Università degli Studi di Padova
Dipartimento di Ingegneria dell'Informazione

Scuola di Dottorato di Ricerca in Ingegneria dell'Informazione
Indirizzo: Scienza e Tecnologia dell'Informazione
XXIV Ciclo

Supélec (Gif-sur-Yvette, France)
Chaire Alcatel-Lucent

École doctorale "Sciences et Technologies de l'Information, des Télécommunications et des Systèmes"
Spécialité: Physique

Flexible Cognitive Small-cells for Next Generation Two-tiered Networks

Direttori di Tesi/Directeurs de Thèse:

Prof. Lorenzo Vangelista

Prof. Mérouane Debbah

Direttore della Scuola/Directeur de l'École:

Prof. Matteo Bertocco

Coordinatore di Indirizzo/Coordinateur de Spécialité:

Prof. Carlo Ferrari

Dottorando/Doctorant: Marco Maso

Acknowledgments

This dissertation would not have been possible without the guidance and the help of several individuals who, in one way or another, contributed and extended their valuable assistance in the preparation and completion of this study.

First and foremost, my family that gave me constant support while pursuing this important goal. Their love, endless patience and comprehension made me feel really privileged and lucky.

My utmost gratitude goes to my two thesis advisors. Prof. Dr. Lorenzo Vangelista triggered my passion for research more than 5 years ago, and I especially thank him for the unselfish and unfailing support he has been giving me ever since. Prof. Dr. Mérouane Debbah, Head of the Alcatel-Lucent Chair on Flexible Radio in Supélec, has been an example of professionalism and expertise for me during this research work. I wish to thank him for his willingness, steadfast encouragement and clear guidance.

My colleagues in the Department of Information Engineering of the University of Padova and Alcatel-Lucent Chair on Flexible Radio in Supélec, for the uncountable discussions and the valuable shared insights and advices.

Last but not least, a heartfelt thanks goes out to my girlfriend for her love, encouragement, understanding, and patience during hard times of this research, and to my friends, old and new, for being by my side whenever I need them.

Abstract

In the last decade, cellular networks have been characterized by an ever-growing user data demand that pushed for more and more network capacity to be satisfied. This caused increasing capacity shortfall and coverage issues, aggravated by inefficient fixed spectrum management policies and obsolete network structures. The development of new technologies and spectrum management policies is seen as a necessary step to take, in order to cope with these issues. Concerning the latter aspect, a significant research effort has been made since the beginning of the century, to investigate the advantages brought by flexible management paradigms, such as new dynamic spectrum access (DSA) schemes based on cognitive radio (CR). On the other hand, technological advancements have been proposed by new standards for mobile communications as well, to guarantee capacity enhancements over current networks.

From a practical point of view, new approaches to network planning have been proposed together with purely technical solutions, to frame next generation cellular networks capable of meeting the identified target performance to satisfy the user data demands. Accordingly, new hierarchical approaches to network planning, where a tier of macro-cell base stations (MBSs) is underlaid with a tier of massively deployed low-power small-cell base stations (SBSs), are seen as promising candidates to achieve this scope. The resulting two-tiered network layout may improve the capacity of current networks in several ways, thanks to a better average link quality between the devices, a more efficient usage of spectrum resources and a potentially higher spatial reuse.

In this thesis, we focus on the challenging problem arising when the two tiers share the transmit band, to capitalize on the available spectrum and avoiding possible inefficiencies. In this case, the coexistence of the two tiers is not feasible, if suitable interference management techniques are not designed to mitigate/cancel the mutual interference generated by the active transmitters in the network. This thesis is divided in three main parts, and proposes a rather exhaustive approach to the development of a new DSA technique, to go from the theoretical basis up to a proof-of-concept development.

We first analyze a simplified two-tiered network obtained when deploying an SBS within the coverage area of a pre-existing MBS. We impose that the physical layer strategy adopted in the first tier, i.e., orthogonal frequency division multiplexing (OFDM), must be left untouched. The rationale for this is that we aim the guaranteeing a higher compliance of any proposed solution with the legacy single-tier network structure. Accordingly, we propose a novel technology called cognitive interference alignment (CIA), to be adopted

uniquely in the second tier, to allow the two tiers to operate side-by-side in a CR setting.

Afterwards, we consider a multi-user extension of the two-tiered network, considering the presence of several SBSs in the second tier. We show how the feasibility of the proposed approach can be extended to such scenarios, designing both a centralized and a distributed approach to manage the multi-user interference in the second tier. The performance of both solutions is evaluated for perfect and imperfect channel state information at the transmitter (CSIT) assumptions, and comparisons with state-of-the-art approaches are provided. Practical implementations issues of both solutions are identified, enlightening main features and drawbacks, and discussing possible solutions.

In the last part of the thesis, we gradually take a step forward from the theoretical basis provided in the first two parts, up to a proof-of-concept development of a hybrid transceiver based on the proposed solution. Specifically, we show how the applicability of CIA is not limited to CR settings, and propose an application of this technique to enhance the energy efficiency of a standalone OFDM femto-cell base station (FBS), typical example of new generation low-power device adopted in heterogeneous network deployments. We investigate the enhancements that can be achieved for different channel conditions and statistics and discuss the impact of the power allocation strategy adopted by the FBS on these results. We finally design a working reconfigurable transceiver based on a software defined radio (SDR) approach, to implement devices capable of transmitting/receiving OFDM/CIA signals, or a flexible combination of both. We conclude the thesis by adopting this new tool to validate the theoretical results of the energy efficiency enhancement solution, showing the effectiveness and merit of both CIA and the designed reconfigurable transceiver.

Sommario

Nell'ultimo decennio, le reti cellulari sono state caratterizzate da una crescita costante della richiesta di dati da parte degli utenti. Unito all'inefficienza delle politiche di gestione dello spettro adottate e all'obsolescenza delle infrastrutture di rete, questo ha generato una crescente necessità di maggiore capacità e copertura di rete. Lo sviluppo di più efficienti politiche di gestione dello spettro radio e di nuove tecnologie è un passo necessario per far fronte a queste problematiche. In questo senso, i vantaggi apportati da nuovi e flessibili schemi di gestione dello spettro, come il cosiddetto dynamic spectrum access (DSA) e gli approcci di tipo cognitive radio (CR), sono stati largamente studiati sin dagli inizi del secolo. Nuove basi per le reti cellulari di prossima generazione sono state poste anche dai più recenti standard, le cui innovazioni tecnologiche promettono un sostanziale aumento di capacità rispetto alle reti esistenti.

Oltre alle innovazioni puramente tecniche, le soluzioni proposte per strutturare reti cellulari evolute, in grado di fornire elevate performance e soddisfare le richieste degli utenti, prevedono nuovi paradigmi che ne guidino la progettazione. In questo senso, approcci gerarchici al network planning, risultanti in reti a due livelli, in cui un livello di stazioni di base di tipo macro (MBS) viene affiancato da un livello di stazioni di base di tipo small (SBS), sono considerati estremamente promettenti. Queste nuove reti a due livelli potranno aumentare la capacità delle reti attuali in molti modi, grazie a minori attenuazioni medie nei canali tra i dispositivi, un uso più efficiente della risorsa spettrale e una miglior copertura di rete.

Il lavoro presentato in questa tesi è concentrato sulla coesistenza tra i due livelli di rete, quando questi adottano la stessa banda in trasmissione per raggiungere un uso più efficiente della risorsa spettrale. In questo caso, se l'interferenza mutualmente generata dai trasmettitori attivi nei due livelli di rete non viene attenuata o eliminata da adeguati meccanismi per la gestione dell'interferenza, la coesistenza può risultare problematica, quando non impossibile. Questa tesi è suddivisa in tre parti e propone un ampia analisi che porta allo sviluppo di una nuova tecnica di tipo DSA, partendo dalle basi teoriche e arrivando allo sviluppo di un proof-of-concept.

Il primo caso studiato è dato da una rete a due livelli semplificata, ottenuta considerando la presenza di una sola SBS all'interno del raggio di copertura di una MBS preesistente. Per garantire la compatibilità delle soluzioni proposte con le operazioni di una classica rete a singolo livello, si impone che la tecnologia di strato fisico adottata dalla MBS, i.e., orthogonal frequency division multiplexing (OFDM), non debba prevedere al-

cuna modifica. Di conseguenza, le relazioni tra i due livelli di rete vengono strutturate secondo il modello CR, e viene proposta una nuova tecnica per realizzare la coesistenza dei due livelli chiamata cognitive interference alignment (CIA), adottata unicamente dalla SBS.

In seguito, l'analisi viene estesa ad una rete multi-utente, considerando la presenza di più di una SBS all'interno del raggio di copertura della MBS preesistente. La fattibilità e l'efficacia di CIA viene analizzata in questo contesto. Di conseguenza, vengono proposte strategie centralizzate e distribuite per la gestione dell'interferenza multi-utente, causata dalla presenza di più SBS all'interno del secondo livello di rete. L'analisi delle prestazioni della rete a due livelli viene effettuata per entrambi gli approcci, in caso di disponibilità di stime di canale al trasmettitore sia perfette sia imperfette (perfect e imperfect CSIT). Questa parte si conclude identificando le problematiche e i meriti principali legati all'implementazione pratica degli approcci proposti, sia centralizzati che distribuiti, e discutendone possibili soluzioni.

Nell'ultima parte della tesi, l'analisi si sposta gradualmente da un approccio di tipo teorico ad uno di tipo pratico, portando allo sviluppo di un transceiver ibrido basato sulla tecnica proposta in precedenza, come proof-of-concept. Particolare attenzione viene dedicata nel mostrare come CIA sia applicabile non solo in caso di scenari di tipo CR, ma possa anche essere utilizzata in modo flessibile per incrementare le prestazioni di una generica stazione di base di tipo femto (FBS) utilizzante OFDM, tipico esempio di dispositivo a bassa potenza adottato nelle attuali reti a più livelli. Viene mostrato come un aumento dell'efficienza energetica del dispositivo sia possibile, grazie all'utilizzo di CIA. Inoltre, viene studiato l'impatto dell'allocazione di potenza effettuata dalla FBS su questo risultato viene studiato, considerando la presenza di canali caratterizzati da varie descrizioni statistiche. La tesi si conclude con la progettazione di un transceiver riconfigurabile, realizzato utilizzando un approccio di tipo software defined radio (SDR), al fine di ottenere uno strumento flessibile per realizzare esperimenti pratici che possano convalidare i precedenti risultati teorici. L'architettura proposta, in grado di trasmettere/ricevere segnali di tipo OFDM/CIA (o combinazioni di entrambi), viene infine utilizzata per testare l'efficacia di CIA nell'aumentare l'efficienza energetica di una classica trasmissione OFDM, con risultati positivi.

Résumé

Au cours de la dernière décennie, les réseaux cellulaires ont connu une augmentation exponentielle de la demande de données, qui a eu pour conséquence directe l'augmentation des capacités que le réseau doit pouvoir satisfaire. Du fait de cette augmentation soudaine de la demande, on constate souvent des chutes de capacités occasionnelles et des problèmes de couverture, aggravés par des politiques de gestion du spectre inefficientes et des structures réseaux obsolètes. Le développement de nouvelles technologies et de nouvelles politiques de management de spectre permettront de traiter les problèmes précédemment évoqués. Concernant ce dernier aspect, un effort significatif a été fait en ce sens depuis le début du siècle pour investiguer les avantages que peuvent offrir de tels paradigmes de management flexibles, tels que les nouveaux schémas de dynamic spectrum access (DSA) basés sur des radios cognitives (CR). D'autre part, des avancées technologiques ont été proposées par les nouveaux standards de communications mobiles, pour garantir des améliorations de capacités offertes au niveau des réseaux actuels.

D'un point de vue pratique, de nouvelles approches pour la planification des réseaux ont également été proposées conjointement avec de nouvelles solutions purement techniques, pour encadrer les réseaux mobiles de prochaine génération, capables d'atteindre les niveaux de performance requis par les demandes de data des utilisateurs. Pour cette raison, les nouvelles méthodes de planification des réseaux hétérogènes, où les stations de base macro (MBS) sont déployées conjointement avec des stations de base small (SBS), constituent des candidats prometteurs pour atteindre cet objectif de performance. Le réseau ainsi considéré pourra augmenter la capacité offerte par les réseaux actuels de nombreuses façons : via une utilisation plus efficiente du spectre disponible et une meilleure réutilisation spectrale, par exemple.

Dans cette thèse, nous nous concentrons principalement sur le problème inhérent au fait de posséder deux niveaux de transmission au niveau de notre réseau (small BS et macro BS) qui doivent dès lors se partager une bande commune, capitaliser sur le spectre disponible et éviter les situations d'interférences où elles s'annihilent mutuellement. Dans ce cas, la question de la coexistence se pose et elle ne peut être atteinte que si des techniques de management d'interférence sont développées pour mitiger/annuler l'interférence générée par ces deux transmetteurs. Le travail se décompose en trois parties principales et propose une approche plutôt exhaustive pour le développement de techniques de DSA, d'un niveau purement théoriques aux premières trames de proof-of-concept.

Nous analysons, tout d'abord, un modèle simplifié de réseau à deux niveaux, dans

lequel une seule SBS est déployée dans le rayon de couverture d'une MBS. Nous imposons, dans ce contexte, que le schéma de transmission utilisé par la MBS, à savoir de l'orthogonal frequency division multiplexing (OFDM), doit être laissé intact. Ce qui légitime ce choix, c'est que l'on cherche à garantir que les SBS qui seront ajoutées se montreront complaisantes vis-à-vis du réseau de MBS déjà existant. Dans ce cadre, nous proposons une nouvelle technologie, nommée cognitive interference alignment (CIA), qui sera adoptée au niveau des SBS, et qui permet aux deux niveaux de transmission de cohabiter dans une configuration de radio cognitive.

Par la suite, nous sommes amenés à considérer une extension multi-utilisateurs du réseau hétérogène précédemment considéré, dans lequel plusieurs SBSs sont déployées. Nous démontrons que notre approche peut être étendue simplement à de tels scénarios, et ce dans une configuration centralisée ou distribuée, afin de traiter l'interférence générée par de multiples utilisateurs au niveau des SBSs. La performance et la qualité des algorithmes est évaluée dans des hypothèses de parfaites et d'imparfaites connaissances l'état des canaux (perfect et imperfect CSIT). Des implémentations pratiques, découlant des algorithmes proposés, sont envisagées et identifient les principaux avantages et inconvénients, laissant ouverte la discussion pour des solutions possibles.

Dans la dernière partie de ce manuscrit, nous discuterons de l'implémentation en pratique d'un proof-of-concept, à partir de la théorie précédemment décrite dans les deux parties précédentes. Il consiste en la réalisation d'un transceiver hybride. Plus particulièrement, nous montrons l'applicabilité de notre technologie CIA et prouvons qu'elle n'est pas limitée qu'aux configurations de radios cognitives. Pour réaliser cela, nous nous plaçons dans un système comportant une station de base femto (FBS) indépendante dont on cherche à augmenter l'efficacité énergétique via notre méthode. Cette FBS constitue alors un exemple typique et illustratif de cette nouvelle génération de transmetteurs à faible puissance devant être utilisé dans les futurs réseaux hétérogènes.

Nous investiguons alors les améliorations offertes par notre méthode pour diverses conditions et statistiques de canaux et nous discutons de l'impact de la stratégie de puissance choisie par la FBS sur ces résultats. Nous réalisons finalement un transceiver reconfigurable basé sur des radios logicielles (SDR), capables de transmettre et de recevoir des signaux OFDM/CIA ou une combinaison des deux. Ce nouvel outil nous permet de valider les résultats théoriques obtenus en termes efficacité énergétique dans les parties théoriques précédentes et démontre donc en pratique les améliorations offertes au réseau par notre méthode CIA et par un tel transceiver hybride reconfigurable.

Contents

List of Acronyms

AWGN	additive white Gaussian noise
BD	block diagonalization
BER	bit error rate
BPSK	binary phase shift keying
CDF	cumulative distribution function
CIA	cognitive interference alignment
CP	cyclic prefix
CR	cognitive radio
CSI	channel state information
CSIT	channel state information at the transmitter
CT	CIA transceiver
DFT	discrete Fourier transform
DL	downlink
DPC	dirty paper coding
DSA	dynamic spectrum access
FBS	femto-cell base station
FDD	frequency division duplexing
FDMA	frequency division multiple access
FFTW	fastest Fourier transform in the West

HT	hybrid transceiver
IDFT	inverse discrete Fourier transform
IA	interference alignment
IBI	inter-block interference
ICI	inter-cell interference
ICIC	inter-cell interference coordination
INNR	interference plus noise to noise ratio
IRBD	iterative regularized block diagonalization
ISI	inter-symbol interference
ISM	industrial, scientific and medical
LAPACK	linear algebra PACKage
LOS	line of sight
LTE	long term evolution
LTE-A	long term evolution advanced
MBSs	macro-cell base stations
MF	matched filter
MIMO	multiple input, multiple output
MIMO-BC	MIMO broadcast channel
MMSE	minimum mean square error
MUEs	macro-cell user equipments
NLOS	non-line-of-sight
OFDM	orthogonal frequency division multiplexing
OFDMA	orthogonal frequency division multiple access
ORBF	opportunistic random beamforming
OT	OFDM transceiver
PAPR	peak to average power ratio
PDCCH	physical downlink control channel

PDP	power delay profile
PRBs	physical resource blocks
QAM	quadrature amplitude modulation
QoS	quality of service
RF	radio frequency
RIBF	regularized inverse beamforming
R.M.S.	root mean square
S-C	Schmidl-Cox
SBSs	small-cell base stations
SDR	software defined radio
SDR4All	Software Defined Radio for All
SINR	signal to interference plus noise ratio
SISO	single input single output
SMMSE	successive minimum mean square error
SNR	signal to noise ratio
SON	self-organizing network
SUEs	small-cell user equipments
SUS-ZFBF	semi-orthogonal user selection ZFBF
SVD	singular value decomposition
TDD	time division duplexing
TD-LTE	time-division long-term evolution
TDMA	time division multiple access
TCP/IP	transmission control protocol / internet protocol
TX/RX	transmitter/receiver
UL	uplink
USB	universal serial bus
USRP	universal software radio peripheral

VFDM	Vandermonde-subspace frequency division multiplexing
WF	water-filling
WiFi	wireless fidelity
WiMAX	worldwide interoperability for microwave access
ZF	zero forcing
ZFBF	zero forcing beamforming

List of Figures

List of Tables

Chapter 1

Introduction

FUTURE CELLULAR NETWORKS are expected to provide ubiquitous broadband access to a large number of mobile users and satisfy the ever-growing user data demand [1]. On the other hand, since the beginning of the century, a spectrum scarcity problem affecting current wireless networks has been noted by the research community [2]. From a practical point of view, this causes the capacity shortfalls and ever-present coverage issues experienced by the already stressed existing 3G networks, that will not likely be able to accommodate the explosion in mobile data demands created by new-generation wireless devices. The development of new technologies and spectrum management policies is seen as a necessary step to take, in order to address these issues.

1.1 Technological Challenges

Recently, new standards for mobile communications have been developed to guarantee capacity enhancements over current networks. In particular, solutions adopted for 4G networks deployment, such as long term evolution (LTE)/long term evolution advanced (LTE-A), are expected to provide a significant capacity increase, up to three times over the current limit. Unfortunately, recent studies have shown that, despite the remarkable technological advancement, LTE/LTE-A may not offer a sufficient performance to address future data traffic, expected to double every year [1]. Accordingly, it is forecast that new approaches to network planning could provide an additional boost and allow these new technologies, e.g., LTE, to consistently meet the performance requirements of future generation networks. The most attractive solution is believed to be a new hierarchical approach to network planning, where a tier of macro-cell base stations (MBSs) is underlaid with a tier of low-power, possibly mobile small-cell base stations (SBSs) [3]. In other words, a network composed of two tiers where transmitters of heterogeneous nature, "serving" cells of different sizes, are deployed in the same area. The resulting two-tiered network layout may improve the capacity of current networks in several ways, thanks

to a better average link quality between the devices, a more efficient usage of spectrum resources and a potentially higher spatial reuse [4, 5]. From a practical point of view, operators are already working in this direction, moving from a static single tier to a more flexible two-tiered approach to network design. Nowadays, more than 16% of the total traffic from the macro-cellular tier is already being diverted to a second tier composed of small form factor base stations, and this is expected to grow to 48% by 2015 [6]. Accordingly, a proliferation of SBSs is expected for the next future.

Deployed by end-users, the SBSs will likely operate in a plug & play manner and lack a predefined network infrastructure. It is foreseen that a massive SBSs' deployment would unlikely be possible without a significant simplification of the network management paradigms [7, 8]. In fact, an explicit cooperation between the two tiers may be unfeasible, due to the massive and unplanned deployment of the SBSs in the second tier. On the other hand, the definition of suitable and reliable strategies to realize the coexistence of the two tiers is mandatory, to be able to experience the desired performance improvements. For these reasons, it is envisioned that future mobile networks will likely be populated by devices that can self-organize and self-optimize their operations, and the so-called self-organizing network (SON) [9] technology is seen as the potential key factor to achieve this goal.

Traditionally, coexistence of different transmitters in two-tiered networks can be achieved adopting three different approaches [10, 11]:

- *Complete separation.* In this case, according to the nomenclature adopted in this thesis, the MBSs and the SBSs operate on disjoint bands, with no need for interference management solutions to mitigate/cancel the inter-cell interference (ICI). For instance, different radio access technologies could be adopted in the two tiers using different frequency bands, i.e., cellular and wireless fidelity (WiFi) [12]. Nevertheless, this approach may significantly decrease the spectral efficiency improvements brought by the two-tiered structure, due to a very large band footprint.

- *Partial sharing.* To reduce the band footprint and raise the spectral efficiency, the two tiers shall re-use a portion of the band. On the other hand, solutions to mitigate/cancel the ICI between the two tiers in the shared band need to be devised.

- *Complete sharing.* The most attractive solution to maximize the potential gains in terms spectral efficiency of the two-tiered network is represented by a co-channel deployment of first and second tier. In other words, in this approach, the MBSs and SBSs share the whole band. Nevertheless, a co-channel deployment of MBSs and SBSs would yield high levels of ICI, potentially limiting the expected spectral efficiency enhancements [8]. The impact of ICI on the performance of a general macro-cell based network has been widely studied in the literature [13]. We note that, in general, the nature of the ICI in two-tiered network is twofold. In particular, each standalone base station operating in these networks may generate *co-tier interference* towards receivers belonging to the same tier, and *cross-tier interference* towards receivers belonging to a different tier. Therefore, if on the one hand

the overall spectral efficiency potentially increases when the two tiers communicate over the same bandwidth, on the other hand high levels of cross-tier interference are generated. Therefore, despite its notable features, this approach is not feasible if appropriate interference management techniques, to allow the coexistence of the two tiers in a co-channel deployment scenario, are not adopted.

During the standardization phase of recent systems, e.g., LTE-A, inter-cell interference coordination (ICIC) techniques have been extensively discussed, and are still considered an open problem, especially in the self-configuring and self-optimizing network use cases [14]. Consequently, the two-tiered network paradigm requires in general not only the aforementioned design of new protocols to allow simplified network operations, but also the study of novel signal processing techniques to provide the expected spectral efficiency gains at physical layer [15, 16].

1.1.1 State-of-the-art Interference Management Solutions

Several state-of-the-art interference management solutions have been proposed in the literature, to realize the coexistence of the two tiers, in case of co-channel deployment, and enhance the spectral efficiency of the network. However, as previously said, the unplanned and dense deployment of SBSs in the second tier does not allow both coordination and cooperation between the two tiers. From a practical point of view, this implies that no information about the first tier in terms of spectrum characteristic, time resource allocation, transmitted messages and power allocation is available at the SBSs. The work in this thesis starts from these considerations to develop the desired interference management strategies to realize the coexistence of the two tiers, when a complete spectrum sharing approach is adopted.

On the one hand, this frames a scenario that does not rely on too unrealistic assumptions, as well as on hardly practically implementable algorithms in terms of required time and computational capabilities. On the other hand, this prevents the implementation of state-of-the-art interference management solutions, to realize the coexistence in two-tiered networks, that require a certain degree of cooperation between the tiers to be adopted:

- Approaches based on dirty paper coding (DPC) [17] cannot be adopted in both tiers since the messages transmitted in one tier are not available in the other.

- Approaches based on interference alignment (IA) [18], coping with cross-tier interference by isolating the received and interference signal subspaces, require a smart coordination of the devices in the network and special decoding at the receiver to realize the alignment. Thus, if the two tiers do not explicitly cooperate, these solutions can not be adopted. Additionally, they depend on the existence of exploitable degrees of freedom in the spatial [19], frequency [20] or time [21] domain, very challenging condition to consistently meet in many realistic scenarios.

- Coordinated beamforming [22, 13] based solutions do not usually require special decoding at the receiver, but have rather stringent channel state information at the transmitter (CSIT) and signaling constraints. In fact, they typically require global CSIT all over the network, cooperation between the two tiers and a backhaul connecting all the transmitters involved in the transmission. Thus, they can not be implemented in the considered scenario.

A different approach to the interference management problem can be considered if the two-tiered network is framed according to the so-called cognitive radio (CR) paradigm [23]. Specifically, the relationships between the network tiers can be modeled according to a licensee-opportunistic scheme, i.e., one tier is the licensee of the band and the other opportunistically operates in the already licensed band without being the licensee, as discussed in the following section.

1.1.2 Cognitive Radio

As previously said, current generation networks are rapidly aging due to an increasing spectrum scarcity, caused by the emergence of various bandwidth-consuming wireless services. However, several studies on spectrum utilization performed by regulatory agencies such as Federal Communication Commission [24, 25] demonstrated that the radio spectrum is extremely under-utilized, due to the unreasonable command-and-control spectrum regulation. In a response to this issue, the adoption of flexible rules for spectrum usage has been suggested to promote a more efficient exploitation of the already allocated physical spectrum [26]. As a consequence, the so-called CR approach has drawn great attention in the last decade within the research community, and is seen as the most promising candidate to enable a more efficient spectrum usage [27].

According to the first definition given by Mitola et al. in [23], CR are a class of smart radio devices capable of extracting a wide range of informations out of the surrounding environment and adapting accordingly. Specifically, the CR exploits this situation awareness to opportunistically transmit in the licensed band by adopting approaches that are encompassed in the so-called dynamic spectrum access (DSA) category [28, 29, 30, 31], that allow the transmission of a secondary flow of information while shielding the primary transmission from undesired interference. Examples of such informations on the licensee system, usually obtained either by means of sensing oriented techniques, e.g., spectrum sensing [27], or by deterministic side knowledge about the nature of the licensee transmission, e.g., the adopted communication standard, could be:

- Spectrum usage.
- Performed resource allocation in time, frequency o space domain.
- Data traffic patterns or statistical models, e.g., data-centric, bursty, variable/constant bit-rate and so on.

- Performed power allocation, e.g., uniform power allocation or optimal according to a given metric.

- Maximum tolerable interference levels, e.g., interference temperature [32, 33].

Now, let us turn the focus to the aforementioned two-tiered network layout. We note that, if the two tiers do not cooperate, the two-tiered network could be easily framed in a CR perspective [8]. For instance, let us consider the usual situation characterizing any commercially-based wireless network, e.g., a cellular network. In this scenario, the first tier would host the licensee network, likely owned by the provider of the service, and would have full rights to the spectrum and possibly need to satisfy one or more quality of service (QoS) requirements while serving the customers. Thus, any SBS deployed in the second tier should sense the environment to change and adapt its transmit parameters accordingly [34, 35]. As a consequence, a re-use of the available resources and opportunistic transmit strategies would be performed in the second tier, in a way not to cause negative impacts on the ongoing transmission in the first tier [16]. In this case, the latter would have the role of the primary system, protected from the interference generated by the former, operating as the secondary system. We note that, in this approach, the SBSs would suffer from full cross-tier interference generated by the active MBSs in the first tier, being the secondary system subordinated to the primary by definition.

As previously said, interference management techniques that can be adopted if the two-tiered network is framed according to the CR paradigm can be derived following a different approach if compared to the approaches discussed in Section 1.1.1. On the other hand, they belong to the same family and can be derived following the same underlying concepts and ideas. For instance, solutions based on IA or transmit beamforming have been proposed for the CR setting [36, 37, 38], usually requiring several degrees of cross-tier and co-tier coordination and multiple spatial dimensions at the transmitter and/or receiver. It is important to note that all these solutions involve a bi-directional signaling between the MBSs/SBSs to be implemented, requiring the existence of a link dedicated to this aim, e.g., a backhaul. Therefore, since no cooperation can be reliably established between the two tiers (and in general within the second tier) as discussed in the first part of this chapter, the implementation of these approaches could be unfeasible, even if the SBSs were cognitive devices. In particular, we remark that:

- The lack of knowledge on both the power allocation and the existence of left-over spatial degrees of freedom in the first tier disqualifies opportunistic IA based approaches as proposed in [39, 40, 36].

- Cognitive beamforming approaches [37, 41, 42] could be adopted if multiple spatial dimensions, i.e., antennas, were available at the SBSs. In this case, the cross-tier interference could be mitigated by satisfying one or more signal to interference plus noise ratio (SINR) constraints at the primary receivers, while at the same time serving one or more secondary receivers at a non-negligible rate. On the other hand, these approaches would not be implementable if the SBSs were single-antenna

devices, a condition that may limit their implementability only to very specific scenarios.

- More general DSA strategies such as spectrum shaping [35] and cooperative frequency reuse [34] can be adopted at an SBS if a special spectrum management approach is adopted at the MBS. If frequency reuse 1 is adopted, as suggested by recent standards such as LTE/LTE-A, and the transmission is performed over the whole band these approaches are not implementable.

In this thesis, we will start from these considerations to develop suitable strategies for interference management in two-tiered networks, to realize the coexistence of the two tiers with no need for cooperation between them. However, the co-channel deployment assumption, made for matters of potential spectral efficiency enhancements, frames a very challenging situation. The non-regulated access to the spectrum could lead to unbearable level of cross-tier interference, limiting if not canceling the spectral efficiency gains brought by the presence of the second tier. For this reason we will assume a flexible approach to spectrum access, and frame the two-tiered network according to the CR paradigm as discussed in this Section. Accordingly, in this thesis, the first tier will be always considered as the primary licensee system, whereas the second tier will be modeled as an opportunistic secondary system. In the following section, the reference scenario considered throughout the thesis will be described.

1.2 Reference Scenario

Consider a two-tiered network operating under the complete sharing approach, with first tier populated by an MBS serving a group of macro-cell user equipments (MUEs) and a second tier composed of several cognitive SBSs serving a group of small-cell user equipments (SUEs), as in Figure 1.1. We assume time division duplexing (TDD) communications in both tiers. Recently, this mode has raised an increasing interest in the wireless communications community as the key factor for many state-of-the-art technological advancements, e.g., massive (or network) multiple input, multiple output (MIMO) [43, 44, 45], to provide significant spectral efficiency gains w.r.t. legacy frequency division duplexing (FDD) mode approaches.

In fact, despite the much stronger requirements in terms of network synchronization that TDD must satisfy if compared to FDD[1], the former brings a number of important technical advantages for future-generation networks that the latter cannot offer.

- FDD is best suited for applications that generate symmetric traffic whereas TDD is best suited for bursty, asymmetric traffic, such as internet or other data-centric

[1]In TDD communications, the transmit and receive cycles of different base stations must be synchronized. If this were not the case, the uplink transmission of user equipments inside a given cell may suffer from high co-channel interference generated by the downlink transmission of any out-of-cell base station, and vice versa. FDD communications do not have this requirement.

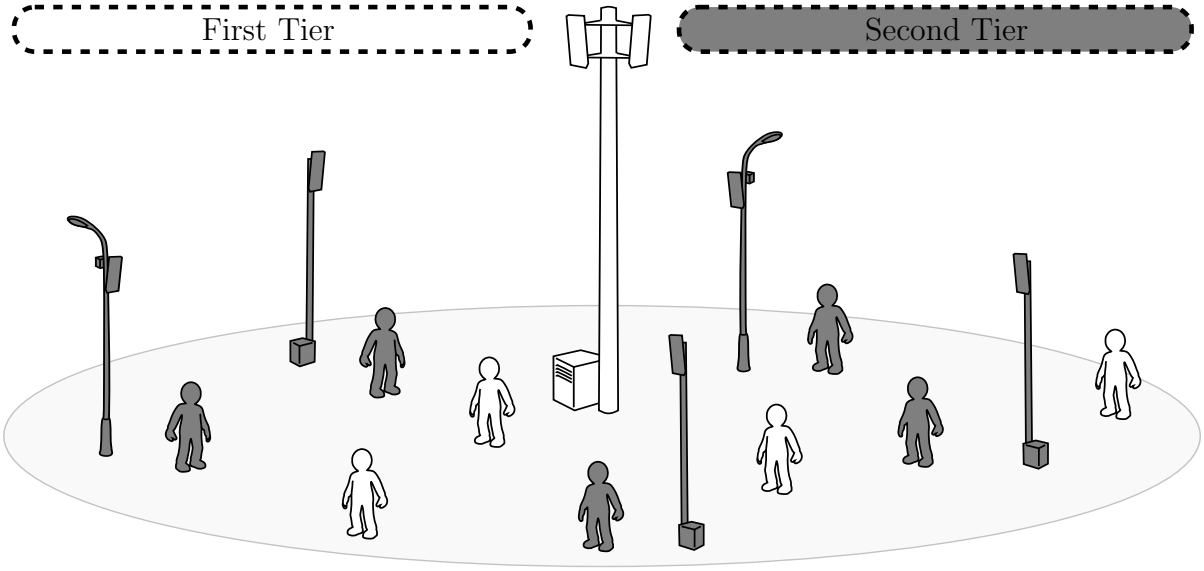

Figure 1.1: Two-tiered network model.

services [46]. The current user demand in 3.5G/4G network is mainly data-oriented. Therefore, a flexible resource allocation scheme is highly advisable and can be realized in case of TDD communications, where the duration of downlink (DL) and uplink (UL) time slot can be defined at software level and changed at any time. This is not possible for FDD communications, where the DL and UL bandwidth are not parameters that can be flexibly tuned during the operations [47].

- TDD does not require paired channels, or large guard bands to be effective. Potentially, this results in higher spectral efficiency if compared to FDD, since only one contiguous channel is needed and shared by the DL and UL transmission. The potential capacity enhancements that this approach can yield are very attractive both for current and next generation networks, due to the ever-growing data demand [1].

- In TDD communications the DL and UL channel impulse responses are reciprocal (i.e., channel reciprocity), thus no explicit channel estimation feedback needs to be transmitted by the receiver. The transmitter can directly acquire the CSI by estimating the UL channel. This implies a higher precision in the CSIT w.r.t. what can be achieved in FDD communications, where both the quantization of the CSI and the UL channel attenuation can significantly degrade the quality of the CSI, that is fed back from the receiver to the transmitter. Consequently, beamforming and power allocation strategies and, in general, transmit parameters optimization can be performed more effectively in TDD communications.

- In frequency selective channels, the ratio between the coherence bandwidth of the channel and channel bandwidth is directly proportional to the frequency diversity order experienced by both DL and UL links [48]. Therefore, TDD communications may experience a grater frequency diversity if compared to FDD communications,

thanks to the wider bandwidth in the spectrum of the UL and DL signals.

- Despite the larger sampling frequency due to the wider single band, and the higher peak transmission power needed to achieve high data rate in a shorter period (if compared to FDD), the hardware required for a device operating in TDD mode is in general cheaper [49]. In particular, only a single oscillator is required by both DL and UL and no duplexer is needed, given the time slotted nature of the transmission.

- Thanks to the channel reciprocity, TDD can exploit spatial diversity even if the receiver is a single-antenna device. For instance, if the transmitter has two antennas, the two received UL signals will experience a different attenuation due to the spatial diversity. Thus, the antenna receiving the stronger UL signal at the transmitter can be used in the DL, and the spatial diversity is exploited irrespective of the presence of only one antenna at the receiver [47].

Big efforts have been devoted in the research community to solve the most prominent practical implementation issues inherent to TDD communications[2], to allow for the practical implementation of devices adopting this promising approach. Recent standards are already including the TDD as one of their possible operating mode, e.g., LTE/LTE-A [50][3], and first commercial products will be soon available on the market, to exploit this technology [51]. This is believed to be a first step towards the introduction of a new generation of network devices able to communicate in TDD mode and, as a result, both academic and industrial environments are very active on this front [52, 53, 54].

For all these reasons, we believe the TDD mode to be a very attractive solution for next generation networks. As a consequence, in this thesis, we have chosen to consider a two-tiered network operating in TDD mode, to be compliant with the state-of-the-art advancements in the wireless communications community. Specifically, we will focus on the DL, unless otherwise stated.

1.3 Contribution

As specified and discussed in Section 1.2, in this thesis we focus on the DL of a two-tiered network and consider the case of co-channel deployment of the two tiers. We study the problem of the coexistence between a MBS (first tier) and several cognitive SBSs (second tier). The main contributions of this thesis are:

- We implement a one-way test-bed based on a software defined radio (SDR) platform, to serve as a proof-of-concept of Vandermonde-subspace frequency division multiplexing (VFDM) [55, 56], state-of-the-art technique adopted by a cognitive SBS operating in a two-tiered network, to null the cross-tier interference towards an

[2]Examples of these issues are the aforementioned network synchronization constraint or the so-called cross-slot and inter-operator interference problems [48], just to name a few.

[3]The so-called time-division long-term evolution (TD-LTE).

orthogonal frequency division multiplexing (OFDM) MUE. We identify the main implementation issues and analyze their impact on the performance of this DSA technique for two-tiered networks.

- We propose a novel DL DSA technique based on a linear precoding scheme at the transmitter, called cognitive interference alignment (CIA), able to deal with the cross-tier interference generated by an opportunistic SBS towards one MUE in the first tier. We derive the optimal linear precoder structure to maximize the spectral efficiency of a second tier operating under a cross-tier interference nulling constraint.
- We extend CIA for the multi-user two-tiered network hosting any number of MUEs and SBS/SUE pairs, designing both a centralized and a distributed solution for the co-tier interference management problem in the second tier.
- We discuss the possible practical implementation issues characterizing the multi-user extension of CIA. We analyze the impact of the relaxation of the perfect CSIT assumption at the SBSs on the performance of the two-tiered network;
- We show the usefulness of CIA not only as a DSA enabler technique in CR settings, but also as an effective strategy to enhance the energy efficiency of the DL transmission of a standalone FBS. We model the FBS as a virtual two-tiered network and propose a hybrid approach, by means of CIA, for the DL transmission.
- We design a novel SDR-based reconfigurable transceiver for flexible cognitive networks, that can be used to implement and test physical layer strategies such as OFDM or CIA. We profit of the capabilities of this novel architecture to demonstrate the effectiveness of the previously proposed hybrid scheme.

1.4 Thesis Outline

The thesis is organized in four main parts after the first chapter.

- **Part I: Single Small-cell Deployment.** In this part, we start by considering a 2×2 scenario, modeled as a two-tiered network with first tier hosting an OFDM MBS and second tier hosting a single cognitive SBS. As a first step, we consider the aforementioned state-of-the-art technique to realize the coexistence of the two tiers in such scenarios, i.e., VFDM, and thoroughly analyze its theoretical and practical limitations. Afterwards, we propose a novel approach to the two-tiered network deployment based on cognitive flexible small-cells, for a single-user setting, i.e., CIA. This contribution is organized as follows:
  - **Chapter 2.** In this chapter, we first briefly introduce the state-of-the-art solution for OFDM-based 2×2 systems, i.e., VFDM. Then, we describe the implementation of an experimental test-bed using the new Software Defined Radio for All (SDR4All) platform [57], to take a first step towards a

proof-of-concept of a VFDM-based system. The practical feasibility of a VFDM transmission over a secondary link is shown. Practical implementation issues are identified and discussed.

- **Chapter 3.** In this chapter, we keep our focus on the OFDM-based 2×2 scenario, modeled as a simplified two-tiered network and derive the optimal linear precoder-based strategy that can be adopted by a cognitive SBS, operating in such scenario, to serve one SUE while satisfying an interference nulling constraint to protect one MUE, i.e., CIA. We note that, this approach, is optimal w.r.t. the spectral efficiency of the secondary link. Interestingly, the proposed technique is indeed optimal for any interference channel for which the channel matrix representing the link from the interference nulling transmitter and the shielded receiver has a non-empty null-space. Numerical findings show how the adoption of CIA at the cognitive SBS enable a fruitful coexistence inside the OFDM-based two-tiered network if perfect CSIT is available in the second tier.

- **Part II:** The considered two-tiered network is extended to a multi-user setting, where several secondary SBS/SUE pairs are deployed inside the coverage area of an OFDMA MBS, serving multiple MUEs. We first show how the feasibility of the proposed technique can be extended in case of multiple MUEs to be protected in the first tier. Afterwards, we study the co-tier interference mitigation problem in the second tier and provide both a centralized and a distributed solution. Then, we focus on the implementation requirements of the proposed approaches and identify their limitations, discussing possible issues and solutions. The performance of both approaches is evaluated in case of perfect and imperfect CSIT, and enhancements w.r.t. to traditional solutions for coexistence in two-tiered networks are shown. This part is organized as follows:

  - **Chapter 4.** A centralized coordinated beamforming strategy based on a network MIMO configuration, to mitigate the co-tier interference in the second tier, is presented in this chapter. The proposed approach enables the coexistence of the two multi-user tiers, by mitigating the co-tier interference in the second tier, while satisfying the cross-tier interference nulling constraint at each SBS. Spectral efficiency enhancements w.r.t to traditional solutions for coexistence in two-tiered networks are shown, assuming perfect CSIT and SBSs' synchronization in the second tier.

  - **Chapter 5.** In this chapter, we first deeply investigate the impact of the relaxation of the important assumption related to the perfect CSIT in the second tier. Then, the comparison provided in Chapter 4 for a perfect CSIT assumption is repeated in case of imperfect CSIT. Interestingly, the results are rather consistent with the previous case, and confirm the spectral efficiency enhancements brought by the proposed approach, even in case of imperfect CSIT in the second tier. Finally, we discuss general implementation requirements of the centralized solution and identify the limitations of such approach, mainly

focusing on possible showstopper issues and possible solutions.

- **Chapter 6.** To address important issues impacting the feasibility of the previously introduced centralized approach, a distributed co-tier interference mitigation strategy for the SBSs is proposed in this chapter. We show that a second tier composed by self-organizing autonomous SBSs adopting a CIA-based strategy can provide capacity enhancements to the two-tiered network, without requiring cooperation, backhaul-based communications between SBSs and coordinated beamforming. The performance of the proposed strategy is evaluated and analyzed for several second tier's configurations, under both perfect and imperfect CSIT assumption. Numerical findings show significant spectral efficiency enhancements over traditional solutions adopted in such networks, i.e., user orthogonalization approaches. Finally, the main differences between the centralized and distributed solution are illustrated, specifically focusing on the advantages in terms of feasibility and implementability that the latter brings w.r.t. the former.

- **Part III:** In this third part we take a step back and give an example of the flexibility of CIA, whose applicability is not necessarily limited to CR settings. Accordingly, we consider a simpler single transmitter DL scenario, given by a standalone OFDM femto-cell base station (FBS) [4] communicating with two user equipments, and propose a strategy to increase the energy efficiency of the transmission. Finally, we implement a flexible hybrid transceiver based by means of an SDR approach, making use of the insights drawn throughout the thesis, to demonstrate the feasibility of the energy efficiency enhancing solution. Concluding remarks close the thesis.

  - **Chapter 7.** A hybrid OFDM/CIA transmitter is proposed in this chapter, as a flexible solution to enhance the performance of next generation two-tiered networks. Specifically, we design a green strategy to recycle unused resources of a standalone FBS performing an OFDM transmission, with the goal to increase its spectral efficiency while maintaining the same total transmit power, thus increasing the energy efficiency as well. We model the considered scenario as a virtual two-tiered network and propose a novel hybrid approach to the FBS design, such that both a CIA and an OFDM transmission can be performed simultaneously by the new hybrid FBS. We study the optimal power splitting among the OFDM and CIA transmissions numerically, and show non-negligible energy efficiency enhancements for several operating conditions.

  - **Chapter 8.** The design of a reconfigurable transceiver for flexible cognitive networks is proposed in this chapter, to provide a proof of concept of the hybrid energy efficiency enhancer strategy presented in Chapter 7. We first describe the architecture of the SDR-based transceiver, focusing on its base-band design and capabilities. Afterwards, we validate the channel reciprocity assumption, inherent theoretical feature of the TDD mode communication required to implement CIA, by means of specific field tests. Finally, the results of a set of experiments is provided to confirm the theoretical results and the effective-

ness of the proposed technique. We show that additional spectral and energy efficiency can be added to the standalone OFDM transmission thanks to the adoption of the hybrid strategy realized by means of CIA.

- **Part III:** In the last part we provide concluding remarks and discuss possible future research directions, to close the thesis.
  - **Chapter 9.** A summary of the main contributions and results of the thesis is proposed in this chapter. Moreover, a discussion on possible perspectives is provided.
  - **Appendix A.** In this appendix, the computation of the structure of a null-space precoder to cancel the undesired interference in the 2×2 scenario analyzed in Chapter 1 is detailed.

1.5 Scientific Production

The work in this thesis has been summarized and presented in the following contributions:

Journal Articles

- M. Maso, L. S. Cardoso, E. Bastug, L.-T. Nguyen, M. Debbah and O. Ozdemir, *On the practical implementation of VFDM-based opportunistic systems: issues and challenges*, REV Journal on Electronics and Communications, Vol. 2, No. 1–2, January – June, 2012.

- M. Maso, E. Bastug, L. S. Cardoso, M. Debbah and O. Ozdemir, *Implementation of a Reconfigurable Cognitive Transceiver for Opportunistic Networks*, submitted IEEE Journal on Selected Areas in Communications: Cognitive Radio Series, 2012.

- M. Maso, L. S. Cardoso, M. Debbah and L. Vangelista, *Cognitive Orthogonal Precoder for Two-tiered Networks Deployment*, to appear in IEEE Journal on Selected Areas in Communications: Cognitive Radio Series, March 2013.

- M. Maso, M. Debbah and L. Vangelista, *A Distributed Approach to Interference Alignment in OFDM-based Two-tiered Networks*, to appear in IEEE Transactions on Vehicular Technology, 2013.

Conference Proceedings

- L. S. Cardoso, M. Maso, M. Kobayashi and M. Debbah, *Orthogonal LTE two-tier Cellular Networks*, IEEE International Conference on Communications (ICC 2011), Kyoto, Japan, 2011.

- M. Maso, L. S. Cardoso, E.Bastug, M. Debbah and O.Ozdemir *VFDM: a prototype of cognitive transceiver*, International Workshop on Communication Systems (IWCS) 2011, Hanoi, Vietnam, 2011.
- L. S. Cardoso, M. Maso, E.Bastug, M. Debbah and O.Ozdemir *Prototype of Orthogonal Precoder-based Technique for Two-Tiered Cellular Networks*, 27$^{\text{th}}$ World Wireless Research Forum (WWRF), Düsseldorf, Germany, 2011.
- M. Maso, L. S. Cardoso, M. Debbah and L. Vangelista, *Channel Estimation Impact for LTE Small Cells based on MU-VFDM*, WCNC 2012, Paris, France, 2012.
- M. Maso, L. S. Cardoso, M. Debbah and L. Vangelista, *Cognitive Interference Alignment for OFDM two-tiered networks*, SPAWC 2012, Çeşme, Turkey, 2012.
- L. S. Cardoso, M. Maso and M. Debbah, *A Green Approach to Femtocells Capacity Improvement by Recycling Wasted Resources*, accepted for publication at WCNC, 2013.

Part I

Single Small-cell Deployment

Chapter 2

Vandermonde-subspace Frequency Division Multiplexing: Implementation and Issues

In the previous chapter we have seen how next generation cellular networks are expected to provide significant capacity enhancements over 3G networks. A new hierarchical approach to network planning is considered as one of the main candidates to achieve this goal. Accordingly, two-tiered network deployments, where a tier of macro-cell base stations is underlaid with a tier of low-power, small-cell (micro/pico/femto) mobile base stations, have already been proposed in recent standards, e.g., LTE-A [58]. On the other hand, co-channel deployments of tiered networks are in general very challenging, due to the presence of high levels of ICI. If no cooperation is established between the two tiers, ICI may largely limit the potential spectral efficiency gains provided by the frequency reuse 1. Smart interference management techniques to be implemented at physical layer to address this issue are required. In this chapter, we start our study by considering a simplified scenario including a LTE-A OFDM macro-cell sharing the spectrum with one small-cell.

2.1 Problem Statement

Consider the downlink of the a simplified two-tiered network composed of two transmitter/receiver (TX/RX) pairs, as depicted in Figure 2.1. We note that, this simplified model mimics a scenario where an operator willing to increase the performance of the network, delegates the installation of a new radio device to an end-user. Several efforts in the literature clearly stated that a co-channel deployment of the two tiers is highly advisable, to be able to profit of the potential spectral efficiency enhancements brought by the resulting two-tiered network structure [11, 10]. Nevertheless, a key factor to achieve the

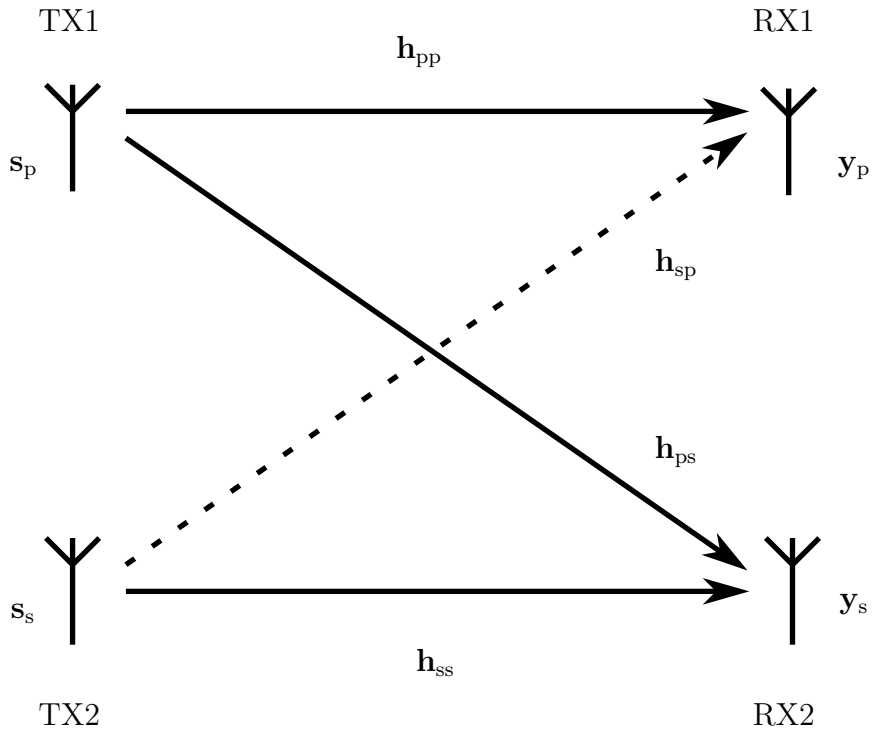

Figure 2.1: Dowlink of two-tiered network [Interference channel].

benefits promised by the frequency reuse 1 is the effectiveness of the strategies adopted to mitigate/cancel to ICI affecting such network deployments. As discussed in Chapter 1, the expected massive and unplanned deployment of small-cell base stations in next generation networks disqualifies attracting but hardly realizable cooperative approaches for ICI management in the two tiers. Moreover, in such scenarios, the transmitters operating in the first tier are likely unaware of the existence of the secondary system, hence no cooperating between the two tiers is feasible. Consequently, the two tiers must operate autonomously, and coordinated signal processing strategies at the transmitter, such as DPC [17], zero forcing (ZF) [59] or any other joint linear beamforming strategy, are not implementable.

On the other hand, due to the hierarchical structure and the spectrum access policy of the considered network, the CR approach provides a set of tools and models to address the ICI issue. Accordingly, as in classical CR settings, we can denote the TX/RX pair operating in the first tier as the primary system (TX2/RX2), and the TX/RX pair operating in the second tier as the secondary system. The primary system communicates a message $\mathbf{s}_{\mathrm{p}}$ over a given licensed band, whereas the secondary system opportunistically accesses the spectrum to communicate a message $\mathbf{s}_{\mathrm{s}}$ over the same bandwidth. In particular, no strategy is implemented at the former to mitigate the ICI generated to the latter. Conversely the opportunistic system has to adhere to one of the interference management policies prescribed by the CR paradigm, i.e., cancelation (overlay or interweave

approach) or mitigation (underlay approach) [29], to protect the licensee system from the undesired interference. Usually, the opportunistic system exploits its cognitive capabilities to acquire side knowledge on the transmission of the primary system. Depending on the amount and nature of available information, the secondary transmit signal can be shaped to assume specific interference properties at the primary receiver.

Wireless communications are typically affected by multi-path signal propagation, resulting in frequency selectivity of the channels. Recent standards, e.g., LTE-A, propose block transmission systems to combat this phenomenon and provide high data rates. Accordingly, we consider that TX1 is a legacy OFDM transmitter, transmitting over N subcarriers, with CP size of L. Concerning the primary receiver RX1, OFDM provides interesting features that allows to eliminate inter-symbol interference (ISI) and inter-block interference (IBI) and equalize the signal using single-tap linear equalizers. In order to obtain this result, RX1 discards the L leading symbols of each received OFDM symbol/block, once time and frequency synchronizations have been achieved. The same operations are performed at RX2 that consequently acts as an OFDM-like receiver. This choice is due both to the aforementioned physical argument (ISI and IBI suppression) and to architectural reasons. In fact, thanks to this assumption, RX1 may act as RX2 and vice-versa, with a simple software reconfiguration, enhancing the flexibility of the considered framework.

We remark that, in the considered scenario, the redundancy adopted at TX1, i.e., cyclic prefix (CP), to deal with the multi-path propagation of the signal is not used to extract information at RX1. Therefore, TX2 can exploit these *unused* resources to design the opportunistic transmission such that the desired interference constraint is respected. We know from [55, 56] that in such scenarios, if the communication is performed in TDD mode, an overlay cognitive approach can be adopted, and an interference cancelation linear precoder based technique called VFDM is implementable at TX2 if perfect CSI is available, as shown in the following. To the best of the author's knowledge, VFDM is the only available state-of-the-art solution in the literature adoptable by a small-cell to harmlessly coexist with an LTE OFDM macro-cell. At present, only theoretical studies on the subject are available. Therefore, herein we aim at investigating the feasibility of this DSA approach to provide a bridge between the theoretical results and a practical implementation of VFDM. Consequently, a first implementation of a cognitive VFDM transmitter/receiver pair prototype, based on the SDR4All platform [57] is proposed as a step forward towards a new flexible approach to small-cells deployment in next generation network. The outcoming demonstrator shows the feasibility of a VFDM-based transmission in the considered scenario. On the other hand, a significant BER detriment w.r.t. to the theoretical results provided in [56] is obtained. A thorough analysis is performed to better characterize the issues affecting VFDM, both from a theoretical and practical point of view. Concerning the notation adopted throughout this work, we note that the primary system (first tier) is always referred by the subscript "p" and the secondary (second tier) by "s", unless otherwise stated. Furthermore, given a matrix $\mathbf{A}$, we define $[\mathbf{A}]_{m,n}$ as its element at the m^{th} row and the n^{th} column

2.2 Signal Model

Consider the modulated symbol vector at TX1. Let $\mathbf{s}_{\mathrm{p}} \in \mathbb{C}^{N\times 1}$ be a complex zero mean unit norm input symbol vector. The OFDM transmit symbol vector $\mathbf{x}_{\mathrm{p}} \in \mathbb{C}^{(N+L)\times 1}$ is then

$$\mathbf{x}_{\mathrm{p}} = \mathbf{A}\mathbf{F}^{-1}\mathbf{s}_{\mathrm{p}}, \tag{2.0}$$

where $\mathbf{A}$ is an $(N+L)\times N$ CP insertion matrix given by

$$\mathbf{A} = \begin{bmatrix} \mathbf{0_{L,N-L}} & \mathbf{I}_L \\ & \mathbf{I}_N \end{bmatrix}, \tag{2.0}$$

and $\mathbf{F} \in \mathcal{C}^{N\times N}$ a unitary discrete Fourier transform (DFT) matrix with $[\mathbf{F}]_{(k+1)(j+1)} = \frac{1}{\sqrt{N}} e^{-i2\pi\frac{kj}{N}}$ for $k, j = 0, \ldots, N-1$.

Now let $\mathbf{h}_{\mathrm{ab}} \sim \mathcal{CN}(0, \mathbf{I}_{l+1}/(l+1))$ be i.i.d. Rayleigh fading channel vectors of $l+1$ taps, representing the link between a transmitter in the tier "a" and a receiver in the tier "b". In general, in practical OFDM implementations, the CP is over dimensioned with respect to the number of channel paths, to avoid ISI and IBI. The operations of convolution of the transmit symbol vectors with the channels can be expressed by the matrices $\mathbf{H}_{\mathrm{ab}} \in \mathbb{C}^{N\times(N+L)}$, given by

$$\mathbf{H}_{\mathrm{ab}} \;= [\mathbf{0}_{N\times(L-l)}\mathbf{G}_{\mathrm{ab}}]\ , \tag{2.0}$$

where $\mathbf{0}_{N\times M}$ is an $N\times M$ all zeros matrix and $\mathbf{G}_{\mathrm{ab}} \in \mathbb{C}^{N\times(N+l)}$ are Toeplitz matrices defined as

$$\mathbf{G}_{\mathrm{ab}} = \begin{bmatrix} h_{\mathrm{ab},l} & \cdots & h_{\mathrm{ab},0} & 0 & \cdots & 0 \\ 0 & \ddots & & \ddots & \ddots & \vdots \\ \vdots & \ddots & \ddots & & \ddots & 0 \\ 0 & \cdots & 0 & h_{\mathrm{ab},l} & \cdots & h_{\mathrm{ab},0} \end{bmatrix}.$$

Note that, in (2.2), $\mathbf{H}_{\mathrm{ab}}$ can assume different structures depending on the relationship between L and l. We remark that, the number of rows of $\mathbf{H}_{\mathrm{ab}}$, i.e, N, that is the number of received symbols at RX1 and RX2 results, from the CP removal operation performed at the receiver.

We switch our focus on TX2 and similarly let $\mathbf{x}_{\mathrm{s}} \in \mathbb{C}^{(N+L)\times 1}$ be the transmit symbol vector at TX2. Then, if we define $\mathbf{y}_{\mathrm{p}}$, $\mathbf{y}_{\mathrm{s}} \in \mathbb{C}^{N\times 1}$ as the received signals at RX1 and RX2, respectively, we can write

$$\mathbf{y}_{\mathrm{p}} = \mathbf{F}(\mathbf{H}_{\mathrm{pp}}\mathbf{x}_{\mathrm{p}} + \mathbf{H}_{\mathrm{sp}}\mathbf{x}_{\mathrm{s}} + \mathbf{n}_{\mathrm{p}}) \tag{2.0}$$

$$\mathbf{y}_{\mathrm{s}} = \mathbf{F}(\mathbf{H}_{\mathrm{ss}}\mathbf{x}_{\mathrm{s}} + \mathbf{H}_{\mathrm{ps}}\mathbf{x}_{\mathrm{p}} + \mathbf{n}_{\mathrm{s}}), \tag{2.1}$$

with $\mathbf{n}_{\mathrm{p}}$ and $\mathbf{n}_{\mathrm{s}}$ additive white Gaussian noise (AWGN) vectors of length N. Perfect time and frequency synchronization at the receiver in both systems are assumed. In the

considered overlay scenario, TX2 must process its signal such that RX1 does not see any residual interference after the CP removal, regardless of the distribution or the realization of $\mathbf{s}_\mathrm{s}$. This is in contrast with alternative approaches for cognitive network deployment that limit the maximum power used by the secondary system [33], hence limiting its usefulness mainly to short range communications [60]. As previously said, when coping with an LTE-A OFDM base first tier, this result can be achieved by means of a linear precoding strategy at TX2, thanks to the TDD assumption. In fact, in TDD networks, the DL and UL channels between any TX/RX are reciprocal within their coherence time (in principle identical). Thus, an opportunistically performed channel estimation of the UL channel, may be used as the required channel state information (CSI) to design the linear precoder for the DL transmission. Accordingly, let $\mathbf{s}_s x \in \mathbb{C}^{L\times 1}$ be a zero mean input symbol vector such as $\mathbf{s}_\mathrm{s}\mathbf{s}_\mathrm{s}^\mathrm{H} = \mathbf{I}_L$, then we can write

$$\mathbf{x}_\mathrm{s} = \mathbf{V}\mathbf{s}_\mathrm{s}, \tag{2.1}$$

where $\mathbf{V} \in \mathbb{C}^{(N+L)\times L}$ is the linear VFDM precoder [55], derived as Vandermonde matrix [61] constructed from the roots of $S(z)$, polynomial associated to the interfering channel $\mathbf{h}_\mathrm{sp}$

$$S(z) = \sum_{i=0}^{l} h_{\mathrm{sp},i} z^{l-i}, \tag{2.1}$$

In [55], the author shows that, for $l = L$ and uniform power delay profile (PDP) of $\mathbf{h}_\mathrm{sp}$, such a $\mathbf{V}$ yields

$$\mathbf{H}_\mathrm{sp}\mathbf{x}_\mathrm{s} = \mathbf{H}_\mathrm{sp}\mathbf{E}\mathbf{s}_\mathrm{s} = \mathbf{0}_{\mathbf{N}\times\mathbf{L}}, \tag{2.1}$$

$\forall \quad \mathbf{s}_\mathrm{s} \in \mathbb{C}^{L\times 1}$. Alternatively, in case of unbalanced power distribution for the roots of $S(z)$, a Gram-Schmidt orthonormalization [62] of the original Vandermonde matrix or an approach based on a singular value decomposition (SVD) of $\mathbf{H}_\mathrm{sp}$ may be preferable [56, 63].

From an algebraic point of view, we note that regardless of the adopted strategy to derive $\mathbf{V}$, or its orthonormalized version defined as $\mathbf{E} \in \mathbb{C}^{(N+L)\times L}$, such a linear precoder projects the transmitted signal onto the null-space of the interfering channel from TX2 to RX1. This results in an interference free transmission in the primary system if TX2 disposes of perfect CSIT.

2.3 SDR4All

To implement the VFDM demonstrator, the SDR4All platform is adopted [57]. This is a novel hardware/software solution developed for teaching and development purposes in telecommunications and SDR. The hardware part is composed of plug-and-play universal software radio peripheral (USRP) version 1 cards [64] that includes filters, amplifiers and oscillators, analog-to-digital/digital-to-analog converters, samplers and is responsible for the communication over the universal serial bus (USB) link. These cards are composed of two parts: a mother-board and one or two daughter-boards. The mother-board controls

the RF, USB circuitry and sampling. The adopted daughter-board is the RFX 2400. The radio frequency (RF) circuitry, responsible of the analog signal generation, operates in the widely popular 2.4 GHz industrial, scientific and medical (ISM) band, chosen by standards such as 802.11(b/g) [65], Bluetooth [66] and worldwide interoperability for microwave access (WiMAX) [67]. Furthermore, standard isotropic antennas made for the 2.4 and 2.49 GHz ISM band are adopted. The main parameters of the SDR4All hardware are provided in Table 2.1. The base-band processing is provided by a user-friendly software

Table 2.1: Parameters for the hardware part.

parameter	**value**
Operating band	ISM 2.4 $\sim$ 2.49 GHz
base-band filtering	20 MHz
Channels	1 to 13 (802.11)
Total TX power	up to 50 mW
Data bandwidth	up to 16 MHz

toolbox, developed specifically to this end [68], operating in MATLAB® environment and providing full communication chains as well as basic communication blocks. In other words, SDR4All provides a platform that allows the user to deal with actual base-band symbols processed in MATLAB®, and this is one of its most interesting features. The inherent flexibility brought by such an approach allows the implementation of new and customized algorithms and metrics, thanks to the direct access to the transmission/reception chain code. Accordingly, well-tailored results can be obtained to assess both the effectiveness and the performance of the physical layer algorithm of interest.

From a structural point of view, a dedicated non real-time driver allows the toolbox to communicate with a single daughter-board inside the USRP. In particular, due to the lack of real-time functionalities, an on the fly detection of the signal before the decoding is not feasible. Such a process would require much more processing power and memory than MATLAB® can cope with at the base-band rate. Accordingly, a signaling procedure performed through a transmission control protocol / internet protocol (TCP/IP) network can be adopted to trigger the detection. This approach minimizes the number of samples processed by the transmitter/receiver to be compliant with the hardware and software constraints, increasing the feasibility of the packet detection and decoding step. Note that, both wired and wireless network can act as bearer for the trigger. Nevertheless, in the latter case, the transmission/reception takes place one second after the trigger has been sent to guarantee that the wireless network will not interfere with the toolbox packet transmission.

Figure 2.2: Experimental setup.

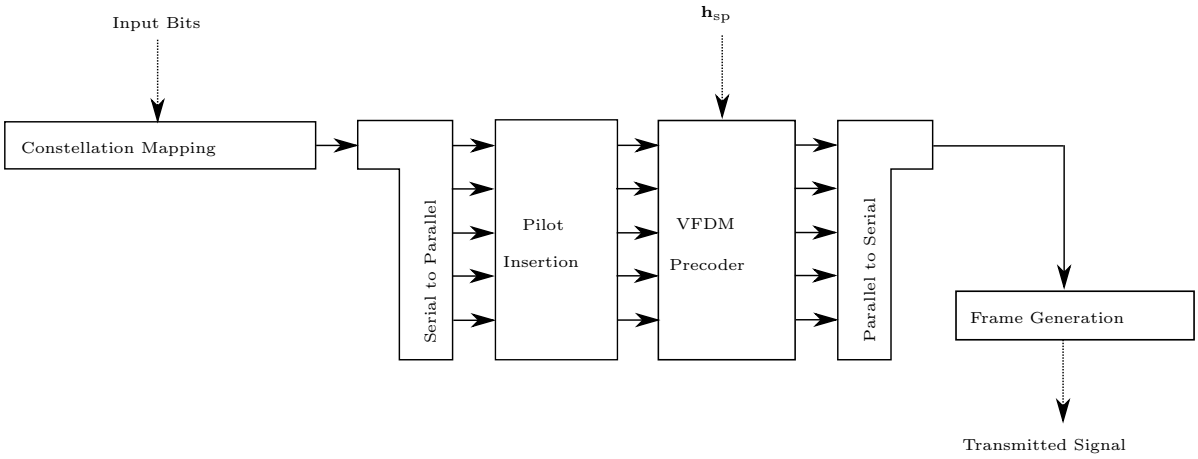

Figure 2.3: VFDM TX block diagram.

2.4 VFDM Implementation

The block scheme of the implemented experimental setup is depicted in Figure 2.2. As previously stated, herein we want to study the feasibility and performance of a practical implementation VFDM-based opportunistic transmitter. Thus we focus on the secondary link and consider the data transmission from TX2 to RX2. Consequently, no interference channel estimation is performed by TX2. We assume that the null-space precoder is derived using an $L+1$ path Rayleigh fading channel realization $\mathbf{h}_{\text{sp}}$, generated for test purposes and used by the VFDM block as hypothetical interference channel between TX2 and RX1. We first analyze the secondary transmitter. The kernel driver of the toolbox handles the data streams and communicates with the USRP over the USB link. Further details about the configuration and logic of the USRP's hardware can be found in [69].

2.4.1 VFDM Base-band Transmitter

The block diagram of the VFDM transmitter is shown in Figure 2.3. The input bits to be coded and transmitted are obtained by a deterministic source, i.e., a file, and mapped into ML symbols, adding padding bits if necessary. Such a symbol stream is then successively parallelized into L sub-streams, according to the requirements of the VFDM precoder as illustrated in Section 2.2. The resulting matrix $\mathbf{S} \in \mathbb{C}^{L\times M}$ is fed to the pilot insertion block, where the transmit frame is built by alternating groups of symbol blocks and pilot blocks. Let N_{Pilots} be a parameter defining the number of groups of pilot blocks inside one frame. The pilot insertion procedure is articulated in three steps:

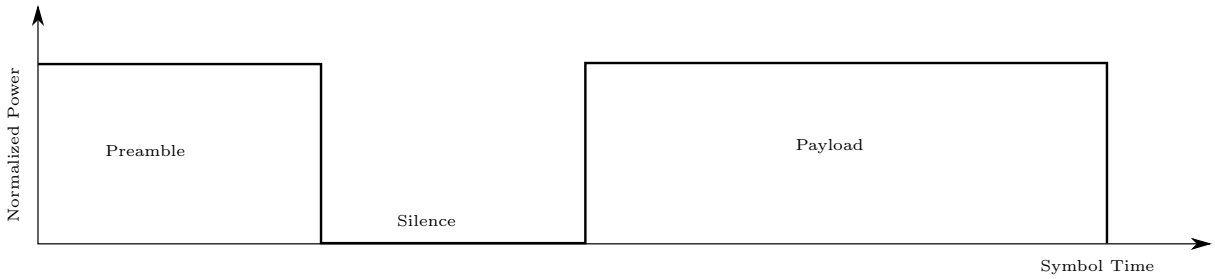

Figure 2.4: Frame Structure.

1. The input data stream is divided into N_{Pilots} groups of blocks denoted as $\mathbf{U}_j \in \mathbb{C}^{L\times(M/N_{\text{Pilots}})}$, with $j = 1, ..., N_{\text{Pilots}}$.

2. A pilot symbol matrix $\mathbf{P_L}$ of size $L \times M_{\text{Pilots}}$ is generated, such that

$$\begin{cases} [\mathbf{P_L}]_{(k+1)(l+1)}\alpha e^{-i2\pi\frac{kl}{M_{\text{Pilots}}}}, \\ k = 0, ..., L-1, \\ l = 0, ..., M_{\text{Pilots}}. \end{cases} \tag{2.1}$$

3. The uncoded payload $\mathbf{P_L} \in \mathbb{C}^{L\times(M+N_{\text{Pilots}}M_{\text{Pilots}})}$ is composed by alternating $\mathbf{P_L}$ to $\mathbf{U}_j$, as follows

$$\mathbf{P_L} = [\mathbf{U}_1|\mathbf{P}_{\mathbf{L},1}|\mathbf{U}_2|\mathbf{P}_{\mathbf{L},2}|\mathbf{U}_3|\cdots], \tag{2.1}$$

where $Pm_{\mathbf{L},j}$, with $j = 1, ..., N_{\text{Pilots}}$, is the j^{th} pilot symbol matrix repetition.

At this stage, the VFDM precoder block generates the coded payload of the transmission, successively serialized to be ready for the frame generation. Let b, $c \in \mathbb{N}_\star$[1] be scaling parameters. The frame generator adds to the payload a preamble known at the receiver, characterized by the following structure:

1. A Golay complementary sequence $\mathbf{g}$ [70] of length N, taking values in $\{1+i, -1-i\}$, for time/frequency synchronization purposes at the receiver.

2. A constant sequence of symbols $\mathbf{o} \in \{1+i\}^N$, introduced to assure correct detection of phase offset variations.

3. A guard time of size cN.

The final frame structure is depicted in Figure 2.4.

2.4.2 VFDM Base-band Receiver

The block diagram of the VFDM receiver is represented in Figure 2.5. The first operation

[1]To avoid ambiguity in the preamble definition, we consider $\mathbb{N}_\star$ as the set of natural number excluding 0.

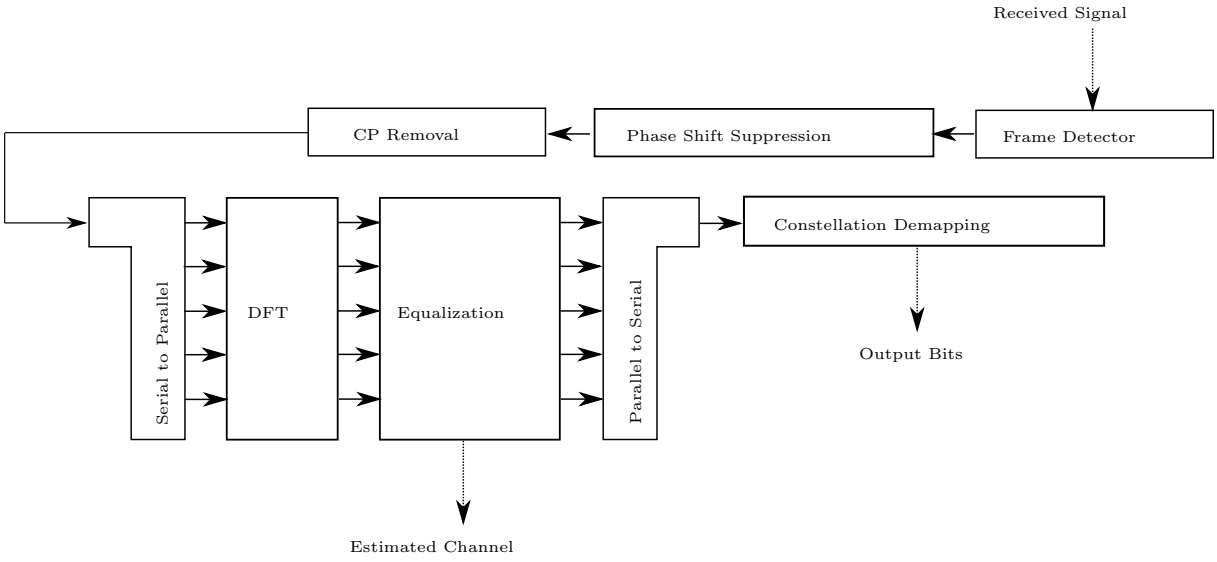

Figure 2.5: VFDM RX block diagram.

performed at the receiver is the frame detection. This is accomplished by means of suitable time and symbol level synchronization, exploiting the structure of the received frame. In the proposed implementation, RX2 exploits the known payload structure to identify the starting point of the VFDM frame with accuracy. As a first step, the cross-correlation between the received signal $\mathbf{y}$, and the known Golay sequence $\mathbf{g}$ is computed as

$$R(n) \triangleq \sum_{m} \mathbf{y}^*(n)\mathbf{g}(n+m). \tag{2.1}$$

The Golay complementary sequence is characterized by good autocorrelation properties, presenting a clear peak for $m = 0$. Therefore, RX2 can detect $\hat{n}$, which is the estimated starting point of the frame, by taking

$$\hat{n} = \max_{n} R(n). \tag{2.1}$$

In any communication system, several non-ideal factors may induce a phase shift of the received frame at the receiver, e.g., analog and RF impairments, imperfections in the phase lock loop (responsible for generating the carrier frequency at the chosen central frequency f_c), channel rotations, thermal noise and so on. The accuracy of the decoding can be severely affected by an unsuppressed phase shift. A two-step procedure is adopted in the implemented test-bed to address this issue. Despite the existence of other more refined techniques in the literature, the following solution provides simple and low complexity operations, and it is adopted by many existing standards [71, 72]. By construction, inside the preamble, the sequence $\mathbf{o}$ is composed of symbols having the same phase. Therefore, if we denote $\phi|\cdot|$ as the phase of a given complex value, RX2 can obtain a first *coarse* phase shift estimation as

$$\hat{\phi_c} = \frac{1}{bN} \sum_{m=\hat{n}}^{\hat{n}+N(b+1)-1} (\phi|r_{m+1}| - \phi|r_m|), \tag{2.1}$$

where each subsequent phase offset computation is averaged to compensate for phase noise. At this stage, a first compensation takes place. Afterwards, $\hat{\phi}_{\mathrm{f}}$, hereafter *fine* phase shift, is estimated. Similar to what is described in [71] for 802.11a, $\mathbf{o}$ is divided in two equal portions, $\mathbf{o}_1$ and $\mathbf{o}_2$, and RX2 can estimate $\hat{\phi}_{\mathrm{f}}$ as

$$\hat{\phi}_{\mathrm{f}} = \frac{4}{(bN)^2} \sum_{m=\hat{n}}^{\hat{n}+\frac{N(b+1)}{2}-1} \phi |r_m r^*_{\frac{N(b+1)}{2}}|. \tag{2.1}$$

The *fine* phase shift compensation ends the preamble processing. After a CP removal operation, the stream is parallelized and a DFT is performed, according to the model introduced in Section 2.2. At this stage, each symbol block has size N, number of carriers used in the OFDM primary system. If we let $\tilde{\mathbf{P}}_{\mathbf{L},i}$ be the i^{th} repetition of $\mathbf{P_L}$ corrupted by the channel and $\tilde{\mathbf{U}}_i$ be the i^{th} received data matrix of size $N \times \frac{M}{N_{\mathrm{Pilots}}}$, we can write the frequency domain representation of the received frame as

$$\tilde{\mathbf{G}} = [\tilde{\mathbf{U}}_1 | \tilde{\mathbf{P}}_{\mathbf{L},1} | \tilde{\mathbf{U}}_2 | \tilde{\mathbf{P}}_{\mathbf{L},2} | \tilde{\mathbf{U}}_3 | \cdots] \in \mathbb{C}^{N \times (M + N_{\mathrm{Pilots}} M_{\mathrm{Pilots}})}. \tag{2.1}$$

Note that, the equalizer can benefit from the repetition of the matrix $\mathbf{P_L}$ inside the frame to update the channel estimation frequently. Each data block is equalized using the channel estimation provided by the previous $\mathbf{P_L}$ evaluation. Consequently, in general, RX2 does not need any a priori information about the coherence time of the channel. Furthermore, a frequent channel estimation can mitigate the impact of an overly noisy environment and improve the overall decoding performance. By definition, we have $\mathbf{P}_{\mathbf{L},i}\mathbf{P}^{\mathrm{H}}_{\mathbf{L},i} = \mathbf{I}_L$, thus the i^{th} equivalent channel estimation is obtained by pilot evaluation as follows:

$$\widehat{\mathbf{H}}_i = \tilde{\mathbf{P}}_{\mathbf{L},i}\mathbf{P}^{\mathrm{H}}_{\mathbf{L},i}. \tag{2.1}$$

Finally, a simple ZF equalizer [59] is implemented. The equalized payload can be written as $\widehat{\mathbf{G}} = [\widehat{\mathbf{U}}_1 | \widehat{\mathbf{U}}_2 | ... | \widehat{\mathbf{U}}_{\frac{M}{N_{\mathrm{Pilots}}}}] \in \mathbb{C}^{N \times M}$, where

$$\widehat{\mathbf{U}}_i = \mathbf{H}_i^{\dagger} \tilde{\mathbf{U}}_i. \tag{2.1}$$

The resulting symbols are then serialized and demapped to obtain the output bit sequence. We remark that the proposed VFDM receiver has the same decoding structure as a classic OFDM receiver, increasing the flexibility of the proposed solution. Nevertheless, a difference between the two architectures is represented by the pilot structure. By construction, the VFDM precoder accepts L symbols as an input, whereas the DFT block accepts N. This feature has a direct impact on the structure of the pilot symbol matrix that can be transmitted/received in the two systems.

2.5 Experimental Results

A test-bed composed of a TX/RX pair, managed by two laptops, as illustrated in Figure 2.6, has been set up to validate the proposed solution. As described in Section 2.3,

Table 2.2: User defined parameters.

parameter	**value**
Carrier frequency	ISM 2.412 GHz
Bandwidth	4 MHz
N	64
L	8
N_{Pilots}	$M/120$
M_{Pilots}	10
Golay sequence length	64
Constant sequence length	2048
Zeros sequence length	128
Modulation order	4−QAM

the base-band signal processing is implemented at software level, exploiting a MATLAB® toolbox developed specifically to this end [68]. The SDR4All platform drives the hardware at both side of the transmission. In the considered scenario, TX2 does not send any trigger message to the receiver before starting the VFDM transmission. To make sure that RX2 is able to receive and buffer enough meaningful data, a repetition of the VFDM frame is transmitted. We note that the size of the transmit window can be set at software level using the SDR4All toolbox. TX2 performs a set of 1000 transmissions, such that statistically relevant results can be obtained. The main parameters used for system configuration are provided in Table II.

The frame structure discussed in Section 2.4.1, and represented in Figure 2.4, contemplates a guard band (i.e., zero sequence) insertion between the preamble and the frame, used to compute a first estimate of the experienced signal to noise ratio (SNR) at the

Figure 2.6: Transmission test-bed.

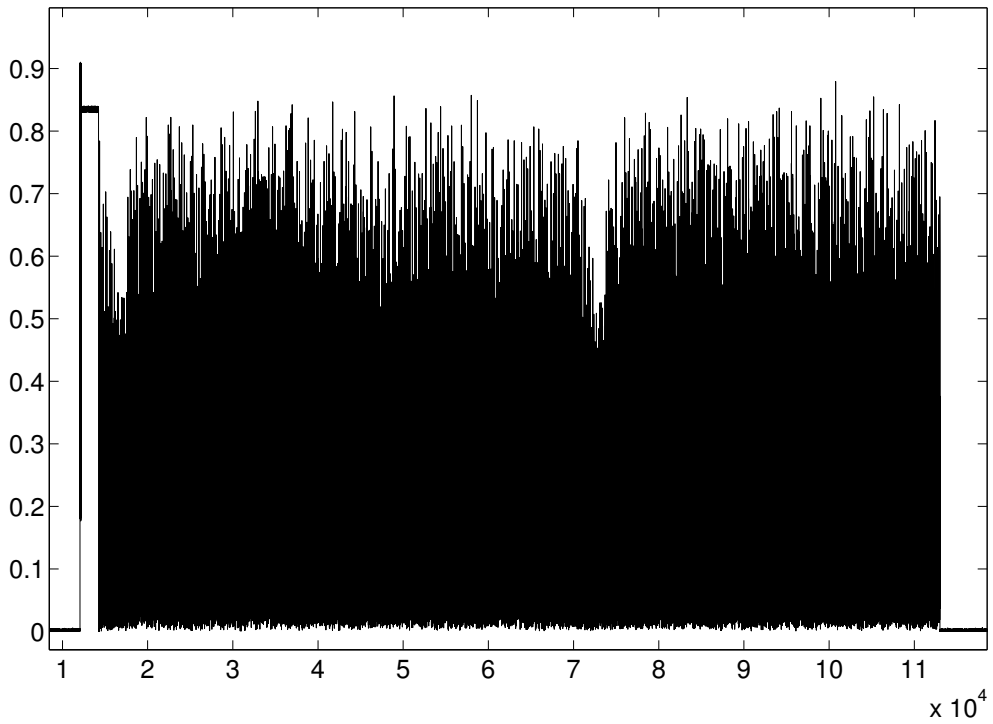

Figure 2.7: Receive frame at RX2.

receiver. In fact, the receiver can evaluate the received power during the second portion of the preamble (i.e., the constant sequence $\mathbf{o}$), and the noise power during the silence and compute their ratio. The power profile of the received frame at RX2 is shown in Figure 2.7. In this case, the preamble SNR is 25.1 dB. We note that the payload exhibits a very irregular power profile, especially if compared to the preamble. This behavior is typically due to a peak to average power ratio (PAPR) problem. In particular, this implies that the payload SNR may be substantially different from the first estimation provided above. For the sake of simplicity, we focus on one of the aforementioned transmissions, whose outcome is presented in Figures 2.8(a) and 2.8(b), where the bitmap file adopted for this test is depicted in its transmitted and received version. As a first observation, we note that the proposed scheme for a standalone VFDM transmission is correctly working. However, the number of faulty pixels in Figure 2.8(b) is unlikely result of a 4-ary quadrature amplitude modulation (QAM), i.e. $4-$QAM, based transmission performed at high SNR, whose bit error rate (BER) should be lower [62]. Let us compute the cumulative distribution function (CDF) of the BER to better characterize its behavior. The result of this operation is presented in Figure 2.9. If we compare these findings to the theoretical results, we see that the average BER for SNR $= 25$ dB in [56] falls into the 10^{th} percentile of the BER of the current test. Interestingly, herein the average BER is 0.0603 that, according to [56], is the average BER of a transmission performed at SNR~ 9 dB. Despite the non-ideal conditions inherent to the realistic implementation, a difference of around

(a) Transmitted data (b) Received data

Figure 2.8: Transmitted and received data.

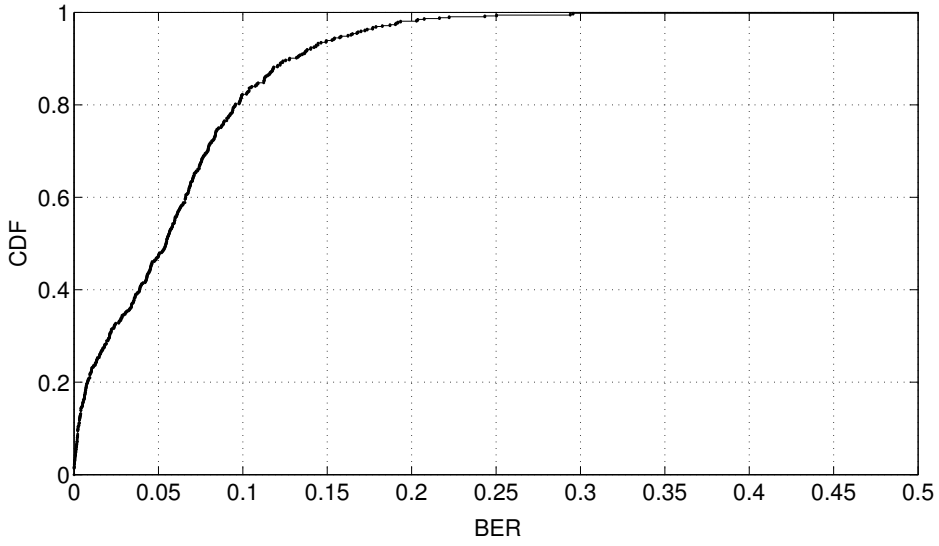

Figure 2.9: CDF of the BER.

16 dB to achieve the same BER of the theoretical results is scarcely justifiable. These findings show that the SNR experienced by the preamble and by the payload have likely very different values. In particular, the SNR experienced by the preamble and the resulting BER of the overall transmission are not in a direct relationship. This is confirmed by Figure 2.10, where the CDF of the preamble SNR is presented. The CDF shows an evident behavior, with an average value of SNR $\sim$ 25 dB, confirming our previous results. The unsuitability of the preamble SNR measurement to give a correct estimate of the likely lower payload SNR is clear. The causes of the inconsistency of the proposed ap-

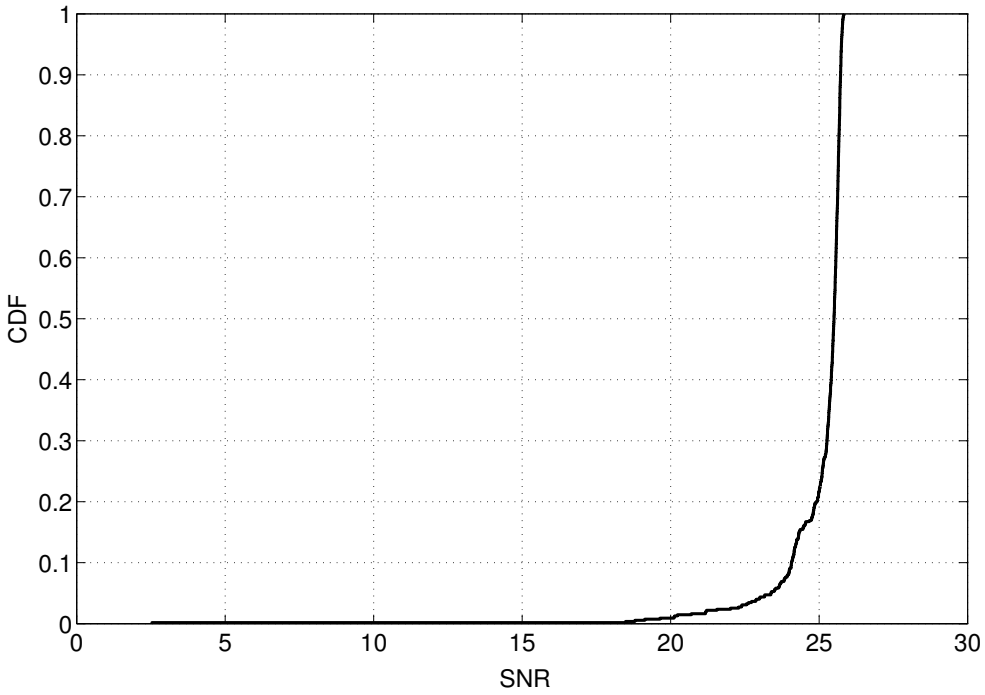

Figure 2.10: CDF of the SNR.

proach for the SNR estimation need a further investigation. Accordingly, the behavior of the power profile of the payload is studied in the following, in order to fully characterize the considered system and address the aforementioned issue.

2.6 Precoder Analysis

The experimental results obtained so far show that a secondary VFDM based transmission can experience significant SNR drops at the receiver, hence rate loss. In this section, we present an analysis of the null-space precoder, in the presence of channels characterized by different PDPs and root mean square (R.M.S.) delay spreads, to investigate their impact on the precoder structure. We specifically target our efforts on TX2's transmission, thus we simplify the model presented in Section 2.2 and write

$$\begin{array}{ll} \mathbf{y}_{\mathrm{p}} & = \mathbf{H}_{\mathrm{sp}}\mathbf{E}\mathbf{s}_{\mathrm{s}} \\ \mathbf{y}_{\mathrm{s}} & = \mathbf{H}_{\mathrm{ss}}\mathbf{E}\mathbf{s}_{\mathrm{s}} \end{array} , \tag{2.1}$$

where the thermal noise has been ignored for simplicity, and only the received signal component coming from TX2 is represented. Additionally, we let $\mathbf{h}_{\mathrm{sp}} = [h_{\mathrm{p},0}, \ldots, h_{\mathrm{p},l}]$, and $\mathbf{h}_{\mathrm{ss}} = [h_{\mathrm{s},0}, \ldots, h_{\mathrm{s},l}]$, to lighten the notation adopted in the following analysis. We recall that the parameters N, L and l define respectively the number of carriers, the CP size and the number of paths of the channel, line of sight (LOS) component excluded.

For simplicity we will consider that the channels in primary and secondary system are characterized by the same parameter l. Our goal is to understand how the precoder acts on the power profile of the input symbol vector $\mathbf{s}_\mathrm{s}$ of size L.

In order to be compliant with (2.2), first TX2 derives a suitable null-space precoder $\mathbf{V} = [\mathbf{v}_1^\mathrm{T}|\mathbf{v}_2^\mathrm{T}|\ldots|\mathbf{v}_L^\mathrm{T}]$ by solving the equation $\mathbf{H}_\mathrm{sp}\mathbf{V} = \mathbf{0}_{N\times 1}$. Afterwards, an orthonormalization of the columns of $\mathbf{V}$ is computed to yield $\mathbf{E}$, to tackle any possible ill-conditioning of $\mathbf{V}$. We note that, the interference nulling constraint in (2.2) can be alternatively expressed as a system of linear equations. Accordingly, let use rewrite $\mathbf{V}$ as

$$\mathbf{V} = \left[\begin{array}{c} \mathbf{r}_1 \\ \vdots \\ \mathbf{r}_{L-l} \\ \hline \\ \mathbf{C} \end{array}\right], \tag{2.1}$$

with $\mathbf{r}_i \in \mathbb{C}^{1\times L}$ row vectors with random entries, $\forall i \in [1, L-l]$, and $\mathbf{C} \in \mathbb{C}^{(N+l)\times L}$ matrix such that $\mathbf{G}_\mathrm{sp}\mathbf{C} = \mathbf{0}_{N\times L}$. Then, the problem in (2.2) can be cast into a set L independent homogeneous systems, associated to the L columns of $\mathbf{C}$. We can represent this set in parametric form as follows

$$\begin{cases} c_{1j}h_{\mathrm{p},l} + \ldots + c_{(l+1)j}h_{\mathrm{p},0} & = 0 \\ c_{2j}h_{\mathrm{p},l} + \ldots + c_{(l+2)j}h_{\mathrm{p},0} & = 0 \\ \vdots & \vdots \\ c_{Nj}h_{\mathrm{p},l} + \ldots + c_{(l+N)j}h_{\mathrm{p},0} & = 0, \end{cases} \tag{2.1}$$

where the notation $[\mathbf{C}]_{(i,j)} = c_{ij}$ has been adopted for compactness. By looking at (2.6), we identify a system of N equations in $N + l$ variables, $\forall j \in [1, L]$. Consequently, each of the L systems given by (2.6) is determined if and only if $l = 0$, i.e., for LOS channels. Conversely, for $l > 0$, i.e., for non-line-of-sight (NLOS) channels, the systems are always under-determined no matter which N, L and l values are selected. Naturally this impacts significantly the structure of $\mathbf{C}$, that is $\mathbf{V}$, thus we need to analyze the different cases separately.

2.6.1 LOS Channels

We start by considering LOS channels, i.e., $l = 0$. As a consequence, $\mathbf{h}_\mathrm{sp} = [h_{\mathrm{p},0}]$ and $\mathbf{h}_\mathrm{ss} = [h_{\mathrm{s},0}]$, and we have

$$\begin{array}{ll} \mathbf{H}_\mathrm{sp} & = h_{\mathrm{p},0}[\mathbf{0}_{N\times L}|\mathbf{I}_N] \\ \mathbf{H}_\mathrm{ss} & = h_{\mathrm{s},0}[\mathbf{0}_{N\times L}|\mathbf{I}_N] \end{array}, \tag{2.1}$$

where $\mathbf{I}_N$ is the $N \times N$ identity matrix. For $l = 0$, (2.6) becomes

$$\begin{cases} c_{1j} h_{\mathrm{p},0} & = 0 \\ c_{2j} h_{\mathrm{p},0} & = 0 \\ \vdots & \vdots \\ c_{Nj} h_{\mathrm{p},0} & = 0. \end{cases} \tag{2.1}$$

The N variables in (2.6.1) do not have any available degree of freedom. By construction, they already appear in fully solvable form. In particular, it can be verified that (2.6.1) admits only the set of solutions given by

$$c_{ij} h_{\mathrm{p},0} = 0, \quad i \in [1, N], j \in [1, L]. \tag{2.2}$$

As a consequence, the desired linear precoder can be obtained by TX2 as

$$\mathbf{V} = \begin{bmatrix} \mathbf{K}_{L \times L} \\ \mathbf{0}_{N \times L} \end{bmatrix},$$

with $\mathbf{K}_{L \times L} \in \mathbb{C}^{L \times L}$ matrix with random entries. Accordingly, $\mathbf{E}$ is given by

$$\mathbf{E} = \begin{bmatrix} \mathbf{I}_{L \times L} \\ \mathbf{0}_{N \times L} \end{bmatrix}. \tag{2.2}$$

Therefore, for LOS channels, the null-space precoder degenerates into a time division multiple access (TDMA) approach. TX2 transmits only over the first L symbols of the OFDM block, and $\mathbf{C} = \mathbf{0}_{N \times L}$. The precoder in (2.6.1) implies also that

$$\mathbf{H}_{\mathrm{ss}} \mathbf{E} = \mathbf{0}_{(N+L) \times L}, \quad \forall\, h_{\mathrm{s},0} \in \mathcal{CN}(0, 1), \tag{2.3}$$

thus $\mathbf{y}_{\mathrm{s}} = 0$, and no symbol can be decoded. In other words, if the secondary transmitter removes the CP, the SNR of the resulting N symbols is always equal to zero. In particular, the obtained result has a stronger implication. In fact, (2.6) is the set of homogeneous systems to be solved by any secondary transmitter willing to cancel its interference towards a primary OFDM receiver. Consequently, we argue that, for LOS channels, no linearly precoded transmission can be performed by a single antenna TX2 communicating with a single antenna secondary OFDM-like receiver, while guaranteeing the interference cancellation at a primary OFDM receiver. In other words, in these scenarios, the structure of any null-space precoder would be as in (2.6.1), yielding a maximum secondary system achievable spectral efficiency equal to zero. This reveals the unfeasibility of the current approach in case of LOS channels and is a potential harm to its effectiveness. We will further analyze this issue in Chapter 3.

2.6.2 NLOS Channels

If $l > 0$, then $\mathbf{h}_{\mathrm{sp}} = [h_{\mathrm{p},0}, \ldots, h_{\mathrm{p},l}]$ and $\mathbf{h}_{\mathrm{ss}} = [h_{\mathrm{s},0}, \ldots, h_{\mathrm{s},l}]$, and we can refer to the general model introduced in Section 2.2. In this case, the set of under-determined systems of N

equations in $N+l$ variables in (2.6) does not present any variable in fully solvable form, and the set of the possible solutions highly hinges on the parameter l. In order to better characterize its impact on the precoder structure, we start our analysis from a simple case, $l=1$, that is a two-path channel.

Two-path channel

Consider a channel with two paths, including the LOS component, i.e., $l=1$. Therefore, $\mathbf{h}_{\mathrm{sp}}=[h_{\mathrm{p},0},h_{\mathrm{p},1}]$ and $\mathbf{h}_{\mathrm{ss}}=[h_{\mathrm{s},0},h_{\mathrm{s},1}]$. In this case, we have

$$\mathbf{H}_{\mathrm{sp}}=\begin{bmatrix} h_{\mathrm{p},1} & h_{\mathrm{p},0} & 0 & 0 & 0 & \dots & 0 \\ 0 & h_{\mathrm{p},1} & h_{\mathrm{p},0} & 0 & 0 & \dots & 0 \\ \vdots & \ddots & & & & \ddots & \vdots \\ 0 & 0 & 0 & \dots & 0 & h_{\mathrm{p},1} & h_{\mathrm{p},0} \end{bmatrix} \tag{2.3}$$

We know from [56] that $\dim\ker(\mathbf{H}_{\mathrm{sp}})=L$, thus the number of columns of $\mathbf{V}$ is dependent on the CP size. Consequently, in the following we will consider several values of L. Note that, $N=4$ if not otherwise stated.

For the simple case of $L=l=1$, a systematic recursive solution can be found

$$c_{ij}=(-1)^{N+i}c_{Nj}\left(\frac{h_{\mathrm{p},0}}{h_{\mathrm{p},1}}\right)^{N-i}, \tag{2.3}$$

where c_{Nj} has been arbitrarily chosen among all the variables, without loss of generality. In fact, in this case, any chosen variable could be factorized out and the behavior will always be depending on the ratio $h_{\mathrm{p},0}/h_{\mathrm{p},1}$. Therefore, when $L=l=1$, the precoder $\mathbf{V}$ degenerates into a column vector that, given the selected variable and $N=4$, can be written as

$$\mathbf{V}_{[1j]}=c_{4j}\left[-\left(\frac{h_{\mathrm{p},0}}{h_{\mathrm{p},1}}\right)^{3},\left(\frac{h_{\mathrm{p},0}}{h_{\mathrm{p},1}}\right)^{2},-\frac{h_{\mathrm{p},0}}{h_{\mathrm{p},1}},1,-\frac{h_{\mathrm{p},1}}{h_{\mathrm{p},0}}\right]^{\mathrm{T}}, \tag{2.3}$$

and its orthonormalized version $\mathbf{E}_{[1j]}=\dfrac{1}{\sqrt{D_1}}\mathbf{V}_{[1j]}$, where

$$D_1=|c_{4j}|^2\left[\left|\frac{h_{\mathrm{p},0}^3}{h_{\mathrm{p},1}^3}\right|^2+\left|\frac{h_{\mathrm{p},0}^2}{h_{\mathrm{p},1}^2}\right|^2+\left|\frac{h_{\mathrm{p},0}}{h_{\mathrm{p},1}}\right|^2+\left|\frac{h_{\mathrm{p},1}}{h_{\mathrm{p},0}}\right|^2+1\right].$$

Unfortunately, this simple solution can not be extended to larger values of L and l. In fact, when these two parameters are greater than 1, the resulting equations yield very long and complex results thus, for the sake of readability, we present the corresponding analysis in Appendix A. Nevertheless, the obtained results show that this approach leads to unmanageable computations. Despite the attempt to simplify the equations in order to identify repeating patterns, a systematic closed-form representation of $\ker(\mathbf{H}_{\mathrm{sp}})$ depending on the three main parameters (N, L, and l) is not derivable. Consequently, we have to face the analysis of the power distribution of the precoded symbols numerically.

2.7 Power Distribution

As seen in the previous section, and in detail in Appendix A, the complexity of the explicit precoder computation brings long and non trivial equations even for very simple configurations. This prevents us to characterize the power profile of the precoded signal systematically, even though we can infer useful insights and have a better understanding on how the power is distributed among the symbols. As a simple example, we can consider the case presented in Section 2.6.2 and analyze the power distribution along the vector given by (2.6.2), i.e., $L = l = 1$. As can be inferred by looking at the equation, the ratio $|h_{\mathrm{p},0}/h_{\mathrm{p},1}|$ imposes an exponentially decreasing/increasing power profile to the precoded symbols. The corresponding outcome is depicted in Figures 2.11 and 2.12, where the trivial case $|h_{\mathrm{p},0}/h_{\mathrm{p},1}| = 1$ is omitted.

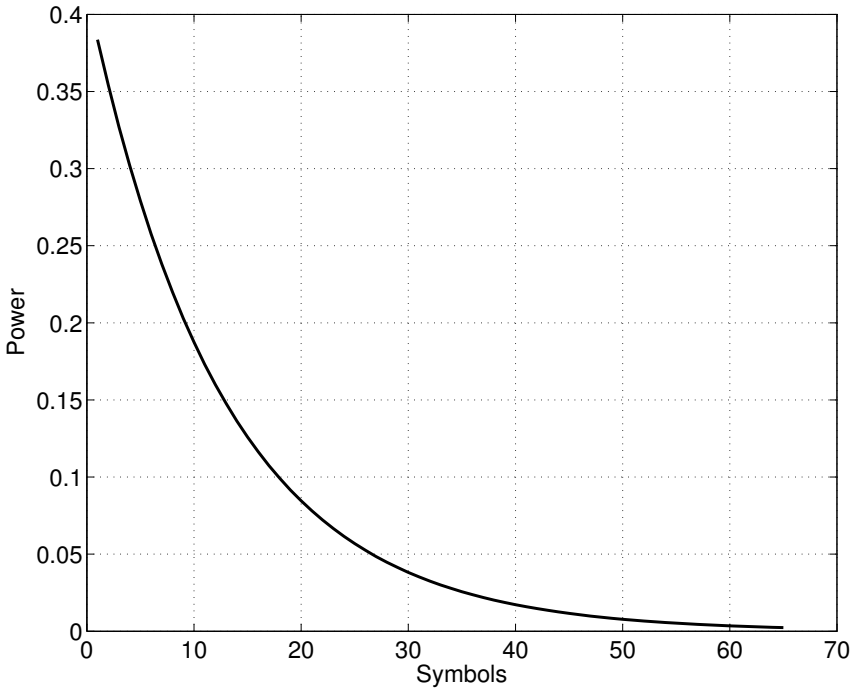

Figure 2.11: Power profile of the column precoder when $L = l = 1$, $\left|\frac{h_{\mathrm{p},0}}{h_{\mathrm{p},1}}\right| < 1$.

For practical purposes, the case $|h_{\mathrm{p},0}/h_{\mathrm{p},1}| > 1$ is unlikely to be occurring in a real transmission, thus we focus on the scenario $|h_{\mathrm{p},0}/h_{\mathrm{p},1}| < 1$. We can immediately notice from Figure 2.11 that the power is not uniformly distributed but, on the contrary, is concentrated in the first part of the symbols. Here the structured nature of $\ker(\mathbf{H}_{\mathrm{sp}})$ assumes a precise characterization. In fact, regardless of the realization of the channel, whenever $|h_{\mathrm{p},0}/h_{\mathrm{p},1}| < 1$ the power profile of the precoder has an exponential decay along the symbols. Moreover, the smaller $|h_{\mathrm{p},0}/h_{\mathrm{p},1}|$ the faster the decay.

If we move from the simple example to the more complicate cases in Appendix A, we

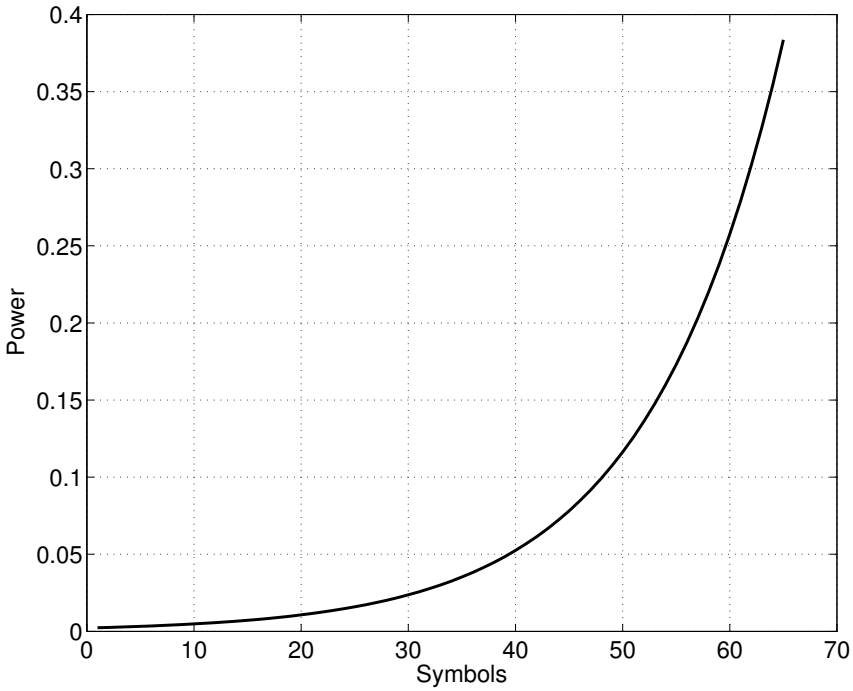

Figure 2.12: Power profile of the column precoder when $L = l = 1$, $\left|\frac{h_{\mathrm{p},0}}{h_{\mathrm{p},1}}\right| > 1$.

can see that, even if we can not easily deduce any characteristic of the power distribution along the precoded symbols, the PDP of the channel plays a fundamental role in this matter. In the following section, we will consider the same setup as in Section 2.2, and we will characterize numerically the relationship between the PDP of the channel and the power distribution of the precoded symbols.

2.7.1 PDP Importance

In the following Monte-Carlo simulations, we assume that the OFDM reference system transmits over $N = 64$ subcarriers, with a CP size of $L = 16$. Three different PDP models for the considered Rayleigh fading channel $\mathbf{h}_{\mathrm{sp}}$ are considered, namely uniform, exponential with fast ($\frac{T_s}{\tau} = 2.5$) and slow ($\frac{T_s}{\tau} = 0.75$) decay, where T_s is the sample time and τ is the R.M.S. delay spread. In Figures 2.13, 2.14 and 2.15, three channel snapshots are depicted, one for each of the aforementioned PDP, where we represent the power associated to each path.

We focus on these snapshots to understand how the power associated to the channel taps can induce a non uniform power distribution of the precoded symbols. Accordingly, a precoder $\mathbf{E}$ is computed for each one of the three cases. For simplicity, let us assume an input symbol vector $\mathbf{s}_{\mathrm{s}} = \mathbf{1}_L$, i.e., an L-sized all ones vector. Then, the outcoming power profile of the precoded symbols is shown in Figures 2.16, 2.17 and 2.18. Even though not

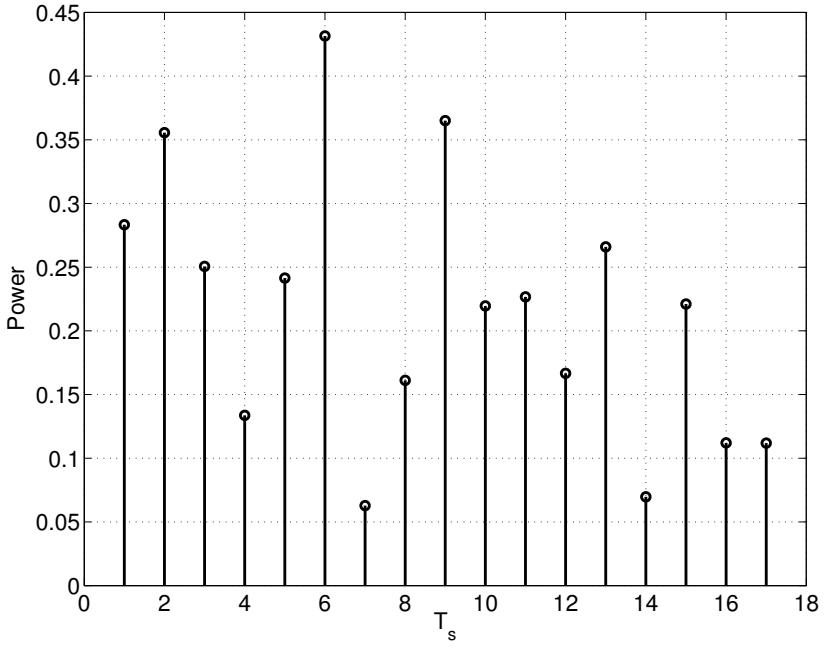

Figure 2.13: Uniform PDP

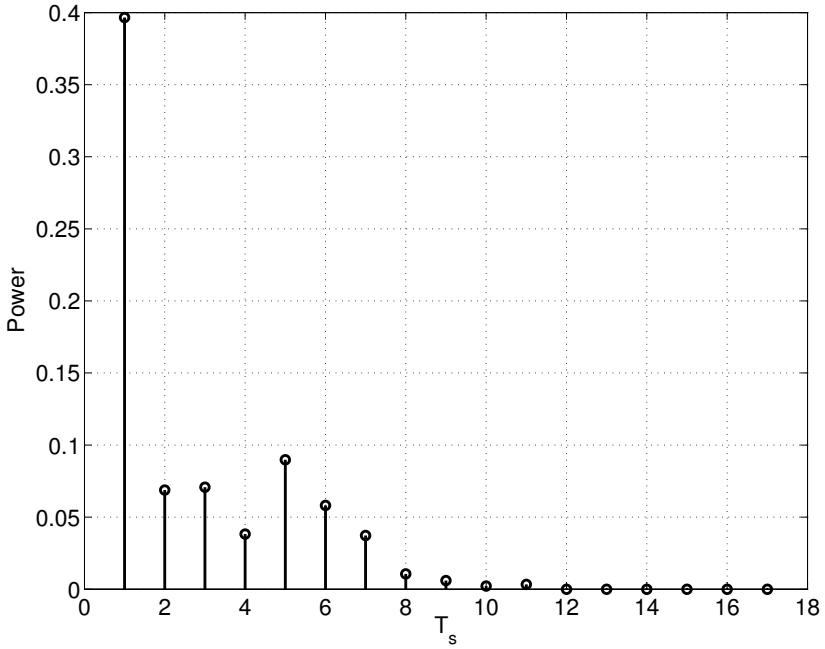

Figure 2.14: Exponential PDP, slow decay, $\frac{T_s}{\tau} = 0.75$

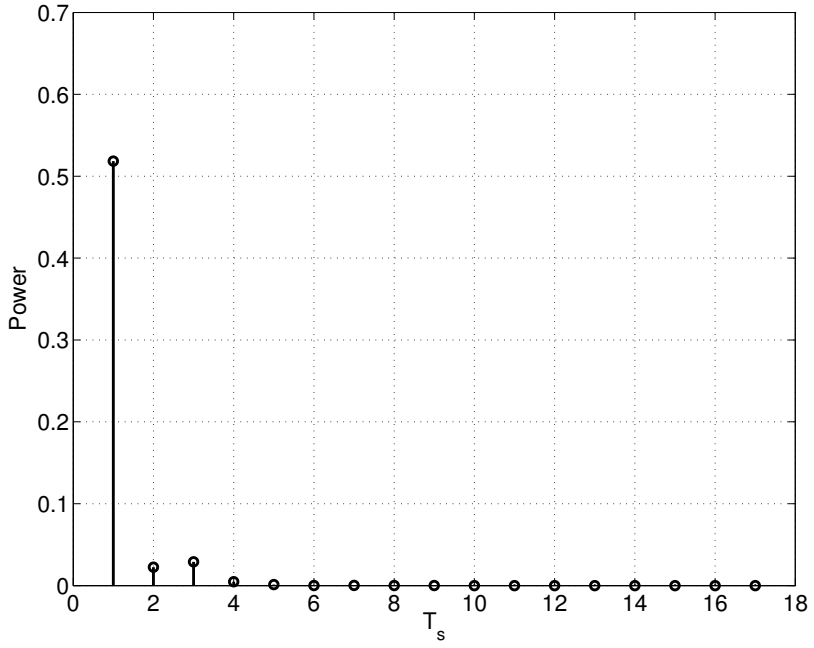

Figure 2.15: Exponential PDP, fast decay, $\frac{T_s}{\tau} = 2.5$

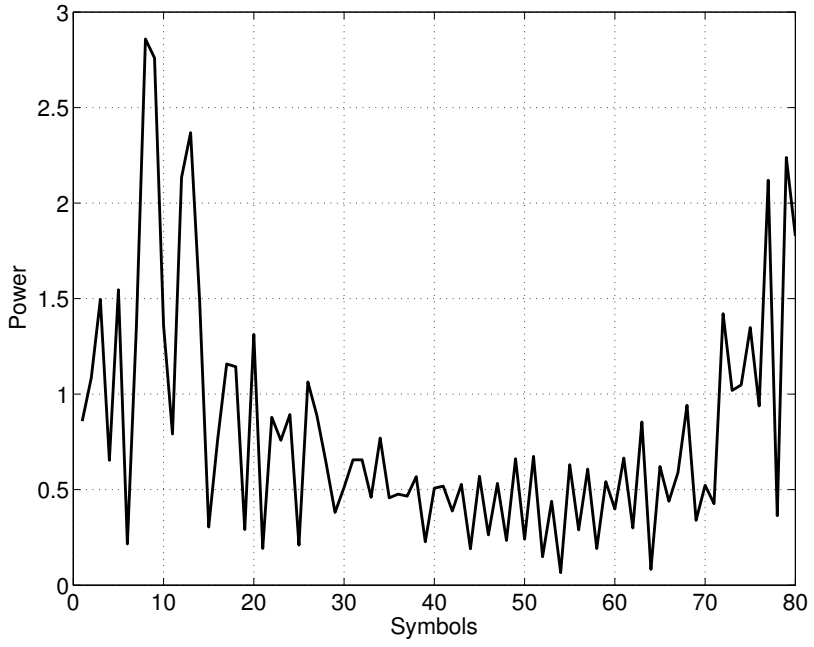

Figure 2.16: Uniform PDP. Power profile

generalized, this approach is meant to show how channels presenting a given statistical

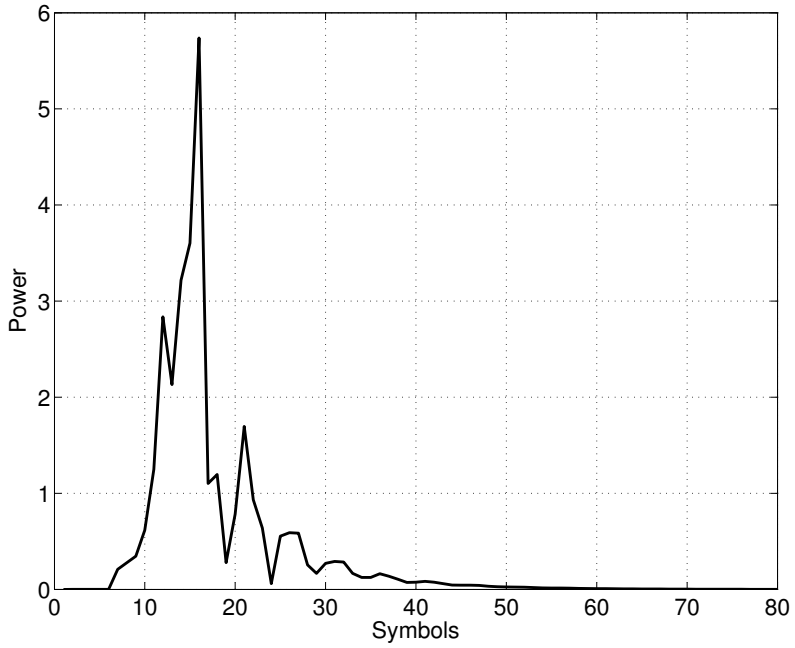

Figure 2.17: Exponential PDP, slow decay, $\frac{T_s}{\tau} = 0.75$. Power profile

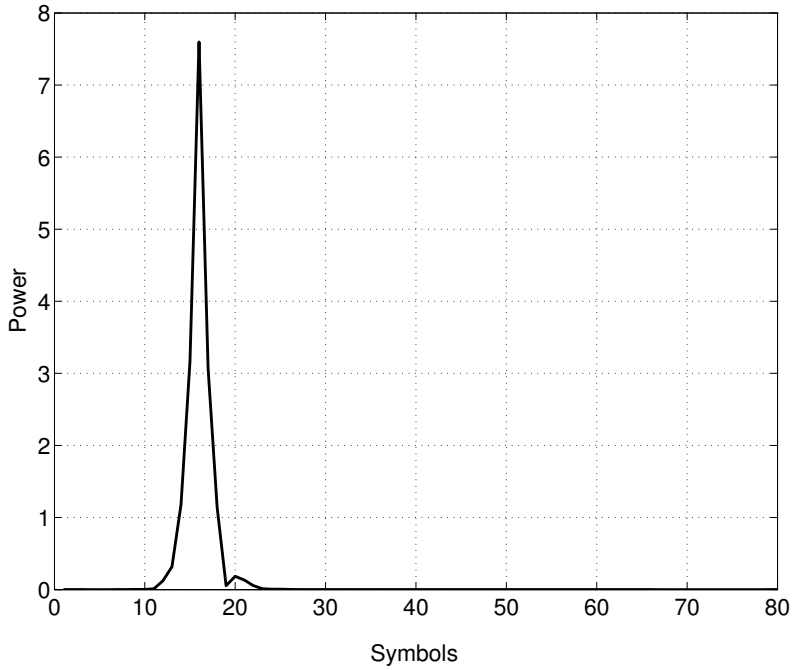

Figure 2.18: Exponential PDP, fast decay, $\frac{T_s}{\tau} = 2.5$. Power profile

description can influence the performance of the secondary system, as seen in previous sections. Aside from the high PAPR that characterizes all the three samples, the impact of the delay spread and PDP of the channel on the power profile of the precoded transmit symbols is significant. The power is never uniformly distributed, and is non-negligible over the whole duration of the precoded signal only for uniform PDP, as depicted in Figure 2.16. Conversely, Figures 2.17 and 2.18 clearly show a power concentration in the first symbols, and very low power level elsewhere. In particular, the power distribution in Figure 2.18 is so tight that the precoded signal is characterized by an impulsive behavior. Usually, RF circuitry at the modulators imposes limits on the precision of the generation of very impulsive signal. Nevertheless, at present we want to understand what would be the outcome of the transmission of such a signal in our scenario. Therefore, we assume that a signal as depicted in Figures 2.17 and 2.18, i.e., its digital representation in our simulations, may be obtained in practice. In the considered scenario the two systems are deployed into the same area hence we can safely assume that $\mathbf{h}_{\text{sp}}$ and $\mathbf{h}_{\text{ss}}$ may be drawn from the same distribution.

Several sources of attenuation can decrease the received power in wireless communications, e.g., distance dependent path loss and/or shadowing effects, thus the corresponding channel is unlikely to be characterized by a uniform PDP. In real applications the channels will most likely fall into the categories represented by the two latter channel snapshots, i.e., exponential PDP with smaller delay spread. Therefore, we focus on this case and analyze both fast and slow decay, considering the uniform PDP case as a benchmark for the other two. Given the precoder computed above, we generate two snapshots of $\mathbf{h}_{\text{ss}}$, as depicted in Figures 2.19 and 2.20.

As previously described, we consider the transmission of the two signals whose power profile is depicted in Figures 2.16 and 2.17, assuming channels as in Figures 2.19 and 2.20, respectively. In compliance to the OFDM receiving chain, the CP is removed from the received signals, shown in Figures 2.21 and 2.22, where the dashed lines represent the transmit signals, plotted for comparison purposes. A huge power penalty can be spotted in both cases, more evident as the delay spread decreases. We remark that this is not related to a particular matching between the computed precoder and the faced channel, because by construction $\mathbf{h}_{\text{sp}}$ and $\mathbf{h}_{\text{ss}}$ are independent, hence $\ker(\mathbf{H}_{\text{sp}})$ and $\ker(\mathbf{H}_{\text{ss}})$ are distinct. The aforementioned power penalty is strictly related to the nature of the channel, i.e., characterized by short delay spread, hence the largest amount of received power is concentrated in the portion of the signal corresponding to the CP. It is important to note that the white Gaussian noise added at the receiver does not experience the same penalty, and its statistical properties are not modified by the CP removal process. As a consequence, the effective SNR of the resulting N symbols could be significantly different from the SNR before the CP removal. Such an SNR drop affects mainly the quality of the following decoding process, thus the achievable rate of this scheme in the considered scenario. The impact of this issue on the achievable spectral efficiency of the secondary link when adopting the analyzed null-space precoder has been enlightened in Section 2.5. We recall that the experimental BER at the receiver achieved by the demonstrator, herein implemented to show the feasibility of such a secondary transmission, was lower than ex-

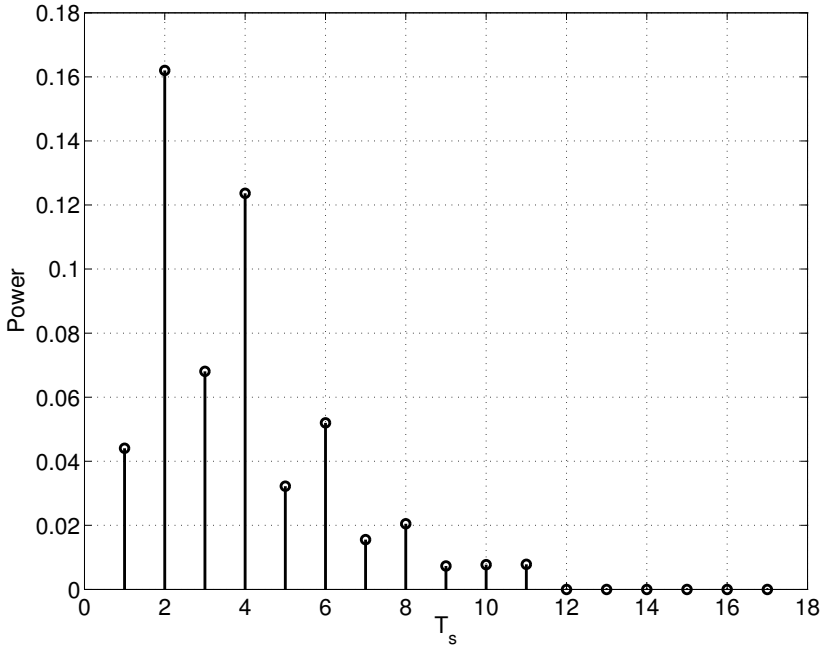

Figure 2.19: Secondary link. Exponential PDP, slow decay, $\frac{T_s}{\tau} = 0.75$

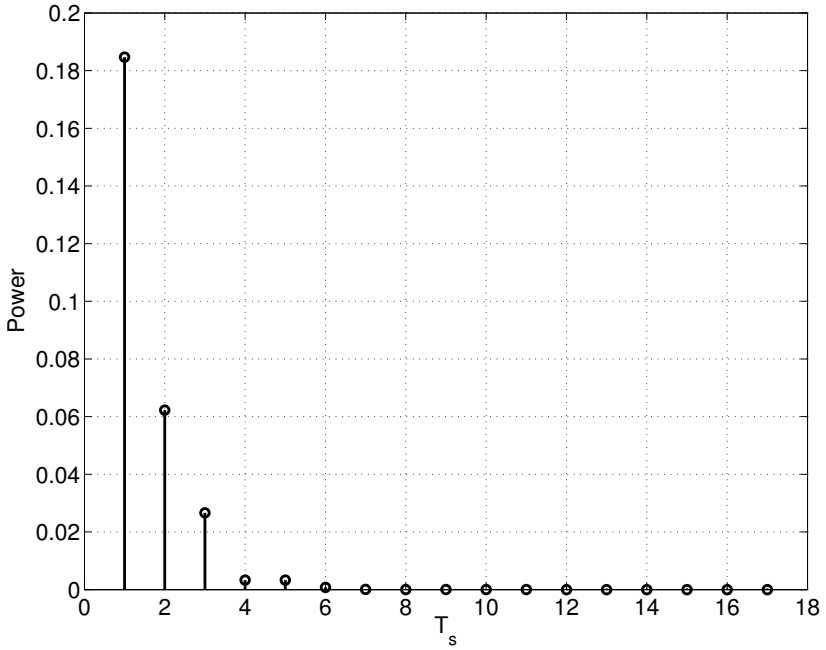

Figure 2.20: Secondary link. Exponential PDP, fast decay, $\frac{T_s}{\tau} = 2.5$

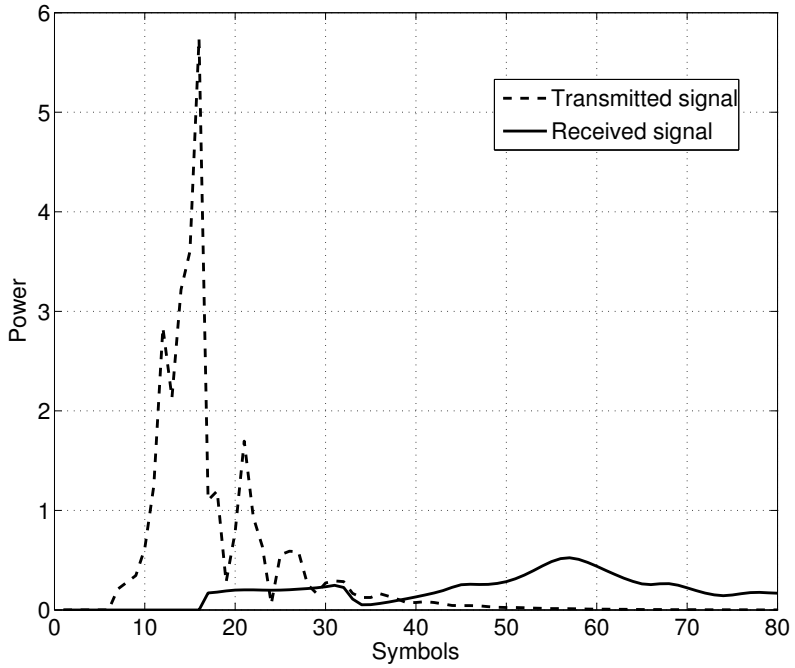

Figure 2.21: Transmitted and received signal. Exponential PDP, slow decay, $\frac{T_s}{\tau} = 0.75$

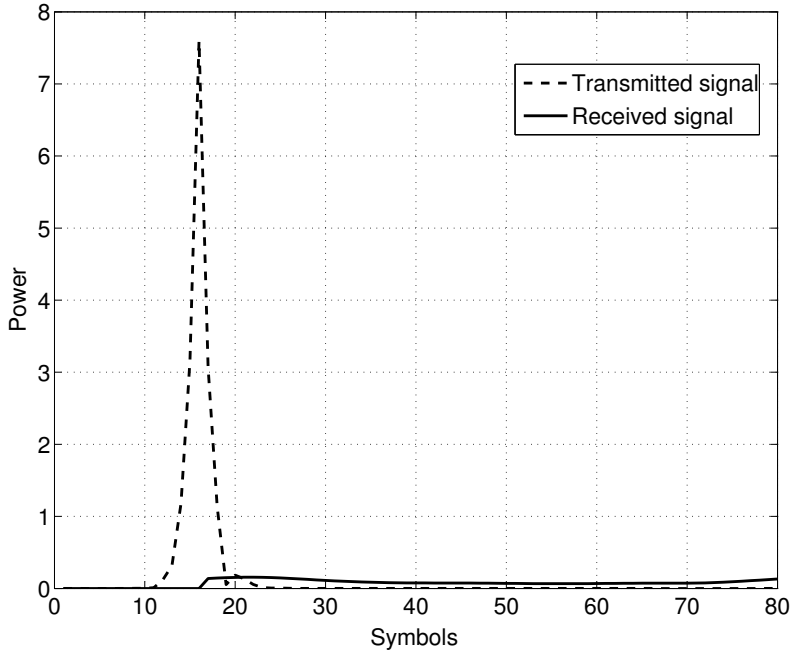

Figure 2.22: Transmitted and received signal. Exponential PDP, fast decay $\frac{T_s}{\tau} = 2.5$

pected and not compatible with the theoretical results. The insights drawn in this section provide a deeper explanation to this result. In the following we will further investigate this problem by studying the optimal null-space precoder structure and corresponding power loading strategy. Additionally, a workaround to improve the performance at the secondary receiver will be proposed. Accordingly, a change in the signal model in the secondary system will be analyzed, evaluating the difference of achievable spectral efficiency between the legacy receiver architecture and an alternative scheme not including a CP removal step.

Chapter 3

Optimal Null-space Precoder: Cognitive Interference Alignment

The analysis provided in the previous chapter showed that the drawbacks that a secondary system may face in the considered spectrum sharing scenario. The opportunistic transmission performed in the secondary system, if the primary system adopts an OFDM-based scheme, may lead to very unfavorable conditions for the secondary receiver. In particular, the structure of the adopted interference nulling precoder, and the secondary receiver architecture are key factors to achieve an interesting opportunistic system's performance. In this chapter, we start from the former aspect and take a step back by re-framing the considered scenario in a more general way. We consider a two users interference channel where one of the two transmitters has to fulfill an interference cancelation constraint w.r.t. the non-served receiver. We derive the optimal precoder structure for any such interference channels when the channel matrices have a non-empty kernel. Afterwards, we extend the result to the considered two-tiered scenario, and a study on the impact on the achievable spectral efficiency of the secondary link of the CP removal operation at the OFDM-like secondary receiver, is presented.

3.1 Two-tiered Network DL Model

As done in Chapter 2, herein we consider the DL of a two-tiered network, operating in TDD mode, composed of a macro-cell in the first tier and a small-cell in the second, as depicted in Figure 3.1. In particular, the licensee OFDM MBS serves one MUE, whereas the cognitive SBS serves one SUE. Each device in the network disposes of a single antenna, thus single input single output (SISO) communications are performed in both tiers, with frequency reuse 1. Concerning the available knowledge at the transmitters, on the one hand the MBS is unaware of the existence of the second tier, on the other hand the SBS is uninformed about left-over space, time or frequency resources or power allocation in

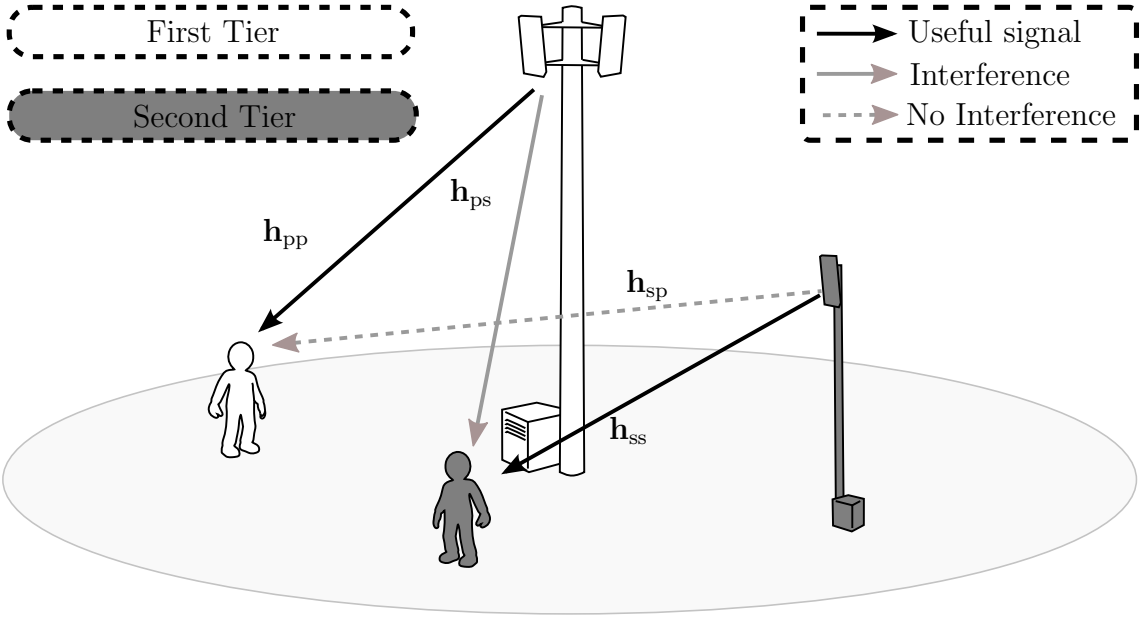

Figure 3.1: DL of a two-tiered network

the macro-cell. Accordingly, no cross-tier cooperation or coordination is established. We note that, at this stage, we are still considering that both MUE and SUE are classic OFDM receivers. Let $\mathbf{h}_{\text{pp}}$, $\mathbf{h}_{\text{ps}}$, $\mathbf{h}_{\text{sp}}$, $\mathbf{h}_{\text{ss}} \sim \mathcal{CN}(0, \mathbf{I}_{l+1}/(l+1))$ be i.i.d. Rayleigh fading channel vectors of $l+1$ taps. For simplicity, but without lack of generality, we consider that all the channel vectors have the same size. Moreover, we assume that both systems adopts Gaussian constellations, and that the channel coherence time in both tiers is largely superior to the block transmission time $N+L$, such that the channel is essentially the same from one block to the other. Let N be number of the subcarriers used by the MBS, and $L \geq l$ the length of the CP, added to the OFDM block to compensate for the ISI IBI.

Now, consider a transmitter in the tier "a" and a receiver in the tier "b". As done in Chapter 2, we define $\mathbf{H}_{\text{ab}} \in \mathbb{C}^{(N+L)\times(N+L)}$ as the channel matrix representing the convolution of the transmit signal with the channel connecting these two devices, as

$$\mathbf{H}_{\text{ab}} = \begin{bmatrix} h_{\text{ab},0} & 0 & \cdots & h_{\text{ab},l} & \cdots & \cdots & h_{\text{ab},1} \\ \vdots & \ddots & \ddots & & \ddots & \ddots & \vdots \\ \vdots & \ddots & \ddots & & \ddots & \ddots & h_{\text{ab},l} \\ h_{\text{ab},l} & \cdots & \cdots & h_{\text{ab},0} & 0 & \cdots & 0 \\ 0 & \ddots & \ddots & \ddots & \ddots & \ddots & \vdots \\ \vdots & \ddots & \ddots & \ddots & \ddots & \ddots & 0 \\ 0 & \ddots & \ddots & h_{\text{ab},l} & \ddots & \ddots & h_{\text{ab},0} \end{bmatrix}. \tag{3.0}$$

where, as an approximation, we neglect the inter-channel interference that may be caused by analog and RF impairments at the MUE/SUE.

Let $\mathbf{x}_\mathrm{p}$, $\mathbf{x}_\mathrm{s} \in \mathbb{C}^{(N+L)\times 1}$ be the transmit symbol vectors and $\mathbf{y}_\mathrm{p}$, $\mathbf{y}_\mathrm{s} \in \mathbb{C}^{(N+L)\times 1}$ be the received symbol vectors for the primary/secondary system respectively. The overall received signal at primary and secondary receiver is

$$\begin{aligned} \mathbf{y}_\mathrm{p} &= \mathbf{H}_{\mathrm{pp}}\mathbf{x}_\mathrm{p} + \mathbf{H}_{\mathrm{sp}}\mathbf{x}_\mathrm{s} + \mathbf{n}_\mathrm{p} \quad (3.1)\\ \mathbf{y}_\mathrm{s} &= \mathbf{H}_{\mathrm{ss}}\mathbf{x}_\mathrm{s} + \mathbf{H}_{\mathrm{ps}}\mathbf{x}_\mathrm{p} + \mathbf{n}_\mathrm{s}, \quad (3.2)\end{aligned}$$

where $\mathbf{n}_\mathrm{p}$, $\mathbf{n}_\mathrm{s} \sim \mathcal{CN}(0, \sigma^2\mathbf{I}_{N+L})$ are $N+L$-sized AWGN noise vectors. The OFDM transmitted signal by the MBS is

$$\mathbf{x}_\mathrm{p} = \mathbf{A}\mathbf{F}^{-1}\mathbf{s}_\mathrm{p}, \quad (3.2)$$

where $\mathbf{A}$ is a $(N+L)\times N$ CP insertion matrix as defined in(2.2), $\mathbf{F} \in \mathbb{C}^{N\times N}$ is a unitary DFT matrix as defined in Chapter 2 and $\mathbf{s}_\mathrm{p} \sim \mathcal{CN}(0, d(p_{\mathrm{p},1}, \ldots, p_{\mathrm{s},N}))$[1] is the primary input symbol vector. The SBS precodes its signal with an appropriate precoding matrix $\mathbf{E}$, such that

$$\mathbf{x}_\mathrm{s} = \mathbf{E}\mathbf{s}_\mathrm{s}, \quad (3.2)$$

with $\mathbf{E}$ and $\mathbf{s}_\mathrm{s}$ detailed in the following.

3.2 Cognitive Interference Alignment

We assume that perfect CSI w.r.t. $\mathbf{h}_{\mathrm{sp}}$ and $\mathbf{h}_{\mathrm{ss}}$ is available at the cognitive SBS and that no spectrum sensing is performed in the second tier. Additionally, no a priori knowledge is available at the SBS about both the time resource allocation in the first tier and the primary transmit input symbol vector. Thus, techniques such as DPC can not be implemented to realize the coexistence between the two concurrent transmissions.

Let us consider the classic OFDM receiver chain, where the following base-band preprocessing is performed

$$\begin{aligned} \tilde{\mathbf{y}}_\mathrm{p} &= \mathbf{F}\mathbf{B}\mathbf{y}_\mathrm{p} = \tilde{\mathbf{H}}_{\mathrm{pp}}\mathbf{A}\mathbf{F}^{-1}\mathbf{s}_\mathrm{p} + \tilde{\mathbf{H}}_{\mathrm{sp}}\mathbf{E}\mathbf{s}_\mathrm{s} + \tilde{\mathbf{n}}_\mathrm{p} \quad (3.3)\\ \tilde{\mathbf{y}}_\mathrm{s} &= \mathbf{F}\mathbf{B}\mathbf{y}_\mathrm{s} = \tilde{\mathbf{H}}_{\mathrm{ps}}\mathbf{A}\mathbf{F}^{-1}\mathbf{s}_\mathrm{p} + \tilde{\mathbf{H}}_{\mathrm{ss}}\mathbf{E}\mathbf{s}_s x + \tilde{\mathbf{n}}_\mathrm{s},\end{aligned}$$

where $\mathbf{B} = [\mathbf{0}_{N\times L}|\mathbf{I}_N]$ is the CP removal matrix and $\tilde{\mathbf{n}}_\mathrm{s}$, $\tilde{\mathbf{n}}_\mathrm{p}$ are the Fourier transforms of the last N elements of the noise vectors $\mathbf{n}_\mathrm{s}$, $\mathbf{n}_\mathrm{p}$, having the same statistics of their time domain versions. In particular $\tilde{\mathbf{H}}_{\mathrm{ab}} = \mathbf{F}\mathbf{B}\mathbf{H}_{\mathrm{ab}}$ reads

$$\tilde{\mathbf{H}}_{\mathrm{ab}} = \mathbf{F}\begin{bmatrix} h_{\mathrm{ab},l} & \cdots & h_{\mathrm{ab},0} & 0 & \cdots & 0 \\ 0 & \ddots & & \ddots & \ddots & \vdots \\ \vdots & \ddots & \ddots & & \ddots & 0 \\ 0 & \cdots & 0 & h_{\mathrm{ab},l} & \cdots & h_{\mathrm{ab},0} \end{bmatrix} \in \mathbb{C}^{N\times(N+L)},$$

and $\mathrm{rank}(\tilde{\mathbf{H}}_{\mathrm{ab}}) = N$. From the rank-nullity theorem [73] we have

$$\dim\ker(\tilde{\mathbf{H}}_{\mathrm{sp}}) = L, \quad (3.1)$$

[1]Given a vector $\mathbf{a}$, we denote as $d(\mathbf{a}) = diag(\mathbf{a})$ a diagonal matrix such that $[d(\mathbf{a})]_{i,i} = a_i$.

$\forall \mathbf{h}_{\mathrm{sp}} \in\sim \mathcal{CN}(0, \mathbf{I}_{l+1}/(l+1))$, where $\ker(\cdot)$ is the kernel of the matrix provided as argument and $\dim\ker(\cdot)$ its dimensions. Therefore, we can always find a matrix $\mathbf{E} \in \mathbb{C}^{(N+L)\times L}$ such that its column space, i.e., the linear span of its columns, can be expressed as

$$\mathrm{span}\,(\mathbf{E}) = \ker(\tilde{\mathbf{H}}_{\mathrm{sp}})^2 \tag{3.1}$$

and

$$\tilde{\mathbf{H}}_{\mathrm{sp}}\mathbf{E} = \mathbf{0}_{N\times L}. \tag{3.1}$$

At this stage, we can let $\mathbf{s}_{\mathrm{s}} \sim \mathcal{CN}(0, d(p_{\mathrm{s},1}, \ldots, p_{\mathrm{s},L}))$ in (3.1) be the secondary input symbol vector.

By substituting (3.1) in (3.1), we obtain

$$\mathbf{y}_{\mathrm{p}} = \mathbf{H}_{\mathrm{pp}}\mathbf{x}_{\mathrm{p}} + \begin{bmatrix} \mathbf{K} \\ \mathbf{0}_{N\times L} \end{bmatrix} \mathbf{s}_{\mathrm{s}} + \mathbf{n}_{\mathrm{p}}, \tag{3.1}$$

where $\mathbf{K} \in \mathbb{C}^{L\times L}$ is a matrix whose size is independent of the size of $\mathbf{h}_{\mathrm{sp}}$, i.e., l. We note that, the structure of this result is analogous to what is obtained by classic IA approaches [18]. In fact, thanks to the adoption of $\mathbf{E}$ at the SBS, the received signal at the MUE can always be decomposed in two constant sized components, $\forall \mathbf{s}_{\mathrm{s}} \sim \mathcal{CN}(0, d(p_{\mathrm{s},1}, \ldots, p_{\mathrm{s},L}))$, i.e., an interference and a useful signal subspace. In particular, if perfect synchronization of the signal transmitted by the MBS and the cross-tier interference signal generated the SBS can be ensured at the MUE, the latter is always confined in a subspace of the overall received signal space at the MUE, whose size is constantly L. As a consequence, the legacy N degrees of freedom of the OFDM transmission in the first tier are preserved. The MUE obliviously discards the aligned interference coming from the SBS by means of the OFDM receiver pre-processing shown in (3.3). The outcoming vector $\tilde{\mathbf{y}}_{\mathrm{p}}$, carrying the desired N interference free dimensions out of the $N + L$ received ones, then reads

$$\tilde{\mathbf{y}}_{\mathrm{p}} = \tilde{\mathbf{H}}_{\mathrm{pp}}\mathbf{x}_{\mathrm{p}} + \tilde{\mathbf{n}}_{\mathrm{p}}. \tag{3.1}$$

For these reasons, hereafter we will refer to this scheme as CIA.

3.3 Optimal Interference Cancelation Precoder

As previously seen, the adoption of the CIA scheme preserves the degrees of freedom of the primary OFDM transmission, hence its maximum achievable spectral efficiency. On the other hand, thanks to the joint effect of the receiver pre-processing and the redundancy introduced by the MBS to combat ISI and IBI, the CIA scheme guarantees the SBS counts with L additional transmit dimensions. Naturally, the efficiency of the secondary transmission hinges on the choice of the precoder $\mathbf{E}$, that has to be designed such that the spectral efficiency of the secondary link is maximized. In this section, we present a constructive approach to design such a precoder. Let us start from a definition.

[2]Let $\mathcal{A}$ and $\mathcal{B}$ be two vector spaces of dimension M. We define $\mathcal{A} = \mathcal{B}$ if and only if $\forall x \in \mathbb{C}^M$, $x \in \mathcal{A} \leftrightarrow x \in \mathcal{B}$.

Definition 1 (Semi-unitary precoder)**.** *A precoder* $\mathbf{W} \in \mathbb{C}^{N\times M}$ *is semi-unitary if and only if* $\text{rank}\,(\mathbf{W}) = min\{N, M\}$ *and all its non zero eigenvalues are equal to 1, thus* $\mathbf{W}\mathbf{W}^H = \mathbf{I}_N$ *or* $\mathbf{W}^H\mathbf{W} = \mathbf{I}_M$*.*

By looking at Def. 1, we note that a unitary precoder $\mathbf{W} \in \mathbb{C}^{N\times N}$ is also *semi-unitary.* In fact, $\text{rank}\,(\mathbf{W}) = min\{N, N\} = N$ and all its eigenvalues are equal to 1 by definition.

Let us now consider the product of semi-unitary precoders. The following holds.

Proposition 2 (Product of semi-unitary precoders)**.** *The product of* K *semi-unitary precoders is a semi-unitary precoder.*

Proof: Let $\mathcal{W} = \{\mathbf{W}_1, \ldots, \mathbf{W}_K\}$ be a set of K semi-unitary precoders $\mathbf{W}_i \in \mathbb{C}^{N_i\times M_i}$, $\forall i \in [1, K]$, such that $M_i = N_{i+1}, \forall i \in [1, K-1]$. We know that if $N_i > M_i$ then $\mathbf{W}_i^{\text{H}}\mathbf{W}_i = \mathbf{I}_{M_i}$, whereas if $M_i > N_i$ then $\mathbf{W}_i\mathbf{W}_i^{\text{H}} = \mathbf{I}_{M_i}$. In the following, we will assume $N_i > M_i$. Let $\mathbf{Q} = \prod_i^K \mathbf{W}_i \in \mathbb{C}^{N_1\times M_K}$ be the product of the K precoders. If we compute the matrix given by $\mathbf{Q}^{\text{H}}\mathbf{Q}$, we obtain

$$\begin{aligned}\mathbf{Q}^{\text{H}}\mathbf{Q} &= \mathbf{W}_K^{\text{H}} \ldots \mathbf{W}_2^{\text{H}}\mathbf{W}_1^{\text{H}}\mathbf{W}_1\mathbf{W}_2 \ldots \mathbf{W}_K \\ &= \mathbf{W}_K^{\text{H}} \ldots \mathbf{W}_2^{\text{H}}\mathbf{I}_{M_1}\mathbf{W}_2 \ldots \mathbf{W}_K \\ &= \mathbf{W}_K^{\text{H}}\mathbf{I}_{M_{K-1}}\mathbf{W}_K \\ &= \mathbf{I}_{M_K},\end{aligned}$$

where we recursively used the definition of the semi-unitary $\mathbf{W}_i$ given in Def. 1. Consequently, $\mathbf{Q}$ is semi-unitary. Note that, if $N_i < M_i$, $\mathbf{Q}\mathbf{Q}^{\text{H}} = \mathbf{I}_{N_K}$ is obtained similarly, demonstrating that $\mathbf{Q}$ is semi-unitary regardless of the considered case, and this ends the proof. ■

The following result provides the optimal linear precoder based strategy to be adopted by any transmitter that aims at maximizing the spectral efficiency of its transmission towards a secondary receiver, while fulfilling a feasible interference cancellation constraint w.r.t. to the interference link towards a primary receiver.

Proposition 3 (Optimal interference cancellation precoder)**.** *Consider an interference channel with a primary and a cognitive secondary transmitter/receiver pair, i.e, TX1/RX1 and TX2/RX2 respectively, characterized by the following equations*

$$\begin{aligned}\mathbf{y}_1 &= \mathbf{H}_{11}\mathbf{x}_1 + \mathbf{H}_{21}\mathbf{x}_2 + \mathbf{n}_1 \\ \mathbf{y}_2 &= \mathbf{H}_{22}\mathbf{x}_2 + \mathbf{H}_{12}\mathbf{x}_1 + \mathbf{n}_2,\end{aligned} \tag{3.-3}$$

with $\mathbf{y}_i$ *N-sized received vectors,* $\mathbf{H}_{ij} \in \mathbb{C}^{N\times M}$ *channel matrices with* $N < M$*,* $\mathbf{n}_i \sim \mathcal{CN}(0, \sigma^2\mathbf{I}_N)$ *AWGN vector and* $\mathbf{x}_i = (\mathbf{x}_{i,j}, \ldots, \mathbf{x}_{i,M})^T \in \mathbb{C}^{M\times 1}$ *transmit vectors. When perfect CSI w.r.t.* $\mathbf{H}_{21}$ *is available at TX2, the interference towards RX1 is cancellable by means of a linear null-space precoder. If also perfect CSI w.r.t.* $\mathbf{H}_{22}$ *is available, a* ***semi-unitary*** *precoder is optimal in the sense of the spectral efficiency of the secondary link under the interference cancellation constraint.*

Proof: We start by isolating the interference plus noise component of the received message at RX2, that performs single-user decoding, as

$$\boldsymbol{\xi}_2 = \mathbf{H}_{12}\mathbf{x}_1 + \mathbf{n}_2. \tag{3.-3}$$

Analogously, can define $\mathbf{S}_{(2,\xi)}$, covariance matrix of $\boldsymbol{\xi}_2$, as

$$\mathbf{S}_{(2,\xi)} = \mathbf{H}_{12} d(p_{1,1}, \ldots, p_{1,M}) \mathbf{H}_{12}^{\mathrm{H}} + \sigma_n^2 \mathbf{I}_N, \tag{3.-3}$$

where $d(p_{1,1}, \ldots, p_{1,M})$ is a diagonal matrix obtained by the vector $(p_{1,1}, \ldots, p_{1,M})$, representing a generic input covariance matrix at TX1. Note that, rank $\mathbf{H}_{21} = N$ by construction, thus $\dim \ker(\mathbf{H}_{21}) = M - N$ and $\ker(\mathbf{H}_{21}) \subseteq \mathcal{R}^{M\times(M-N)}$. Therefore, a linear precoder $\mathbf{Z}_2 \in \mathbb{C}^{M\times(M-N)}$ such that span $(\mathbf{Z}_2) = \ker(\mathbf{H}_{21})$ can always be found.

Now, let $\mathbf{u}_2 \sim \mathcal{CN}(0, d(p_{2,1}, \ldots, p_{2,(M-N)}))$ be an input vector such that $\mathbf{x}_2 = \mathbf{Z}_2\mathbf{u}_2$, $\mathbf{S}_2 = \mathbf{Z}\ d(p_{2,1}, \ldots, p_{2,(M-N)})\mathbf{Z}^{\mathrm{H}}$ be the covariance matrix of $\mathbf{u}_2$ and $P_2 = \mathbb{E}[x_{i,j}x_{i,j}^{\mathrm{H}}]$ be the average transmit power per precoded symbol at TX2, $\forall j \in [1, M]$, where $\mathbb{E}$ is the expectation operator. Then, the maximum achievable spectral efficiency for the secondary link is the solution of the following maximization problem

$$\begin{aligned} \max_{\mathbf{S}_2} \quad & \frac{1}{M}\log_2\left|\mathbf{I}_N + \mathbf{S}_{(2,\xi)}^{-1/2}\mathbf{H}_{22}\mathbf{S}_2\mathbf{H}_{22}^{\mathrm{H}}\mathbf{S}_{(2,\xi)}^{-1/2}\right| \\ \text{s.t.} \quad & \mathbf{H}_{21}\mathbf{Z}_2 = \mathbf{0}_{N\times(M-N)} \\ & \mathrm{tr}(\mathbf{S}_2) \le MP_2, \end{aligned} \tag{3.-3}$$

where $\mathrm{tr}(\mathbf{S}_2) = \sum_i = 1^N[\mathbf{S}_2)]_{i,i}$ denotes the trace of $\mathbf{S}_2$. The presence of the constraint $\mathbf{H}_{21}\mathbf{Z}_2 = \mathbf{0}_{N\times(M-N)}$ restricts the subset of the possible solutions to the kernel of the interference channel. Let $\mathbf{W}$ be a matrix whose columns form an orthonormal basis of span $(\mathbf{Z}_2)$. Such one $\mathbf{W}$ is semi-unitary by definition of orthonormal matrix and many strategies can be adopted to derive it, e.g. LQ factorization. Then, by defining $\boldsymbol{\Gamma} \in \mathbb{C}^{(M-N)\times(M-N)}$ as a matrix with random entries, we can remove the constraint and write

$$\mathbf{Z}_2 = \mathbf{W}\boldsymbol{\Gamma}. \tag{3.-4}$$

The columns of $\mathbf{Z}_2$ are a generic linear combination of the columns of $\mathbf{W}$, thus $\mathbf{H}_{21}\mathbf{Z}_2 = \mathbf{0}_{N\times(M-N)}$ will be satisfied by any optimal $\mathbf{Z}_2^* = \mathbf{W}\boldsymbol{\Gamma}^*$ by construction. Then we can write

$$\mathbf{S}_2 = \mathbf{W}\boldsymbol{\Gamma} d(p_{2,1}, \ldots, p_{2,(M-N)})\boldsymbol{\Gamma}^{\mathrm{H}}\mathbf{W}^{\mathrm{H}} = \mathbf{W}\boldsymbol{\Sigma}_2\mathbf{W}^{\mathrm{H}}$$

with $\boldsymbol{\Sigma}_2 = \boldsymbol{\Gamma} d(p_{2,1}, \ldots, p_{2,(M-N)})\boldsymbol{\Gamma}^{\mathrm{H}}$, and (3.-3) becomes

$$\begin{aligned} \max_{\mathbf{S}_2} \quad & \frac{1}{M}\log_2\left|\mathbf{I}_N + \mathbf{S}_{(2,\xi)}^{-1/2}\mathbf{H}_{22}\mathbf{W}\boldsymbol{\Sigma}_2\mathbf{W}^{\mathrm{H}}\mathbf{H}_{22}^{\mathrm{H}}\mathbf{S}_{(2,\xi)}^{-1/2}\right| \\ \text{s.t.} \quad & \mathrm{tr}(\boldsymbol{\Sigma}_2) \le MP_2. \end{aligned} \tag{3.-3}$$

We further simplify (3.-3), by letting $\mathbf{S}_{(2,\xi)}^{-1/2}\mathbf{H}_{22}\mathbf{W}$. By taking its SVD, we write $\mathbf{G} = \mathbf{U}_{\mathrm{g}}\boldsymbol{\Lambda}_{\mathrm{g}}^{\frac{1}{2}}\mathbf{V}_{\mathrm{g}}^{\mathrm{H}}$, with $\mathbf{U}_{\mathrm{g}} \in \mathbb{C}^{N\times N}$,$\mathbf{V}_{\mathrm{g}} \in \mathbb{C}^{(M-N)\times(M-N)}$ unitary matrices. Moreover,

$\mathbf{\Lambda}_{\mathrm{g}} = [\mathbf{\Lambda}_{\mathrm{g}}^{\lambda}, \mathbf{\Lambda}_{\mathrm{g}}^{0}]^{\mathrm{T}}$, where $\mathbf{\Lambda}_{\mathrm{g}}^{0} = \mathbf{0}_{(M-N)\times 2N-M}$ and $\mathbf{\Lambda}_{\mathrm{g}}^{\lambda} = d(\sqrt{\lambda_{(\mathrm{g},1)}}, \ldots, \sqrt{\lambda_{(\mathrm{g},(M-N))}})$, with $\lambda_{(\mathrm{g},i)}$ eigenvalues of $\mathbf{G}^{\mathrm{H}}\mathbf{G}$. Therefore, we can write

$$\begin{aligned} \max_{\mathbf{\Sigma}_2} \quad & \frac{1}{M}\log_2\left|\mathbf{I}_N + \mathbf{U}_{\mathrm{g}}\mathbf{\Lambda}_{\mathrm{g}}^{\frac{1}{2}}\mathbf{V}_{\mathrm{g}}^{\mathrm{H}}\mathbf{\Sigma}_2\mathbf{V}_{\mathrm{g}}\mathbf{\Lambda}_{\mathrm{g}}^{\frac{1}{2}}\mathbf{U}_{\mathrm{g}}^{\mathrm{H}}\right| \\ \text{s.t.} \quad & \mathrm{tr}(\mathbf{\Sigma}_2) \leq MP_2. \end{aligned} \tag{3.-4}$$

The upper bound for the determinant of a positive definite matrix is given by the product of the elements on its main diagonal, i.e., $|\mathbf{A}| \leq \prod_i \mathbf{A}_{[i,i]}$ (Hadamard inequality). Then, if we let $\mathbf{\Gamma} = \mathbf{V}_{\mathrm{g}}$, thus $\mathbf{\Sigma}_2 = \mathbf{V}_{\mathrm{g}}d(p_{2,1}, \ldots, p_{2,(M-N)})\mathbf{V}_{\mathrm{g}}^{\mathrm{H}}$, the argument of the determinant in (3.-4) is diagonalized and we can write

$$\begin{aligned} \max_{p_{2,i}} \quad & \sum_{i=1}^{M-N}\log_2(1 + p_{2,i}\lambda_{(\mathrm{g},i)}) \\ \text{s.t.} \quad & \sum_{i=1}^{M-N} p_{2,i} \leq MP_2. \end{aligned} \tag{3.-3}$$

Now we can apply a classical water-filling (WF) algorithm to find

$$p_{2,i} = \left[\mu - \frac{1}{\lambda_{(\mathrm{g},i)}}\right]^{+}, \tag{3.-4}$$

with μ, "water level", determined such that $\sum_i^{(M-N)} p_{2,i} \leq MP_2$. At this stage, it is clear that $\mathbf{\Gamma}^* = \mathbf{V}_{\mathrm{g}}$, and the solution to (3.-3) is $\mathbf{S}_2 = \mathbf{W}\mathbf{V}_{\mathrm{g}}d(p_{2,1}, \ldots, p_{2,(M-N)})\mathbf{V}_{\mathrm{g}}^{\mathrm{H}}\mathbf{W}^{\mathrm{H}}$. By plugging $\mathbf{\Gamma}^*$ in (3.3), we obtain

$$\mathbf{Z}^* = \mathbf{W}\mathbf{V}_{\mathrm{g}}, \tag{3.-4}$$

where $\mathbf{W}$ is semi-unitary by construction and $\mathbf{V}_{\mathrm{g}}$ is unitary by definition of SVD. The spectral efficiency maximizing precoder, under the considered constraints, is then semi-unitary by Proposition 2. In particular, in (3.3), $\mathbf{W}$ can be composed by any orthonormal set of columns spanning $\ker(\mathbf{H}_{12})$, whose appropriate linear combination to maximize the spectral efficiency will always be found by means of a suitable $\mathbf{V}_{\mathrm{g}}$, thus $\mathbf{W}$ is optimal and this ends the proof. ∎

Note that, Proposition 3 holds true for any configuration of the interference channel, as long as the system is characterizable by the equations provided in the hypothesis. In particular, the result is independent from parameters such as bandwidth, number of antennas, number of subcarriers and so on. Consequently, we can state the following result.

Corollary 4 (Optimal CIA precoder)**.** *Consider a two-tiered network where a licensee single antenna OFDM base station coexists with a single antenna opportunistic base stations adopting CIA. A semi-unitary CIA precoder* $\mathbf{E}$ *is optimal, in the sense of maximum link spectral efficiency for the SBS/SUE pair.*

Proof: By looking at (3.3), we directly recognize the interference channel equations provided in the hypothesis of Proposition 3, hence the latter can be applied to show that a semi-unitary CIA precoder $\mathbf{E}$ is optimal, and conclude the proof. ∎

3.4 Optimal Precoder Evaluation

In this section we evaluate the performance of the proposed method by means of extensive Monte Carlo simulations of the analyzed transmission system. Three PDP models are considered for the aforementioned Rayleigh fading channels, i.e., uniform, exponential with fast ($\frac{T_s}{\tau} = 2$) and slow ($\frac{T_s}{\tau} = 0.25$) decay, where T_s is the sample time and τ is the R.M.S. delay spread. We first focus on the maximum achievable spectral efficiency of the secondary link. Accordingly, we neglect the impact of the primary system interference on the SUE to isolate the merit of CIA. We compare the achievable performance of the optimal and show the gains that this approach can yield w.r.t. non-semi-unitary precoders (sub-optimal approach according to Lemma 3). As a further complementary benchmark, we consider a unitary root-based VFDM precoder, derived by means of a Gram-Schmidt orthonormalization [56], and evaluate its performance is the considered scenario. To achieve a fair comparison, we adopt for VFDM the same power loading strategy as the optimal CIA solution. We assume that the MBS transmits over $N = 128$ subcarriers, with a CP size of $L = 32$ and that the channel size l coincides with the CP size L.

We start from the uniform PDP case, in Fig. 3.2. If compared to the optimal per-

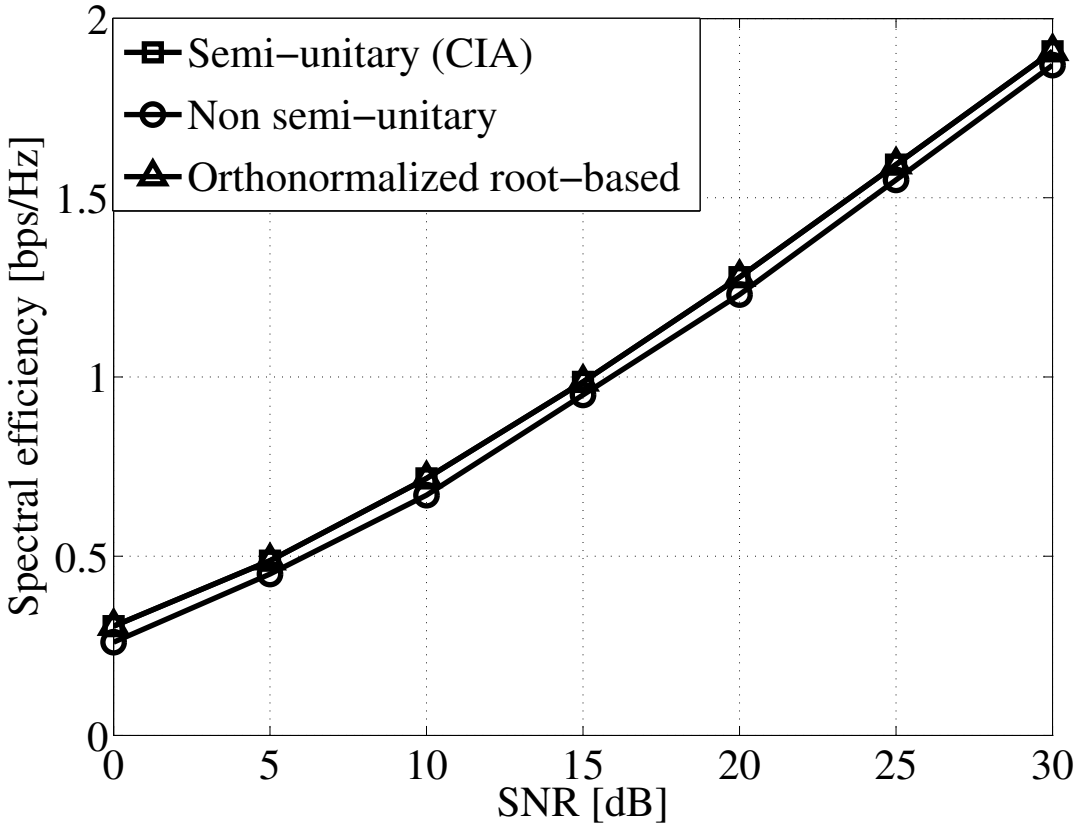

Figure 3.2: Spectral efficiency of the secondary link. Uniform PDP.

formance provided by the semi-unitary optimal precoder, we notice that, by adopting a sub-optimal solution, a loss of less than 3% can be seen for the considered SNR range. On the other hand, the performances of the orthonormal (semi-unitary) root-based VFDM and CIA precoder coincide. This demonstrates the optimality of the results provided in [56] when the considered channels are characterized by a uniform PDP, and $l = L$.

The spectral efficiency for exponential PDP with slow decay is depicted in Figure 3.3. In this case, the sub-optimal solutions achieve less than 93% and 84% of the achievable

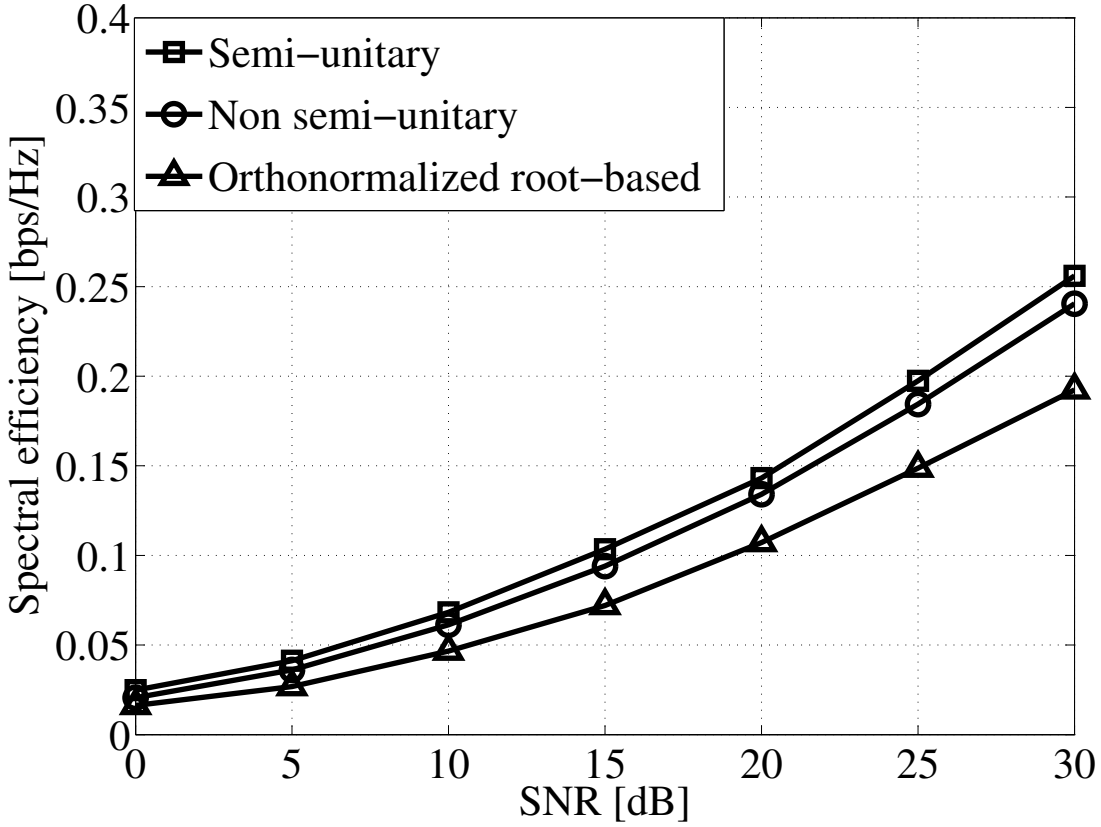

Figure 3.3: Spectral efficiency of the secondary link. Exponential PDP, slow decay, $\frac{T_s}{\tau} = 0.25$.

spectral efficiency of the optimal CIA precoder at high and low SNR respectively. In general, both solutions suffer from a significant loss if compared to the uniform PDP case. This time, the less frequency selective channel resulting from the non uniform power distribution of the channel paths, diminishes the diversity and impacts negatively on the efficiency of the secondary link transmission. In particular, as the PDP departs from a uniform structure, a reduction on the amount of effective eigenmodes of the equivalent channel is seen, irrespective of the fact that the number of transmit dimensions remains the same. This impacts the performance of the orthonormal root-based VFDM precoder as well. In fact, if the effective delay spread of the channel becomes shorter, the amount

of non-zero roots of the channel diminishes. Moreover, their sparse power distribution yields a very ineffective orthonormalization process, resulting in a spectral efficiency loss for the secondary link, w.r.t. the CIA precoder, of as much as 25% at high SNR.

In Figure 3.4, the spectral efficiency for exponential PDP with fast decay is shown. In

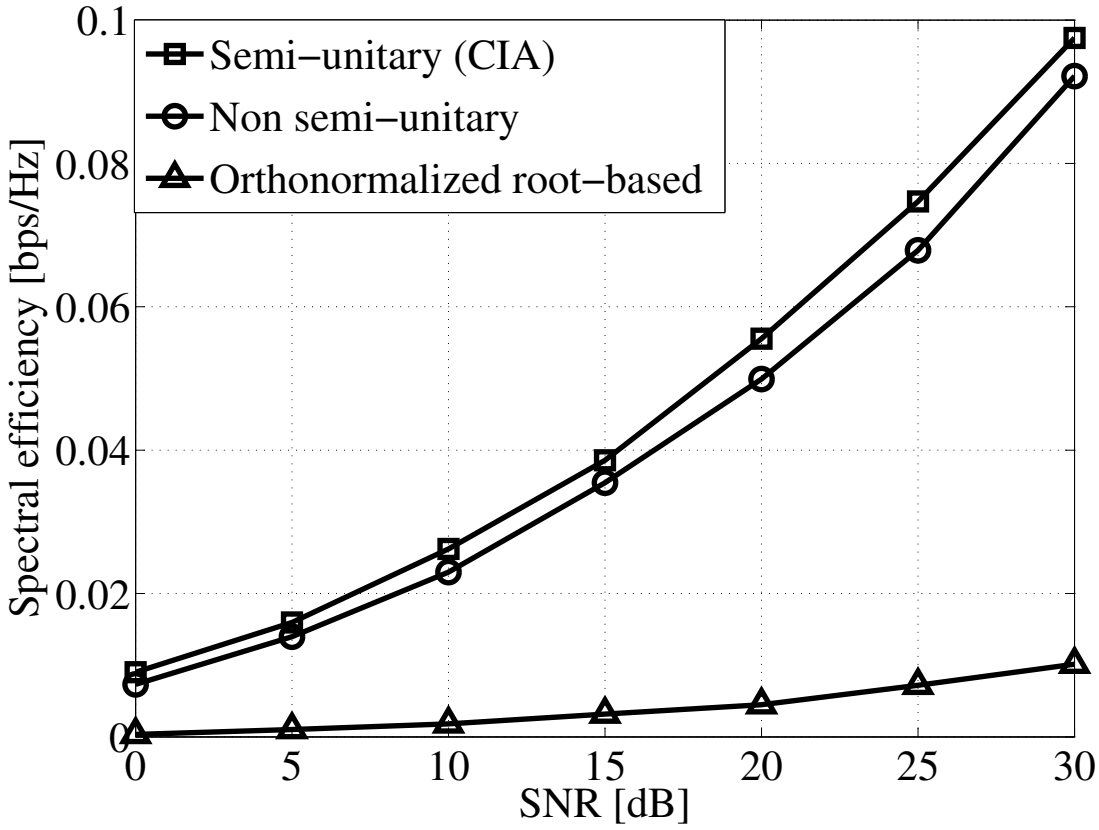

Figure 3.4: Spectral efficiency of the secondary link. Exponential PDP, fast decay, $\frac{T_s}{\tau} = 2$.

this case, all techniques experience a considerable drop in spectral efficiency due to the very low amount of effective eigenmodes of the equivalent channel. Despite this, we note that the behavior of the optimal and sub-optimal strategy maintains a similar trend as in the previous case. Conversely, the orthonormal root-based VFDM precoder performance loss is of more than 90%, confirming the impact of the delay spread on the robustness of the root-based precoder computation.

The results presented herein show the higher consistency of the optimal CIA precoder w.r.t. the sub-optimal solutions. Nevertheless, the non-negligible loss induced by channels characterized by short delay spreads confirms the findings in Chapter 2. In the next section, we will propose a change in the secondary receiver design mitigate this loss and evaluate the difference of achievable spectral efficiency between the legacy strategy and the modified one.

3.5 Cyclic Prefix Removal Impact

In Chapter 2, the impact of the PDP and R.M.S. delay spread of the channel used to create the null-space precoder on the power profile of the latter has been investigated. We have shown that the power is never uniformly distributed, even for uniform PDPs. In particular, the shorter the channel, the more the power of the coded transmit symbol will be concentrated in the first portion of the symbol itself. In other words, the amount of power present in the CP is a fundamental characteristic of the received signal. The more the power, the lower the SNR experienced by the resulting N symbols after the CP removal. Accordingly, the most penalizing drawback is a possibly poor spectral efficiency of secondary transmission when facing particularly short channels. We note that this result depends on the structure of the Toeplitz matrix used to model the convolution with the channel and on its kernel, whose non emptiness is always guaranteed in case of CP removal at the MUE. As a consequence, the only possible workaround to improve the performance at the SUE is a change in its design.

Let us consider (3.3). We focus on the received signal at the SUE, and relax the assumption that this acts as an OFDM-like receiver. In particular, we assume that SUE may consider the entirety of its $N+L$ received symbols to extract the desired L information symbols. We define $\Delta^{(l)}(\cdot)$ and $\Delta^{(u)}(\cdot)$ be two operators that extract the lower and the upper triangular part of a matrix argument, respectively. Then, we can rewrite $\tilde{\mathbf{y}}_{\mathrm{s}} \in \mathbb{C}^{(N+L)}$, the received signal at the SUE, as

$$\begin{aligned} \mathbf{r}_{\mathrm{s}} &= \mathbf{y}_{\mathrm{s}} \\ &= (\Delta^{(l)}(\mathbf{H}_{\mathrm{ss}}) + \Delta^{(u)}(\mathbf{H}_{\mathrm{ss}}))\mathbf{E}\mathbf{s}_{\mathrm{s}} + \mathbf{H}_{\mathrm{ps}}\mathbf{A}\mathbf{F}^{-1}\mathbf{s}_{\mathrm{p}} + \mathbf{n}_{\mathrm{s}} \end{aligned}, \tag{3.-4}$$

where, differently from (3.3), the secondary receiver does neither discard the first L received symbols nor perform the DFT, leading us to let $\mathbf{r}_{\mathrm{s}} = \mathbf{y}_{\mathrm{s}}$. We note that, in (3.5), we decomposed the channel coming from the SBS into two components, i.e., $\Delta^{(l)}(\mathbf{H}_{\mathrm{s}})$ and $\Delta^{(u)}(\mathbf{H}_{\mathrm{s}})$, contribution of the channel generating ISI and IBI, respectively [74]. In fact, since the secondary receiver does not discard CP, the IBI is not eliminated and has to be taken into account into the model. In particular, we have

$$\Delta^{(l)}(\mathbf{H}_{\mathrm{ss}}) = \begin{bmatrix} h_{\mathrm{ss},0} & 0 & \cdots & 0 & \cdots & \cdots & \cdots & 0 \\ h_{\mathrm{ss},1} & h_{\mathrm{ss},0} & \ddots & \ddots & \ddots & \ddots & \ddots & \vdots \\ \vdots & \ddots & \ddots & \ddots & \ddots & \ddots & \ddots & \vdots \\ h_{\mathrm{ss},l} & \cdots & \cdots & h_{\mathrm{ss},0} & 0 & \ddots & \ddots & \vdots \\ 0 & \ddots & \ddots & \ddots & \ddots & \ddots & \ddots & \vdots \\ \vdots & \ddots & \ddots & \ddots & \ddots & \ddots & \ddots & \vdots \\ \vdots & \ddots & \ddots & \ddots & \ddots & \ddots & \ddots & 0 \\ 0 & \ddots & \ddots & h_{\mathrm{ss},l} & \ddots & \ddots & \ddots & h_{\mathrm{ss},0} \end{bmatrix}.$$

and

$$\Delta^{(u)}(\mathbf{H}_{\text{ss}}) = \begin{bmatrix} 0 & 0 & \cdots & \cdots & \cdots & h_{\text{ab},l} & \cdots & h_{\text{ss},1} \\ \vdots & \ddots & \ddots & \ddots & \ddots & \ddots & \ddots & \vdots \\ \vdots & \ddots & \ddots & \ddots & \ddots & \ddots & \ddots & h_{\text{ss},l} \\ \vdots & \ddots & \ddots & \ddots & \ddots & \ddots & \ddots & 0 \\ \vdots & \ddots & \ddots & \ddots & \ddots & \ddots & \ddots & \vdots \\ \vdots & \ddots & \ddots & \ddots & \ddots & \ddots & \ddots & \vdots \\ \vdots & \ddots & \ddots & \ddots & \ddots & \ddots & \ddots & \vdots \\ 0 & \ddots & \ddots & \ddots & \ddots & \ddots & \ddots & 0 \end{bmatrix}.$$

We remark that, the change in the model does not change the optimal precoder computation, but only its realization. The knowledge required at the SBS to derive the optimal $\mathbf{E}$ is unchanged if compared to what was assumed in Section 3.3. In fact, the only additional requirement is an update to (3.3), covariance matrix of the interference at the SUE, to include the IBI component. Consequently, first the subspace that the columns of $\mathbf{E}$ should span to satisfy (3.2) is generated thanks to the knowledge of $\hat{\mathbf{H}}_{\text{sp}}$ as seen in Section 3.2. Afterwards, the power loading strategy is derived as described in Section 3.3.

Consider the set of PDP models introduced in Section 3.4, i.e., uniform, exponentially decreasing with fast and slow decay. The goal of the following study is to understand what would be the achievable spectral efficiency increase for the secondary system, if the SUE could decode the CP as a useful portion of the received signal. We start from the uniform PDP case, i.e., Figure 3.5. In this case, the CP decoding is not yielding any spectral efficiency gain to the SUE. In particular, the achievable spectral efficiency is unchanged until SNR = 15 dB, to decrease for higher values up to a loss of about 5%, due to the presence of strong IBI. This could be expected, in fact for uniform PDP the received symbol carries a non-negligible power throughout its whole duration (see Figure 2.16). Consequently, the power of the IBI is such that the performance of the secondary link slightly decreases at very high SNR, if the CP is not removed.

In Figure 3.6, the performance in case of exponential PDP with slow decay is computed. In this case, when the CP is not discarded, a gain of around 400% and 500% is achievable for low and high SNR respectively, whereas the SNR gain is more than 25 dB. The power penalty experienced by the SUE, after the CP removal operation, is significant. Specifically, the two results have a difference of as much as an order of magnitude at high SNR. If we consider the performance of legacy CIA for uniform PDP as a reference, we notice that the spectral efficiency loss when the PDP is exponentially decreasing with slow decay is around 85% w.r.t. the reference. On the contrary, if the SUE decodes all the $N+L$ received symbols, the rate loss is less than 28%. The importance of the information stored inside the CP, when the channel is characterized by a short delay spread, is now clear and suggests that legacy CIA is not efficient is this scenario. Accordingly, the spectral efficiency of the transmission could be improved significantly with an architectural change at the SUE, highly advisable to guarantee the presence of meaningful gains thanks to the cognitive approach.

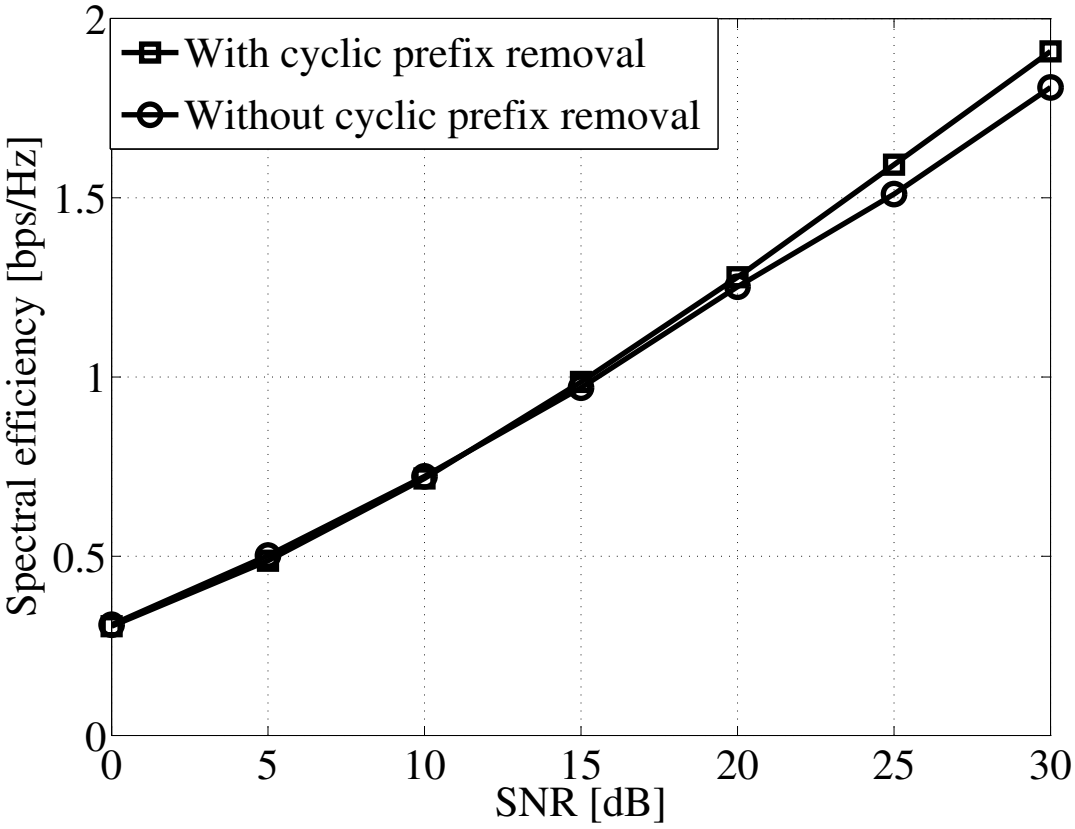

Figure 3.5: Achievable rate in case of CP decoding and CP removal. Uniform PDP.

Finally, in Figure 3.7, we consider an exponential PDP with fast decay. We start by noting that, for this class of fast decaying channels, the legacy OFDM-like receiver architecture limits the spectral efficiency of the transmission to less than 0.05 bit/s/Hz for SNR= $[10, 15]$ dB, result not compliant with the data demands of any future 4^{th} generation device. On the other hand, if the SUE does not discard the CP, a gain of around 350% and 1300% is achievable for low and high SNR respectively. In fact, the power penalty paid after the CP removal operation is so relevant that the performance of the system is strongly affected, hence the order of magnitude of the two results is significantly different. Moreover, as in the previous case, the SNR gain is extremely large, i.e., more than 30 dB. As before, let us investigate how the new SUE architecture can mitigate the spectral efficiency loos experienced by CIA when facing a channel characterized by a fast decaying exponentially decreasing PDP, if compared to the performance for uniform PDP. When the SUE has a legacy OFDM-like structure, the spectral efficiency loss in case of exponential PDP is more than 95% of the achievable spectral efficiency in case of uniform PDP, for both low and high SNR regime. On the other hand, the loss is reduced if the SUE can decode all the $N + L$ symbols, showing the increasing concentration of useful information inside the first L symbols. In particular, the loss at low SNR is around 85%, whereas for high SNR is remarkably only 30%. We note that, the spectral efficiency loss of the

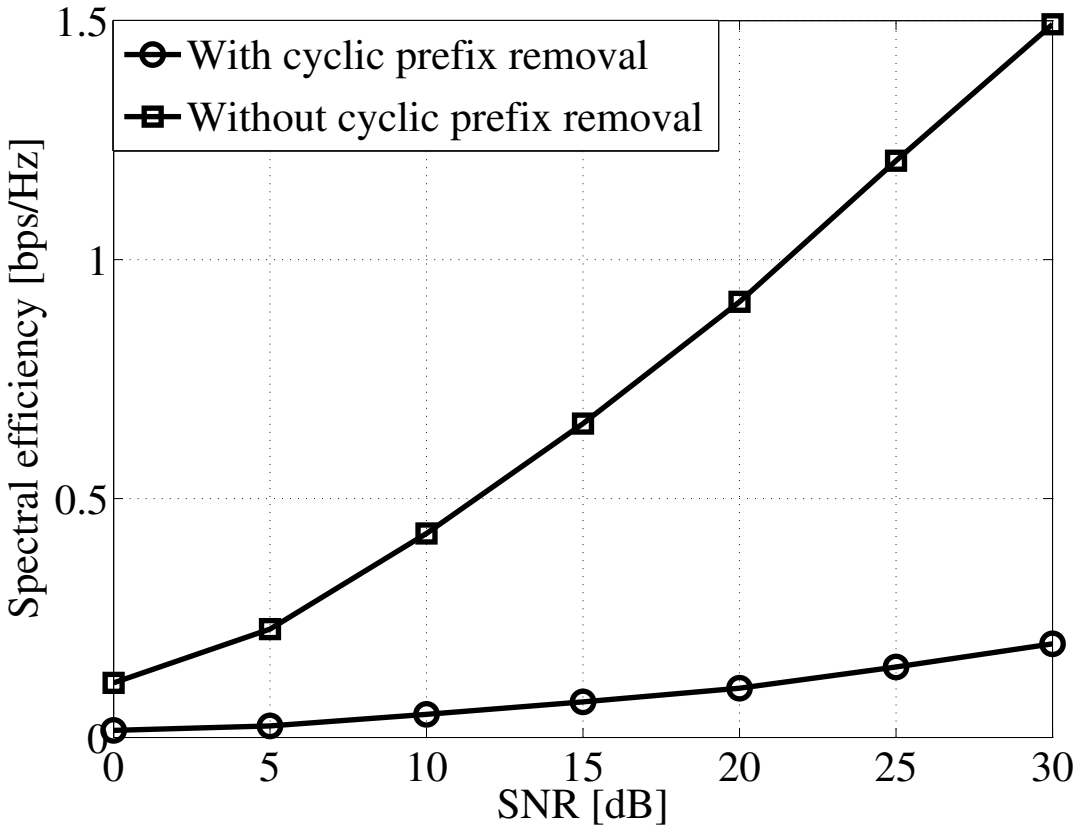

Figure 3.6: Achievable rate in case of CP decoding and CP removal. Exponential PDP, slow decay, $\frac{T_s}{\tau} = 0.25$.

legacy receiver w.r.t. the modified architecture would be even bigger in case of channels dominated by the LOS component, i.e., Rician fading, typically present in short-range or micro-cellular communications. As a consequence, the spectral efficiency gain brought by the CP decoding is fundamental in the CIA receiver design.

The results herein presented show that the operating scenario is of great importance to drive the choice of the most suitable receiver structure for the SUE. In fact, the spectral efficiency of the secondary link highly hinges on the R.M.S. delay spread and PDP of the channel, and a greater frequency selectivity is preferable in terms of performance for CIA. On the other hand, as seen in Figures 3.6 and 3.7, a change in the receiver structure can provide significant enhancements over the OFDM-like receiver structure, mitigating the experienced spectral efficiency loss for channels characterized by lower frequency selectivity.

Accordingly, a flexible approach to receiver design is advisable, to deal with several different channel statistics and conditions and provide a more reliable cognitive solution based on CIA. The increased complexity would necessary yield higher costs, but at the same time would provide better performance, as showed in this section. Depending on the

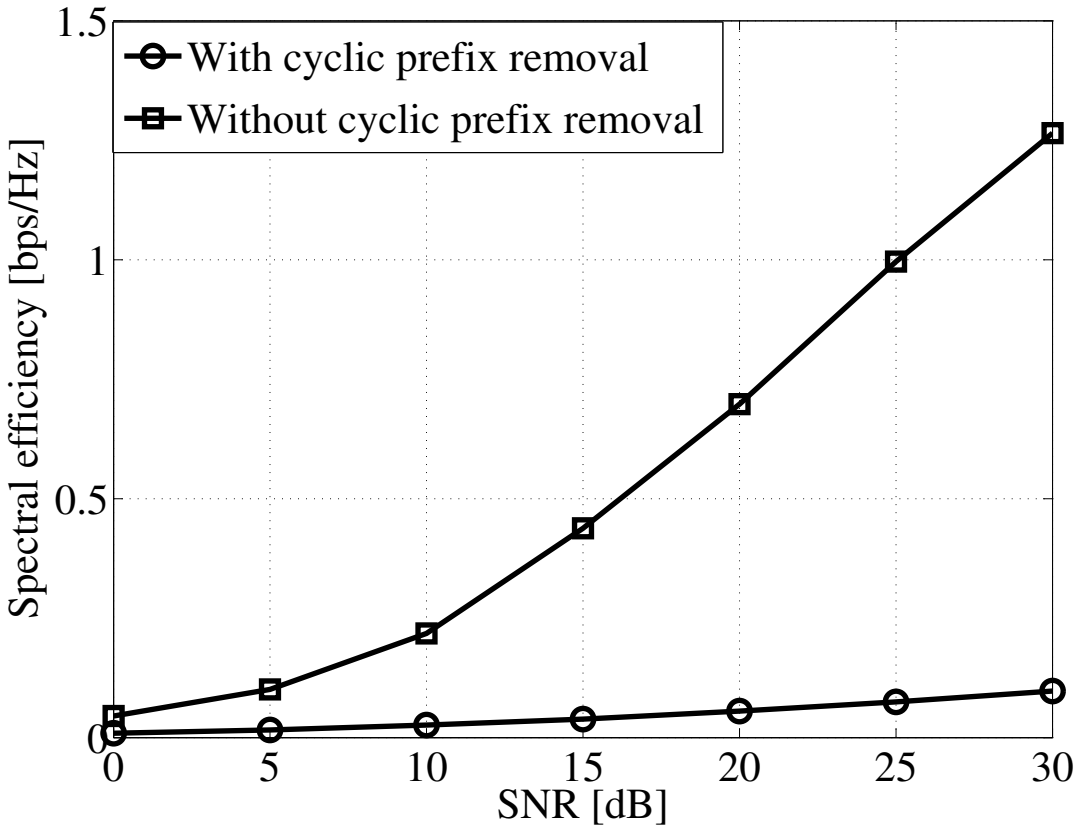

Figure 3.7: Achievable rate in case of CP decoding and CP removal. Exponential PDP, fast decay, $\frac{T_s}{\tau} = 2$.

network requirements and QoS constraints, one solution could be preferable to the other and the network designer should frame the receiver architecture accordingly. A trade-off should most likely be found from time to time, in order to decide which strategy suits the system's needs the most. As a final remark, we note that the interference generated by the MBS towards the SUE, neglected in this chapter for simplicity, could represent another limiting factor for the achievable spectral efficiency of the secondary like. Accordingly, in the following chapters we will take into account to move towards a more realistic representation of the considered two-tiered network.

Part II

Multiple Small-cells Deployment

Chapter 4

Centralized Co-tier Interference Management Solution

The approach proposed so far has shown how a cognitive SBS may be deployed inside the coverage area of a pre-existing OFDM MBS, without decreasing the quality of the OFDM transmission. Specifically, under ideal assumptions, the derived linear precoding strategy allows the SBS to transmit over the same band as the MBS, without causing undesired interference to a MUE connected to the macro-cell. On the other hand, the attractiveness of this result may be limited by the simplicity of the considered network layout. Accordingly, we extend the applicability of the proposed technique to more complex two-tiered network model, considering a multi-user extension of both first and second tier. In particular, we consider the presence of several SBS/SUE pairs inside the coverage area of an orthogonal frequency division multiple access (OFDMA) MBS serving a group of MUEs. Assuming absence of cooperation between the two tiers, we propose a new cascaded precoder structure to be adopted by the SBSs to cancel the cross-tier interference towards the first tier, while mitigating the co-tier interference in the second tier. From an algorithmic point of view, the second task may be carried out by means of either a centralized or a distributed approach. In this chapter, we start from the centralized case and model the second tier as a cooperative network composed of all the deployed SBSs. A centralized mechanism to mitigate the co-tier interference in the second tier is then proposed and analyzed. The distributed case will be studied in Chapter 6.

4.1 Problem Statement

Consider a two-tiered network comprised of an LTE OFDMA MBS and several cognitive SBSs operating in TDD mode, under the complete sharing approach, as in Figure 4.1. We assume that the SBSs may be connected through a backhaul, yielding a coordinated network MIMO system [13]. As typically done in first analysis of new strategies and

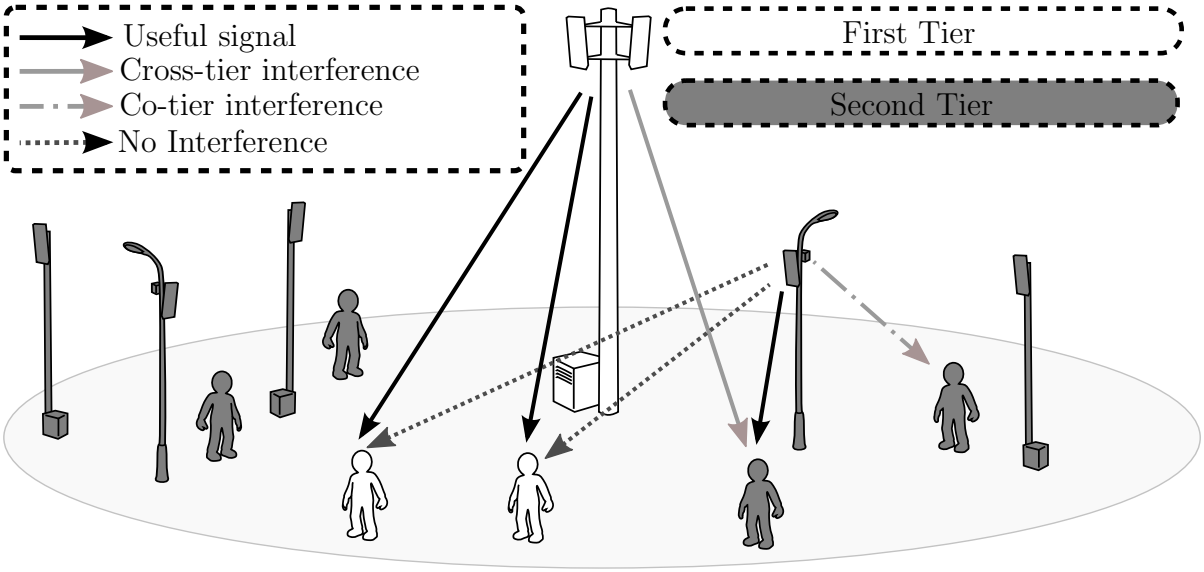

Figure 4.1: Two-tiered network DL model.

techniques in the field of cooperative or network MIMO systems, e.g.,[75, 76, 77, 78, 79, 80] and reference therein, to first characterize their performance and potential, we assume that the backhaul connecting the SBSs may deliver an infinite capacity. We aim at realizing a profitable coexistence of the devices in both tiers. Thus, a strategy must be adopted at the SBSs to cancel the cross-tier interference towards the MUEs (dashed line) and mitigate the co-tier interference. We recall that, no cooperation is established between the two tiers, hence, in contrast with what is done by the opportunistic SBSs, the MBS does not implement any interference avoidance technique to mitigate the cross-tier interference generated towards the SUEs by the OFDMA transmission.

Many techniques have been proposed in the literature for coexistence of multiple devices in such scenarios. Nevertheless, the absence of cooperation between the two tiers makes their implementation very challenging in the best case. Furthermore, as discussed in previous chapters, given the nature of the considered two-tiered network, no special decoding or signal processing should be required at the receivers to ensure the effectiveness of the adopted interference management strategy. From a practical point of view, these assumptions disqualify approaches such as IA [18], where both tiers are required to cooperate. Additionally, in these schemes the receivers usually implement specific signal processing to isolate the useful and interference signal subspaces, and require the presence of available degrees of freedom in the spatial [19], frequency [20] or time [21] domain, to realize the alignment. Opportunistic IA [36] solutions are specifically tailored for CR applications but, despite being less restrictive, they still require a varying level of cooperation between the two tiers [39, 81, 82, 40].

Alternative solutions requiring CSIT only are the so-called coordinated beamforming strategies [22, 13]. Unfortunately, even though signal processing at the receiver is usually not necessary in these strategies, cooperation between the transmitters in the two-tiered

network is required. Accordingly, the application of these strategies to the scenario considered herein is unfeasible. The solutions usually proposed in the literature to manage the cross-tier interference, in case of absence of cooperation between the tiers, are DSA based approaches, e.g, spectrum shaping [35], cooperative frequency reuse [34] to name a few. Nevertheless, these strategies highly depend on the spectrum management approach adopted in the first tier, thus if in the latter the transmissions are always performed over the full bandwidth, the transmit opportunities for the second tier are extremely low.

In this chapter, we start from these considerations and provide an extension of the previously introduced linear precoding strategy to multi-user two-tiered networks. In particular, we will construct a cascaded linear precoder made up by an inner component designed to cancel the cross-tier interference generated by the SBSs towards the first tier, and an outer component to avoid the multi-user co-tier interference interference in the second tier. We show that, not only OFDMA, but any block transmission scheme that deals with multipath interference, provides resources that can be exploited to cancel the cross-tier interference. Under this assumption, the sole requirement is perfect CSIT, used to derive the precoder. This contrasts with the aforementioned state-of-the-art techniques, that either require available time, space or frequency resources, or cooperation between the tiers to be performed.

Finally, concerning the adopted model, we note that the first tier includes only one MBS, whereas no limit is imposed on the number of deployed SBSs. The rationale for this is that if no meaningful performance could be achieved even in a single MBS case (for perfect and imperfect CSI), then there would be no use in pursuing the analysis for more complex cellular layouts including multiple MBSs, structured SBSs' positioning and practical channel models. Accordingly, herein we restrain our attention to a two-tiered network as in Figure 4.1. A discussion on the feasibility of the coexistence between the two tiers, in case of first tier composed of several macro-cells, is carried out in Chapter 5.

4.2 Signal Model

Consider the DL scenario in Figure 4.1. Let K be the number of cognitive SBSs, transmitting over the same frequency band as a pre-existing MBS serving M single-antenna MUEs. For simplicity, and without loss of generality, we assume that each SBS serves one single-antenna SUE. In fact, an extension to a multi-SUEs per SBS model could be seamlessly obtained by means of any multi-user scheduling technique [83], once the solution for single SUE case has been identified. All channel vectors $\mathbf{h} \in \mathcal{CN}(0, \mathbf{I}_{L+1}/(L+1))$, irrespective of the tier, transmitter and receiver, represent the impulse response of i.i.d. frequency-selective Rayleigh fading channels composed of $L+1$ paths.

Concerning the notation, we recall that subscript "p" refers to the first tier, while "s" refers to the second, i.e., $\mathbf{h}_{\text{sp}}^{(i,j)}$ (or $\mathbf{H}_{\text{sp}}^{(i,j)}$) represents a link from the i^{th} SBS to the j^{th} MUE. Conversely, $\mathbf{s}_{\text{s}}^{[i]}$ (or $\mathbf{H}_{\text{sp}}^{([i],j)}$) denotes a vector/matrix related to the transmission from any SBS in the second tier *except* i.

As before, we assume that the MBS adopts an M-user OFDMA based transmission of block size $N + L$ and a CP of size L, to compensate the effects of the multi-path propagation due to the considered frequency selective channel. For simplicity, uniform resource allocation of N/M subcarriers per MUE is adopted, $\mathcal{N}_j$ being the set of subcarrier indices assigned to the j^{th} MUE, i.e., one or more physical resource blocks (PRBs) in LTE/LTE-A [50, 84], with $\bigcup_{j=1}^{M} \mathcal{N}_j = \{1, \ldots, N\}$ and $\bigcap_{j=1}^{M} \mathcal{N}_j = \emptyset$. As a consequence, each MUE selects its own set of subcarriers by means of an $N \times N$ mask receiver filter $\mathbf{B}_j$, such that $\text{tr}(\mathbf{D}_j) = N/M$ and $\sum_{j=0}^{M} \mathbf{D}_j = \mathbf{I}_N$, with $[\mathbf{D}_j]_{(n,n)} = 1$ when the subcarrier n is allocated to the j^{th} MUE and zero otherwise. Let $\mathbf{F} \in \mathbb{C}^{N \times N}$ be a unitary DFT matrix as defined in Chapter 2 and $\mathbf{A}$ a $(N + L) \times N$ CP insertion matrix given by (2.2).

For the sake of compactness, let us directly include the CP removal operation in the channel matrix representing the link from the MBS to the j^{th} MUE, defined as $\mathcal{T}(\mathbf{h}_{\text{pp}}^{(1,j)}) \in \mathbb{C}^{N \times (N+L)}$, where $\mathcal{T}(\cdot)$ is a Toeplitz operator that returns a Toeplitz matrix built from a given vector, i.e., for $\mathbf{h} = [h(0) \cdots h(L)]$:

$$\mathcal{T}(\mathbf{h}) = \begin{bmatrix} h(L) & \cdots & h(0) & 0 & \cdots & 0 \\ 0 & \ddots & & \ddots & \ddots & \vdots \\ \vdots & \ddots & \ddots & & \ddots & 0 \\ 0 & \cdots & 0 & h(L) & \cdots & h(0) \end{bmatrix}. \tag{4.1}$$

Concerning the second tier, we assume the SBSs adopt a block transmission scheme as done in previous chapters, detailed in Section 4.3.1. Additionally, we will still consider that an SUE is not different from an MUE with respect to the reception chains, being distinguished merely by the association point (MBS or SBS). Therefore, like the MUEs, the SUEs discard the leading L symbols and perform a DFT at the reception. Naturally, no mask filter is needed at k^{th} SUE, given that, in general, no OFDMA-based transmission can be performed in the second tier without generating cross-tier interference towards the MUEs. Let $\mathcal{T}(\mathbf{h}_{\text{sp}}^{(i,j)}) \in \mathbb{C}^{N \times (N+L)}$ be the matrix representing the channel from the i^{th} SBS to the j^{th} MUE, constructed from the $\mathbf{h}_{\text{sp}}^{(i,j)}$ channel coefficients. The matrices $\mathcal{T}(\mathbf{h}_{\text{ps}}^{(1,k)})$, $\mathcal{T}(\mathbf{h}_{\text{ss}}^{(i,k)}) \in \mathbb{C}^{N \times (N+L)}$, representing the link from MBS and the i^{th} SBS to the k^{th} SUE respectively, can be similarly constructed.

Now, let $\mathbf{y}_{\text{p}}^{(j)}$, $\mathbf{y}_{\text{s}}^{(k)}$ be the received N-sized vector at the j^{th} MUE and k^{th} SUE, respectively, $\mathbf{s}_{\text{p}}$ be the MBS input vector of size N, composed of M individual zero mean, unit norm symbol vectors $\mathbf{s}_{\text{p}}^{(j)}$, $j \in [1, M]$, and $\mathbf{x}_{\text{s}}^{(i)}$ be the transmit vector at the i^{th} SBS, of size $N + L$, detailed later for clarity. Then, if we let $\mathbf{n}_{\text{p}}^{(j)}$, $\mathbf{n}_{\text{s}}^{(k)} \sim \mathcal{CN}(0, \sigma^2 \mathbf{I}_N)$ be two

AWGN vectors, the received signals at the j^{th} MUE and k^{th} SUE can be expressed as

$$\mathbf{y}_{\mathrm{p}}^{(j)} = \mathbf{D}_j\mathbf{F}\left(\mathcal{T}(\mathbf{h}_{\mathrm{pp}}^{(1,j)})\mathbf{A}\mathbf{F}^{-1}\mathbf{s}_{\mathrm{p}} + \sum_{i=1}^{K}\mathcal{T}(\mathbf{h}_{\mathrm{sp}}^{(i,j)})\mathbf{x}_{\mathrm{s}}^{(i)} + \mathbf{n}_{\mathrm{p}}^{(j)}\right)$$

$$\mathbf{y}_{\mathrm{s}}^{(k)} = \mathbf{F}\left(\mathcal{T}(\mathbf{h}_{\mathrm{ss}}^{(i,k)})\mathbf{x}_{\mathrm{s}}^{(i)} + \sum_{l\neq i}^{K}\mathcal{T}(\mathbf{h}_{\mathrm{ss}}^{(l,k)})\mathbf{x}_{\mathrm{s}}^{(l)} + \mathcal{T}(\mathbf{h}_{\mathrm{ps}}^{(1,k)})\mathbf{A}\mathbf{F}^{-1}\mathbf{s}_{\mathrm{p}} + \mathbf{n}_{\mathrm{s}}^{(k)}\right).$$

Note that, in (4.2), we represented $\mathbf{y}_{\mathrm{s}}^{(k)}$ by separating the useful signal received from the i^{th} SBS from the co-tier interference component generated by the remaining $K-1$ SBSs, operating in the second tier. For $\mathbf{y}_{\mathrm{p}}^{(j)}$, the all of the second tier transmitted signal is seen as interference.

To simplify the subsequent analysis, consider an equivalent aggregate model that includes all users in the system. Let us start by looking at the first tier. By summing up all the contributions of the MUEs, orthogonal in the frequency domain, the equivalent channel matrix from the MBS to the MUEs is

$$\mathbf{H}_{\mathrm{pp}} = \sum_{j=1}^{M}\mathbf{D}_j\mathbf{F}\mathcal{T}(\mathbf{h}_{\mathrm{pp}}^{(1,j)})\mathbf{A}\mathbf{F}^{-1} \in \mathbb{C}^{N\times N}. \tag{4.1}$$

Let us now define

$$\mathbf{H}_{\mathrm{sp}}^{(i,\cdot)} = \sum_{j=1}^{M}\mathbf{D}_j\mathbf{F}\mathcal{T}(\mathbf{h}_{\mathrm{sp}}^{(i,j)}) \in \mathbb{C}^{N\times(N+L)}, \tag{4.1}$$

then the equivalent aggregated interference channel from the SBSs to the MUEs is constructed as

$$\mathbf{H}_{\mathrm{sp}} = \left[\ \mathbf{H}_{\mathrm{sp}}^{(1,\cdot)}, \ldots, \mathbf{H}_{\mathrm{sp}}^{(K,\cdot)}\ \right] \in \mathbb{C}^{N\times K(N+L)}. \tag{4.2}$$

Switching our focus to the second tier, let $\mathbf{H}_{\mathrm{ss}}^{(i,k)} = \mathcal{T}(\mathbf{h}_{\mathrm{ss}}^{(i,k)})$. Then, by defining

$$\widetilde{\mathbf{H}}_{\mathrm{ss}} = \begin{bmatrix} \mathbf{H}_{\mathrm{ss}}^{(1,1)} & \cdots & \mathbf{H}_{\mathrm{ss}}^{(1,K)} \\ \mathbf{H}_{\mathrm{ss}}^{(2,1)} & \cdots & \mathbf{H}_{\mathrm{ss}}^{(2,K)} \\ \vdots & \ddots & \vdots \\ \mathbf{H}_{\mathrm{ss}}^{(K,1)} & \cdots & \mathbf{H}_{\mathrm{ss}}^{(K,K)} \end{bmatrix} \in \mathbb{C}^{KN\times K(N+L)}, \tag{4.2}$$

the equivalent aggregated channel from the SBSs to the SUEs can be written as

$$\mathbf{H}_{\mathrm{ss}} = (\mathbf{I}_K \otimes \mathbf{F})\widetilde{\mathbf{H}}_{\mathrm{ss}} \in \mathbb{C}^{KN\times K(N+L)}, \tag{4.2}$$

with $\otimes$ operator denoting the Kronecker product. The interfering link from the MBS to the SUEs is obtained by following the same approach. Let $\mathbf{H}_{\mathrm{ps}}^{(1,k)} = \mathcal{T}(\mathbf{h}_{\mathrm{ps}}^{(1,k)})\mathbf{A}\mathbf{F}^{-1} \in \mathbb{C}^{N\times N}$. By defining

$$\widetilde{\mathbf{H}}_{\mathrm{ps}} = \begin{bmatrix} \mathbf{H}_{\mathrm{ps}}^{(1,1)} \\ \mathbf{H}_{\mathrm{ps}}^{(1,2)} \\ \vdots \\ \mathbf{H}_{\mathrm{ps}}^{(1,K)} \end{bmatrix} \in \mathbb{C}^{KN\times N}, \tag{4.2}$$

we can write the equivalent aggregated channel as

$$\mathbf{H}_{\mathrm{ps}} = (\mathbf{I}_K \otimes \mathbf{F})\widetilde{\mathbf{H}}_{\mathrm{ps}} \in \mathbb{C}^{KN \times N}. \tag{4.2}$$

Now, we define $\mathbf{y}_{\mathrm{p}} = \sum_{j=1}^{M} \mathbf{y}_{\mathrm{p}}^{(j)}$ as the aggregated received vector at the MUEs of size N, and $\mathbf{y}_{\mathrm{s}} \triangleq [\mathbf{y}_{\mathrm{s}}^{(1)\mathrm{T}}, \ldots, \mathbf{y}_{\mathrm{s}}^{(K)\mathrm{T}}]^{\mathrm{T}}$ as the aggregated received vector at the SUEs of size KN. We also define $\mathbf{x}_{\mathrm{s}} \triangleq [\mathbf{x}_{\mathrm{s}}^{(1)\mathrm{T}}, \ldots, \mathbf{x}_{\mathrm{s}}^{(K)\mathrm{T}}]^{\mathrm{T}}$ as the aggregated transmit vector at the SBSs, of size $K(N+L)$. The equivalent signal model is then obtained as

$$\mathbf{y}_{\mathrm{p}} = \mathbf{H}_{\mathrm{pp}}\mathbf{s}_{\mathrm{p}} + \mathbf{H}_{\mathrm{sp}}\mathbf{x}_{\mathrm{s}} + \mathbf{n}_{\mathrm{p}} \tag{4.3}$$

$$\mathbf{y}_{\mathrm{s}} = \mathbf{H}_{\mathrm{ss}}\mathbf{x}_{\mathrm{s}} + \mathbf{H}_{\mathrm{ps}}\mathbf{s}_{\mathrm{p}} + (\mathbf{I}_K \otimes \mathbf{F})\mathbf{n}_{\mathrm{s}}. \tag{4.4}$$

Note that, in (4.3) and (4.4), $\mathbf{n}_{\mathrm{p}} = \sum_{j=1}^{M} \mathbf{D}_j \mathbf{F} \mathbf{n}_{\mathrm{p}}^{(j)}$ and $\mathbf{n}_{\mathrm{s}} = [\mathbf{n}_{\mathrm{s}}^{(1)\mathrm{T}}, \ldots, \mathbf{n}_{\mathrm{s}}^{(K)\mathrm{T}}]^{\mathrm{T}}$ are the aggregated AWGN vectors of the first and second tier, of size N and KN respectively.

4.3 Precoder Design

As assumed in Chapter 3, the studied two-tiered network is framed according to the cognitive overlay paradigm [29]. As a consequence, the opportunistic transmission performed by the SBSs must protect the MUEs from any undesired interference. By looking at (4.3), this implies

$$\mathbf{H}_{\mathrm{sp}}\mathbf{x}_{\mathrm{s}} = \mathbf{0}_{N \times 1}. \tag{4.4}$$

The SBSs possess no information about unused resources (time, space or frequency) in the first tier and each MUE is a single antenna device. This explains why the previously discussed traditional techniques to design an interference-free transmission can not be implemented in the considered scenario.

Let $\mathbf{s}_{\mathrm{s}}^{(i)}$ be the input symbol vector at the i^{th} SBS, detailed later for clarity. Consequently, let $\mathbf{s}_{\mathrm{s}} \triangleq [\mathbf{s}_{\mathrm{s}}^{(1)\mathrm{T}}, \ldots, \mathbf{s}_{\mathrm{s}}^{(K)\mathrm{T}}]^{\mathrm{T}}$ be the aggregated SBSs' input symbol vector, such that

$$\mathbf{x}_{\mathrm{s}} = \mathbf{E}\mathbf{s}_{\mathrm{s}} \tag{4.4}$$

becomes its precoded version through a linear precoder $\mathbf{E}$, whose design is discussed in the following. Then (4.3) can be rewritten as

$$\mathbf{H}_{\mathrm{sp}}\mathbf{E} = \mathbf{0}_{N \times 1}. \tag{4.4}$$

If we assume that each SBS may independently precode its input vector to cancel the

interference towards the MUEs, we can express $\mathbf{E}$ as the matrix direct sum[1] [85] of K precoders

$$\mathbf{E} = \bigoplus_{i=1}^{K} \mathbf{E}_i, \tag{4.4}$$

where $\mathbf{E}_i$ is the precoder at the i^{th} SBS. It is straightforward to see that when the following holds

$$\mathbf{H}_{\text{sp}}^{(i,\cdot)} \mathbf{E}_i = \mathbf{0}_{N \times L}, \quad \forall i \in [1, K], \tag{4.4}$$

(4.3) is always satisfied, if perfect knowledge of $\mathbf{H}_{\text{sp}}^{(i,\cdot)}$ is available at the i^{th} SBSs. Thus, the SBSs do not need to share any information related to the cross-tier interference channels towards the MUEs to create $\mathbf{E}$. This results in a simpler architecture as well as in a lower backhaul signaling. As a consequence, we can focus on the i^{th} SBS to devise $\mathbf{E}_i$ and then apply (4.3) to find the desired overall precoder. Moreover, we note that a CSI measurement is valid only throughout the coherence time of the channel of interest, e.g., $\mathbf{H}_{\text{sp}}^{(i,\cdot)}$. Therefore, we must seek for one-shot strategies that do not require iterative procedures between the SBSs and the SUEs/MUEs to derive the precoding/decoding matrices, such as the IA-based solutions in [39] and references therein. At this stage, we assume perfect CSIT related to the interfering links from the SBSs towards the MUEs. The impact of imperfect CSIT will be analyzed later.

4.3.1 Single SBS/SUE Precoder Design

We first focus on the pair given by the i^{th} SBS and its served SUE (denoted with k for clarity), thus a scenario as in Figure 4.2, i.e., $K = 1$.

By looking at (4.3), we note that, if a suitable interference nulling precoder exists, then it must lie within the kernel of $\mathbf{H}_{\text{sp}}^{(i,\cdot)}$. Note that, as discussed in Chapters 2 and 3, the non-emptiness of the kernel is guaranteed by the block transmission structure adopted in the first tier, i.e., OFDMA, hence a solution to (4.3) can always be found. In fact, the redundancy introduced at the MBS, to combat the multipath interference, ensures that $\text{rank}\left(\mathbf{H}_{\text{sp}}^{(i,\cdot)}\right) = N$, thus $\dim\left(\ker\left(\mathbf{H}_{\text{sm}}^{(i,\cdot)}\right)\right) = L$. Now, let $\mathbf{H}_{\text{sp}}^{(i,\cdot)} = \mathbf{L}_{\text{sp}}^{(i,\cdot)} \mathbf{Q}_{\text{sp}}^{(i,\cdot)}$ be the LQ decomposition [61] of the equivalent channel matrix representing the interfering link between the i^{th} SBS and the MUEs, where $\mathbf{L}_{\text{sp}}^{(i,\cdot)} \in \mathbb{C}^{N \times (N+L)}$ is a lower triangular matrix and $\mathbf{Q}_{\text{sp}}^{(i,\cdot)} \in \mathbb{C}^{(N+L) \times (N+L)}$ is a unitary matrix given by

$$\mathbf{Q}_{\text{sp}}^{(i,\cdot)} \triangleq \left[\, \mathbf{q}_1 \mid \mathbf{q}_2 \mid \cdots \mid \mathbf{q}_{N+L} \, \right]. \tag{4.4}$$

[1] Let $\mathcal{W} = \{\mathbf{W}_1, \ldots, \mathbf{W}_K\}$ be a set of K matrices $\mathbf{W}_i \in \mathbb{C}^{N_i \times M_i}$, $\forall i \in [1, K]$. The matrix direct sum of the matrices in $\mathcal{W}$ is denoted $\bigoplus_{i=1}^{K} \mathbf{W}_i$ and is defined as $\bigoplus_{i=1}^{K} \mathbf{W}_i = \begin{bmatrix} \mathbf{W}_1 & \mathbf{0} & \ldots & \mathbf{0} \\ \mathbf{0} & \mathbf{W}_2 & \ldots & \mathbf{0} \\ \vdots & \ddots & \ddots & \vdots \\ \mathbf{0} & \ldots & \mathbf{0} & \mathbf{W}_K \end{bmatrix}$.

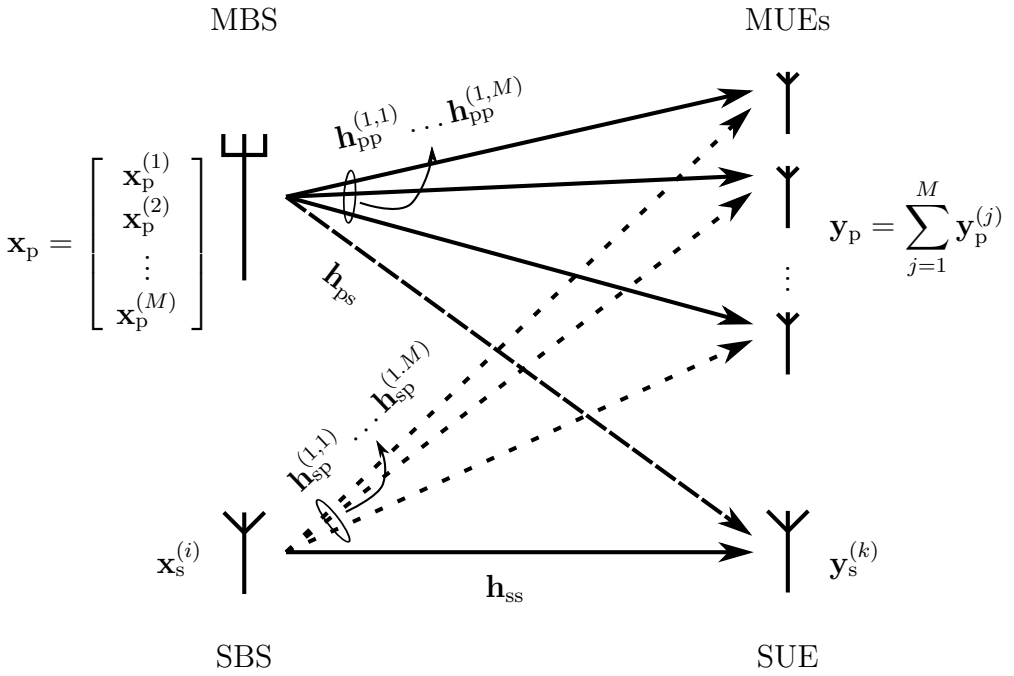

Figure 4.2: OFDMA DL interference channel model, single SBS.

By construction, we know that the last L orthonormal columns of $\mathbf{Q}_\mathrm{sp}^{(i,\cdot)\mathrm{H}}$ lie within $\ker\left(\mathbf{H}_\mathrm{sp}^{(i,\cdot)}\right)$. Therefore, if we define

$$\mathbf{E}_i \triangleq \left[\ \mathbf{q}_{N+1} \mid \cdots \mid \mathbf{q}_{(N+L)-1} \mid \mathbf{q}_{N+L}\ \right] \in \mathbb{C}^{(N+L)\times L}, \tag{4.4}$$

we have an semi-unitary (thus optimal) precoder that fulfills (4.3). If we substitute (4.3.1) into (4.3), we see that the precoder $\mathbf{E}$ is obtained as a $K(N+L) \times KL$ matrix, whose dimension determines the size of the previously defined aggregated zero mean, unit norm SBSs' input symbol vector $\mathbf{s}_\mathrm{s}$, i.e., KL.

We first focus on the macro-cell. If we plug (4.3) into (4.3), then we obtain

$$\mathbf{y}_\mathrm{p} = \mathbf{H}_\mathrm{pp}\mathbf{s}_\mathrm{p} + \boldsymbol{\nu}_\mathrm{p}, \tag{4.4}$$

realizing the desired cross-tier interference cancelation. Note that, in (4.3.1), $\boldsymbol{\nu}_\mathrm{p} \in \mathcal{CN}(0, \sigma_n^2\mathbf{I}_N)$ is the DFT of the AWGN vector $\mathbf{n}_\mathrm{p}$, having the same size and statistic.

Concerning the received signal at the considered SUE, we can rewrite (4.2) as

$$\mathbf{y}_\mathrm{s}^{(k)} = \mathbf{F}\mathbf{H}_\mathrm{ss}^{(i,k)}\mathbf{E}_i\mathbf{s}_\mathrm{s}^{(i)} + \mathbf{F}\mathbf{H}_\mathrm{ps}^{(1,k)}\mathbf{s}_\mathrm{p} + \boldsymbol{\nu}_\mathrm{s}^{(k)}, \tag{4.4}$$

where the co-tier interference component is absent, being the focus of the section on a single SBS/SUE pair. In (4.3.1), $\mathbf{E}_i$ is a linear precoder as defined in (4.3.1), $\mathbf{H}_\mathrm{ps}^{(1,k)}\mathbf{s}_\mathrm{p}$ is the cross-tier interference coming from the MBS and $\boldsymbol{\nu}_\mathrm{s}^{(k)} \in \mathcal{CN}(0, \sigma_n^2\mathbf{I}_N)$ is the DFT of $\mathbf{n}_\mathrm{s}^{(k)}$.

At this stage, the dimension of $\mathbf{s}_{\mathrm{s}}^{(i)}$, zero mean, unit norm input symbol vector at the i^{th} SBS, is clear. In particular, the size of $\mathbf{s}_{\mathrm{s}}$, i.e., KL, implies that $\mathbf{s}_{\mathrm{s}}^{(i)}$ is an L-sized vector. Consequently, each SBS has an implicit upper bound (L) on the number of input symbols that can be precoded by $\mathbf{E}_i$. This, together with the perfect CSIT assumption, is the cost of the cross-tier interference cancelation constraint induced by the overlay cognitive approach. The absence of cross-tier interference towards the first-tier is then guaranteed if perfect CSIT is available at the SBSs, regardless of the number of MUEs served by the MBS. Remarkably, in this scheme, a change in the nature of the transmission performed by the MBS (OFDM or OFDMA) does not require a different interference cancelation approach, but only the construction of a suitable equivalent channel matrix, for which the LQ decomposition can always be computed.

Furthermore, we remark that unlike other interference management schemes that exploit the spatial degrees of freedoms by the use of multiple antennas, i.e. zero forcing beamforming (ZFBF) [86], and/or special decoding strategies at the receiver, i.e., IA, the proposed technique requires only one antenna per SBS and MUE and legacy OFDM decoding at the latter. In fact, the interference towards the first tier is canceled by adopting a precoder $\mathbf{E}_i$ that opportunistically exploits the redundancy introduced by the MBS to combat IBI, e.g. the CP. In the following, we start from these findings to analyze the multi SBS/SUE scenario described in Section 4.2.

Finally, we note that, the complexity of the LQ decomposition of an $N \times (N+L)$ matrix, e.g $\mathbf{H}_{\mathrm{sp}}^{(i,\cdot)}$, is $\mathcal{O}(N(N+L)^2 - (N+L)N^2 + (N+L)^3)$ [61]. Consequently, a centralized approach to find the null space of the aggregated cross-tier interference channel matrix, i.e., $\mathbf{H}_{\mathrm{sp}}$ in (4.2), would require an LQ decomposition of complexity $\mathcal{O}(N[K(N+L)]^2 - [K(N+L)]N^2 + [K(N+L)]^3)$, growing exponentially with K. Therefore, the distributed nature of the proposed $\mathbf{E}_i$ precoding not only reduces the backhaul signaling requirements, but dramatically decreases the complexity of the processing in the second tier, where K low complexity LQ decompositions are performed in parallel to derive the K individual precoders.

4.3.2 Multi SBS/SUE Precoder Design

As seen in Section 4.3.1, the SBSs separately design the precoders $\mathbf{E}_i$, $\forall i \in [1, K]$, such that the overall precoder $\mathbf{E}$ as shown in (4.3) successfully satisfies (4.3). As a consequence, we can rewrite the signal model in (4.3) and (4.4) as

$$\mathbf{y}_{\mathrm{p}} = \mathbf{H}_{\mathrm{pp}}\mathbf{s}_{\mathrm{p}} + \mathbf{n}_{\mathrm{p}} \tag{4.5}$$

$$\mathbf{y}_{\mathrm{s}} = \mathbf{H}_{\mathrm{ss}}\mathbf{E}\mathbf{s}_{\mathrm{s}} + \mathbf{H}_{\mathrm{ps}}\mathbf{s}_{\mathrm{p}} + \boldsymbol{\nu}_{\mathrm{s}}., \tag{4.6}$$

with $\boldsymbol{\nu}_{\mathrm{s}} = [\boldsymbol{\nu}_{\mathrm{s}}^{(1)\mathrm{T}}, \ldots, \boldsymbol{\nu}_{\mathrm{s}}^{(1)\mathrm{T}}]^{\mathrm{T}}$. We focus on the second tier and, for clarity, we simplify the notation by introducing

$$\overline{\mathbf{H}}_{\mathrm{ss}} = \mathbf{H}_{\mathrm{ss}}\mathbf{E} \in \mathbb{C}^{KN \times KL}. \tag{4.6}$$

The structure of the received signal is the same for any SUE, hence we can rewrite (4.3.1) for the multi-user case as

$$\mathbf{y}_{\mathrm{s}}^{(k)} = \mathbf{F}\mathbf{H}_{\mathrm{ss}}^{(i,k)}\mathbf{s}_{\mathrm{s}}^{(i)} + \overline{\mathbf{H}}_{\mathrm{ss}}^{([i],k)}\mathbf{s}_{\mathrm{s}}^{[i]} + \mathbf{F}\mathbf{H}_{\mathrm{ps}}^{(1,k)}\mathbf{s}_{\mathrm{p}} + \boldsymbol{\nu}_{\mathrm{s}}^{(k)}, \tag{4.6}$$

in which we identify a useful component, two interfering terms and the thermal noise. In (4.3.2), $\overline{\mathbf{H}}_{\mathrm{ss}}^{([i],k)}\mathbf{s}_{\mathrm{s}}^{[i]} \in \mathbb{C}^{N\times(K-1)L}$ represents the co-tier interference experienced by each SUE. Clearly, the performance of the second tier hinges on the mutual interference between the SBSs and is strongly interference limited as K increases. Note that, as in the single user case, the absence of cooperation between the two tiers implies that the MBS' interference on the SUEs is always present. Consequently, in this scenario, each SUE deals with a stronger interference if compared to the single SBS case in Section 4.3.1. To address this issue we exploit the cooperative nature of the SBSs, that may communicate over an infinite-capacity backhaul realizing a coordinated network MIMO system, as assumed in Section 4.1. Despite being hardly realistic, this assumption is usually made in similar scenarios for first studies on newly-proposed algorithms, to focus on the ultimate bounds of such solutions and achieve a better understanding of their potential [13, 78]. The cooperating SBSs can be therefore modeled as a MIMO broadcast channel (MIMO-BC), whose capacity is given by DPC [87]. However, DPC is usually not considered an appropriate scheme for real applications, due to its extremely challenging implementation. DPC involves successive encoding and decoding operations at the transmitter and receiver, respectively, thus significant additional complexity is required at both sides of the transmission. The problem of finding practical dirty paper codes that approach the capacity limit is still unsolved [88]. Because of its complexity, many suboptimal but linear strategies have been introduced lately. Accordingly, we propose to address the co-tier interference problem at the cooperating SBSs by adding one linear suboptimal precoding layer, resulting in an overall cascaded precoder, as detailed in the following sections.

4.3.3 Dimensionality Problem and Linear Techniques

Having solved the cross-tier interference problem, now we devote our attention to mitigating the co-tier interference by means of a linear suboptimal precoder. As such, in (4.6), we focus on the SBSs' transmission by isolating the term $\overline{\mathbf{H}}_{\mathrm{ss}}$ of dimension $KN \times KL$, as defined in (4.3.2). Note that, in any block transmission system, the added redundancy L to the block of N useful symbols is always such that $\frac{L}{N} < 1$, for matters of efficiency. As seen in Section 4.3.1, the proposed approach imposes a dimensionality constraint to the transmitters in the second-tier since each SBS precodes up to L input symbols while each SUE receives N symbols. This implies that a direct application of techniques such as ZFBF or block diagonalization (BD) [89] is not possible, since both require that the number of columns (transmit dimensions) of the channel matrix be bigger or equal than the number of rows (receive dimensions). Solutions base on regularized inverse beamforming (RIBF) [90] are applicable, but they generally achieve poor performance at high SNR, due to the aforementioned dimensionality issue ($N > L$ received symbols) that yields a

very poor condition number to the equivalent channel representation built upon Toeplitz matrices. Similar results are achieved by matched filter (MF) precoding [91] strategies, largely suboptimal at high SNR. It is known from [92], and for the multiple beams case from [93], that opportunistic random beamforming (ORBF) based techniques are able to yield the optimal capacity scaling of $KL \log\log KN$ in dense networks with a large number of receivers. Unfortunately, in our scenario the ratio $\frac{N}{L}$ is such that we can not achieve good performance using these techniques.

In general, most of the results in the literature regarding linear precoding techniques under given optimization criteria assume only one antenna/symbol at the receiver. For this reason, a direct extension of these techniques to our scenario is not possible. In order to overcome this limitation, algorithms that consider multiple symbols/antennas at each receiver such as successive minimum mean square error (SMMSE) precoding [94] or iterative regularized block diagonalization (IRBD) [95], have been proposed for multi-user networks. The higher diversity gain experienced when adopting these techniques is due to the suppression of the interference only between the symbols received by two different receivers. These algorithms perform better than other techniques that rely on the single antenna/symbol assumption. On the other hand, they require a joint receiver decoding, with a consequent increase in the complexity of the receivers' architecture.

Simpler solutions to deal with an arbitrary number of dimensions at each receiver are user/antenna selection based algorithms. It is known that by scheduling only a subset of antennas or eigenmodes [89] to be served using a classical ZFBF, the achievable sum-rate is asymptotically optimal [96]. In spite of this, the condition for the asymptotic optimality is never met in the considered OFDM-based two-tiered network. As a consequence, neither an exhaustive search of the optimal subset nor a faster and suboptimal greedy selection algorithm [97] can achieve good results in our scenario.

Looking at the schemes presented so far, we note that the inherent dimensionality constraint limits the performance of the second tier, in terms of both achievable sum-rate and complexity of the SBSs/SUEs. Starting from this consideration, we propose a low complexity solution to overcome the dimensionality constraint and mitigate the co-tier interference in the following section.

4.3.4 RIBF Flexible Network Solution

Consider a flexible approach to the second tier deployment in which the network designer can modify the dimensionality of the system by installing more antennas at each SBS/SUE, or alternatively by increasing the SBS' density. We let γ_{tx}, γ_{rx} be two parameters such that $\gamma_{tx}L, \gamma_{rx}N \in \mathbb{N}$ are the number of transmit and receive dimensions respectively, with L and N fixed due to the OFDMA symbol structure. This way, the network designer can tune γ_{tx} and γ_{rx} to capitalize on the flexibility of the model, effectively changing the number of available channels for the transmission, and obtaining different operating scenarios. For instance, when $\gamma_{tx} = 1$ and γ_{rx} grows large, the system experiences a large increase of the number of receive dimensions, i.e., implying a greater

number of SUEs (or SUEs' antennas) from which the best ones to serve are selected, and this represents the condition under which ORBF is optimal (a very "tall" overall channel matrix). Conversely, if γ_{rx} is kept constant ($\gamma_{rx} = 1$ for simplicity) and we let γ_{tx} increase, the SBSs can exploit the abundance of transmit dimensions to achieve a higher transmit diversity, thanks to the greater number of considered channels. Another interesting configuration is given by $\gamma_{tx} = N$ and $\gamma_{rx} = L$, that is a network where the number of transmit and receive dimensions coincides, i.e., channel inversion based techniques such as ZFBF and RIBF become efficient in terms of degrees of freedom exploitation. These strategies do not require iterative or greedy algorithms to be implemented, thus represent an attractive solution to manage the co-tier interference by means of a one-shot technique. In particular, it is known from [90] that RIBF offers better performance for a wider class of channels, by regularizing the matrix to be inverted whenever its condition number is poor. Consequently, in the following we will focus on RIBF, and we note that it can be implemented effectively in the considered scenario if the dimensionality constraint is overcome, thus if the following holds

$$\gamma_{tx} L \geq \gamma_{rx} N. \tag{4.6}$$

Now, without loss of generality, we let $\gamma_{rx} = 1$ and γ_{tx} increase. In particular, we note that this preserves the legacy number of antennas per SUE, i.e., 1, and their disjoint decoding strategy. Differently from the strategy adopted in Chapter 3 when introducing CIA for the simple 2×2 scenario analyzed, herein we consider a uniform power allocation strategy due to the large number of SBSs (or antennas per SBS) involved in the process. As a consequence, the computational burden for the SBSs is reduced.

We remark that, thanks to the γ_{rx} and γ_{tx} tuning, the second tier is characterized by a greater number of channels. Therefore, in the new setup, $\mathbf{s}_\mathrm{s}$ is a vector of size $\gamma_{tx} KL$, $\mathbf{E} \in \mathbb{C}^{\gamma_{tx} K(N+L) \times \gamma_{tx} KL}$ and $\overline{\mathbf{H}}_\mathrm{ss} \in \mathbb{C}^{KN \times \gamma_{tx} KL}$. At this stage, we can define

$$\mathbf{\Phi} = \overline{\mathbf{H}}_\mathrm{ss}^\mathrm{H} \left(\frac{\sigma_n^2}{P_\mathrm{s}} \mathbf{I}_{KN} + \overline{\mathbf{H}}_\mathrm{ss} \overline{\mathbf{H}}_\mathrm{ss}^\mathrm{H} \right)^{-1} \tag{4.6}$$

as the joint RIBF precoder, with $\mathbf{\Phi} \in \mathbb{C}^{\gamma_{tx} KL \times KN}$. Then, if we let $\mathbf{u}_\mathrm{s} \in \mathbb{C}^{KN \times 1}$ be a new aggregated SBSs' input symbol vector, such that $\mathbf{s}_\mathrm{s} = \mathbf{\Phi} \mathbf{u}_\mathrm{s}$ we can rewrite the signal model given by (4.5) and (4.6) as

$$\mathbf{y}_\mathrm{p} = \mathbf{H}_\mathrm{pp} \mathbf{s}_\mathrm{p} + \mathbf{n}_\mathrm{p} \tag{4.7}$$

$$\mathbf{y}_\mathrm{s} = \mathbf{H}_\mathrm{ss} \mathbf{W} \mathbf{u}_\mathrm{s} + \mathbf{H}_\mathrm{ps} \mathbf{x}_\mathrm{p} + \boldsymbol{\nu}_\mathrm{s}, \tag{4.8}$$

where

$$\mathbf{W} = \frac{\mathbf{E}\mathbf{\Phi}}{\sqrt{\mathrm{tr}(\mathbf{E}\mathbf{\Phi}\mathbf{\Phi}^\mathrm{H}\mathbf{E}^\mathrm{H})}} \in \mathbb{C}^{\gamma_{tx} K(N+L) \times KN} \tag{4.8}$$

is the overall normalized cascaded precoder, such that $\mathrm{tr}(\mathbf{W}^\mathrm{H}\mathbf{W}) = 1$. We emphasize that, the cascaded precoder structure is intrinsically different from that of the precoder introduced in Chapter 3, even for the $K, M = 1$ case. In fact, the use of an outer linear precoding scheme, while preserving the interference cancelation condition towards the first tier, substantially changes the dimensionality of the system.

4.4 Numerical Analysis

In this section, we present a numerical performance analysis of the proposed technique. Note that, according to Section 4.2 and 4.3, the matrices $\mathbf{H}_{\text{sp}}$ and $\mathbf{E}$ are not composed of i.i.d. random entries, but are strongly structured. No closed form of their eigenvalue/eigenvector distribution is available, and a purely theoretical performance analysis can not be carried out. Consequently, we proceed by means of Monte Carlo based simulations of the considered DL scenario. Specifically, we consider an OFDMA/LTE MBS serving a macro-cell hosting $M = 4$ MUEs, and second tier composed of cooperative SBSs adopting the proposed cascaded precoder to serve a group of SUEs. For simplicity, we consider the least resource-demanding extended mode proposed by the standard [50], and characterized by $N = 128$ subcarriers, a CP of length $L = 32$, for a total bandwidth of 1.92 MHz. Noise and channel vectors are generated as described in Section 4.2. We assume that perfect CSI is available at the SBSs. The impact of noisy channel estimations, yielding imperfect CSIT, on the sum-rate of the two-tiered network is studied in Chapter 5. Note that, in the first part of the section, we do not consider any interference from the MBS to the SUEs to isolate the effect of the cascaded precoder on second tier's performance. In particular, this assumption is crucial to evaluate the effect of the imperfect channel estimation at the SBSs on the effectiveness of both inner and outer interference management precoders. Conversely, the cross-tier interference generated by the MBS towards the SUEs is taken into account in the second part of the section, when evaluating the overall achievable sum-rate of the two-tiered network. Finally, for the sake of compactness of the notation in our plots, we introduce the *load rate* β as the ratio between the number of transmit and receive dimensions as defined in Section 4.3.4, and given by

$$\beta = \frac{\gamma_{tx} L}{\gamma_{rx} N}. \tag{4.8}$$

4.4.1 Performance of the Second Tier

Consider the presence of $K = 3$ SBSs/SUEs in the second tier. Let us assume that the SBSs null the interference towards the MUEs by (4.3.1), then the upper bound capacity $C_{\text{DPC}}^{\text{SUM}}$ achieved by adopting DPC, for a uniform power allocation is given by [59]

$$C_{\text{DPC}}^{\text{SUM}} = \frac{\mathcal{B}}{N+L} \mathbb{E}\left[\log_2 \left| \mathbf{I}_{KN} + \left(\frac{N+L}{\sigma^2 L \gamma_{tx}} \right) P_{\text{s}} \overline{\mathbf{H}}_{\text{ss}} \overline{\mathbf{H}}_{\text{ss}}^{H} \right| \right], \tag{4.8}$$

where $\mathcal{B}$ is the considered bandwidth and P_{p} and $P_{\text{s}} = \frac{P_{\text{p}}}{K}$ are the power per transmit symbol at the MBS and at each SBS, respectively. Note that, the adopted model implies that the total transmit power per tier is the same, i.e., $P_{\text{p}}(N + L)$, and the larger K becomes, the lower the power budget available at each SBS. This is imposed to model the second tier in compliance with the lower energy consumption requirements that the SBSs will likely have w.r.t. a legacy MBS in 4G networks [3].

The perfect CSIT assumption ensures that the achievable sum-rate of the first tier is unaltered by the presence of a second tier composed of SBSs adopting the interference cancelation precoder, thus we focus on the performance of the second tier. Let us assume that instead of computing the outer precoder $\mathbf{\Phi}$ according to Section 4.3.4, the SBSs may mitigate the co-tier interference in the second tier by computing $\mathbf{\Phi}$ according to the strategies discussed in Section 4.3.3, including the semi-orthogonal user selection ZFBF (SUS-ZFBF) algorithm [96]. Accordingly, in Figure 4.3, $C^{\text{SUM}}_{\text{DPC}}$ is compared to C^{SUM}, achievable ergodic sum-rate for a cascaded precoder where $\mathbf{\Phi}$ is computed by means of the techniques discussed in Section 4.3.3, for SNR $\in [0, 30]$. This result confirms

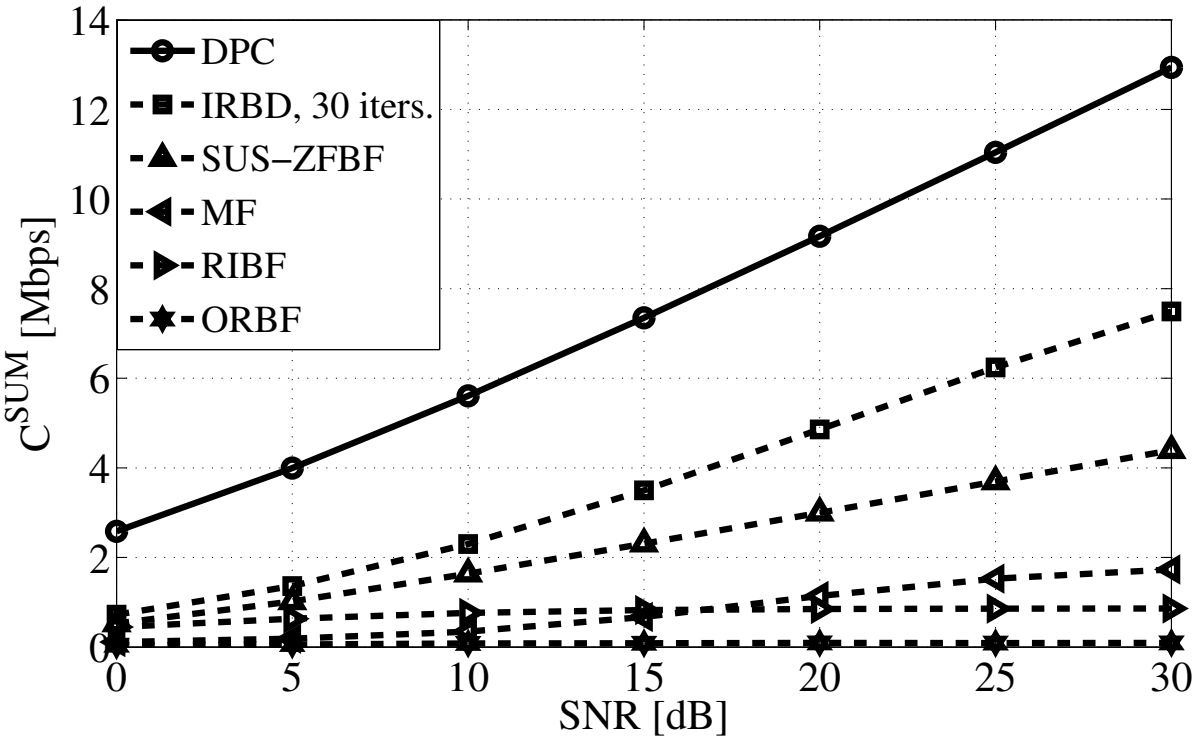

Figure 4.3: Rate of the SBSs for different transmit schemes, $K = 3$ ($N = 128, L = 32$ and bandwidth of 1.92 Mhz).

the insights provided in Section 4.3.3. In fact, if the SBSs mitigate the co-tier interference in the second tier by adopting the techniques discussed therein, a largely sub-optimal performance is achievable if compared to the upper bound given by $C^{\text{SUM}}_{\text{DPC}}$, showing a big rate offset w.r.t. to the optimal performance.

We now investigate the performance for a second tier adopting the cascaded precoder $\mathbf{W}$ proposed in Section 4.3.4, with SBSs deployed and operating according to the flexible RIBF-based solution. To compute the corresponding achievable ergodic sum-rate, $C^{\text{SUM}}_{\text{RIBF}}$, we need to evaluate the SINR for each of the KN received symbols at the SUEs. Let $\mathbf{\Phi} = [\boldsymbol{\phi}^{(1)}, \ldots, \boldsymbol{\phi}^{(KN)}]$. Let $\overline{\mathbf{h}}^{(j)}_{\text{ss}} = [[\overline{\mathbf{H}}_{\text{ss}}]_{j1}, \ldots, [\overline{\mathbf{H}}_{\text{ss}}]_{j\gamma_{tx}KL}]$ denote the j^{th} row of $\overline{\mathbf{H}}_{\text{ss}}$, then

we can write

$$\mathrm{SINR}_{(\mathrm{s}),j} = \frac{|\overline{\mathbf{h}}_{\mathrm{ss}}^{(j)}\boldsymbol{\phi}^{(j)}|^2}{\sum_{i\neq j}^{KN}|\overline{\mathbf{h}}_{\mathrm{ss}}^{(j)}\boldsymbol{\phi}^{(i)}|^2 + \frac{\mathrm{tr}(\mathbf{W}\mathbf{W}^{\mathrm{H}})\sigma_n^2}{P_{\mathrm{s}}K(N+L)}}, \quad \forall j \in [1, KN] \tag{4.8}$$

where the dimension of $\overline{\mathbf{H}}_{\mathrm{ss}}$ depends strictly on the value assumed by β. Then, it is straightforward to see that for a K-SBS system the achievable ergodic sum-rate, when perfect CSIT is available, is given by

$$C_{\mathrm{RIBF}}^{\mathrm{SUM}} = \frac{\mathcal{B}}{N+L}\mathbb{E}[\sum_{j=1}^{KN}\log_2(1+\mathrm{SINR}_{(\mathrm{s}),j})]. \tag{4.8}$$

In Figure 4.4 a comparison between $C_{\mathrm{RIBF}}^{\mathrm{SUM}}$ and $C_{\mathrm{DPC}}^{\mathrm{SUM}}$ is shown, for a load rate of $\beta = 3$. The proposed strategy achieves a promising performance, approaching the upper bound

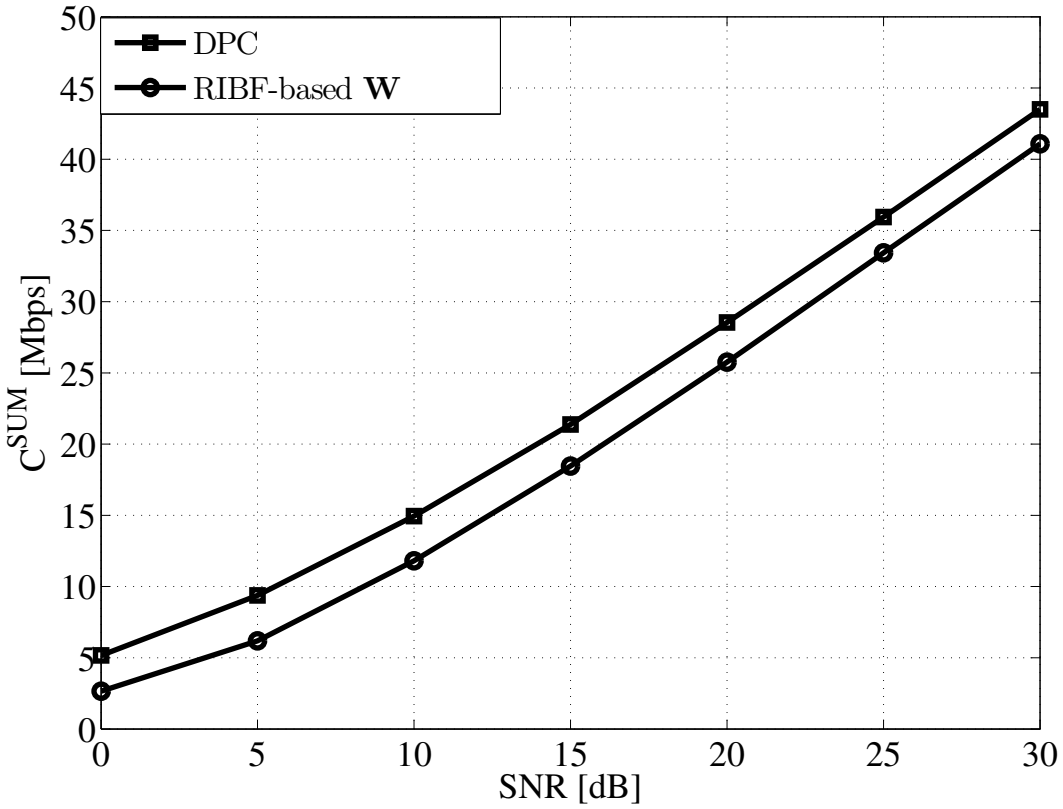

Figure 4.4: Achievable rate for SBSs adopting the RIBF-based $\mathbf{W}$ precoder compared to the upper bound provided by DPC, $K = 3$, $\beta = 2.5$ ($N = 128, L = 32$ and bandwidth of 1.92 Mhz).

throughout the whole considered SNR ranges showing a comparable performance to the

hardly implementable state-of-the-art solution for the co-tier interference management problem. In particular, due to the inherent simplicity and flexibility of the proposed solution, the SBSs' performance can be made arbitrarily close to the upper bound, by increasing the number of dimensions at the transmit side. We remark that, the complexity of the linear precoding techniques outperforming RIBF in Figure 4.3 prevents their implementability for $\beta > \frac{L}{N}$. This consideration further motivates the proposed solution in case of second tier composed of massively deployed SBSs.

4.4.2 Comparison with existing solutions

In this section, we include the first tier in our analysis to evaluate the percent increase in achievable sum-rate that the proposed two-tiered network brings to the classical single tier deployment, if any. Herein, we aim at better characterizing the merit of the cascaded precoder structure w.r.t. to alternative approaches usually adopted in real-life scenarios. The state-of-the-art approaches that allow the deployment of two-tiered networks are divided in three main categories [10]: 1) *complete separation*, 2) *partial sharing*, 3) *complete sharing*. In *complete separation* approaches, the MBS and SBSs operate on disjoint bands, avoiding mutual cross-tier interference. However, the transmission band is limited for both systems to decrease their footprint, hence the overall spectral efficiency enhancement is reduced. To mitigate this problem, *partial sharing* can be implemented. In this case, the two tiers share part of the total available band, and solutions for cross-tier interference management in the shared band need to be devised, yielding complex, possibly cooperative, hybrid strategies. When *complete sharing* is adopted, the MBS and SBSs re-use the same band, creating opportunities for increased spectrum efficiency. Nevertheless, despite its notable features, this approach can easily bring unbearable amount of cross-tier interference generated by the SBSs to the MUEs.

The strategy proposed in this chapter follows the third approach, and aim at allowing the coexistence of SBSs and MBS inside the same area, canceling the interference from the former to the latter, adopting a complete sharing approach. Among the aforementioned bandwidth management schemes, only the complete separation approach always guarantees zero cross-tier interference from the SBSs to the MUEs. Therefore, for a fair comparison, we focus on this approach and divide the available bandwidth in two portions assigned exclusively to the MBS and the SBSs. As seen in Section 4.3.1, by adopting $\mathbf{W}$, each SBS can transmit up to L input symbols from each antenna. On the other hand, the MBS transmits N information symbols to the MUEs, i.e., the number of active subcarriers. Consequently, in the complete separation approach, we assign a bandwidth $\mathcal{B}_s = \frac{\mathcal{B}L}{N}$ to the SBSs and $\mathcal{B}_p = \mathcal{B} - \mathcal{B}_s$ to the MBS. By means of this division, we ensure that, in both the complete separation and the cascaded precoder case, each SBS' antenna is transmitting the same number of symbols. Moreover, in order to exploit all the available transmit dimensions in the complete separation case, we assume that the SBSs may perform a network MIMO-OFDMA transmission towards the SUEs, adopting a ZF precoding such that no linear processing at the SUEs is required, as when adopting $\mathbf{W}$. We note that, a legacy OFDMA transmission is performed by the MBS, as described previously.

Additionally, and differently from what we have assumed so far, we assume that when the transmission in the second tier is performed over the same bandwidth adopted in the first tier, the SUEs suffer from full interference from the MBS. This allows for a more realistic and fair comparison, accounting both for advantages and drawbacks of the two different bandwidth management approaches. We let $\beta = 3$ and $K \in \{2, 8\}$, where the number of considered SBSs has been set to be computationally feasible in our simulations. In Figure 4.5, the percent increase in achievable sum-rate of the two-tiered network w.r.t. a classical OFDMA single tier network is shown for the two schemes and perfect CSIT assumption. We first note that, both approaches provide a remarkable rate increase w.r.t.

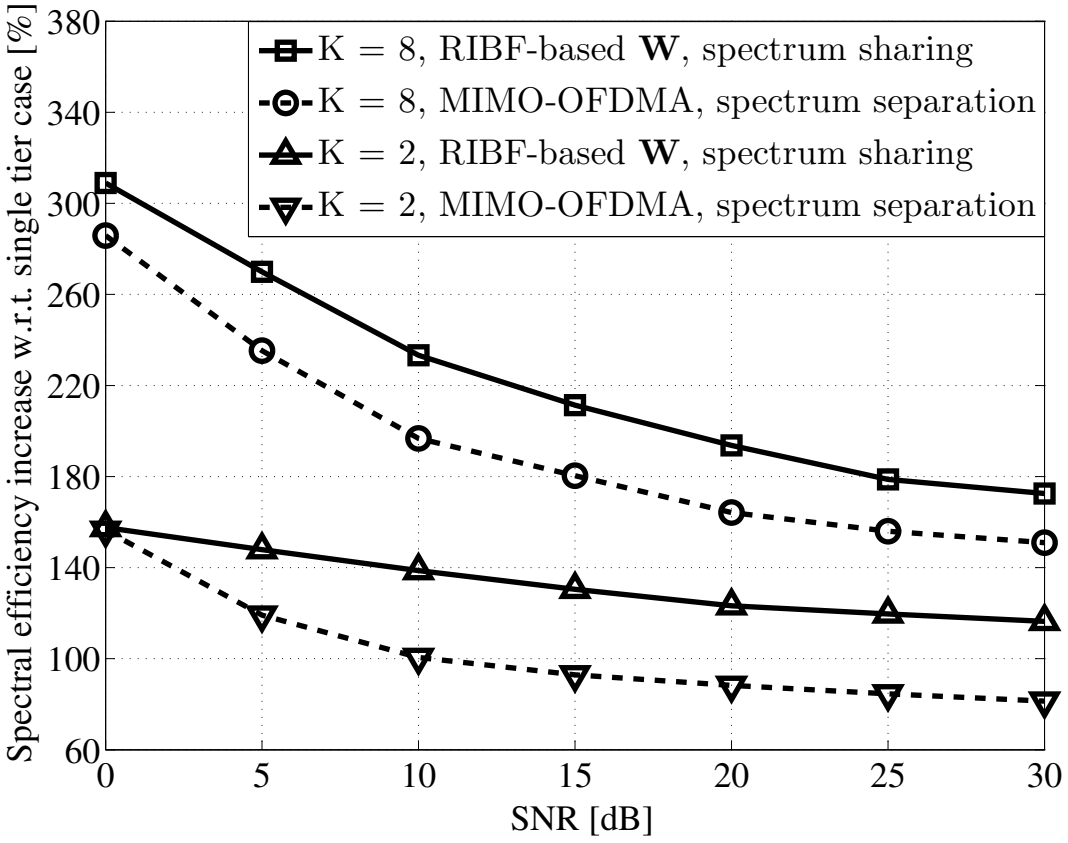

Figure 4.5: Percent increase in achievable sum-rate of a two-tiered network, $K \in \{2, 8\}$, $\beta = 3$ and cross-tier interference MBS $\rightarrow$ SUEs ($N = 64, L = 16$ and bandwidth of 0.96 Mhz). Perfect CSIT.

the single tier case, and the higher K the larger the increase throughout the whole considered SNR range. Therefore, in case of perfect CSIT, the two-tiered network structure always yields a non-negligible rate increase growing with K, w.r.t. the single tier deployment.

On the other hand, if we compare the two approaches, we see that the complete sharing strategy implemented thanks to $\mathbf{W}$ shows a clear advantage over the complete separation

scheme, for both considered values of K, number of SBSs. In particular, the cascaded precoder solution yields gains up to 60% over the complete separation case, for $K = 2$, and between 10% and 20%, for $K = 8$. Thus, the gains grow with K at the low-to-medium SNR values, and decrease for medium-to-high SNR values, due to the larger condition number of $\overline{\mathbf{H}}_{\text{ss}}$ for higher values of K. In fact, we recall that $\mathbf{W}$ is normalized in (4.3.4) by $\sqrt{\text{tr}(\mathbf{E}\boldsymbol{\Phi}\boldsymbol{\Phi}^{\text{H}}\mathbf{E}^{\text{H}})}$, whose value increases with the condition number of $\overline{\mathbf{H}}_{\text{ss}}$ and impacts the achievable sum-rate by reducing the available power at the SBS for the information symbols. Despite this penalizing issue affecting the cascaded precoder, we note that a non-negligible increase in achievable sum-rate is consistently provided by the spectrum sharing over the complete separation approach at all SNR regimes. Remarkably, the SBSs adopting $\mathbf{W}$ are able to exploit efficiently the higher multiplexing gain provided by the complete sharing approach, in spite of the large impact of the cross-tier interference from the MBS to the SUEs, clearly noticeable at medium and high SNR values. This confirms the potential of the proposed strategy and enlighten its advantages w.r.t. the state-of-the-art solution for two-tiered networks deployment.

The findings in this chapter show that a multi-user extension of the technique introduced in the previous chapter is not only feasible, but also convenient in terms of sum-rate enhancement if compared to state-of-the-art approaches for spectrum management in two-tiered networks. Specifically, for two-tiered networks where an MBS and several cooperative SBSs coexist inside the same area, the achievable overall sum-rate can be effectively enhanced when moving from a complete spectrum separation to a spectrum sharing approach. This reinforces our previous findings, showing that the proposed approach can be seamlessly extended from a simple 2×2 system to more complex two-tiered network layouts.

We recall that, the analysis in this chapter aimed at investigating the potential of the proposed approach for a second tier composed of a group of cooperative SBSs communicating over an infinite-capacity backhaul. Despite being hardly realistic, this assumption frames an ideal two-tiered network scenario, allowing to focus on the technical merits of the proposed approach. In fact, assuming a finite-capacity backhaul may generally lead to worse performance. Thus, from a practical point of view, it would be very difficult to understand what is the impact of the backhaul limitations on the poorer performance and which flaws the proposed techniques have by construction. If the proposed solution could not provide meaningful performance even in an ideal fully cooperative SBSs case (for perfect and imperfect CSIT), then there would be no use in considering the case of autonomous self-organizing SBSs, which is studied in Chapter 6.

Chapter 5

Practical Aspects

In the previous chapter, the study of a suitable technique to realize the coexistence problem in two-tiered networks has been extended to a multi-cell network layout. Assuming complete spectrum sharing between the two tiers, we focused on the coexistence of multiple DL transmissions performed by an OFDM MBS and several SBSs, being the latter deployed within the coverage area of the former. As a first step, we considered a cooperative and centralized approach to the problem, assuming the presence of an infinite-capacity backhaul connecting the SBSs. The second tier has then been modeled as a network MIMO system, transforming a potentially interference limited channel into a MIMO-BC. A novel cascaded linear precoder has been derived to allow the SBSs to mitigate the co-tier interference in the second tier, while guaranteeing absence of interference towards the first tier, in case of perfect CSIT. Promising performance have been shown in terms of achievable sum-rate of the second tier. The feasibility of this proposed approach depends on some very stringent assumptions that may not always be realistic in real-life scenarios. Accordingly, in this chapter, a discussion on the constraints that the proposed approach may face in practical network implementations is carried out. We start by analyzing the performance of the cascaded precoder when the perfect CSIT assumption is relaxed. The losses that a two-tiered network may suffer in this case are shown, and a comparison with the performance of alternative approaches is provided for both perfect and imperfect CSIT assumption. A general discussion on further challenges and issues for real-life scenario applications of the centralized solution concludes the chapter.

5.1 Channel State Information

One common way to acquire CSI in modern wireless communications is through pilot/training symbols estimation. Typically, the transmitters/receivers may obtain the desired CSI in different ways, depending on the adopted standard and underlying technology. For instance, the estimation can be performed by evaluating the received instance

of known pilot symbols, carried throughout the whole duration of the frame by reserved tones present in each received symbol [98]. Alternatively, training sequences carrying solely known pilot symbols, and exclusively devoted to channel estimation purposes, may be periodically inserted into the transmit frame (e.g., every time slot) to allow the estimating devices to acquire more accurate and possibly long-term channel estimations [50, 99]. We note that, for networks operating in FDD mode, independent channel estimations are required for UL and DL channels, whereas only the estimation related to the DL (or the UL) channel is necessary at each device, for networks operation in TDD mode. In fact, in the latter case, if a reasonably correct calibration of the RF circuitry is performed at both sides of the communication [100], the UL and DL channels are reciprocal, and their CSI coincides. We recall that, in this work, we are considering that all communications are carried out in TDD mode, thus the reciprocity of the UL and DL channels can be exploited.

In the previous chapter, we extended the two-tiered network model considered in Chapter 3 from a simple 2×2 model, to a more complex multi-user scenario where an OFDM MBS serves a group of MUEs in the first tier, whereas several cognitive SBSs serve more a group of SUEs in the second tier, with both tiers sharing the spectrum. We showed that when perfect CSIT is available at the SBSs, a linear precoder $\mathbf{W}$ capable of nulling the cross-tier interference towards the first tier and mitigating the co-tier interference in the second tier can always be designed. However, in a realistic implementation, the available CSI at each transmitter in the system is the result of noisy, thus imperfect, channel estimations. Herein, we seek for a deeper understanding of the impact of the CSIT acquisition on the overall network sum-rate. We recall that, in Section 4.3.2, we assumed the presence of an infinite-capacity backhaul connecting all the SBSs. As discussed in Chapter 4, this assumption frames an ideal two-tiered network scenario, given that, in general, a finite-capacity backhaul assumption may generally lead to worse performance. If the latter case were considered, it would be very difficult to understand if the poorer performance of the two-tiered network were caused by the impact of the backhaul limitations or by technical flaws that the proposed technique has by construction. If the proposed solution could not provide meaningful performance even in an ideal case (for perfect and imperfect CSIT), then there would be no use in considering the case of autonomous self-organizing SBSs, whose study is proposed in Chapter 6. This allows us to target our efforts on the analysis of the effect of a noisy channel estimation onto the performance of the considered two-tiered network.

Let us focus on the first tier. As previously done, we consider as a reference a recent standard adopting OFDMA as physical layer technique for the DL transmission, i.e., LTE/LTE-A. In general, the LTE specifications mandate performance requirements for both DL and UL transmissions, but let freedom in channel estimation implementation [101]. However, regardless of the chosen implementation, channel estimations at the receiver are necessary in such scenarios to equalize the data transmitted by the OFDMA transmitter, guarantee the desired decoding quality and meet the performance requirements. Additionally, in practical implementations, the receiver could possibly need to adopt a precoder based transmit strategy to enhance the quality of the communication

with the OFDMA transmitter over the UL, as shown in [102] and reference therein. As a consequence, reliable channel estimations should always be available at the receiver in the first tier.

Consider for simplicity that a classic training/transmission scheme [103] may be adopted in the first tier to obtain the necessary channel estimations, as follows. Consider a block fading channel model where a channel estimation is valid throughout the duration of the coherence time of the channel, i.e., T. The channel estimations at the different devices are performed during a period $\tau \leq T$, hence the available time for transmission is upper bounded by $T - \tau$. In TDD networks, τ is usually composed of two phases, τ_1 and τ_2: the UL (or DL) channel estimation phase, during τ_1, and the DL (or UL) channel estimation phase, during τ_2. At this stage, and without loss of generality, we assume that the UL channel estimation is performed during τ_1. Accordingly, this this phase, the MUEs send UL OFDM training symbols to the MBS. Analogously, DL OFDM training symbols are sent by the MBS to the MUEs during τ_2, to allow the DL channel estimation at the latter. A graphical representation of the estimation and transmission times is provided in Figure 5.1. Now we switch our focus to the second tier. By construction, the SBSs do

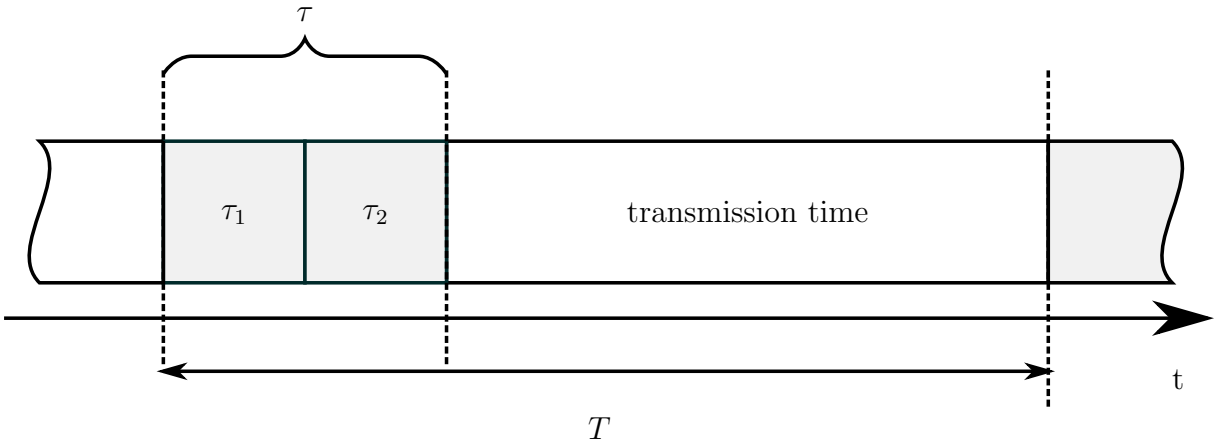

Figure 5.1: Channel estimation and transmission times.

not cooperate with the MBS and the latter may be in general oblivious of the existence of the former. Nevertheless, the SBSs being endowed with cognitive capabilities, they can serve the SUEs by means of an opportunistic strategy, by exploiting some side knowledge of the technology and procedures adopted in the first tier, as seen in previous chapters. The goal of this section is to show that, given a reference procedure in the first tier, the SBSs may obtain the CSI required to design the cascaded precoder derived in Chapter 4, i.e., $\mathbf{W} = \mathbf{E}\mathbf{\Phi}$, by adopting an opportunistic channel estimation procedure. Let us consider the CSI requirements for the SBSs. First each SBS must dispose of reliable channel estimations w.r.t. the interference channels towards each MUE. If this knowledge is available at the i^{th} SBS, then a suitable cross-interference nulling precoder $\mathbf{E}_i$ can be devised, and $\mathbf{E}$ computed as in (4.3). Additionally, the SBSs must dispose of a global CSI w.r.t the

channels towards the SUEs to jointly derive the co-tier interference mitigating precoder $\mathbf{\Phi}$.

In the following, we start from an example of possible channel estimation protocol and illustrate the corresponding practical opportunistic channel estimation protocol that could be adopted in the second tier. The actions performed by the SBSs and SUEs are detailed for both τ_1 and τ_2, in order to provide a complete working example of a practical channel estimation protocol that could be adopted in a realistic two-tiered network implementations.

5.1.1 UL channel estimation (τ_1)

We start from τ_1. During this phase, the MUEs transmit OFDM training symbols used by the MBS to estimate the channels and perform DL resource block allocation and input power optimization, as depicted in Figure 5.2. Specifically, the MBS needs a reliable

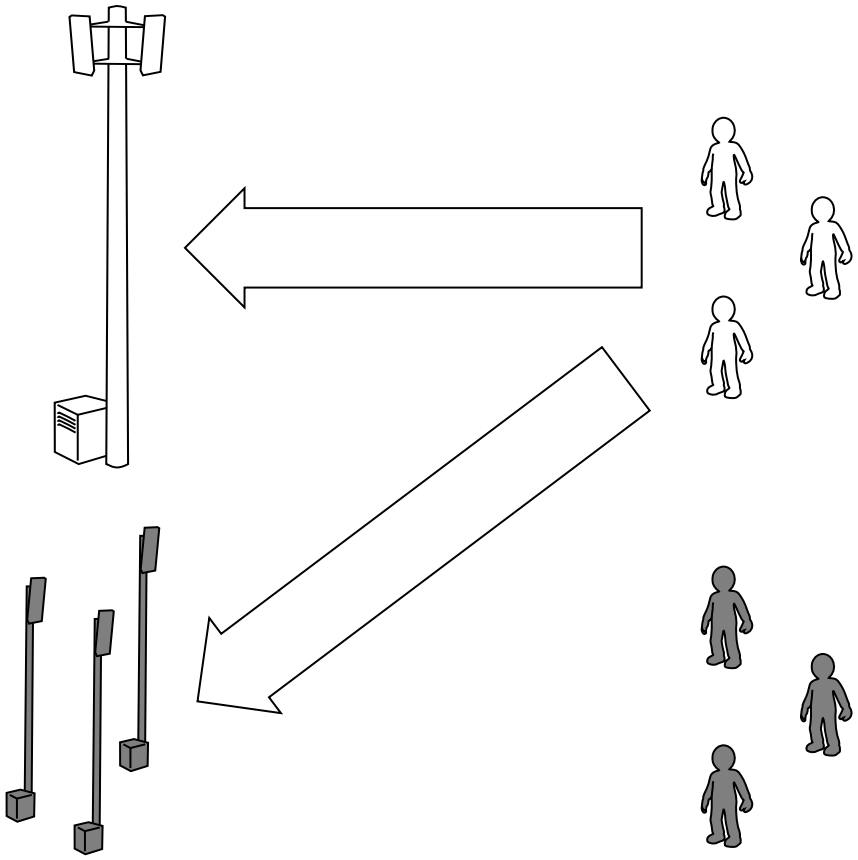

Figure 5.2: UL channel estimation.

estimation of $\mathbf{h}_{\text{pp}}^{(i,j)}, \forall j \in [1, M]$, to perform the PRBs allocation for the MUEs. Note that, each transmitted training symbol is received by both the MBS and the SBSs. We assume that, in this phase, the transmission is slotted in time, thus τ_1 is divided into M

slots, one per each MUE. Therefore, each MUE transmits during a time slot of length τ_1/M. Now, consider the second tier. We recall that the SBSs have cognitive capabilities, so we can safely assume that they are aware of the adopted pilot patterns as the MBS [84] and can decode the signal transmitted by the MUEs. In the following, we show how the CSIT w.r.t. the interfering link between the SBSs and the MUEs can be acquired. Since the interference cancelation precoder is computed autonomously by the SBSs, then we can focus on a single SBS to describe the procedure. Let $\overline{\mathbf{H}}_{\text{ps}}^{(j,i)} = \mathbf{F}\mathcal{T}(\mathbf{h}_{\text{ps}}^{(j,i)})\mathbf{A}\mathbf{F}^{-1} \in \mathbb{C}^{N\times N}$ be the channel matrix representing the frequency domain realization of the link between the j^{th} MUE and the i^{th} SBS. Then $\mathbf{y}_{\text{s,SBS}}^{(i)}(t) \in \mathbb{C}^N$, received signal at the i^{th} SBS from the j^{th} MUE at the discrete time t is

$$\mathbf{y}_{\text{s,SBS}}^{(i)}(t) = \overline{\mathbf{H}}_{\text{ps}}^{(j,i)}\mathbf{s}_{\text{p}} + \boldsymbol{\nu}_{\text{s,SBS}}^{(i)}(t), \tag{5.0}$$

where $\mathbf{s}_{\text{p}} = \frac{1}{\sqrt{N}}[1,\ldots,1]$ is a unit norm training symbol vector, t is the discrete time at which $\mathbf{y}_{\text{s}}^{(j,i)}(t)$ is measured and $\boldsymbol{\nu}_{\text{s},tx}^{(i)}(t) \sim \mathcal{CN}(0,\sigma_n^2\mathbf{I}_N)$ is a vector modeling the effect of the AWGN at the i^{th} SBS' circuitry after the DFT[1]. Thus, at the end of the j^{th} time slot of τ_1, $\widehat{\overline{\mathbf{H}}}_{\text{ps}}^{(j,i)} = d\left(\left[\widehat{\overline{\mathbf{H}}}_{\text{ps}}^{(j,i)}\right]_{1,1},\ldots,\left[\widehat{\overline{\mathbf{H}}}_{\text{ps}}^{(j,i)}\right]_{N,N}\right)$, estimation of $\overline{\mathbf{H}}_{\text{ps}}^{(j,i)}$, is computed as

$$\begin{aligned}\left[\widehat{\overline{\mathbf{H}}}_{\text{ps}}^{(j,i)}\right]_{n,n} &= \frac{M\sqrt{N}}{\tau_1}\sum_{t=1}^{\frac{\tau_1}{M}}\left[\mathbf{y}_{\text{s,SBS}}^{(i)}(t)\right]_n \\ &= \left[\overline{\mathbf{H}}_{\text{ps}}^{(j,i)}\right]_{n,n} + \frac{M\sqrt{N}}{\tau_1}\sum_{t=1}^{\frac{\tau_1}{M}}\left[\nu_{\text{s,SBS}}^{(i)}(t)\right]_n,\end{aligned} \tag{5.0}$$

where, as a result of the average over the time slot duration, the estimation error is inversely proportional to τ_1. Therefore, the higher the required estimate accuracy the shorter the period to transmit for each SBS.

Now, let $\widehat{\mathbf{g}} = \mathbf{F}^{-1}\left[[\widehat{\overline{\mathbf{H}}}_{\text{ps}}^{(j,1)}]_{1,1},\ldots,[\widehat{\overline{\mathbf{H}}}_{\text{ps}}^{(j,i)}]_{N,N}\right]^{\text{T}}$. Then, by taking the first $L+1$ components of $\widehat{\mathbf{g}}$, corresponding to the number of paths in the considered channel model, we define the time domain version of the channel between the j^{th} MUE and the i^{th} SBS as

$$\widehat{\mathbf{h}}_{\text{ps}}^{(j,i)} = \widehat{\mathbf{h}}_{\text{sp}}^{(i,j)} \triangleq [\widehat{\mathbf{g}}_1,\ldots,\widehat{\mathbf{g}}_{L+1}]^{\text{T}},$$

where $\widehat{\mathbf{h}}_{\text{ps}}^{(j,i)} = \widehat{\mathbf{h}}_{\text{sp}}^{(i,j)}$ due the reciprocity of the DL and UL channels in a TDD communication. Accordingly, the i^{th} SBS can construct $\mathcal{T}(\widehat{\mathbf{h}}_{\text{sp}}^{(i,j)})$ and the end of the j^{th} slot of τ_1. At this point, we can safely assume that each SBS is aware of the PRBs allocation performed by the MBS. In fact, in LTE/LTE-A, the result of the allocation is communicated by the MBS to the MUEs through the physical downlink control channel (PDCCH), within

[1]The subscript SBS in $\boldsymbol{\nu}_{\text{s,SBS}}^{(i)}(t)$ (and $\mathbf{y}_{\text{s,SBS}}^{(i)}(t)$) is added to the notation to avoid confusion with $\boldsymbol{\nu}_{\text{s}}^{(k)}$ (and $\mathbf{y}_{\text{s}}^{(k)}$) as introduced in Chapter 4.

each DL sub-frame [104]. This information is meant to reach all the MUEs hosted in the macro-cell, thus it is received by the SBSs as well, the latter being deployed in the coverage area of the MBS. Using this information, the i^{th} SBS can construct $\mathbf{B}_j$, as defined in Chapter 4. Then, at the end of τ_1, $\mathbf{H}_{\text{sp}}^{(i,\cdot)} = \sum_{j=1}^{M} \mathbf{B}_j \mathbf{F} \mathcal{T}(\widehat{\mathbf{h}}_{\text{sp}}^{(i,j)})$ is finally computed as in (4.2) and the interference nulling precoder $\mathbf{E}_i$ is derived according to the procedure described in Section 4.2.

5.1.2 DL channel estimation (τ_2)

Consider the first tier. During this phase, the MBS transmits to the MUEs a unit norm sequence $\mathbf{s}_{\text{p}} \in \mathbb{C}^{\tau_2}$ of length τ_2 on each subcarrier. This is done to allow $\overline{\mathbf{H}}_{\text{pp}}^{(1,j)} = \mathbf{F}\mathcal{T}(\widehat{\mathbf{h}}_{\text{pp}}^{(1,j)})\mathbf{A}\mathbf{F}^{-1} \in \mathbb{C}^{N \times N}$ to be known at the j^{th} MUE, mainly for signal equalization purposes. Note that, the size of τ_2 depends on the number of both subcarriers and performed channel estimations, with the latter number impacting the accuracy of the channel estimation. The structure of the received signal during τ_2 is the same for each MUE, hence we can safely focus on j^{th} MUE, without loss of generality. At the end of τ_2, the matrix representation of the signal received by the j^{th} MUE is

$$\mathbf{Y}_{\text{p}}^{(j)} = \overline{\mathbf{H}}_{\text{pp}}^{(1,j)} \mathbf{S}_{\text{p}} + \Upsilon_{\text{p}}^{(j)}, \tag{5.0}$$

where $\mathbf{S}_{\text{p}} = [\ \mathbf{s}_{\text{p}} \mid \cdots \mid \mathbf{s}_{\text{p}}\ ]^{\text{H}}$ and and $\Upsilon_{\text{p}}^{(j)} = \left[\ \boldsymbol{\nu}_{\text{p}}^{(j)}(1) \mid \cdots \mid \boldsymbol{\nu}_{\text{p}}^{(j)}(\tau_2)\ \right]$ are $(N \times \tau_2)-$sized matrices, with $\boldsymbol{\nu}_{\text{p}}^{(j)}(l) \sim \mathcal{CN}(0, \mathbf{I}_N)$ vector modeling the effect of the AWGN at the j^{th} MUE's circuitry after the DFT. At the end of τ_2, the j^{th} MUE estimates the frequency domain representation of the channel to the MBS as

$$\begin{aligned} \widehat{\overline{\mathbf{H}}}_{\text{pp}}^{(1,j)} &= \frac{1}{N} d\left(\mathbf{Y}_{\text{p}}^{(1,j)} \mathbf{S}_{\text{p}}^{\text{H}} \mathbf{1}_N\right) \\ &= \left(\overline{\mathbf{H}}_{\text{pp}}^{(1,j)} + \frac{1}{N} \Upsilon_{\text{p}}^{(j)} \mathbf{S}_{\text{p}}^{\text{H}}\right) \mathbf{1}_N, \end{aligned} \tag{5.0}$$

with $\mathbf{1}_{\tau_2}$ all ones column vector of size τ_2. Note that, (5.1) is feasible thanks to the properties of $\mathbf{s}_{\text{p}}$, i.e., $\mathbf{s}_{\text{p}}^{\text{H}} \mathbf{s}_{\text{p}} = 1$. Then, if necessary, $\widehat{\mathbf{h}}_{\text{pp}}^{(1,j)}$ is obtained as done for $\widehat{\mathbf{h}}_{\text{sp}}^{(1,j)}$ in Section 5.1.1.

Turning our focus back to the second tier, we recall that its cognitive capabilities and the similarity between an MUE and an SUE allow us to assume that the SUEs know the physical layer characteristics of the first tier (i.e. any receiver in the two-tiered network may act be an MUE or an SUE, depending on which base station it is associated to). It is clear from (4.3.4) that, to design the $\mathbf{\Phi}$ precoder, the SBSs need to dispose of the CSI with respect to each SUE. Accordingly, during τ_2, the SUEs transmit training symbols to the SBSs for channel estimation purposes, as depicted in Figure 5.3. To avoid interference towards the MUEs, the SUEs make use of the structure of the pilot symbols used in the channel estimation process into the first tier. Accordingly, $\tau_2 - 1$ unit norm mutually orthonormal sequences that are orthogonal to $\mathbf{s}_{\text{p}}$ can be found in the second tier, by

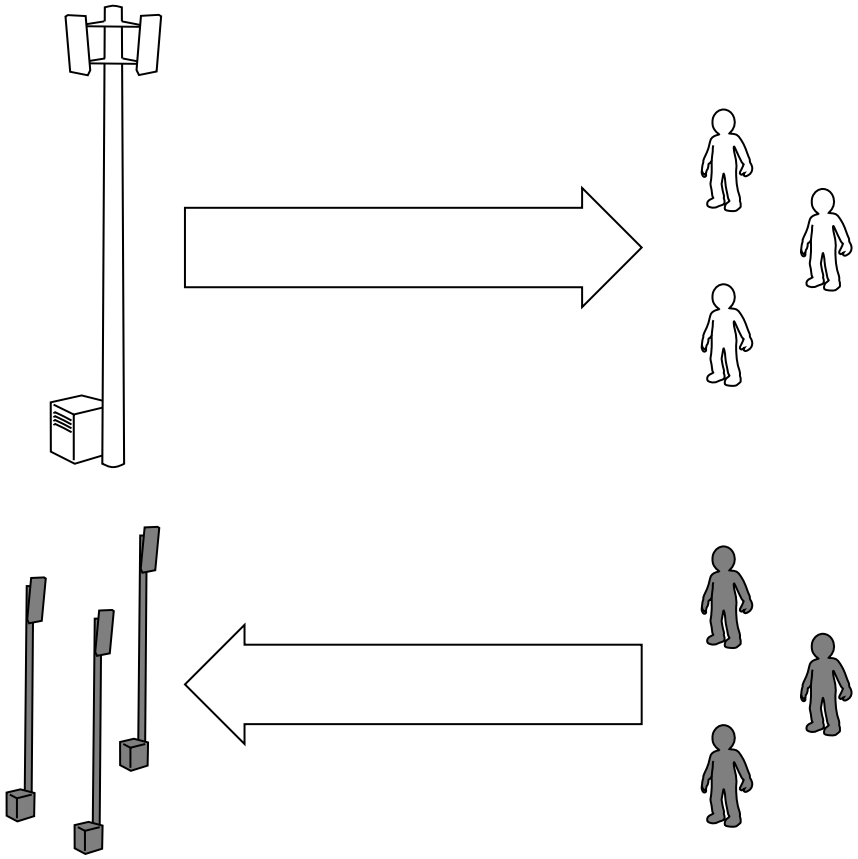

Figure 5.3: DL channel estimation.

construction. Therefore, if we define $K' \in \mathbb{N}$ such that $K' \leq (\tau_2 - 1)$, up to K' SUEs can select a unit norm training sequence $\mathbf{s}_{\mathrm{s}}^{(k)} \in \mathbb{C}^{\tau_2}$, such that

$$\mathbf{s}_{\mathrm{s}}^{(k)\mathrm{H}} \, \mathbf{s}_{\mathrm{p}} = 0, \ \forall k \in [1, K'], \tag{5.0}$$

and perform an OFDM transmission towards the SBSs. By construction, this approach is scalable only up to $K' \sim N$ SBS/SUE pairs. On the other hand, if we consider the parameters of a realistic operative scenario (i.e., $N \sim \alpha * 10^{\{2,3\}}$, $\alpha \in \mathbb{Z}_+$), we can easily see that a scalability issue would arise only in practical network deployment involving an unlikely number of SBSs. At this stage, we do not impose any mechanism to choose the sequences in the second tier. Depending on the designer's goal, one of the many schemes proposed in the literature, i.e. [105, 106], could be adopted.

Now, let $\mathbf{h}_{\mathrm{sp,SUE}}^{(k,j)} \in \mathbb{C}^{L+1}$ be the channel vector representing the link between the k^{th} SUE and the j^{th} MUE[2], and $\mathcal{T}(\mathbf{h}_{\mathrm{sp,SUE}}^{(k,j)}) \in \mathbb{C}^{N \times (N+L)}$ be its corresponding channel matrix. Then, the matrix representation of the signal received by the j^{th} MUE at the end

[2]The subscript SUE in $\mathbf{h}_{\mathrm{sp,SUE}}^{(k,j)}$ denotes that, in this case, the transmitting device in the second tier is the k^{th} SUE and not the k^{th} SBS. This additional notation is added to avoid confusion with $\mathbf{h}_{\mathrm{sp}}^{(i,j)}$, channel vector representing the link between the i^{th} SBS and the j^{th} MUE, introduced in Chapter 4.

of τ_2 can be rewritten as

$$\begin{aligned} \mathbf{Y}_{\mathrm{p}}^{(j)} &= \mathbf{H}_{\mathrm{pp}}^{(1,j)}\mathbf{S}_{\mathrm{p}} + \\ &\sum_{k=1}^{K}\mathbf{F}\mathcal{T}(\mathbf{h}_{\mathrm{sp,SUE}}^{(k,j)})\mathbf{A}\mathbf{F}^{-1}\mathbf{S}_{\mathrm{s}}^{(k)} + \Upsilon_{\mathrm{p}}^{(j)}, \end{aligned} \tag{5.1}$$

with $\mathbf{S}_{\mathrm{s}}^{(k)} = \left[\, \mathbf{s}_{\mathrm{s}}^{(k)} \mid \cdots \mid \mathbf{s}_{\mathrm{s}}^{(k)} \,\right]^{\mathrm{H}} \in \mathbb{C}^{N\times\tau_2}$. Now, to obtain the desired CSI, the j^{th} MUE computes $\mathbf{Y}_{\mathrm{p}}^{(j)}\mathbf{S}_{\mathrm{p}}^{\mathrm{H}}$. Then, the result of this operation is given by (5.1), since $\sum_{i=1}^{K}\mathbf{B}_j\mathbf{F}\mathcal{T}(\mathbf{h}_{\mathrm{sp,SUE}}^{(i,j)})\mathbf{A}\mathbf{F}^{-1}\mathbf{S}_{\mathrm{s}}^{(j)}\mathbf{S}_{\mathrm{p}}^{\mathrm{H}} = \mathbf{0}_{N\times N}$ by construction, thus no interference is generated from the SUEs towards the MUEs.

We note that, the absence of interference guaranteed by (5.1.2) is verified only if the $K+1$ different signals received at the j^{th} MUE are perfectly synchronized. In this example of protocol, we assume that this condition is always verified. Nevertheless, it is worth noting that, despite the popularity of this assumption in the literature (i.e., [107, 108, 109] and references therein), the achievement of perfect synchronization of multiple signals at the receiver is a very challenging problem in realistic implementations. Several efforts have been recently made by the research community to develop practically implementable techniques to realize multiple synchronized transmissions. The interested reader may refer to [110, 111, 112, 113, 114, 115], and references therein, for further details on the subject.

Now, we keep our focus on the second tier, and consider the matrix representation of the received signal at the j^{th} SBS at the end of τ_2, given by

$$\begin{aligned} \mathbf{Y}_{\mathrm{s,SBS}}^{(j)} &= \sum_{k=1}^{K}\overline{\mathbf{H}}_{\mathrm{ss}}^{(k,j)}\mathbf{S}_{\mathrm{s}}^{(k)} + \\ &\overline{\mathbf{H}}_{\mathrm{ps}}^{(1,j),\mathrm{SBS}}\mathbf{S}_{\mathrm{p}} + \Upsilon_{\mathrm{s,SBS}}^{(j)}, \end{aligned} \tag{5.1}$$

where $\overline{\mathbf{H}}_{\mathrm{ss}}^{(k,j)} = \mathbf{F}\mathcal{T}(\widehat{\mathbf{h}}_{\mathrm{ss}}^{(k,j)})\mathbf{A}\mathbf{F}^{-1} \in \mathbb{C}^{N\times N}$ and $\overline{\mathbf{H}}_{\mathrm{ps,SBS}}^{(1,j)} = \mathbf{F}\mathcal{T}(\widehat{\mathbf{h}}_{\mathrm{ps,SBS}}^{(1,j)})\mathbf{A}\mathbf{F}^{-1} \in \mathbb{C}^{N\times N}$ are the channel matrices representing the frequency domain realization of the link between the k^{th} SUE and the j^{th} SBS and the link between the MBS and the j^{th} SBS, respectively[3]. Note that, in (5.1), $\Upsilon_{\mathrm{s,SBS}}^{(j)} = \left[\, \boldsymbol{\nu}_{\mathrm{s,SBS}}^{(j)}(1) \mid \cdots \mid \boldsymbol{\nu}_{\mathrm{s,SBS}}^{(j)}(\tau_2) \,\right] \in \mathbb{C}^{N\times\tau_2}$ is the matrix collecting the effect of the AWGN at the j^{th} SBS after the DFT, with $\boldsymbol{\nu}_{\mathrm{s,SBS}}^{(j)}(i) \sim \mathcal{CN}(0, \sigma_n\mathbf{I}_N)$, $\forall$ natural number $i \leq \tau_2$.

The j^{th} SBS performs K different channel estimations during τ_2 to find $\mathbf{H}_{\mathrm{ss}}^{(i,j)}$, $\forall\ i \in [1, K]$, CSI w.r.t. the channels towards each SUE. As before, we focus on a single

[3]The subscript SBS in $\overline{\mathbf{H}}_{\mathrm{ps,SBS}}^{(1,j)}$ and $\mathbf{h}_{\mathrm{ps,SBS}}^{(1,j)}$ denotes that, in this case, the receiving device in the second tier is the j^{th} SBS and not the j^{th} SUE. This additional notation is added to avoid confusion with $\mathbf{h}_{\mathrm{ps}}^{(1,j)}$ (and $\mathbf{H}_{\mathrm{ps}}^{(1,k)}$), channel vector (matrix) representing the link between the MBS and the j^{th} SUE, introduced in Chapter 4. Analogously, the notation $\mathbf{Y}_{\mathrm{s,SBS}}^{(j)}$ has been adopted.

link, being the remaining channels estimated similarly. Specifically, let us consider the link between the j^{th} SBS and i^{th} SUE. Due to the previous consideration about the cognitive capabilities of the second tier, we assume that the j^{th} SBS knows $\mathbf{S}_{\mathrm{s}}^{(i)}, \forall\, i \in [1, K]$. For instance, this may be possible in the considered centralized and cooperative case if the orthonormal sequence to be used by each SUE were chosen and assigned to the SUEs by the SBSs. As a consequence, if perfect synchronization of the received signals is achieved at the j^{th} SBS, $\widehat{\overline{\mathbf{H}}}_{\mathrm{ss}}^{(i,j)}$ is given by

$$\begin{aligned}\widehat{\overline{\mathbf{H}}}_{\mathrm{ss}}^{(i,j)} &= \frac{1}{N} d\left(\mathbf{Y}_{\mathrm{s,SBS}}^{(j)} \mathbf{S}_{\mathrm{s}}^{(i)\mathrm{H}} \mathbf{1}_N\right) \\ &= \overline{\mathbf{H}}_{\mathrm{ss}}^{(i,j)} + d\left(\frac{1}{N} \Upsilon_{\mathrm{s,SBS}}^{(j)} \mathbf{S}_{\mathrm{s}}^{(i)\mathrm{H}}\right) \mathbf{1}_N, \end{aligned} \tag{5.0}$$

since, by construction $\mathbf{F}\mathcal{T}(\mathbf{h}_{\mathrm{ps,SBS}}^{(1,j)})\mathbf{A}\mathbf{F}^{-1}\mathbf{S}_{\mathrm{p}}\mathbf{S}_{\mathrm{s}}^{(i)\mathrm{H}} = \mathbf{F}\mathcal{T}(\mathbf{h}_{\mathrm{ss}}^{(k,j)})\mathbf{A}\mathbf{F}^{-1}\mathbf{S}_{\mathrm{s}}^{(k)}\mathbf{S}_{\mathrm{s}}^{(i)\mathrm{H}} = \mathbf{0}_{N\times N}$, $\forall i \in [1, K]$, $i \neq k$. Once again, the estimating device, i.e. the j^{th} SBS, does not suffer from undesired interference thanks to the mutual orthogonality of the training sequences. Finally, $\widehat{\mathbf{h}}_{\mathrm{ss}}^{(i,j)}$ can be computed following the steps described in Section 5.1.1 for $\widehat{\mathbf{h}}_{\mathrm{ps}}^{(j,i)}$. The precoder $\mathbf{W}$ is then constructed at the end of τ_2 as described in Section 4.3.

After the completion of τ_2, the channel estimation phase τ reaches its end and the MBS engages in the transmission phase during $T - \tau$. On the other hand, as previously seen, all the required informations to compute $\mathbf{W}$ are already available in the opportunistic second tier at the end of τ, hence the SBSs can engage in the transmission phase as well.

5.2 Performance Evaluation

In this section, we present a numerical performance analysis of the cascaded precoder $\mathbf{W}$, when only imperfect CSIT is available in the network. In particular, all the concerned devices perform the noisy channel estimations according to the procedure described so far. The nature of the sum-rate loss experienced by the two tiers is twofold. On the one hand, the imperfectly built $\mathbf{W}$ causes residual cross-tier interference towards the first tier and reduced co-tier interference mitigation in the second tier. On the other hand, the time spent performing UL and DL channel estimations necessarily reduces the available time for the transmissions, reducing the achievable sum-rate. Accordingly, we aim at showing how the sum-rate loss in the two tiers may vary as different $\frac{\tau}{T}$ proportions are set. Note that, in the first part of the section, we do not consider any interference from the MBS to the SUEs to isolate the effect of the imperfect CSIT on the effectiveness of $\mathbf{W}$. w.r.t. to both cross-tier interference cancelation and co-tier interference mitigation. Conversely, this important source of interference is taken into account in the second part of the section. Therein, the comparison provided in Section 4.4.2 between the proposed spectrum sharing approach (realized by the adoption of the cascaded precoder in the second tier) and the complete spectrum separation approach is re-proposed under the light of the imperfect CSIT discussion carried out in this chapter. This way, we aim at

quantifying the performance enhancement, if any, that the proposed strategy may yield over the state-of-the-art approach for two-tiered network deployment, in a more realistic scenario where only noisy channel estimations are available in both tiers.

As done in Section 4.4, we consider an OFDMA/LTE MBS serving a macro-cell hosting $M = 4$ MUEs, and second tier composed of cooperative SBSs adopting the proposed cascaded precoder to serve a group of SUEs. To reduce Monte Carlo simulation times, we consider $N = 64$, $L = 16$ (for a total bandwidth of $\mathcal{B} = 0.96$ MHz) and a load rate of $\beta = 1$. Noise and channel vectors are generated as described in Section 4.2.

5.2.1 Impact of the Channel Estimation

In Section 4.3, we showed that when perfect CSIT is available at the SBSs, an interference nulling precoder $\mathbf{E}$ can be designed. However, as discussed so far, in a realistic implementation, each transmitter in the system performs noisy channel estimations, yielding imperfect CSIT. Accordingly, the zero interference constraint in (4.3) can no longer be satisfied and the SBSs may generate interference towards the MUEs. If we denote the j^{th} row of $\overline{\mathbf{H}}_{\text{pp}}^{(1,j)}$ as $\mathbf{h}_{\text{pp}}^{(j)} = [[\overline{\mathbf{H}}_{\text{pp}}]_{j,1}, \ldots, [\overline{\mathbf{H}}_{\text{pp}}]_{j,N}]$, and the j^{th} row of $\mathbf{H}_{\text{sp}}$ as $\mathbf{h}_{\text{sp}}^{(j)} = [\mathbf{H}_{\text{sp}}]_{j,1}, \ldots, [\mathbf{H}_{\text{sp}}]_{j,\gamma_{tx}KL}]$, then the SINR per received symbol at the MUEs reads

$$\text{SINR}_{(\text{p}),j} = \frac{P_p K |\mathbf{h}_{\text{pp}}^{(j)}|^2}{\sum_{i=1}^{KN} |\mathbf{h}_{\text{sp}}^{(j)} \boldsymbol{\phi}^{(i)}|^2 + \sigma_n^2}, \forall j \in [1, N]. \tag{5.0}$$

Note that, the imperfect CSI at the SBSs has an impact on the general design of $\mathbf{W}$, worsening the SINR per received symbol at the SUEs, due to channel estimation effects and increased co-tier interference component. Therefore, (4.4.1) does not hold for this case and, adopting the notation introduced in Chapter 4 each SUE experiences an effective SINR value [103] per received symbol given by

$$\text{SINR}_{(\text{s}),j} = \frac{\left(\frac{|\bar{\mathbf{h}}_{\text{ss}}^{(j)} \boldsymbol{\phi}^{(j)}|^2}{\sum_{i \neq j}^{KN} |\bar{\mathbf{h}}_{\text{ss}}^{(j)} \boldsymbol{\phi}^{(i)}|^2 + \frac{\text{tr}(\mathbf{W}\mathbf{W}^{\text{H}})\sigma_n^2}{P_s K(N+L)}} \right)^2 \tau}{1 + (1+\tau) \frac{|\bar{\mathbf{h}}_{\text{ss}}^{(j)} \boldsymbol{\phi}^{(j)}|^2}{\sum_{i \neq j}^{KN} |\bar{\mathbf{h}}_{\text{ss}}^{(j)} \boldsymbol{\phi}^{(i)}|^2 + \frac{\text{tr}(\mathbf{W}\mathbf{W}^{\text{H}})\sigma_n^2}{P_s K(N+L)}}}, \tag{5.0}$$

$\forall j \in [1, KN]$, where we assume that the same transmit power is used for training and data symbols. Then, the sum-rate of the first and second tier respectively is

$$C_{\text{p}}^{\text{SUM, I}} = \frac{T - \tau}{T(N+L)} \sum_{j=1}^{N} \log_2(1 + \text{SINR}_{(\text{p}),j}) \tag{5.1}$$

$$C_{\text{s}}^{\text{SUM, I}} = \frac{T - \tau}{T(N+L)} \sum_{j=1}^{KN} \log_2(1 + \text{SINR}_{(\text{s}),j}). \tag{5.2}$$

Finally, for the sake of compactness, we let η_p and η_s be two parameters that measure the ratio between the sum-rate obtained with imperfect CSIT and the sum-rate obtained with perfect CSIT, for the first and second tier respectively.

In Figure 5.4, η_p and η_s are computed as different $\frac{\tau}{T}$ proportions are chosen, for SNR $\in \{0, 10, 20\}$ dB. Consider the MBS. We note that the optimal τ hinges on the SNR

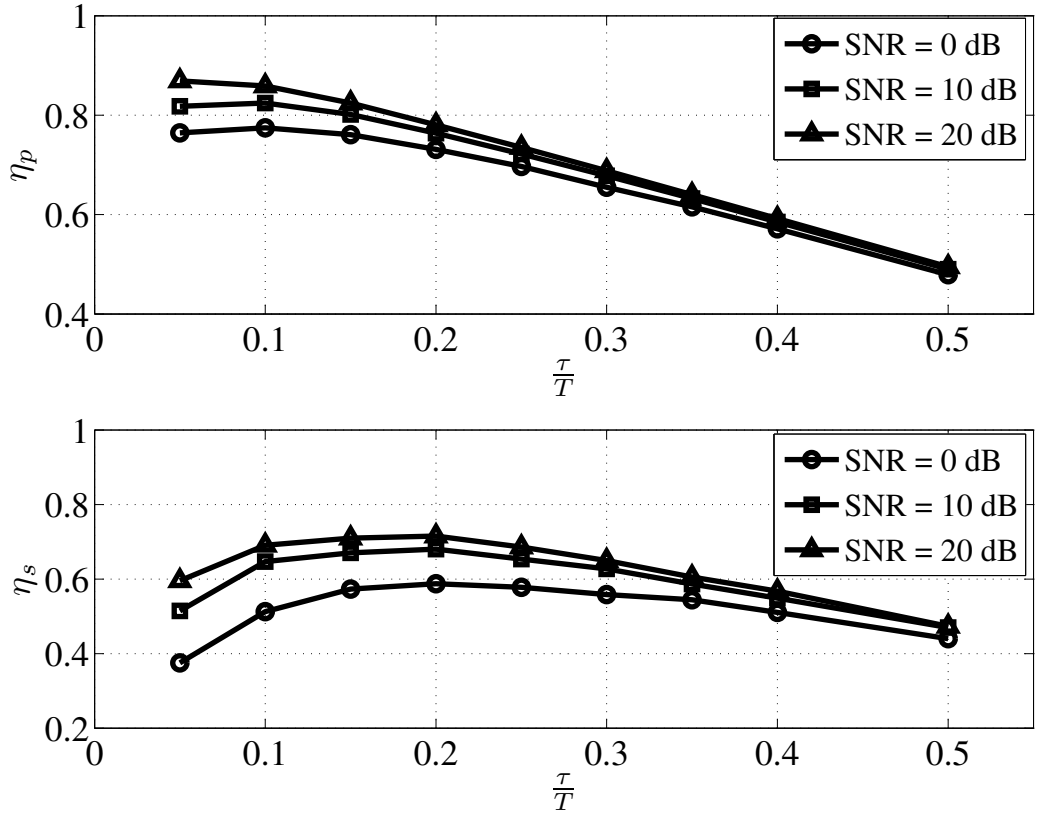

Figure 5.4: Ratio between the rate obtained with imperfect CSIT and the rate obtained with perfect CSIT for first and second tier as the SNR changes, $\beta = 1$ and $K = 3$ ($N = 64, L = 16$ and bandwidth of 0.96 Mhz).

and, in particular, $\tau = 0.1T$ is the optimal value in the low to medium SNR regime. On the other hand, the result for SNR= 20 dB shows that the pre-log factor dominates the sum-rate in this regime, and the best performance is obtained for the minimum value considered in the simulation, i.e., $\tau = 0.05T$. Interestingly, the rate loss experienced by the MBS for SNR= 0 dB is around 22%. Thus, the cross-tier interference cancelation provided by the inner stage of $\mathbf{W}$, i.e., $\mathbf{E}$, shows a promising robustness to imperfect CSIT even if the experienced SNR is very low. Switching our focus to the second tier, we see that the impact of the channel estimation errors at the SBSs on the effectiveness of the co-tier interference mitigation is larger. As a result, the SBSs experience a non-negligible sum-rate loss for imperfect CSIT, especially at very low SNR. However, differently from what we have seen for the MBS, the optimal value for τ does not show a clear dependence on the SNR, being consistently $\tau = 0.2T$ throughout the considered SNR range. In particular, we note how the sum-rate loss varies slowly with τ. This implies that small variations on the available time for the channel estimation w.r.t. the optimal τ are

acceptable by the SBSs, allowing for faster suboptimal channel estimations if necessary.

As seen in Section 4.3.3, the dimensionality of the system has a fundamental impact on the performance of the second tier. As a consequence, we now compute the performance of the cascaded precoder $\mathbf{W}$ as the number of transmit dimensions in the second tier increases. There are two choices at hand: 1) we modify the ratio between the number of transmit and receive dimensions, i.e., γ_{rx}, K fixed and β increases, 2) we simply deploy more SBS/SUE pairs, i.e., γ_{rx}, β fixed and K increases. Therefore, we let the load rate $\beta \in \{1, 2, 3\}$ in Figure 5.5 (with $\gamma_{rx} = 1$, $K = 3$), and the number of SBSs $K \in \{1, 3, 6\}$ in Figure 5.6 (with $\gamma_{rx} = 1$, $\beta = 3$). We assume a constant SNR= 10 dB. We first focus on η_p.

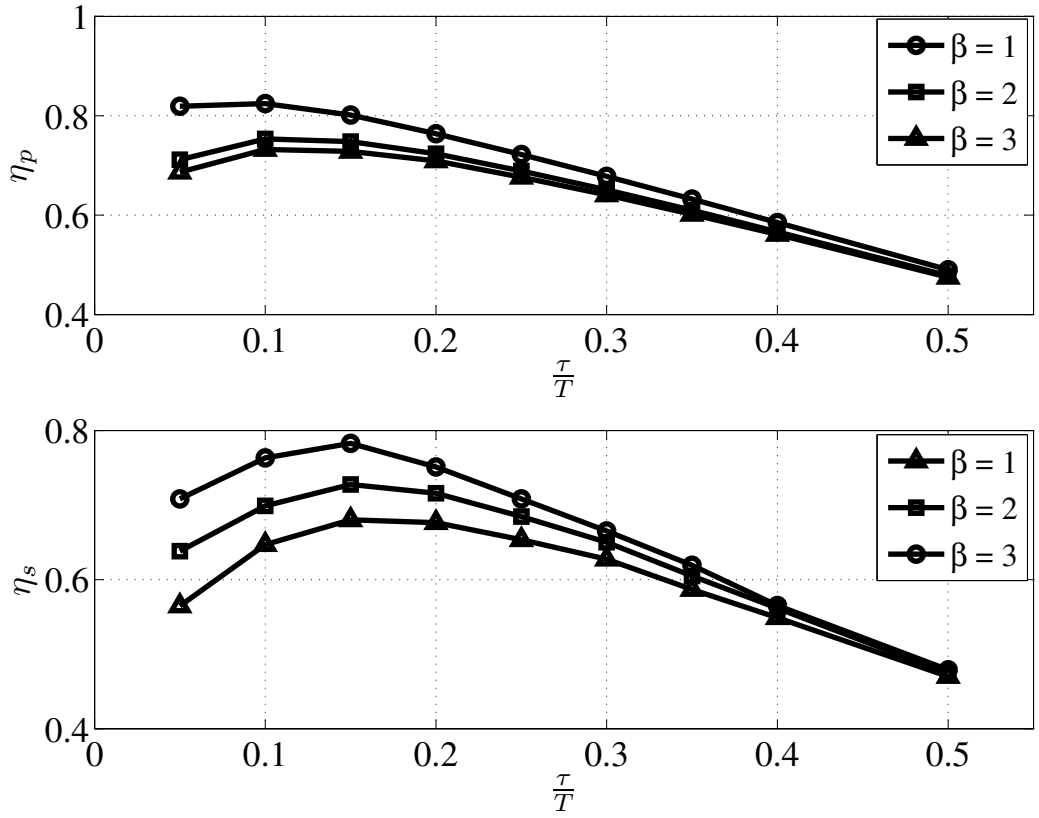

Figure 5.5: Ratio between the rate obtained with imperfect CSIT and the rate obtained with perfect CSIT for first and second tier as β changes, SNR = 10 dB and $K = 3$ ($N = 64, L = 16$ and bandwidth of 0.96 Mhz).

By comparing the two cases, the cascaded precoder confirms its robustness to imperfect CSIT and effectiveness for what concerns the cross-tier interference cancelation, regardless of the adopted approach. In particular, we note that $\tau = 0.1T$ is optimal for every tested configuration. The sum-rate loss of the SBSs shows a similar trend for the two considered approaches, despite the difference in the optimal value for τ, i.e., $\tau = 0.1T$ in Figure 5.5 and $\tau = 0.15T$ in Figure 5.6. Nevertheless, we notice that the sum-rate loss for the SBSs

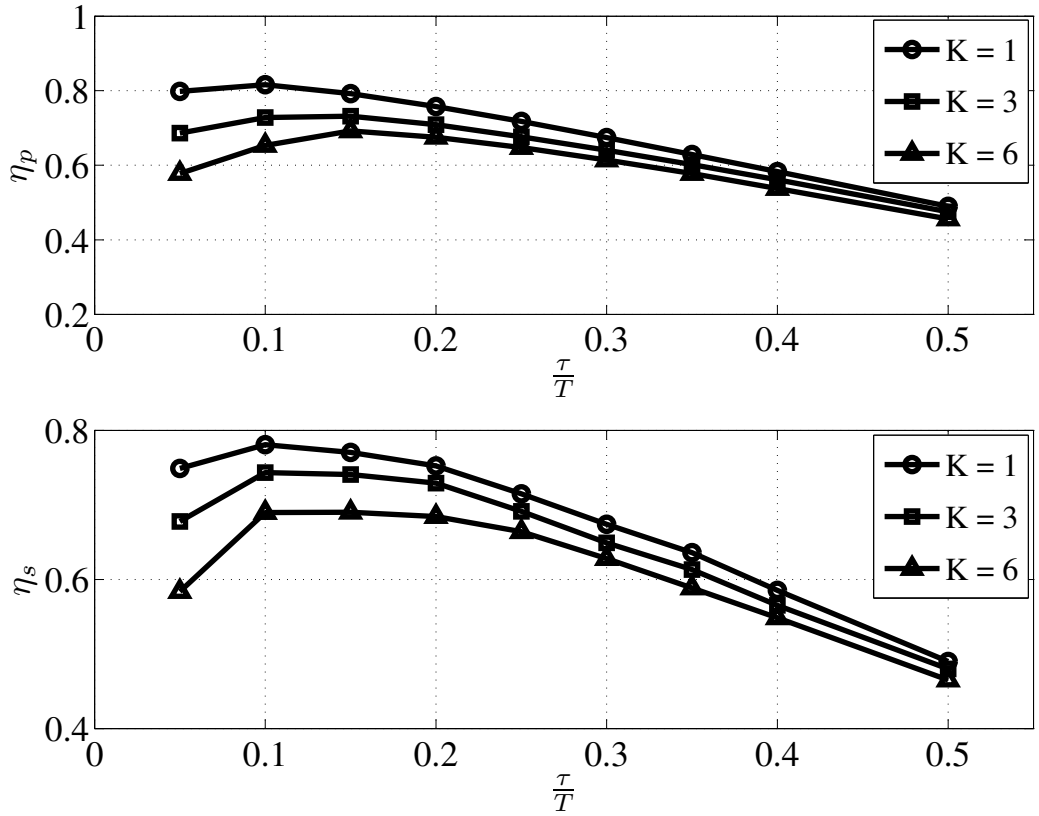

Figure 5.6: Ratio between the rate obtained with imperfect CSIT and the rate obtained with perfect CSIT for first and second tier as K changes, SNR = 10 dB and $\beta = 1$ ($N = 64, L = 16$ and bandwidth of 0.96 Mhz).

increases as K increases, but remarkably shows a decreasing behavior as β increases. This interesting result is due to the higher transmit diversity gain experienced by the SBSs as β increases. If the number of transmit dimensions is largely greater than the number of receive dimensions, the diversity gain can compensate the rate loss due to the reduced co-tier interference mitigation provided by the outer stage of $\mathbf{W}$ for imperfect CSIT, showing the potential of a densely deployed second-tier adopting the proposed technique.

Comparison with Existing Solutions

At this stage, we take a step back and consider the comparison proposed in Section 4.4.2. The interesting result obtained therein for perfect CSIT motivates a further study, when only imperfect CSIT is available. Let the channel estimations at the interested devices be performed according to the procedure described in this chapter. As before, the percent increase in achievable sum-rate of the two-tiered network is then computed for two different spectrum management strategies: 1) spectrum sharing between

the tiers thanks to the adoption of the cascaded precoder $\mathbf{W}$ at the SBSs, 2) complete spectrum separation between the tiers.

As done in Section 4.4.2 we assume $N = 64, L = 16$ (for a total bandwidth of 0.96 Mhz), a number of SBSs $K \in \{2, 8\}$, load rate $\beta = 3$ and cross-tier interference generated by the MBS towards the SUEs. The results of this comparison are depicted in In Figure 5.7. Both approaches provide a significant rate increase w.r.t. the single tier

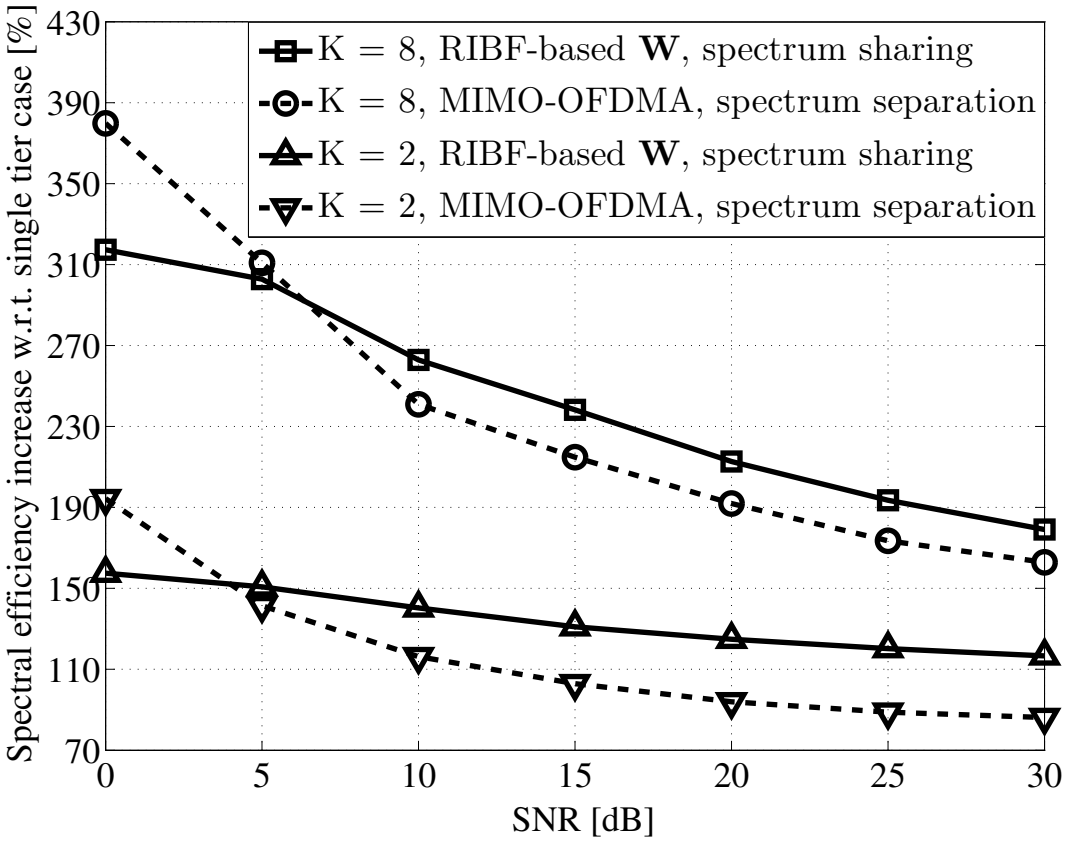

Figure 5.7: Percent increase in achievable sum-rate of a two-tiered network, $K \in \{2, 8\}$, $\beta = 3$ and cross-tier interference MBS $\rightarrow$ SUEs ($N = 64, L = 16$ and bandwidth of 0.96 Mhz). Imperfect CSIT.

case even in case of imperfect CSIT, and the higher K the larger the increase throughout the whole considered SNR range. Additionally, we remark that the range of the percent increase for imperfect CSIT is very similar to the outcome of the perfect CSIT study, showing a remarkable numerical consistency with the latter. However, a qualitative difference is present for the behavior at low SNR values. In particular, the proposed technique outperforms the complete separation approach for SNR values greater than 4 dB and 7 dB for $K = 2$ and $K = 8$, respectively. Accordingly, when the SNR are the estimating device is very low the quality of the performed channel estimations decreases, hence the effectiveness of the resulting $\mathbf{W}$ is reduced, both w.r.t. the co-tier interference mitigation

and cross-tier interference cancelation.

On the other hand, the advantage for other SNR regimes is evident and non-negligible, even though lower if compared to the perfect CSIT case. Therefore, the SBSs adopting $\mathbf{W}$ are able to exploit efficiently the higher multiplexing gain provided by the complete sharing approach even in case of imperfect CSIT, at the expense of a worse performance for low SNR if compared to the complete separation strategy. We remark that, as before, the impact of the cross-tier interference generated by MBS towards the SUEs on the performance of the second-tier is significant for medium and high SNR. Nevertheless, the percent increase in achievable sum-rate for this SNR values is still above 100%, confirming the findings in Chapter 4.

5.3 Synchronization

The second important issue that may affect the implementability of the proposed techniques, i.e., single user or centralized multi-user CIA, is synchronization at the receiver. An example of the importance of this aspect has been briefly discussed Section 5.1.2. In fact, if perfect synchronization of the received signals at the MUEs and SUEs is not ensured during τ_2, then residual interference may decrease the quality of the performed channel estimations, despite the adoption of orthonormal training sequences at the SBSs. As stated before, the implementation of suitable algorithms as the ones in [110, 111, 112, 113, 114, 115] may eliminate or reduce the issue, but in general the implementability of any of these techniques decrease with the number of involved devices. Therefore, for very dense network deployments, i.e., larger K and M in our scenario, achieving an accurate synchronization of many signals at each receiver might be extremely challenging.

It is important to note that synchronization does not have a crucial role only during the channel estimation phase, but also when the SBSs actually engage in the opportunistic transmission after the CSI acquisition. Specifically, the interference cancelation effect provided by the proposed precoder-based techniques is completely dependent on the CP removal at the MUEs. The development of techniques to achieve the synchronization of multiple signals at a given receiver is out of our scope. Nevertheless, we would like to discuss the challenges associated to this task and its implications for the practical implementation of the strategies proposed so far.

Let us consider 3.2, that is

$$\mathbf{y}_{\mathrm{p}} = \mathbf{H}_{\mathrm{pp}}\mathbf{x}_{\mathrm{p}} + \begin{bmatrix} \mathbf{K} \\ \mathbf{0}_{N\times L} \end{bmatrix} \mathbf{s}_{\mathrm{s}} + \mathbf{n}_{\mathrm{p}},$$

rewritten here for clarity, where $\mathbf{K} \in \mathbb{C}^{L\times(N+L)}$. Hence, if the primary and secondary signals are poorly synchronized at sample level at the receiver, the CP removal operation discards the wrong part of the secondary signal, leaving the primary receiver prone to an interference contribution collected from the $\mathbf{K}$ matrix. In order to have a visual

representation of this effect, let us focus on a single MUE receiving both the primary OFDM signal and the secondary CIA signal. If the latter signal arrives at the MUE before the former we have a situation as the one depicted in Figure 5.8. In particular, if

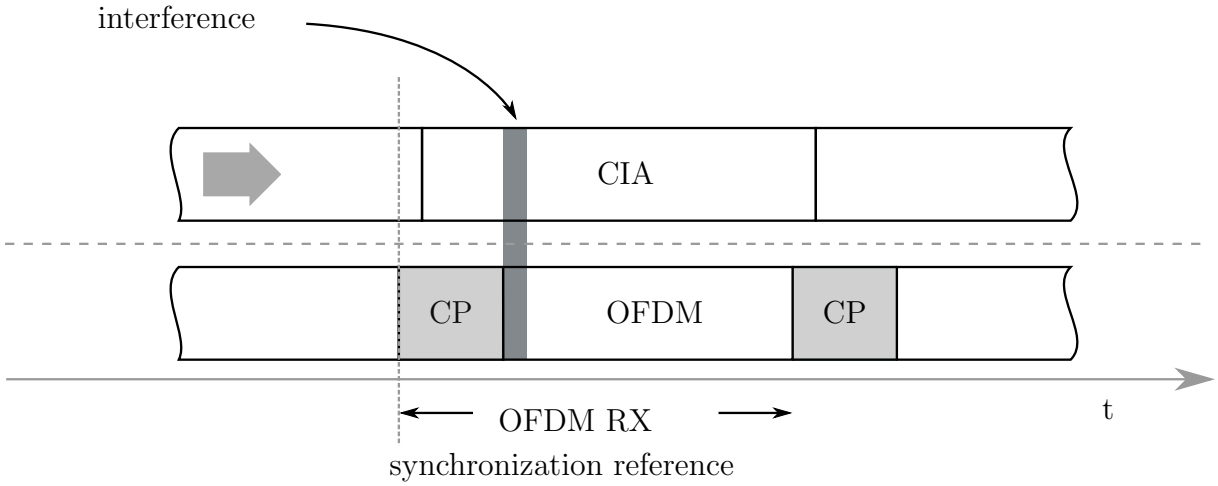

Figure 5.8: Wrong synchronization: CIA signal arriving at the OFDM receiver after the OFDM signal.

we let $w \in \mathbb{N}$ be the difference in number of samples between the beginning of the CIA and OFDM symbols, then the MUE experiences the residual interference carried by the last w rows of the matrix $\mathbf{K}$. A very similar problem occurs if the OFDM signal arrives at the MUE before the CIA signal, as in Figure 5.9. In this case, the MUE experiences the

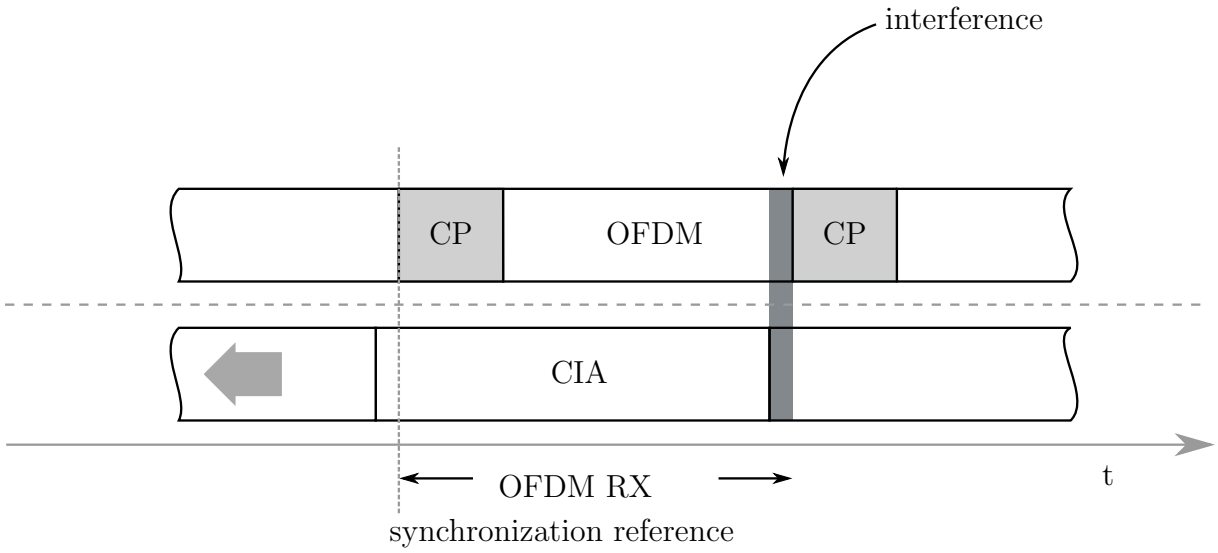

Figure 5.9: Wrong synchronization: CIA signal arriving at the OFDM receiver before the OFDM signal.

residual interference carried by the first w rows of the matrix $\mathbf{K}$. We remark that, in both

cases, the larger the difference in number of samples between the beginning of the CIA and OFDM symbols the stronger the resulting residual interference experienced by the MUE. Indeed, this problem is not exclusively inherent to CIA, but to any opportunistic null-space precoder that exploits the redundancy in OFDM, e.g., VFDM, for which a residual interference growing rapidly with the number of unsynchronized samples has been shown [116].

Now, let us consider the multi-user scenario introduced in Chapter 4. In this case, perfect synchronization of the received signals should be guaranteed at each MUE served by the MBS. In real-life scenarios, this operation would likely become more difficult as M, number of MUEs, increases. Thus, the amount of residual cross-tier interference generated to the MUEs could be non-negligible. If only one SBS is active in the second tier, two signals need to be synchronized at each MUE, i.e., CIA and OFDM signals. However, in case of K active SBSs, the synchronization of $K + 1$ signals must be guaranteed at each one of the M MUEs, due to the coordinated transmission performed in the second tier to mitigate the co-tier interference. On the other hand, only K transmitters would be cooperating to achieve the synchronization, being the MBS an autonomous device oblivious of the existence of the SBSs. This problem may be a showstopper for practical implementations of the cooperative solution studied in Chapter 4. Algorithms as the ones in [110, 111, 112, 113, 114, 115] might not be sufficient to ensure the fundamental synchronization requirement to guarantee the perfect cross-tier interference cancelation from the second to the first tier, especially for large numbers of MUEs and SBSs.

As a final observation, we would like to note that the nature of the communication in the first tier is another important element affecting the feasibility of the synchronization of the primary and secondary signals at the MUEs. Specifically, the synchronization task would be easier in case of structured communications, e.g. LTE/LTE-A, if compared to random access communications. In fact, in the former case, the SBSs could adapt their clock to match that of the MBS once the first synchronization has been acquired, and avoid re-synchronization procedures. Conversely, this would be unfeasible if random access communications were performed in the first tier. In this case, a new synchronization would be necessary in the second tier at each transmission performed by the MBS. Accordingly, the implementation of the proposed cascaded precoder structure might be impossible due to the lack of available time for transmission, after the synchronization algorithm and precoder computation performed in the second tier.

5.4 System-Level Overview

Up to now, a discussion on the impact of some physical layer aspects on the performance of the proposed strategy for two-tiered network deployments has been carried out. Several other system-level practical aspects have an important role on both the performance and the feasibility of the cascaded precoder solution in real-life scenarios. Nevertheless, a detailed discussion on this topic would highly depend on very specific assumptions on the architecture of the considered network. Conversely, in this section, we aim at providing

a general overview on the subject that may encompass more than one specific network configuration. Accordingly, we restrain our our attention to some important system-level aspects and qualitatively discuss their impact on the feasibility of the proposed strategy.

5.4.1 Backhaul Availability

Let us take a step back and consider the structure of the two-tiered scenario considered so far. In Chapter 4 we have introduced a model where a first tier composed of an OFDMA macro-cell is underlaid by a second tier populated by several cooperative SBSs. Therein, the presence of an infinite-capacity backhaul connecting all the SBSs has been assumed. Additionally, we note that this assumption has been exploited in this Chapter as well, when providing the example of adaptive channel estimation protocol for the second tier.

From a practical perspective, a backhaul can be divided in two main components: 1) a physical link, 2) network interfaces specifically designed for device-to-device communications, e.g., X2 interfaces [9] or similar. We start by considering the first component. Due to the expected massive deployment of SBSs in next generation networks, the resulting second tier will probably lack a predefined infrastructure. In fact, the SBSs will not necessarily be installed by provider but more likely by end-users [16]. As a consequence, the presence of a reliable and well-performing physical link connecting all the transmitters in the second tier may not always be guaranteed. On the other hand, even if the physical link were present, the massive and unplanned deployment of SBSs could also prevent the existence of the aforementioned network interfaces, necessary to establish a fruitful cooperation between the devices [117]. Finally, even if the SBSs could dispose of both a physical link and appropriate network interfaces, the resulting backhaul may not provide sufficient performance to meet the latency and delay requirements of state-of-the-art techniques for smart interference management in multi-cell networks [16, 117]. Analogously, the effectiveness of the cross-tier interference cancelation and co-tier interference management proposed in Chapter 4 could be largely reduced, and many of the advantages brought by the cascaded precoder approach could be nullified.

Naturally, if the presence of a backhaul between the SBSs could not be guaranteed, a fundamental requirement for the computation of the cascaded precoder in the second tier would not be fulfilled. In such scenarios, a practical implementation of the proposed cooperative solution would be impossible.

5.4.2 Dimensionality Aspect

Consider the model described in Section 4.2, where K single antenna SBS/SUE pairs populate the second tier. In this case, the load rate, as defined in Section 4.4, is computed as $\beta = \frac{L}{N}$. As seen in Section 4.3.3, the RIBF precoder can be constructed if the number of transmit dimensions is at least equal to the number of receive dimensions, i.e., $\beta = 1$. Accordingly, the proposed cooperative strategy can be implemented in a real-life scenario only if at least one of the two following approaches is adopted: 1) additional $\frac{N}{L} - 1$

antennas are installed at each SBS, 2) additional $\frac{N}{L} - 1$ SBSs are deployed in the second tier.

As thoroughly discussed in Chapter 4, the performance of the proposed cooperative solution highly depends on the value assumed by the load rate β. In particular, the larger β the more effective the outer precoder step by $\mathbf{\Phi}$, as given by (4.3.4), becomes. In fact, even though $\beta = 1$ is already a sufficient condition to compute an effective $\mathbf{\Phi}$, larger values are advisable to achieve a sum-rate for the second tier that can be compared to the upper bound capacity given by DPC, i.e., $\beta = 2.5$, as shown in Figure 4.4. In the following, we consider a numerical example to better understand the implications of this condition.

Let $\frac{L}{N} = \frac{1}{4}$, as in the extended mode of LTE/LTE-A [58]. Then a load rate $\beta = 2.5$ is obtained if each SBS is a 10-antennas device, or if the number of SBSs is 10-fold greater than the number of SUEs in the second tier. It is worth nothing that,if $\frac{L}{N} > \frac{1}{4}$, as is the case in the normal mode of LTE/LTE-A [58], the number of antenna per SBSs (or the ratio between the number of SBSs and SUEs) to have a second tier with a load rate $\beta = 2.5$ could be even larger. Accordingly, a very dense SBSs' deployment (or a very large number of antennas per SBS) is required to experience a sum-rate for the second tier that can be compared to the upper bound capacity given by DPC.

As a consequence, the implementation of the proposed technique in real-life scenarios would require specific network configurations to be effective. Despite being very promising, its application may be possible only for specific network deployments, due to environmental or economical constraints. On the other hand, the recent introduction in the market of new small-form factor transceivers is opening new fronts in network planning and could provide the necessary tools to simplify the implementation of strategies as the centralized solution herein proposed. These new base-stations, based on the concept of *system-on-a-chip*, are meant to blaze a new trail towards denser and more sophisticated network deployments, promising a radical change in the network design paradigms. For instance, products as the LightRadio® [118], are designed to work either as standalone devices or as parts of massive aggregated multi-device structures that can provide single or multiple-antenna capabilities. These technological advancements may significantly reduce the challenges associated to an implementation of the proposed centralized solution, despite the dimensionality constraint discussed in this section.

5.4.3 Cell-Edge Scenario

Consider the scenario described in Section 4.2. Therein, the two-tiered network has been modeled as a single macro-cell, hosting a group of MUEs, underlaid by a second tier populated by several cooperative SBSs, serving a group of SUEs. The development of the cascaded precoder structure proposed in Chapter 4 has been carried out in compliance with this model. Nevertheless, in real-life scenarios, the first tier is populated by more than one MBS. Accordingly, in this section, we discuss the possible impact that the presence of more than one macro-cell in the first tier may have on the feasibility of the proposed

cascaded precoder solution. Let us assume that the SBSs may be deployed in any point inside the coverage areas of the MBSs in the first tier and that, in the latter, the overlap between macro-cells is minimized. Accordingly, we can divide the SBSs in two categories: 1) *cell-center* SBSs, 2) *cell-edge* SBSs.

According to this distinction, the SBSs deployed in proximity to an MBS belong to the first category. We note that, in a real-life scenario, any wireless signal experiences propagation effects such as distance dependent path-loss and shadow fading, just to mention the most notable. Thus, we can safely assume that, in such scenarios, cell-center SBSs will likely generate interference only towards the MUEs associated to the closest MBS. In this case, the cross-tier interference cancelation precoder $\mathbf{E}_i$ (inner stage of the cascaded precoder $\mathbf{W}$) can be computed by the i^{th} SBS with no difference w.r.t. the procedure described in Section 4.3.2.

Now, we switch our focus to the SBSs belonging to the second aforementioned category, i.e., deployed in the cell-edge of one or more macro-cells. For simplicity in the representation, let us consider the case of two nearby macro-cells as pictured in Figure 5.10. Consider the SBS denoted by the bulb, deployed close to the edge of both

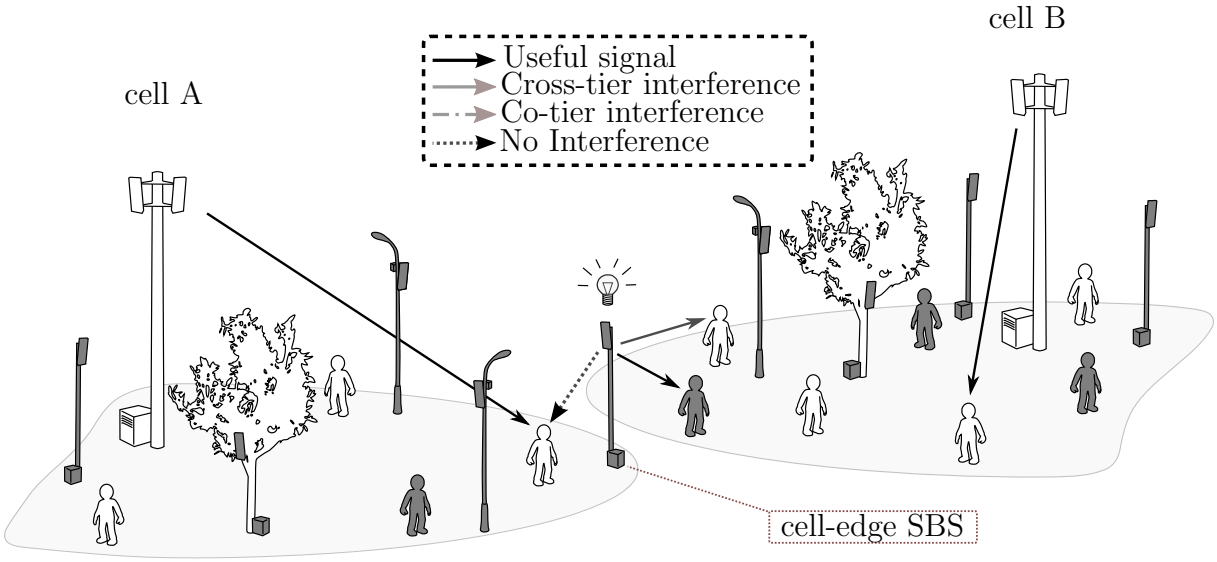

Figure 5.10: Cell-edge scenario.

cells and closer to the MBS of cell A. This cell-edge SBS must serve its associated SUE while canceling the interference generated towards a very close MUE hosted in cell A. In a single macro-cell scenario this could be accomplished by adopting the standard CIA approach, as described in previous chapters. Nevertheless, in this scenario, the situation is more complex. In particular, another MUE associated to cell B is close to the cell-edge and may suffer from severe cross-tier interference generated by the considered SBS, if not properly managed. This is a potentially serious problem for the practical implementation of the proposed technique in such scenarios. In fact, the opportunistic SBS might not be able to synchronize its transmission to more than one macro-cell, and adapt its precoder

accordingly. On the other hand, the cognitive nature of the devices in the second tier could offer practical solutions to tackle this challenging issue, by adapting to the specific operating scenario and network configuration, as follows:

- If a fractional frequency reuse is adopted in the first tier, each macro-cell will operate at a different carrier frequency w.r.t. the neighboring macro-cells, thus no problem exist for the cell-edge SBSs. In this case, the proposed technique can be seamlessly adapted to a macro-cellular first tier layout. Nevertheless, most last-generation standards for cellular networks suggest a frequency reuse 1.

- If a frequency reuse 1 is adopted in the first tier, then the proposed technique could be implemented in case of smart resource allocation in the first tier, by means of coordinated approaches between the MBSs (see [119, 120, 121, 122] and references therein for some examples). In this case, the cell-edge SBSs could find equivalent channel representations w.r.t. the neighboring MUEs belonging to different macro-cells, thanks to the coordinated resource allocation in the first tier, and compute the appropriate cross-tier interference cancelation precoder.

- If a frequency reuse 1 is adopted in the first tier, but no coordinated strategy is implemented by the MBSs, then the cell-edge SBSs could not be able to cancel or mitigate the cross-tier interference towards the neighboring MUEs belonging to different macro-cells, without requiring additional antennas. In fact, by exploiting the additional antennas (or a portion of the already installed antennas on the devices), specific beamforming techniques [123] may be used to cancel or mitigate the cross-tier interference towards the MUEs belonging to different macro-cells. We remark that, if a portion of the already installed antennas on the devices were used to perform the aforementioned additional beamforming tasks, then the load rate β, as defined in (4.4), would be lower. As a consequence, the achievable sum-rate for the second tier would be reduced if compared to the performance of the cascaded precoder approach for the single macro-cell case.

The aforementioned list is by no means exhaustive and only meant to provide possible hints to address the practical issues arising when implementing the proposed approach in the presence of more than one macro-cell. In fact, as previously discussed, the implementation of the cascaded precoder solution for cell-edge SBSs coexisting with several macro-cells is not straightforward. Nevertheless, the active SBSs in the second tier could always capitalize on the flexibility provided by their cognitive nature, to increase the feasibility of the proposed technique by adapting to the specific operating scenario and network configuration, as discussed above. Accordingly, if the first tier were not characterized by any of the above configurations, the nature of the SBSs' deployment may provide the tools to cope with the cell-edge SBSs problem. For instance, special subsets (clusters) of active SBSs may be created instead of considering a single larger cluster of SBSs (as the case in Chapter 4), or some cell-edge SBSs may declare themselves as unavailable for the current time slot if one or more MUEs belonging to a different macro-cell is detected in their proximity, and so on.

5.4.4 Mobility Pattern and Coeherence Time of the Channel

In general, cellular networks are characterized by mobility of the user equipments w.r.t. the base stations, regardless of the size of the cells in the network. The impact of the mobility of the users on the achievable capacity of the network can be significant. In fact, the coherence time of the channel between the base station and any receiver depends on the speed and mobility pattern of the latter [124]. Accordingly, several studies have been proposed to assess the relationship between user mobility and performance of the network.

It is known that a moderate mobility can increase the multi-user diversity inside a network, positively impacting its throughput [125, 126]. However, in case of highly mobile receivers, the benefits are usually overshadowed by the cost in terms of reduced coherence time of the channel and increased uncertainty in CSIT [127]. Modern networks host users that may be characterized by very different mobility patterns and profiles, moving at pedestrian as well as high speed when inside vehicles and trains. As a consequence, the effectiveness of many state-of-the-art signal processing techniques, relying on the quality and timeliness of the CSIT, depends on the homogeneity of these patterns and profiles [128]. In case of significant differences between them, the CSIT needed to perform the required optimization could be outdated or in general imperfect. Thus, strategies for an optimized transmission in these scenarios need to be robust enough to compensate for the lack of completely reliable global CSIT [129, 130].

In a two-tiered network, with both tiers sharing the available spectrum, the importance of the mobility profiles of the user equipments is possibly larger. In this scenario, the first tier operates as a typical single tier network, coping with the user mobility depending on the adopted standard, e.g., LTE/LTE-A, facing the aforementioned problems in case of optimized transmission. On the other, the opportunistic second tier must face a twofold issue as follows.

In a cooperative case as the one considered so far, the SBSs must dispose of CSIT w.r.t. the links towards both the MUEs and the SUEs. From a physical perspective, the coherence time of these channels constrain both the cross-tier interference cancelation and the co-tier interference mitigation problem. Solutions as [131, 132], and references therein, have been proposed for second tiers hosting only one SBS, serving one or more SUEs. In case of second tiers composed of several cooperative SBSs, the problem is more challenging. Specifically, the amount of time required by the signal processing at the SBSs may render the implementation of cooperative solutions hardly feasible. This is true especially in real-life scenarios, where many of the ideal assumptions considered in the first part of this work can not be guaranteed. The evidence of this problem is clear if we consider the proposed cascaded precoder structure, strongly dependent on a reliable CSIT to be effective. Accordingly, if the speed of the MUEs and SUEs were too high, and their mobility patterns and profiles were not sufficiently homogeneous, a practical implementation of the proposed approach might be impossible.

Furthermore, we note that the amount of data that each SBS must process to imple-

ment the proposed solution depends on the size of the bandwidth adopted in the first tier, being the total number of received symbols proportional to the bandwidth. Then, for a given processing capability at the SBSs, a larger bandwidth would require a longer processing time in the second tier, to compute the cascaded precoder $\mathbf{W}$. As a consequence, the feasibility of the proposed approach might depend not only on the mobility of the users but also on the size of the transmit bandwidth. From a practical point of view, the presence of the computational limitations at the SBSs may seem a further complication for the implementability of the solution based on the cascaded precoder. On the other hand, this permits to establish an interesting relationship between the mobility of the users and the computational capabilities of the SBSs, possibly providing opportunities to overcome the aforementioned limitations imposed by the mobility of the users. For instance, for a given number of MUEs and SUEs, the smaller the transmit bandwidth in the first tier the easier it would be for the SBSs to cope with a higher mobility of the users, thanks to the reduced computational time.

5.5 Concluding Observations

In this chapter we focused on some potential key and critical aspects related to the techniques presented so far. Accordingly, possible practical implementation issues have been identified and discussed, to underline what the limits of the centralized approach proposed in Chapter 4 are. In the next chapter, we will see how a distributed solution to the co-existence problem in two-tiered networks can possibly address some of these issues, or reduce their impact on the practical feasibility of the co-channel deployment of several SBSs inside the coverage area of a pre-existing MBS.

Chapter 6

Distributed co-tier interference management solution

In the previous chapter, we discussed the limitations that the centralized solution proposed in Chapter 4 may have in real-life implementations. In this chapter, we start from the previously drawn insights and propose a completely self-organizing approach to cross- and co-tier interference management at the SBSs that does not require explicit cooperation and signaling in the second tier, or among tiers, to be implemented. Accordingly, no specific network interfaces, i.e., X2 interface, or backhaul are assumed to be present in the second tier. We show that a local input signal subspace reduction at the SBSs, relying only on the information about the number of neighboring SUEs, is sufficient to each SBS to derive a suitable precoder to realize the coexistence between the two tiers, in a completely autonomous fashion. Numerical findings show that the proposed solution yields an overall spectral efficiency enhancement for the network, increasing with the number of SBSs. Subsequently, the impact of imperfect CSI at the SBSs is studied.

6.1 Problem Statement

Consider the DL of a two-tiered network as depicted in Figure 6.1, where, for clarity, only a reduced number of channels are represented. As done in previous chapters, we assume that the communications in the two tiers are performed in TDD mode, in compliance with the supported transmit modes in 4G standards as LTE/LTE-A [58, 50]. In the first tier, a group of M MUEs is served by a licensee single antenna MBS, by means of an OFDMA transmission. A second tier, comprised of K single antenna cognitive SBSs, is deployed inside the same area. Frequency reuse 1 is adopted for matters of spectral efficiency, thus each SBS opportunistically transmits over the same bandwidth as the MBS. As before, we assume that each SBS serves only one SUE, for clarity and simplicity in the model. The first tier is oblivious of the existence of the second, thus the two tiers are completely

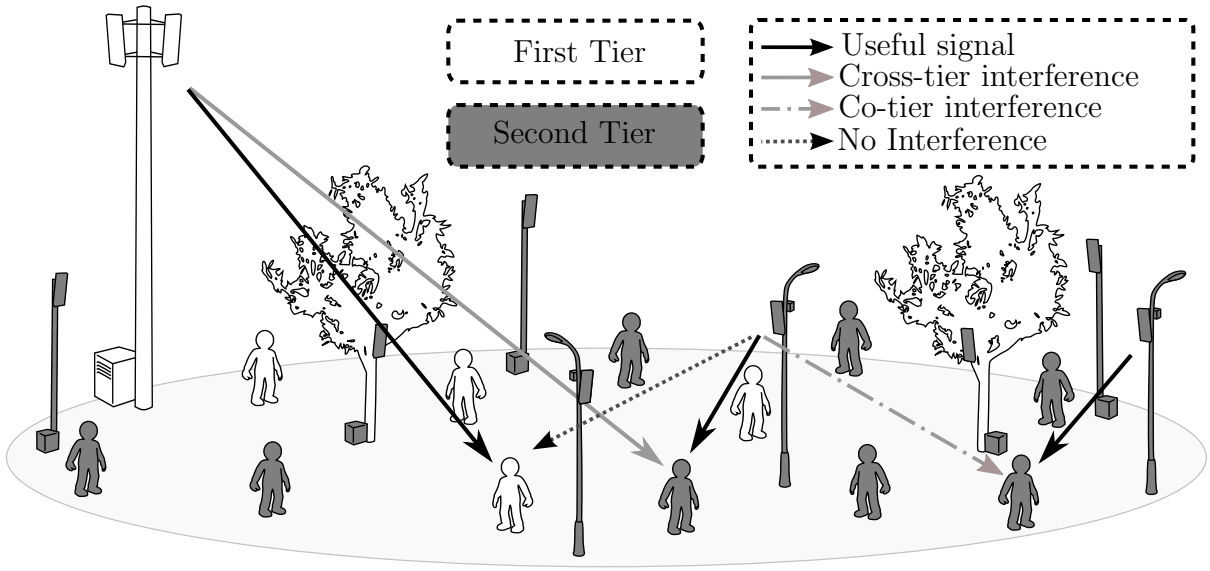

Figure 6.1: Two-tiered network [DL].

independent and no cross-tier cooperation is established. Therefore, the MBS does not implement any interference mitigation strategy, whereas according to the CR paradigm, the SBSs must protect the MUEs from undesired cross-tier interference.

From a practical point of view, the SBSs operating in two-tiered networks are expected to operate in a plug & play manner. These devices may be massively deployed by end-users and likely lack a predefined network infrastructure connecting them, as discussed in Chapter 1. Thus, a significant simplification of the network management paradigms is necessary to cope with this very dense network layout [7, 8]. The so-called SON [9] technology is believed to be one of the potential key factors to achieve this goal in future mobile networks. This new paradigm requires not only the design of new protocols to allow simplified network operations, but also the study of novel signal processing techniques to provide the expected spectral efficiency gains of the two-tiered network approach, at physical layer [15, 16]. In fact, as discussed in previous chapters, a co-channel deployment of MBSs and SBSs might yield high levels of ICI, potentially limiting the expected spectral efficiency enhancements of the two-tiered network layout [8]. For this reason, ICIC techniques have been extensively discussed during the standardization phase of recent systems, e.g., LTE-A,, and are still considered an open problem in the SON use cases [14].

A discussion on the coordinated interference management techniques proposed in the literature, to realize the coexistence of the two tiers and enhance the spectral efficiency of the network, has been proposed in Section 1.1.1. If the two tiers cooperate, popular strategies to achieve this goal include IA or coordinated beamforming, proposed and studied for several CSI/CSIT assumptions in [18, 22, 13] and references therein. In general, IA requires the presence of exploitable degrees of freedom in time, frequency or spatial domain, and a peculiar decoding at the receiver to realize the alignment. Con-

versely, coordinated beamforming involves signal processing at the transmitter only, but has more stringent CSI and signaling constraints. On the other hand, if the two tiers do not cooperate, CR approaches [27] are usually adopted to design the two-tiered network. In fact, by denoting the first tier as the primary system and the second opportunistic tier as the secondary system, any two-tiered network can be easily framed according to the CR paradigm [8]. In these approaches, the SBSs typically adopt opportunistic strategies and adapt their transmit parameters according to the surrounding environment [16, 34, 35]. Adaptation of IA or beamforming solutions to the CR setting have been recently proposed and analyzed for several network configurations [36, 37, 38]. Nevertheless, these approaches may usually require multiple spatial dimensions at the transmitter and/or receiver, several degrees of cross-tier and co-tier cooperation and bi-directional signaling between the MBSs/SBSs, requiring the existence of a link to this scope, e.g., X2 interfaces [9] and/or dedicated backhauls. However, as discussed in Chapter 5, due to the massive and likely unplanned SBSs' deployment, this link may be either nonexistent or unable to meet the latency and delay requirements of any of the discussed state-of-art techniques [117]. Accordingly, in this chapter, we start from these considerations (together with the discussion in Chapter 5) and consider a second tier where the existence of a link connecting the SBSs can not be ensured. Differently from the centralized approach proposed in Chapter 4, we assume that the SBSs must be able to operate autonomously and in a completely self-organizing fashion.

6.2 Model

Herein, we briefly describe the signal model adopted in this chapter. Let $\mathbf{h}_{\mathrm{ab}}^{(\cdot,\cdot)} \sim \mathcal{CN}(0, \mathbf{I}_{l+1}/(l+1))$ be i.i.d. Rayleigh fading channel vectors of size $l+1$ taps. As in previous chapters, we assume that Gaussian constellations are adopted in both tiers. The MBS transmits over N active subcarriers and add to the OFDM block a CP of size $L \geq l$, to combat ISI and IBI, for a total transmitted block size of $N+L$. Concerning the second tier, we assume that each SBS adopts a block transmission scheme as the MBS, i.e., block size of $N+L$.

Let $\mathbf{s}_{\mathrm{p}} \sim \mathcal{CN}(0, d(p_{\mathrm{p},1}, \ldots, p_{\mathrm{p},N}))$ be the N-sized MBS' input symbol vector. Then we can write the MBS' transmit symbol vector, of size $N+L$, as

$$\mathbf{x}_{\mathrm{p}} = \mathbf{A}\mathbf{F}^{-1}\mathbf{s}_{\mathrm{p}}, \tag{6.0}$$

where, as before, $\mathbf{F} \in \mathbb{C}^{N\times N}$ is a unitary DFT matrix as defined in Chapter 2 and $\mathbf{A}$ is an $(N+L)\times N$ CP insertion matrix given by (2.2). We focus on the j^{th} MUE. Let $\mathbf{B} = [\mathbf{0}_{N\times L}|\mathbf{I}_N]$ be a CP removal matrix, hence we can write $\mathbf{y}_{\mathrm{p}}^{(j)} \in \mathbb{C}^{N\times 1}$, received signal at j^{th} MUE as

$$\mathbf{y}_{\mathrm{p}}^{(j)} = \mathbf{F}\mathbf{B}\left(\mathbf{H}_{\mathrm{pp}}^{(1,j)}\mathbf{A}\mathbf{F}^{-1}\mathbf{x}_{\mathrm{p}} + \sum_{i=1}^{K}\mathbf{H}_{\mathrm{sp}}^{(i,j)}\mathbf{x}_{\mathrm{s}}^{(i)} + \mathbf{n}_{\mathrm{p}}^{(j)}\right), \tag{6.0}$$

where $\mathbf{n}_{\mathrm{p}}^{(j)} \sim \mathcal{CN}(0, \sigma^2 \mathbf{I}_{N+L})$ is an AWGN vector, $\mathbf{x}_{\mathrm{s}}^{(i)} \in \mathbb{C}^{(N+L)\times 1}$ is the i^{th} SBS' transmit symbol vector and $\sum_{i=1}^{K} \mathbf{H}_{\mathrm{sp}}^{(i,j)} \mathbf{x}_{\mathrm{s}}^{(i)}$ is the overall cross-tier interference generated by the SBSs. Now we switch our focus to the received signal at k^{th} SUE, i.e., $\mathbf{y}_{\mathrm{s}}^{(k)} \in \mathbb{C}^{N\times 1}$, and write

$$\mathbf{y}_{\mathrm{s}}^{(k)} = \mathbf{F}\mathbf{B}\left(\mathbf{H}_{\mathrm{ps}}^{(1,k)}\mathbf{A}\mathbf{F}^{-1}\mathbf{x}_{\mathrm{p}} + \mathbf{H}_{\mathrm{ss}}^{(k,k)}\mathbf{x}_{\mathrm{s}}^{(k)} + \sum_{i=1, i\neq k}^{K} \mathbf{H}_{\mathrm{ss}}^{(i,k)}\mathbf{x}_{\mathrm{s}}^{(i)} + \mathbf{n}_{\mathrm{s}}^{(k)}\right), \tag{6.0}$$

where $\mathbf{n}_{\mathrm{s}}^{(k)} \sim \mathcal{CN}(0, \sigma^2 \mathbf{I}_{N+L})$ is an AWGN vector. Note that, in (6.2), $\mathbf{H}_{\mathrm{ss}}^{(k,k)}\mathbf{x}_{\mathrm{s}}^{(k)}$ is the received signal coming from the k^{th} SBS and $\mathbf{H}_{\mathrm{ss}}^{(i,k)}\mathbf{x}_{\mathrm{s}}^{(i)}$ the co-tier interference component coming from the other SBSs.

6.3 Distributed solution

An opportunistic secondary tier can perform its operations according to different policies, depending on the adopted spectrum access approach. Accordingly, its cross-tier interference towards the licensee tier can be canceled, i.e., as in *overlay* CR networks [133], or mitigated, i.e., as in *underlay* CR networks [134]. On the other hand, if both tiers act opportunistically, adaptively accessing the spectrum to avoid collisions, an *interweave* CR network is realized [27]. As discussed in previous chapters, herein we model the considered scenario according to the overlay paradigm. Thus, we look for a technique that nulls the cross-tier interference coming from the SBSs, while mitigating the co-tier interference in the second tier, in a distributed way.

We recall the assumptions related to the knowledge available in the second tier. No spectrum sensing is performed by the SBSs, and no information about the spectrum characteristic, time resource allocation, primary system's message and power allocation is available. Thus, techniques based on DPC [17] or opportunistic IA [36] can not be implemented. Furthermore, due to the absence of a backhaul in the second tier, and the lack of information about the presence or performance of the network interfaces, no signaling is exchanged among SBSs. Consequently, techniques relying on coordinated beamforming at the transmitter are not implementable, and each SBS must adopt self-configuring and self-optimizing procedures. Finally, no cooperation is established between the SUEs/MUEs, i.e., single user decoding is performed. This is made to frame a scenario that does not rely on too unrealistic assumptions, as well as on hardly practically implementable algorithms in terms of required time and computational capabilities.

On the other hand, the TDD mode assumed herein provides a structured transmission scheme that can be opportunistically exploited in the second tier to design a suitable interference management strategy and enhance the network performance. Consider the following example. Let us assume that the first tier operates according to a recent standard as LTE/LTE-A, whose DL communications are performed by means of OFDMA. In such a scenario, each cognitive SBS in the second tier can exploit the TDD structure of the communication to acquire informations such as local CSIT w.r.t. the links towards the

SUEs/MUEs reached by its opportunistic transmission, and knowledge about the DL PRBs [50] allocation performed by the MBS in the first tier. For instance, one possible way to perform the DL channel estimation in LTE/LTE-A scenarios has been proposed in [135], where the UL channel is estimated by evaluating the sounding reference signals present in the LTE/LTE-A frame [50]. If said estimations are performed within the coherence time of the channel, then the UL and DL channels are considered reciprocal, hence the estimation of the former is sufficient to have the CSIT related to the latter. Concerning the PRBs allocation in LTE-A, as discussed in Chapter 5, this is communicated by the MBS to the MUEs through the PDCCH, within each DL sub-frame [104]. This information is meant to reach all the MUEs hosted in the cell, thus it is received by the SBSs as well, being the latter deployed in the coverage area of the MBS. From a practical point of view, these informations are limited, and cannot be shared among the SBSs. However, they are sufficient to design a suitable self-organizing strategy based on a linear transmit scheme for the SBSs, i.e., a cascaded precoder, as detailed in the following.

First, in Section 6.3.1, we will briefly revise the CIA model providing its adaptation to the considered scenario, and describe the structure of the inner precoder that nulls the cross-tier interference towards the MUEs in the first tier. Afterwards, the design of the outer precoder that mitigates the co-tier interference in the second tier, in a distributed fashion, is presented in Section 6.3.2.

6.3.1 Cross-tier interference alignment

As discussed in Chapter 4, CIA is implementable in OFDMA-based multi-user two-tiered networks thanks to the simple base-band processing that each OFDM receiver performs after the DFT operation in (6.2). As before, we assume that the MBS uniformly assigns the N active subcarriers to the MUEs, for simplicity. Let $\mathcal{N}$ be the set of active subcarriers, and $\mathcal{N}_j$ the set of $\frac{N}{M}$ subcarrier indices assigned to the j^{th} MUE, i.e., one or more PRBs, with $\bigcup_{j=1}^{M} \mathcal{N}_j = \mathcal{N}$ and $\bigcap_{j=1}^{M} \mathcal{N}_j = \emptyset$ by construction. Then we can express $\mathbf{D}_j \in \{0,1\}^{(N \times N)}$, filter adopted by the j^{th} MUE to recover $\mathcal{N}_j$, with $[\mathbf{D}_j]_{(n,n)} = 1$ if $n \in \mathcal{N}_j$ and zero otherwise, as

$$\begin{cases} \sum_{n=1}^{N} \mathbb{1}_{\{n \in \mathcal{N}_j\}} [\mathbf{D}_j]_{(n,n)} = \frac{N}{M} \\ \sum_{j=1}^{M} \mathbf{D}_j = \mathbf{I}_N{}^1, \end{cases} \tag{6.0}$$

Therefore, the j^{th} MUE can extract the PRBs of interest by means of $\mathbf{D}_j$ and we can rewrite (6.2) as

$$\mathbf{y}_{\mathrm{p}}^{(j)} = \mathbf{D}_j \mathbf{F} \mathbf{B} \left(\mathbf{H}_{\mathrm{pp}}^{(1,j)} \mathbf{A} \mathbf{F}^{-1} \mathbf{x}_{\mathrm{p}} + \mathbf{n}_{\mathrm{p}}^{(j)} \right) + \sum_{i=1}^{K} \mathbf{T}_{\mathrm{sp}}^{(i,j)} \mathbf{x}_{\mathrm{s}}^{(i)}, \tag{6.0}$$

with $\mathbf{T}_{\text{sp}}^{(i,j)} = \mathbf{D}_j\mathbf{F}\mathbf{B}\mathbf{H}_{\text{sp}}^{(i,j)} \in \mathbb{C}^{N\times(N+L)}$ equivalent representation of the interference link from the i^{th} SBS to the j^{th} MUE. The user orthogonality in the frequency domain is then realized thanks to the filter $\mathbf{D}_j$, and an equivalent representation of the overall received signal in the first tier can be written from (6.3.1) as

$$\mathbf{y}_{\text{p}} = \sum_{j=1}^{M} \mathbf{y}_{\text{p}}^{(j)} = \sum_{j=1}^{M} \mathbf{D}_j\mathbf{F}\mathbf{B}\left(\mathbf{H}_{\text{pp}}^{(1,j)}\mathbf{A}\mathbf{F}^{-1}\mathbf{x}_{\text{p}} + \sum_{i=1}^{K}\mathbf{H}_{\text{sp}}^{(i,j)}\mathbf{x}_{\text{s}}^{(i)} + \mathbf{n}_{\text{p}}^{(j)}\right). \tag{6.0}$$

Similarly, an equivalent representation of the overall interference channel between the i^{th} SBS and the MUEs in the first tier can be found, thanks to the structure of $\mathbf{D}_j$, i.e., $\mathbf{T}_{\text{sp}}^{(i,\cdot)} = \sum_{j=1}^{M}\mathbf{T}_{\text{sp}}^{(i,j)}$. We note that, the number of MUEs inside the coverage area of the i^{th} SBS will likely be lower than M, total number of MUEs in the first tier. This does not alter the validity of the previous and following equations. In fact, if the j^{th} MUE were not inside the coverage area of the i^{th} SBS, then we could safely consider $\mathbf{T}_{\text{sp}}^{(i,j)} = \mathbf{0}_{N\times(N+L)}$, preserving the consistency of the general signal model.

In the considered scenario, by construction, $\text{rank}(\mathbf{T}_{\text{sp}}^{(i,\cdot)}) = N$, thus for the rank-nullity theorem [73] we have

$$\dim\ker(\mathbf{T}_{\text{sp}}^{(i,\cdot)}) = L, \tag{6.0}$$

$\forall\mathbf{H}_{\text{sp}}^{(i,j)} \in \mathbb{C}^{(N+L)\times(N+L)}$. As seen in Chapter 4, if we assume perfect CSI at the SBSs w.r.t. the cross-tier interference links $\mathbf{h}_{\text{sp}}^{(\cdot,\cdot)}$, the i^{th} SBS can always find a matrix $\mathbf{E}^{(i)} \in \mathbb{C}^{(N+L)\times L}$ such that

$$\text{span}(\mathbf{E}^{(i)}) = \ker(\mathbf{T}_{\text{sp}}^{(i,\cdot)}), \tag{6.0}$$

and $\mathbf{T}_{\text{sp}}^{(i,\cdot)}\mathbf{E}^{(i)} = \mathbf{0}_{N\times L}$. Now, let us introduce $\mathbf{s}_{\text{s}}^{(i)} \sim \mathcal{CN}(0, d(p_{\text{s},1}^{(i)}, \ldots, p_{\text{s},L}^{(i)}))$ as an L-sized input symbol vector at the i^{th} SBS, and define

$$\mathbf{x}_{\text{s}}^{(i)} = \mathbf{E}^{(i)}\mathbf{s}_{\text{s}}^{(i)}. \tag{6.0}$$

For the sake of clarity, we keep our focus on the j^{th} MUE and let $\tilde{\mathbf{T}}_{\text{sp}}^{(i,j)} = \mathbf{T}_{\text{sp}}^{(i,j)}\mathbf{E}^{(i)} \in \mathbb{C}^{N\times L}$. We can rewrite (6.3.1) as

$$\mathbf{y}_{\text{p}}^{(j)} = \mathbf{D}_j\mathbf{F}\mathbf{B}\left(\mathbf{H}_{\text{pp}}^{(1,j)}\mathbf{A}\mathbf{F}^{-1}\mathbf{x}_{\text{p}} + \mathbf{n}_{\text{p}}^{(j)}\right) + \sum_{i=1}^{K}\tilde{\mathbf{T}}_{\text{sp}}^{(i,j)}\mathbf{s}_{\text{s}}^{(i)}, \tag{6.0}$$

where $\tilde{\mathbf{T}}_{\text{sp}}^{(i,j)}$ has the $\frac{N}{M}$ rows whose indexes $n \in \mathcal{N}_j$ composed of zero entries. Consequently, we can write

$$\sum_{n\in\mathcal{N}_j}\sum_{m=1}^{L}[\tilde{\mathbf{T}}_{\text{sp}}^{(i,j)}]_{(n,m)} = 0, \tag{6.0}$$

and this holds $\forall\mathbf{s}_{\text{s}}^{(i)} \in \mathbb{C}^{L\times 1}$, regardless of the size of $\mathbf{h}_{\text{sp}}^{(i,j)}$, according to (6.3.1) and (6.3.1). The interference signal coming from i^{th} SBS is aligned at the j^{th} MUE, and confined into the same constant sized subset of subcarriers given by $\mathcal{N}\setminus\mathcal{N}_j$, $\forall i \in [1, K]$. As a consequence, the desired $\frac{N}{M}$ interference free dimensions at the j^{th} MUE can be

obliviously extracted by processing the received signal in (6.2) with $\mathbf{D}_j$, as in the classic OFDMA receiver processing, to finally obtain

$$\mathbf{y}_{\mathrm{p}}^{(j)} = \mathbf{D}_j \mathbf{B}\mathbf{F} \left(\mathbf{H}_{\mathrm{pp}}^{(1,j)} \mathbf{A}\mathbf{F}^{-1} \mathbf{x}_{\mathrm{p}} + \mathbf{n}_{\mathrm{p}}^{(j)} \right), \tag{6.0}$$

where the cross-tier interference coming from the second tier has been completely canceled. At this stage, we can define the spectral efficiency for the j^{th} MUE as

$$R_{\mathrm{p}}^{(j)} = \frac{1}{N+L} \sum_{i=1}^{N} \log_2 \left(1 + \mathrm{SINR}_{(\mathrm{p},i)}^{(j)} \right), \tag{6.0}$$

with

$$\mathrm{SINR}_{(\mathrm{p},i)}^{(j)} = \frac{p_{\mathrm{p},i} \left| \left[\mathbf{D}_j \mathbf{F}\mathbf{B}\mathbf{H}_{\mathrm{pp}}^{(1,j)} \mathbf{A}\mathbf{F}^{-1} \right]_{(i,i)} \right|^2}{\sigma^2}, \tag{6.0}$$

SINR of its i^{th} received symbol. We remark that the choice of $\mathbf{D}_j$ depends uniquely on the resource allocation performed at the MBS. As a consequence, the degrees of freedom of the primary OFDMA transmission and its overall spectral efficiency $R_{\mathrm{p}} = \sum_{j=1}^{M} R_{\mathrm{p}}^{(j)}$ are preserved, regardless of the transmit power at the i^{th} SBS.

Now we switch our focus to the second tier. As in the centralized approach analyzed in Chapter 4, herein each of the K SBSs can potentially exploit up to L degrees of freedom, $\forall K \in \mathbb{N}$. Accordingly, the number of input symbol that the i^{th} SBS can precode cannot exceed L, if perfect cross-tier interference cancelation must be ensured. On the other hand, the co-tier interference generated by concurrent transmissions in the second tier may strongly limit its overall achievable spectral efficiency, if unmanaged. A strategy to mitigate this co-tier interference is introduced in the following section.

6.3.2 Co-tier interference mitigation

The CIA solution presented in Section 6.3.1 guarantees up to L transmit dimensions per SBS. The interference alignment and consequent nulling can be obtained regardless of K, number of SBSs. This remarkable achievement shows the potential of CIA when perfect CSIT w.r.t. the cross-tier interference link is available in the second tier. Nevertheless, a channel estimation in real-life scenarios is valid only throughout the duration of the coherence time of the channel, which is finite. This imposes hard constraints for a practical implementation of any co-tier interference management scheme in this scenario, thus fast and preferably one-shot strategies are needed. For instance, the centralized solution for the co-tier interference mitigation proposed in Chapter 4 may not always be implementable, due to the tight time constraints to fulfill, as discussed in Chapter 5. Additionally, since the SUEs are standard OFDM receivers, no further decoding for subspace decomposition to realize the IA can be adopted. Thus, a fundamental requirement to implement standard distributed IA schemes relying on iterative schemes between transmitter and receiver

[21] is not met. The distributed approach relying only on transmitter processing for DL multi-cell scenarios proposed in [136] can not be adopted as well. Despite the promising achievable spectral efficiency, this approach is hardly applicable in our scenario, since it is DPC-based, thus affected by practical implementability issues. As assumed in Section 6.1, each SBS disposes of only one antenna. Therefore, due to dimensionality issues, i.e., $N >> L$, no coordinated [13] or distributed beamforming [136] can be performed efficiently, as seen in Chapter 4. Finally, as discussed in Section 6.1, due to the unplanned SBSs' deployment, no bi-directional signaling can be guaranteed in the second tier, and the co-tier interference problem must be addressed by means of a self-organizing technique implementable by the SBSs in an autonomous manner. Accordingly, we seek for a linear outer precoder to be adopted by the SBSs to provide the desired spectral efficiency enhancements for the considered two-tiered network, and a novel distributed interference mitigation scheme is proposed.

We note that, the co-tier interference in the second tier is completely unrelated to the cross-tier interference generated by the MBS towards the SUEs. Regardless of the number of active SBSs, the latter will always impact the performance of the second tier and does not represent a parameter that can be appropriately tuned by means of a mechanism at the SBSs. Consequently, the equations provided in this section will not include the cross-tier interference coming from the first tier. We remark that this simplification is made to simplify the equations in the algorithm derivation and does not imply the assumption of absence of cross-tier interference from the MBS to SUEs. We start by plugging the previously derived precoder into (6.2). We focus on the k^{th} SUE and write

$$\mathbf{y}_{\mathrm{s}}^{(k)} = \mathbf{F}\mathbf{B}\left(\mathbf{H}_{\mathrm{ss}}^{(k,k)}\mathbf{E}^{(k)}\mathbf{s}_{\mathrm{s}}^{(k)} + \sum_{i=1,i\neq k}^{K}\mathbf{H}_{\mathrm{ss}}^{(i,k)}\mathbf{E}^{(i)}\mathbf{s}_{\mathrm{s}}^{(i)} + \mathbf{n}_{\mathrm{s}}^{(k)}\right), \tag{6.0}$$

Let

$$\mathbf{T}_{\mathrm{ss}}^{(j,k)} = \mathbf{F}\mathbf{B}\mathbf{H}_{\mathrm{ss}}^{(j,k)}\mathbf{E}^{(j)} = [\mathbf{t}_{\mathrm{ss},1}^{(j,k)} \mid \ldots \mid \mathbf{t}_{\mathrm{ss},N}^{(j,k)}]^{\mathrm{T}} \in \mathbb{C}^{N\times L} \tag{6.0}$$

be the equivalent representation of the channel between the j^{th} SBS and the k^{th} SUE, $\forall j \in [1, K]$. Note that, $\mathbf{F}$ is unitary, hence $\tilde{\mathbf{n}}_{\mathrm{s}} = \mathbf{F}\mathbf{B}\mathbf{n}_{\mathrm{s}}^{(k)} \sim \mathcal{CN}(0, \sigma^2\mathbf{I}_N)$. After the DFT, the k^{th} SUE disposes of N received symbols, i.e., N different linear combinations of the $L << N$ input symbols transmitted by the k^{th} SBS, corrupted by the interference coming from the remaining $K-1$ SBSs and by the thermal noise. As a consequence, the equivalent CIA channel representation always provides a significant receive diversity effect to the second tier transmission, by construction. Interestingly, the SBSs may exploit this inherent feature of the system to induce a power gain at each SUE [59], with no need for cooperation or coordinated beamforming strategies. Consider the i^{th} received symbol at k^{th} SUE, its SINR is defined as

$$\mathrm{SINR}_{(\mathrm{s},i)}^{(k)} = \frac{\mathbf{t}_{\mathrm{ss},i}^{(k,k)\mathrm{H}} d(p_{\mathrm{s},1}^{(k)}, \ldots, p_{\mathrm{s},L}^{(k)})\mathbf{t}_{\mathrm{ss},i}^{(k,k)}}{\sigma^2 + \sum_{j=1,j\neq k}^{K}\mathbf{t}_{\mathrm{ss},i}^{(j,k)\mathrm{H}} d(p_{\mathrm{s},1}^{(j)}, \ldots, p_{\mathrm{s},L}^{(j)})\mathbf{t}_{\mathrm{ss},i}^{(j,k)}}. \tag{6.0}$$

Moreover, we let $R_{\mathrm{s}} = \sum_{k=1}^{K} R_{\mathrm{s}}^{(k)}$ be the spectral efficiency of the second tier, where

$$R_{\mathrm{s}}^{(k)} = \frac{1}{N+L} \sum_{i=1}^{N} \log_2 \left(1 + \mathrm{SINR}_{(\mathrm{s},i)}^{(k)}\right) \tag{6.0}$$

is the spectral efficiency of the link between the k^{th} SBS/SUE pair, logarithmic function of $\mathrm{SINR}_{(\mathrm{s},i)}^{(k)}$. Diversity and power gains directly impact the SINR at the receiver. Therefore, the input signal subspace dimension at the SBSs, affecting the dimensionality of the system, has a fundamental role in the performance of the second tier.

No communication is established between the SBSs, hence no cooperation can be realized. However, an implicit coordination mechanism could be adopted to aim at an overall network spectral efficiency enhancement. In particular, we can design a transmit strategy that constrains the input symbol subspace to belong to $\mathbb{C}^{1\times\theta}$, with $\theta \in [1, L]$ natural number. This way, the k^{th} SBS may adaptively reduce the number of input symbols to transmit to its served SUE depending on the number of detected neighboring SUE/SBS pairs, to improve the receive diversity, thus the SINR per received symbol. Then let $\mathbf{u}_{\mathrm{s}}^{(k)} \sim \mathcal{CN}(0, d(p_{\mathrm{s},1}^{(k)}, \ldots, p_{\mathrm{s},\theta}^{(k)}))$ be a new θ-sized input symbol vector at the k^{th} SBS. If we define $\mathbf{\Theta}^{(k)} \in \mathbb{C}^{L\times\theta}$ as an outer precoder such that $\mathbf{s}_{\mathrm{s}}^{(k)} = \mathbf{\Theta}^{(k)}\mathbf{u}_{\mathrm{s}}^{(k)}$ and $\mathbf{Z}^{(k)} = \mathbf{E}^{(k)}\mathbf{\Theta}^{(k)} \in \mathbb{C}^{L\times\theta}$, then we can rewrite (6.3.1) as

$$\mathbf{x}_{\mathrm{s}}^{(k)} = \mathbf{Z}^{(k)}\mathbf{u}_{\mathrm{s}}^{(k)}. \tag{6.0}$$

At this stage, each SBS has two degrees of freedom to design $\mathbf{\Theta}^{(k)}$, i.e., the choice of a suitable signal subspace structure and its dimension θ. We first focus on the former and, for the moment, assume that θ is known at each SBS. We remark that, the eigenvalue and eigenvector distribution of a finite dimension Toeplitz matrix is currently not known, and the same holds true for its kernel structure, e.g. $\ker(\mathbf{T}_{\mathrm{sp}}^{(i,\cdot)})$. Thus, neither deterministic nor stochastic information about the interference generated to the k^{th} SUE by the neighboring non-serving SBSs is available. On the other hand, by looking at (6.3.2), we see that the signal transmitted by each SBS contributes to $\mathrm{SINR}_{(\mathrm{s},i)}^{(k)}$ either at the numerator or at the denominator. Consequently, only two possible strategies can be identified to increase the SINR per received symbol, and consequently enhance $R_{\mathrm{s}}^{(k)}$, i.e., the k^{th} SBS contribution to R_{s}, as follows.

CIA A

The first approach, hereafter denoted as *CIA A*, is an aggressive strategy adopted by the k^{th} SBS aiming at the maximization of (6.3.2), without considering the impact on the SINR per received symbol at the non-served SUEs, given by (6.3.2). The scenario reduces to a point-to-point link connecting the k^{th} SBS/SUE pair, disturbed by an unknown source of interference generated by the non-serving SBSs and by the thermal noise. The interference generated by the non-serving SBSs to the k^{th} SUE cannot be predicted by

the k^{th} SBS, thus it is ignored and only the CSIT related to $\mathbf{h}_{\mathrm{ss}}^{(k,k)}$ is needed to perform the input subspace selection. Now, we let $\mathbf{T}_{\mathrm{ss}}^{(k,k)} = \mathbf{U}_{\mathbf{T}}^{(k)}\mathbf{\Lambda}_{\mathbf{T}}^{(k)}\mathbf{V}_{\mathbf{T}}^{(k)}$ be the SVD of the equivalent channel matrix representing the link connecting the k^{th} SBS/SUE pair, with $\mathbf{U}_{\mathbf{T}}^{(k)} = [\mathbf{u}_{\mathbf{T},1}^{(k)}|\dots|\mathbf{u}_{\mathbf{T},N}^{(k)}] \in \mathbb{C}^{N\times N}$, $\mathbf{V}_{\mathbf{T}}^{(k)} = [\mathbf{v}_{\mathbf{T},1}^{(k)}|\dots|\mathbf{v}_{\mathbf{T},L}^{(k)}] \in \mathbb{C}^{L\times L}$ unitary matrices and $\mathbf{\Lambda}_{\mathbf{T}}^{(k)} = \left[\Delta\left(\sqrt{\lambda_{\mathbf{T},1}^{(k)}},\dots,\sqrt{\lambda_{\mathbf{T},L}^{(k)}}\right), \mathbf{0}_{L\times(N-L)}\right]^T$, where $\sqrt{\lambda_{\mathbf{T},i}^{(k)}}$ are the non negative singular values of $\mathbf{T}_{\mathrm{ss}}^{(k,k)}$ such that $\sqrt{\lambda_{\mathbf{T},1}^{(k)}} \geq \sqrt{\lambda_{\mathbf{T},2}^{(k)}} \geq \cdots \geq \sqrt{\lambda_{\mathbf{T},L}^{(k)}}$. Then the k^{th} SBS can approximate (6.3.2) as a sum of decreasing positive terms and write

$$\widehat{R}_{\mathrm{s}}^{(k)} = \frac{1}{N+L}\sum_{i=1}^{L}\log_2\left(1+\frac{\lambda_{\mathbf{T},i}^{(k)}}{\sigma^2}\right). \tag{6.0}$$

A this stage, we can define $\Theta^{(k)} = [\mathbf{v}_{\mathbf{T},1}^{(k)}|\dots|\mathbf{v}_{\mathbf{T},\theta}^{(k)}] \in \mathbb{C}^{L\times\theta}$, with $\theta \in [1, L]$, as the outer precoder that aligns the input signal to the θ strongest eigenmodes of $\mathbf{T}_{\mathrm{ss}}^{(k,k)}$, i.e., the most efficient subspace of span $(\mathbf{E}^{(k)})$ for the direct link spectral efficiency maximization. Then, (6.3.2) can be rewritten as

$$\widehat{R}_{\mathrm{s}}^{(k)}(\theta) = \frac{1}{N+L}\sum_{i=1}^{\theta}\log_2\left(1+\frac{\lambda_{\mathbf{T},i}^{(k)}}{\sigma^2}\right), \tag{6.0}$$

where the dependency of the spectral efficiency on θ has been explicitly shown for clarity. Note that, in (6.3.2) and (6.3.2), a uniform power allocation at the k^{th} SBS has been assumed for simplicity in the representation, with $p_{\mathrm{s},i}^{(k)} = 1$, $\forall i \in [1, L]$. This does not reduce the generality of the approach. In fact, for a given power budget, stronger eigenmodes always result in a more efficient transmission, regardless of the power loading strategy [59].

CIA B

The second approach, hereafter denoted as *CIA B*, is a conservative strategy aiming at the reduction of k^{th} SBS' contribution to the denominator of $\mathrm{SINR}_{(\mathrm{s},i)}^{(j)}$, $\forall j \in [1, K] \setminus k$. In this case, the scenario reduces to a point-to-multi-point link between the k^{th} SBS and its $K-1$ non-served SUEs, whose equivalent channel representation can be expressed as

$$\begin{aligned}\mathbf{T}_{\mathrm{ss}}^{(k,[k])} &= [\mathbf{T}_{\mathrm{ss}}^{(k,1)\mathrm{T}},\dots,\mathbf{T}_{\mathrm{ss}}^{(k,k-1)\mathrm{T}},\mathbf{T}_{\mathrm{ss}}^{(k,k+1)\mathrm{T}},\dots,\mathbf{T}_{\mathrm{ss}}^{(k,K)\mathrm{T}}]^{\mathrm{T}} \\ &= [\mathbf{t}_{\mathrm{ss},1}^{(k,[k])} \mid \dots \mid \mathbf{t}_{\mathrm{ss},L}^{(k,[k])}] \in \mathbb{C}^{N(K-1)\times L}.\end{aligned} \tag{6.1}$$

The impact of the j^{th} SBSs' transmission on (6.3.2), $\forall j \neq k$, is not known at the k^{th} SBS. Thus, without loss of generality, the latter can safely assume that

$$\begin{cases}\mathbf{t}_{\mathrm{ss},i}^{(j,j)\mathrm{H}}\mathbf{t}_{\mathrm{ss},i}^{(j,j)} &= 1, \quad \forall j \in [1,K]\setminus k, \\ \mathbf{t}_{\mathrm{ss},i}^{(m,j)\mathrm{H}}\mathbf{t}_{\mathrm{ss},i}^{(m,j)} &= 0, \quad \forall m \in [1,K]\setminus\{j,k\}\end{cases}, \tag{6.0}$$

and compute an approximation of (6.3.2) accordingly. Note that, in (6.3.2), the first approximation is related to the direct link between the j^{th} SBS/SUE pair, and the second to the co-tier interference generated by the j^{th} SBS towards its non-served SUEs. Consequently, the k^{th} SBS derives $\widehat{R}_{\mathrm{s}}$, approximation of $R_{\mathrm{s}} = \sum_{i=1}^{K} R_{\mathrm{s}}^{(i)}$, overall spectral efficiency of the second tier, as

$$\widehat{R}_{\mathrm{s}} = \frac{1}{N+L} \sum_{i=1}^{L} \log_2 \left(1 + \frac{1}{\sigma^2 + \mathbf{t}_{\mathrm{ss},i}^{(k,[k])\mathrm{H}} \mathbf{t}_{\mathrm{ss},i}^{(k,[k])}} \right), \tag{6.0}$$

where, as before, a uniform power allocation at the SBSs is assumed. Let $\mathbf{g_T} = (\mathbf{t}_{\mathrm{ss},1}^{(k,[k])\mathrm{H}} \mathbf{t}_{\mathrm{ss},1}^{(k,[k])}, \ldots, \mathbf{t}_{\mathrm{ss},L}^{(k,[k])\mathrm{H}} \mathbf{t}_{\mathrm{ss},L}^{(k,[k])})$ be the vector containing the power values associated to the L columns of $\mathbf{T}_{\mathrm{ss}}^{(k,[k])}$. Now let $\mathbf{g}_{\mathbf{T}}^{\theta} \in [1, L]$ be the θ-sized vector containing the indices of the θ smallest elements of $\mathbf{g_T}$, and $\mathbf{e}_i$ be the vector of the canonical basis with its i^{th} entry equal to 1. At this stage, we can define $\Theta^{(k)} = [\mathbf{e}_{\mathbf{g}_{\mathbf{T}}^{\theta}(1)} | \ldots, |, \mathbf{e}_{\mathbf{g}_{\mathbf{T}}^{\theta}(\theta)}]$ as the outer precoder that selects the columns of $\mathbf{T}_{\mathrm{ss}}^{(k,[k])}$ that minimize the co-tier interference generated by the k^{th} SBS towards its non-served SUEs. Thus, the input signal at the k^{th} SBS is aligned to the most efficient subspace of span $(\mathbf{E}^{(k)})$ for co-tier interference mitigation, and the overall spectral efficiency of the second tier in (6.3.2) can be rewritten as

$$\widehat{R}_{\mathrm{s}}(\theta) \;=\; \frac{1}{N+L} \sum_{i \in \mathbf{g}_{\mathbf{T}}^{\theta}} \log_2 \left(1 + \frac{1}{\sigma^2 + \mathbf{t}_{\mathrm{ss},i}^{(k,[k])\mathrm{H}} \mathbf{t}_{\mathrm{ss},i}^{(k,[k])}} \right). \tag{6.0}$$

The choice of θ is the second degree of freedom available at the k^{th} SBS to design $\mathbf{\Theta}^{(k)}$. As previously seen, θ has a direct impact on the diversity effect provided by the equivalent channel matrices. Intuitively, we expect that a bigger K, number of SBS/SUE pairs, will yield a smaller value for θ to maximize the spectral efficiency of the k^{th} SBS/SUE pair, and vice versa. Consequently, from now on we will refer to $\theta(K)$ to explicitly show this dependency. Due to the self-organizing nature of the second tier, and to the aforementioned lack of knowledge on the eigenvalues distribution of finite dimension Toeplitz matrices and respective kernels, no analytic optimization of the parameter can be performed. A numerical approach is the only viable way to identify a suitable spectral efficiency maximizing $\theta(K)$ at the k^{th} SBS. Assuming a given model for the cross- and co-tier channels, e.g., the channel models described in Section 6.2, each SBS can find a numerical solution by means of offline Monte Carlo simulations, iterating the following algorithm until statistical relevance of the result is reached.

Algorithm 1 Optimal $\theta(K)$

Require: Set a value for K and select an approach between CIA A and CIA B

1: **for** θ in $[1, L]$ **do**
2: Compute $\widehat{R}_{\mathrm{s}}(\theta)$
3: **end for**
4: **return** $\theta(K) = \arg\max_{\theta} \widehat{R}_{\mathrm{s}}(\theta)$

The outcome of this algorithm is a map adoptable by the SBSs to implement the aforementioned implicit coordination mechanism as follows. This map hinges on the channel model peculiar to the surrounding operative environment and can be computed offline as a self-optimizing operation to be performed once, before the transmit operations. No online adjustment to the map is required after the self-optimization, hence no particular timing constraints are imposed on the SBSs for this process. As a design policy, each SBS assumes that the number of SUEs inside its coverage area corresponds to an equal number of potential neighboring interferers, i.e., other SBSs serving the detected SUEs, that is $K-1$. Note that, in a TDD scenario, the number of surrounding SUEs is given by the number of detected sounding reference signals [50] provided by each SUE to its serving SBS for channel estimation purposes. This information is used during the transmit procedures to identify the best value for $\theta(K)$ instantaneously, by means of the offline-computed map. As a consequence, the CIA cascaded precoder can be immediately derived, according to the chosen one-shot co-tier interference management strategy. The last step before engaging in the transmission is the choice of the optimal precoder realization and power loading strategy at the k^{th} SBS, in the sense of spectral efficiency maximization.

6.4 Optimal precoder

As seen in Section 6.3.1, CIA preserves the spectral efficiency of the primary OFDMA transmission. On the other hand, the spectral efficiency of the self-organizing second tier highly depends on the realization of the precoder $\mathbf{Z}^{(k)}$ at each SBS. Thus, in order to maximize the spectral efficiency enhancement brought by the two-tiered network approach, each SBS must self-optimize the spectral efficiency of its link to the served SUE, while complying with the adopted interference management strategy, i.e., CIA A or B.

In the following, we will focus on the k^{th} SBS/SUE pair and show that the distributed CIA cascaded precoder $\mathbf{Z}^{(k)}$ as computed in Section 6.3.2 is optimal in the sense of maximum link spectral efficiency for the k^{th} SBS/SUE pair. The following result can be stated.

Corollary 5 (Optimal distributed CIA precoder)**.** *Consider a two-tiered network where a licensee OFDMA base station coexists with several non cooperative single antenna opportunistic base stations adopting CIA. The distributed CIA cascaded precoder $\mathbf{Z}^{(k)}$ is optimal, in the sense of maximum link spectral efficiency for the k^{th} SBS/SUE pair, regardless of the chosen co-tier interference mitigation approach.*

Proof: Consider (6.3.1) and (6.3.2). We are focusing on the link from the k^{th} SBS to the k^{th} SUE, thus, according to (6.3.2), we can rewrite them as follows

$$\begin{aligned}\mathbf{y}_{\mathrm{p}}^{(j)} &= \mathbf{D}_j\mathbf{F}\mathbf{B}\left(\mathbf{H}_{\mathrm{pp}}^{(1,j)}\mathbf{A}\mathbf{F}^{-1}\mathbf{x}_{\mathrm{p}}+\mathbf{n}_{\mathrm{p}}^{(j)}\right)+\mathbf{T}_{\mathrm{sp}}^{(k,j)}\mathbf{Z}^{(k)}\mathbf{u}_{\mathrm{s}}^{(i)}\\ \mathbf{y}_{\mathrm{s}}^{(k)} &= \mathbf{F}\mathbf{B}\left(\mathbf{H}_{\mathrm{ss}}^{(k,k)}\mathbf{Z}^{(k)}\mathbf{u}_{\mathrm{s}}^{(k)}+\mathbf{H}_{\mathrm{ps}}^{(1,k)}\mathbf{x}_{\mathrm{p}}+\mathbf{n}_{\mathrm{s}}^{(k)}\right),\end{aligned} \tag{6.0}$$

where we omitted the co-tier interference component at the k^{th} SUE, $\sum_{i=1,i\neq k}^{K} \mathbf{H}_{\mathrm{ss}}^{(i,k)}\mathbf{Z}^{(i)}\mathbf{u}_{\mathrm{s}}^{(i)}$, not known at the k^{th} SBS, in compliance with the model described in Section 6.1. Moreover, we isolated the cross-tier interference component coming from the k^{th} SBS to the j^{th} MUE for clarity. This comes without loss of generality, given that $\mathbf{T}_{\mathrm{sp}}^{(k,j)}\mathbf{Z}^{(k)} = \mathbf{0}_{N\times\theta}$, $\forall j \in [1, M]$, $k \in [1, K]$, by construction. By looking at (6.4), we recognize the interference channel equations provided in the hypothesis of Proposition 3. Now we switch our focus on the cascaded precoder $\mathbf{Z}^{(k)} = \mathbf{E}^{(k)}\boldsymbol{\Theta}^{(k)}$. Consider CIA A and CIA B as described in Section 6.3.2. In the former, both $\mathbf{E}^{(k)}$ and $\boldsymbol{\Theta}^{(k)}$ are semi-unitary by construction, hence so is $\mathbf{Z}^{(k)}$ for Proposition 2, and Proposition 3 can be applied. In the latter, $\boldsymbol{\Theta}^{(k)}$ is not semi-unitary but, by construction, selects the θ columns of $\mathbf{E}^{(k)}$ associated to the θ indexes belonging to $\mathcal{N}^{\theta}$. Then, $\mathbf{Z}^{(k)}$ is composed of orthonormal columns, thus it is semi-unitary by definition, and Proposition 3 can be applied to conclude the proof. ∎

6.5 Spectral efficiency computation

At this stage, we dispose of all the necessary tools to derive the spectral efficiency of the two tiers. We recall that, in Section 6.3.2, the cross-tier interference generated by the MBS towards the SUEs has been omitted from the equations describing CIA, for the sake of clarity and simplicity of the notation. Even though not necessary at the k^{th} SBS to derive $\boldsymbol{\Theta}^{(k)}$, this interference may strongly limit the achievable spectral efficiency at the k^{th} SUE. Accordingly, hereafter, the cross-tier interference generated by the MBS will be taken into account in the performance evaluation of the considered two-tiered network. We remark that, macro-cell and small-cell coverage areas have very different size, thus the distance between the MBS and the SUEs served by the active SBSs hinges on the second tier deployment and varies depending on the considered network layout. In order to capture this crucial parameter, we define an interference factor $\alpha \in [0, 1]$ to scale the cross-tier interference generated by the MBS towards the k^{th} SUE. In particular, $\alpha \simeq 1$ models a scenario where the active SBSs are operating near the MBS, whereas if the second tier is deployed very far the MBS we have $\alpha \simeq 0$. Moreover, for the sake of compactness of the notation, we let

$$\begin{aligned}\overline{\mathbf{T}}_{\mathrm{sp}}^{(k,j)} &= \tilde{\mathbf{T}}_{\mathrm{sp}}^{(k,j)}\boldsymbol{\Theta}^{(k)} = [\overline{\mathbf{t}}_{\mathrm{sp},1}^{(k,j)} \mid \ldots \mid \overline{\mathbf{t}}_{\mathrm{sp},N}^{(k,j)}]^{\mathrm{T}} \in \mathbb{C}^{N\times\theta} \\ \overline{\mathbf{T}}_{\mathrm{ss}}^{(k,k)} &= \mathbf{T}_{\mathrm{ss}}^{(k,k)}\boldsymbol{\Theta}^{(k)} = [\overline{\mathbf{t}}_{\mathrm{ss},1}^{(k,k)} \mid \ldots \mid \overline{\mathbf{t}}_{\mathrm{ss},N}^{(k,k)}]^{\mathrm{T}} \in \mathbb{C}^{N\times\theta}\end{aligned} \tag{6.0}$$

be the equivalent channel representation of the link connecting the k^{th} SBS to the j^{th} MUE and to k^{th} SUE respectively. The spectral efficiency for perfect and imperfect CSIT is computed as follows.

6.5.1 Perfect CSIT

We start by noting that for perfect CSI at the SBSs, the spectral efficiency at the j^{th} MUE is given by (6.3.1). Thus, we can switch our focus to the k^{th} SUE and redefine

(6.3.2), SINR of its i^{th} received symbol, as

$$\mathrm{SINR}_{(\mathrm{s},i)}^{(k)} = \frac{\overline{\mathbf{t}}_{\mathrm{ss},i}^{(k,k)\mathrm{H}} d(p_{\mathrm{s},1}^{(k)}, \ldots, p_{\mathrm{s},\theta}^{(k)}) \overline{\mathbf{t}}_{\mathrm{ss},i}^{(k,k)}}{\sum_{m \neq k}^{K} \overline{\mathbf{t}}_{\mathrm{ss},i}^{(m,k)\mathrm{H}} d(p_{\mathrm{s},1}^{(m)}, \ldots, p_{\mathrm{s},\theta}^{(m)}) \overline{\mathbf{t}}_{\mathrm{ss},i}^{(m,k)} + \alpha p_{\mathrm{p},i} \left| \left[\mathbf{F}\mathbf{B}\mathbf{H}_{\mathrm{ps}}^{(1,k)} \mathbf{A}\mathbf{F}^{-1} \right]_{i,i} \right|^2 + \sigma^2}, \quad (6.0)$$

with $\alpha p_{\mathrm{p},i} \left| \left[\mathbf{F}\mathbf{B}\mathbf{H}_{\mathrm{ps}}^{(1,k)} \mathbf{A}\mathbf{F}^{-1} \right]_{i,i} \right|^2$ cross-tier interference generated by the MBS. Accordingly, the spectral efficiency at the k^{th} SUE is computed by plugging (6.5.1) into (6.3.2).

6.5.2 Imperfect CSIT

As discussed in Chapter 5, in realistic implementations of wireless communications systems, the transmitter only disposes of noisy channel estimations, i.e., imperfect CSIT. The design of a channel estimation procedure for the self-organizing scenario is out of our scopes. In fact, differently from the centralized case in Chapter 4, herein the SBSs do not need to cooperate or communicate to perform the opportunistic transmission. Thus, in principle, any channel estimation strategy that exploits the structure of the UL frame (e.g., [135] or similar strategies in case of LTE/LTE-A frame structure [58, 50, 104]), can be adopted at the k^{th} SBS to acquire the necessary CSI. Therefore, we assume a classic training/transmission scheme as in [103] for simplicity. As done in Chapter 5, we consider a block fading channel model characterized by a coherence time T. Thus, each transmitter must perform the necessary channel estimations with periodicity T, in both tiers. We denote as $\tau \leq T$ the time spent estimating the channel. The available time for transmission at each SBS, until the next channel estimation is necessary, is then $T - \tau$. Accordingly, a longer τ yields better channel estimations, but reduces the available time for transmission. Typically, the outcome of a channel estimation in such a model can be represented as [103]

$$\mathbf{r} = \sqrt{\rho\tau}\mathbf{h} + \mathbf{n},$$

where $\mathbf{h}$ is the channel vector, ρ is the transmit power and $\mathbf{n} \sim \mathcal{CN}(0, \sigma^2 \mathbf{I}_{(l+1)})$ is the thermal noise at the devices' antennas. We assume that each transmitter estimates $\mathbf{h}$ by evaluating the observation $\mathbf{r}$, e.g., by means of a minimum mean square error (MMSE) approach, to obtain

$$\mathbf{h} = \hat{\mathbf{h}} + \tilde{\mathbf{h}},$$

with $\hat{\mathbf{h}}$ desired channel estimation and $\tilde{\mathbf{h}}$ independent error.

As seen in Section 6.3.1, a perfect channel estimation of $\mathbf{h}_{\mathrm{sp}}^{(k,j)}$, $\forall j \in [1, M]$, is required to derive $\mathbf{E}^{(k)}$ and fulfill the cross-tier interference constraint in (6.3.1) at the k^{th} SBS. If perfect CSIT is not available, then $\overline{\mathbf{T}}_{\mathrm{sp}}^{(k,j)} \neq 0$ and the $k^{(th)}$ SBS generates cross-tier interference towards the MUEs. Consequently, the SINR of i^{th} received symbol at the

j^{th} MUE reads

$$\mathrm{SINR}_{(\mathrm{p},i)}^{(j)} = \frac{p_{\mathrm{p},i}\left|\left[\mathbf{F}\mathbf{B}\mathbf{H}_{\mathrm{pp}}^{(1,j)}\mathbf{A}\mathbf{F}^{-1}\right]_{i,i}\right|^2}{\sum_{k=1}^{K}\bar{\mathbf{t}}_{\mathrm{sp},i}^{(k,j)\mathrm{H}}d(p_{\mathrm{s},1}^{(k)},\ldots,p_{\mathrm{s},\theta}^{(k)})\bar{\mathbf{t}}_{\mathrm{sp},i}^{(k,j)}+\sigma^2}. \tag{6.0}$$

Concerning the second tier, as seen in Section 6.3.2, the k^{th} SBS adopting CIA A or CIA B needs CSI w.r.t. to the links towards the served SUE or neighboring SUEs, respectively. We note that, the SINR of the i^{th} received symbol at the k^{th} SUEs is always computed by (6.5.1). Nevertheless, imperfect CSIT may decrease the effectiveness of the outer precoder $\mathbf{\Theta}^{(k)}$ and yield higher co-tier interference, i.e., the term $\sum_{m\neq k}^{K}\bar{\mathbf{t}}_{\mathrm{ss},i}^{(m,k)\mathrm{H}}d(p_{\mathrm{s},1}^{(m)},\ldots,p_{\mathrm{s},\theta}^{(m)})\bar{\mathbf{t}}_{\mathrm{ss},i}^{(m,k)}$ in (6.5.1) may increase. This in general worsens the SINR per received symbol at the SUEs, resulting in spectral efficiency losses. Additionally, we know from [103] that the time and resources spent for channel estimation have an impact on the effective SINR experienced at each receiver. If training and data symbols carry the same average power, we can define $\overline{\mathrm{SINR}}_{(\cdot,i)}^{(j)}$, effective SINR value of the i^{th} symbol at the j^{th} receiver, as

$$\overline{\mathrm{SINR}}_{(\cdot,i)}^{(j)} = \frac{\left(\mathrm{SINR}_{(\cdot,i)}^{(j)}\right)^2\tau}{1+(1+\tau)\mathrm{SINR}_{(\cdot,i)}^{(j)}}, \quad \forall j\in[1,KN]. \tag{6.0}$$

Therefore, we can compute $R_{\mathrm{p}}^{\mathrm{I}}$ and $R_{\mathrm{s}}^{\mathrm{I}}$, spectral efficiency of first and second tier respectively, for imperfect CSIT, as

$$R_{\mathrm{p}}^{\mathrm{I}} = \frac{T-\tau}{T(N+L)}\sum_{j=1}^{M}\sum_{i=1}^{N}\log_2(1+\overline{\mathrm{SINR}}_{\mathrm{p},i}^{(j)}) \tag{6.1}$$

$$R_{\mathrm{s}}^{\mathrm{I}} = \frac{T-\tau}{T(N+L)}\sum_{m=1}^{K}\sum_{i=1}^{N}\log_2(1+\overline{\mathrm{SINR}}_{\mathrm{s},i}^{(m)}).. \tag{6.2}$$

6.6 Numerical analysis

In this section we focus on the achievable spectral efficiency of the proposed CIA scheme, for several configurations of the studied two-tiered network. Throughout the analysis, unless otherwise stated, an interference factor $\alpha = 1$ is assumed, to model a two-tiered network characterized by high cross-tier interference generated by the MBS towards the second tier. Extensive Monte Carlo simulations are performed to obtain statistically relevant results.

No particular channel model is adopted in this study, hence we consider frequency-selective Rayleigh fading channels with uniform power delay profile, as described in Section 6.2. For computational tractability, we assume that the OFDMA transmission at the MBS is performed over a bandwidth of 1.92 MHz, divided in $N = 128$

subcarriers, with CP size of $L = l = 32$, as in the extended mode of the least resource demanding LTE/LTE-A DL configuration [50].

Concerning the power budget available at the MBS and the SBSs, we adopt the same policy as in Chapter 4, imposing that the total power budget per tier is the same, i.e., $P_p(N + L)$. Thus, we assume that

$$\begin{aligned} \mathrm{tr}(\mathbf{x}_{\mathrm{p}}\mathbf{x}_{\mathrm{p}}^{\mathrm{H}}) &= P_{\mathrm{p}}(N+L) \\ \mathrm{tr}(\mathbf{x}_{\mathrm{s}}^{(k)}\mathbf{x}_{\mathrm{s}}^{(k)\mathrm{H}}) &= \frac{P_{\mathrm{p}}}{K}(N+L), \forall k \in [1,K] \end{aligned}$$

such that $\sum_{k=1}^{K} \mathrm{tr}(\mathbf{x}_{\mathrm{s}}^{(k)}\mathbf{x}_{\mathrm{s}}^{(k)\mathrm{H}}) = \mathrm{tr}(\mathbf{x}_{\mathrm{p}}\mathbf{x}_{\mathrm{p}}^{\mathrm{H}})$ Accordingly, the larger K becomes, the lower the power budget available at each SBS becomes. This models the second tier in compliance with the lower energy consumption requirements that the SBSs will likely have w.r.t. a legacy MBS in 4G networks [3]. Throughout the section, the SNR at the receiver will be used to model different operating conditions and better assess the overall two-tiered network spectral efficiency enhancements, brought by the presence of the second tier. Without loss of generality, we assume that the average power of the thermal noise affecting the receiving devices is the same in both tiers, i.e., σ^2. From a practical point of view, for each target SNR value considered in the simulation, we consider a value for σ^2 such that the average SNR of the i^{th} received received symbol at the j^{th} MUE, given by

$$\mathrm{SNR}_{(\mathrm{p},i)}^{(j)} = \log_{10} \mathbb{E}\left[\frac{p_{\mathrm{p},i} \left| \left[\mathbf{F}\mathbf{B}\mathbf{H}_{\mathrm{pp}}^{(1,j)}\mathbf{A}\mathbf{F}^{-1} \right]_{(i,i)} \right|^2}{\sigma^2} \right], \forall j \in [1,M], \tag{6.0}$$

coincides with the target SNR, unless otherwise stated. This way, due to the different power budgets available at the MBS and at each SBS, the SUEs will likely experience a lower average SNR if compared to the MUEs. In other words, by considering the same noise level for both MUEs and SUEs, and by computing it such that a target SNR per received symbol at the MUEs is achieved, we mimic the SNR reduction experienced by the SUEs w.r.t. the MUEs, due to the different power budget per transmitter in the first and second tier. We note that, this choice allows a fair comparison with the performance of the single tier network case, i.e., no SBS/SUE pairs, for which the average SNR per received symbol at the MUEs is the same as in the two-tiered case.

As a first step, we analyze the performance for perfect CSIT in the second tier. We compare our results to what is achievable by means of an orthogonalization strategy such as TDMA, where only one SBS is active at each iteration (time slot), considered an appropriate benchmark for the following reasons. TDMA is the first traditional benchmark for the performance of interference alignment solutions for the interference channel [18]. In fact, it is a classical distributed solution for self-organizing and ad-hoc networks [137], commonly adopted in many commercial standards and applications [99], when no cooperation or communication can be established between potentially interfering transmitters. Finally, differently from a frequency division multiple access (FDMA) approach, equivalent in terms of achievable spectral efficiency, a TDMA approach to address the co-tier

interference issue in the second tier is compliant with the frequency reuse 1 assumption made in Section 6.1.

As a second step, we investigate the robustness of CIA when dealing with channel estimation errors, i.e., imperfect CSIT. Afterwards, we complete our study by analyzing the percent increase in achievable spectral efficiency that the proposed approach could yield w.r.t. the legacy single tier based network deployment. Accordingly, we compare the spectral efficiency of a two-tiered network composed of an OFDMA MBS underlaid with K self-organizing SBSs adopting CIA, with the performance of a standalone legacy OFDMA MBS, for imperfect CSIT and different values of α.

As a preliminary study, we identify the optimal $\theta(K)$, for both CIA A and CIA B, iterating the algorithm described in Section 6.3.2. We aim at finding the optimal input signal subspace dimension at the SBSs such that the second tier does not suffer from co-tier interference limitation. For this study, the considered thermal noise is such that the SNR of the i^{th} received symbol at the k^{th} SBS is

$$SNR_{(\mathrm{s},i)}^{(k)} = \mathbb{E}\left[\log_{10}\left(\frac{\mathbf{t}_{\mathrm{ss},i}^{(k,k)\mathrm{H}} \mathbf{t}_{\mathrm{ss},i}^{(k,k)}}{\sigma^2} \right) \right] = 30\mathrm{dB}, \quad \forall i \in [1,N], k \in [1,K]. \tag{6.0}$$

We let $K \in \{4,6,8,16\}$ and depict the performance for CIA A and CIA B in Figure 6.2 and Figure 6.3 respectively. A clear dependency of the optimal input signal subspace

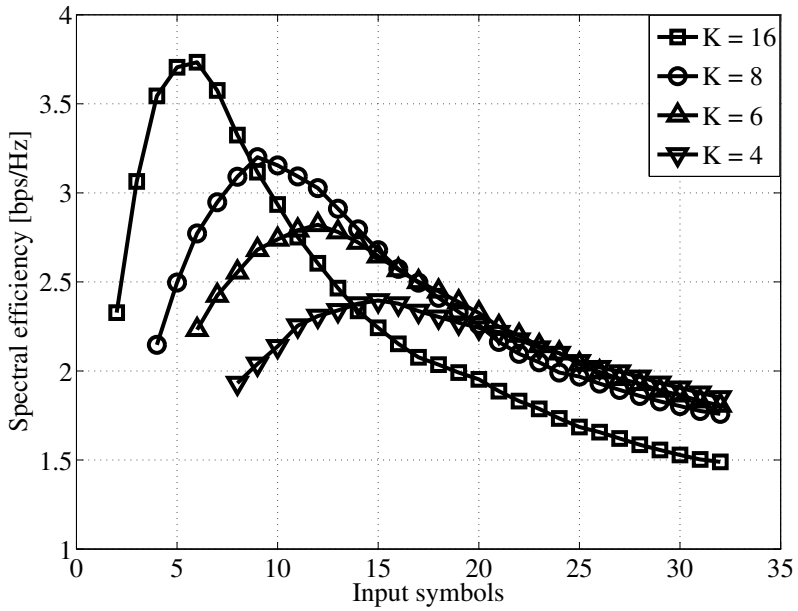

Figure 6.2: Spectral efficiency of the second tier for CIA A for $K \in \{4,6,8,16\}$ SBSs, as the dimension of the input signal subspace changes. $N = 128$, $L = 32$ and bandwidth of 1.92 Mhz.

dimension on the number of active SBSs is shown for both approaches, further motivating

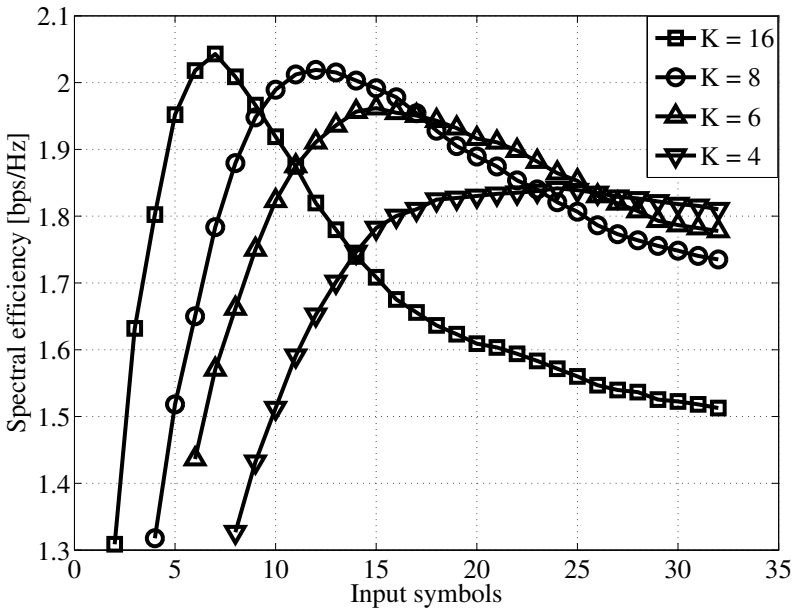

Figure 6.3: Spectral efficiency of the second tier for CIA B for $K \in \{4, 6, 8, 16\}$ SBSs, as the dimension of the input signal subspace changes. $N = 128$, $L = 32$ and bandwidth of 1.92 Mhz.

the intuition given in Section 6.3.2, i.e., the larger K the smaller the optimal $\theta(K)$. Intuitively, due to the lack of cooperation between the SBSs, we could expect that the co-tier interference may cause a progressive decrease of the performance of the second tier as the number of SBSs K grows, regardless of the chosen approach. Conversely, the achievable spectral efficiency in case of optimal $\theta(K)$ increases with K thanks to an effective co-tier interference mitigation, and a consistent robustness against the cross-tier interference generated by the MBS. On the other hand, these results show both higher achievable spectral efficiency lower $\theta(K)$ values for CIA A than for CIA B, for all values of K. Therefore, a smaller but more efficient input signal subspace is a preferable choice if compared to a larger less interfering one, in the sense of the overall self-organizing second tier performance. In other words, a larger input signal subspace reduction at the k^{th} SBS, followed by a selfish maximization of the spectral efficiency of the link towards the served SUE, i.e., as in CIA A, provides a higher diversity effect at the receivers, thus induces a larger power gain at the k^{th} SUE.

Now we consider the previously obtained optimal $\theta(K)$ and we let $SNR_{(s,i)}^{(k)} \in [-10, 30]$ dB. We compute the achievable spectral efficiency for the two proposed methods for $K \in \{4, 8, 16\}$, in Figure 6.4, Figure 6.5 and Figure 6.6, respectively.

Significant SNR gains brought by CIA A over CIA B are evident for each configuration, confirming the previous findings. In particular, the larger K the higher is the experienced SNR gain. As previously stated, we provide a comparison with a commonly implemented

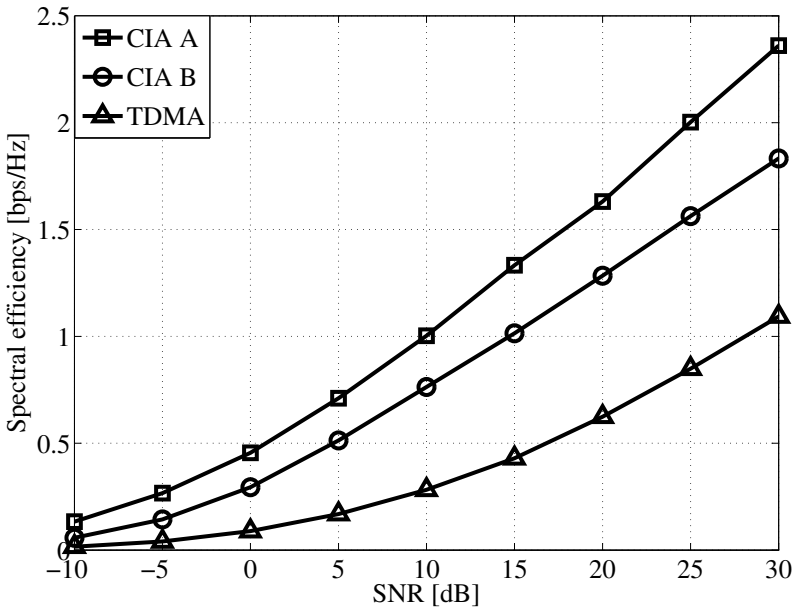

Figure 6.4: Spectral efficiency of the second tier as the SNR changes, $K = 4$ SBSs, $N = 128, L = 32$ and bandwidth of 1.92 Mhz.

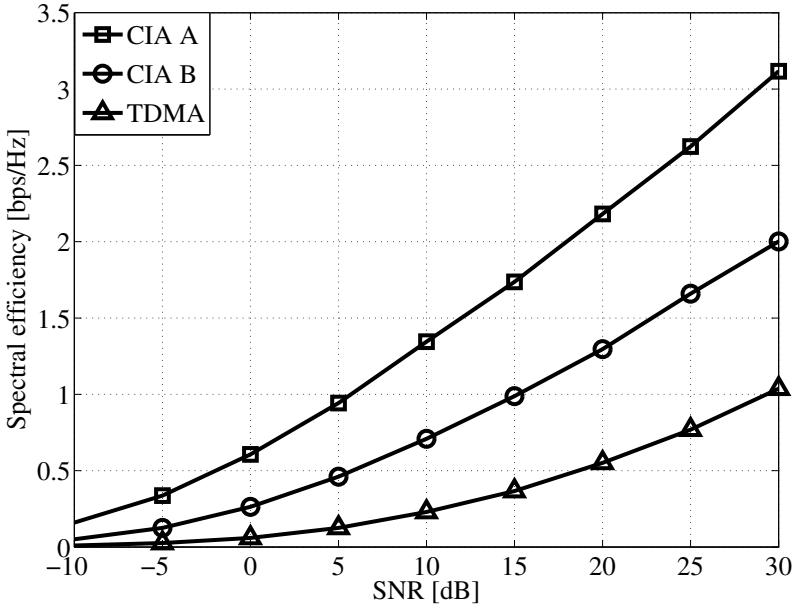

Figure 6.5: Spectral efficiency of the second tier as the SNR changes, $K = 8$ SBSs, $N = 128, L = 32$ and bandwidth of 1.92 Mhz.

distributed TDMA approach, where only one SBS is active at each iteration (time slot). We remark that, to guarantee a fair comparison, the active SBS in the TDMA scheme

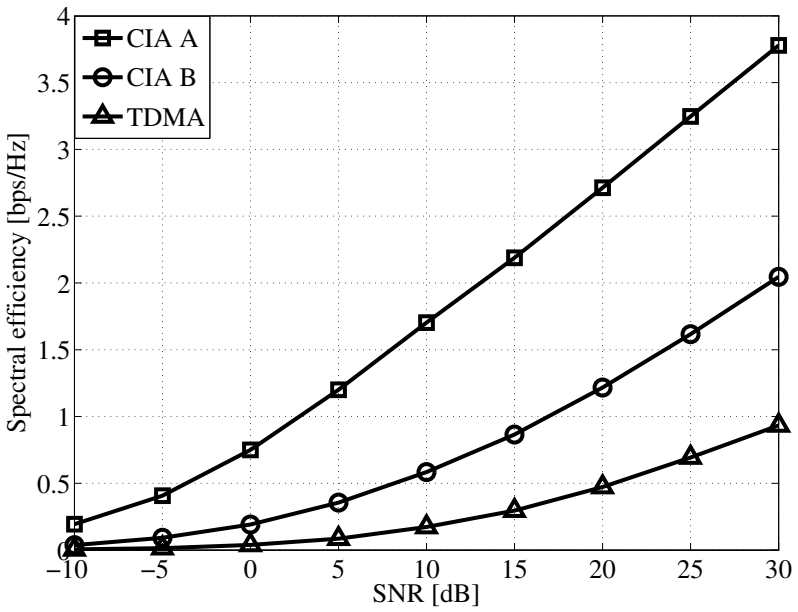

Figure 6.6: Spectral efficiency of the second tier as the SNR changes, $K = 16$ SBSs, $N = 128, L = 32$ and bandwidth of 1.92 Mhz.

adopts an optimal water-filling power loading strategy [59]. Interestingly, both proposed methods outperform the TDMA approach in the considered SNR range. Furthermore, if we focus on the best performer out of the proposed strategies, i.e., CIA A, we observe remarkable SNR gains up to 20 dB for $K = 4$ and 30 dB for $K = 16$ w.r.t. TDMA. Let us now focus on the CSI requirements of the considered approaches. According to Section, CIA A requires less CSI than CIA B to be performed. In fact, an SBS adopting CIA A needs only CSI w.r.t. the direct link towards its served SUE, whereas for CIA B the CSI related to all the links towards the K SUEs inside its coverage area are needed. As a consequence, CIA A has the same CSI requirements as TDMA and is not affected by scalability issues as K increases[2]. For these reasons, in the remainder of the section, we will consider CIA A as the selected approach to implement CIA at the self-organizing SBSs.

Now, we compute the performance of CIA when perfect CSIT is not available in the second tier as discussed in Section 6.5.2. We evaluate the impact of an imperfectly built $\mathbf{Z}^{(k)}$ precoder on the overall network performance as the ratio $\frac{\tau}{T}$ changes. As in Chapter 4, we let $\eta_p = \dfrac{R_{\mathrm{p}}^{\mathrm{I}}}{R_{\mathrm{p}}}$ and $\eta_s = \dfrac{R_{\mathrm{s}}^{\mathrm{I}}}{R_{\mathrm{s}}}$ be two parameters that measure the percentage of the achievable spectral efficiency for perfect CSIT that is achievable when only imperfect CSIT is available, for the first and second tier, respectively. Consider a first tier with $M = 4$ MUEs and a second tier composed of $K = 8$ SBS/SUE pairs. In Figure 6.7, η_s

[2]The same is not true for CIA B. If the k^{th} SBS adopts this approach, then the amount of necessary channel estimations to construct $\mathbf{Z}^{(k)}$ increases with number of SUEs inside its coverage area

and η_p are computed as different $\frac{\tau}{T}$ proportions are chosen, for SNR $\in \{0, 10, 20\}$ dB. We note that, η_s is inversely proportional to $\frac{\tau}{T}$. In particular, when $\frac{\tau}{T}$ is too high, the

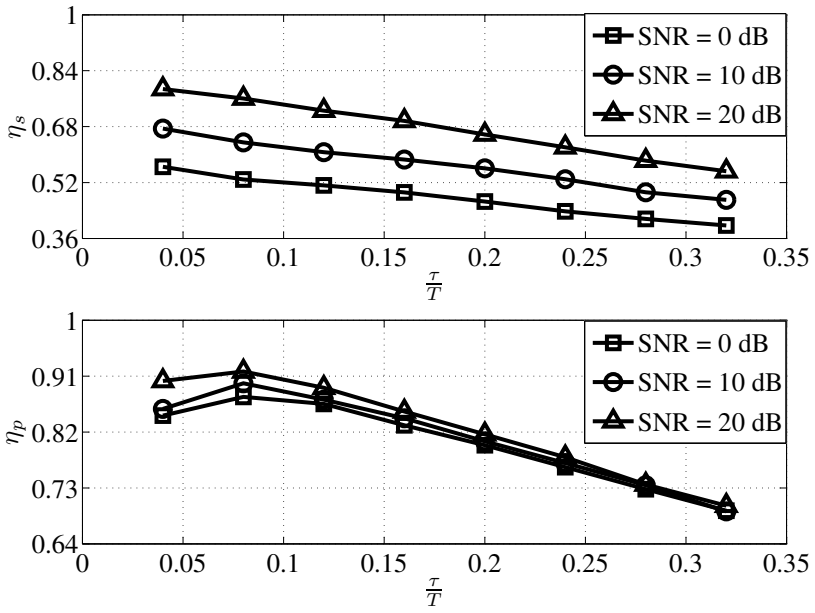

Figure 6.7: Ratio between the achievable spectral efficiency of the SBSs and MBS for imperfect CSIT and perfect CSIT in the second tier, SNR$\in \{0, 10, 20\}$ dB, $K = 8$ SBSs, $N = 128, L = 32$ and bandwidth of 1.92 Mhz.

time spent to acquire the CSI at the SBSs is such that the experienced SINR gains are not sufficient to compensate the loss induced by the lack of time available for the transmission. In other words, the pre-log factor in (6.2) is dominant and η_s scales linearly with $\frac{\tau}{T}$. Remarkably, this behavior is independent from the SNR value at the receiver, showing the robustness of the proposed co-tier interference management mechanism to channel estimation errors. On the other hand, the maximum value for η_s decreases with the SNR, as could be expected, and shows a non-negligible spectral efficiency loss even for medium to high target SNR, i.e., more than 15% at SNR = 20 dB and more than 30% at SNR = 10 dB. We recall that, each SBS requires only the CSI related to the direct link towards its served SUE to compute the CIA A precoder. Thus, the spectral efficiency loss for imperfect CSIT w.r.t. the perfect CSIT case, measured by η_s, is not due to additional co-tier interference generated towards the non-served SUEs, but only to a less effective power allocation w.r.t. the direct link connecting each SBS/SUE pair. As a consequence, a larger number of active SBSs, i.e. K, would not yield different values for η_s, thanks to the scalability of the proposed solution.

Switching our focus to η_p we clearly see a constructive impact of a longer τ on the effectiveness of the cross-tier interference alignment technique, thus on the spectral efficiency of the first tier. In particular, differently from the previous case, the pre-log factor in (6.1) becomes dominant (η_p scales linearly with $\frac{\tau}{T}$) only for $\frac{\tau}{T} > 0.12$. In fact, by estimating

the channels during the optimal $\frac{\tau}{T}$ portion of the coherence time, i.e., $\frac{\tau}{T} = 0.08$, regardless of the power of the noise affecting the estimations, each SBS can compute a more precise precoder $\mathbf{E}^{(k)}$, inducing a consequent power gain at the MUEs. We note that, in general, the cross-tier interference alignment strategy is more robust against imperfect CSIT than the co-tier interference mitigation mechanism. For very low target SNR values, i.e., 0 dB, the first tier's loss is around 15% of its achievable spectral efficiency for perfect CSIT, whereas for medium to high SNR, i.e., 20 dB, the loss can be reduced to less than 10%.

We keep focusing on the first tier and analyze the impact of the cross-tier interference generated by the second tier as the number of active SBSs increases. In Figure 6.8, η_p is computed for $M = 4$ MUEs and $K \in \{4, 8, 16\}$ SBSs. We note that, to achieve

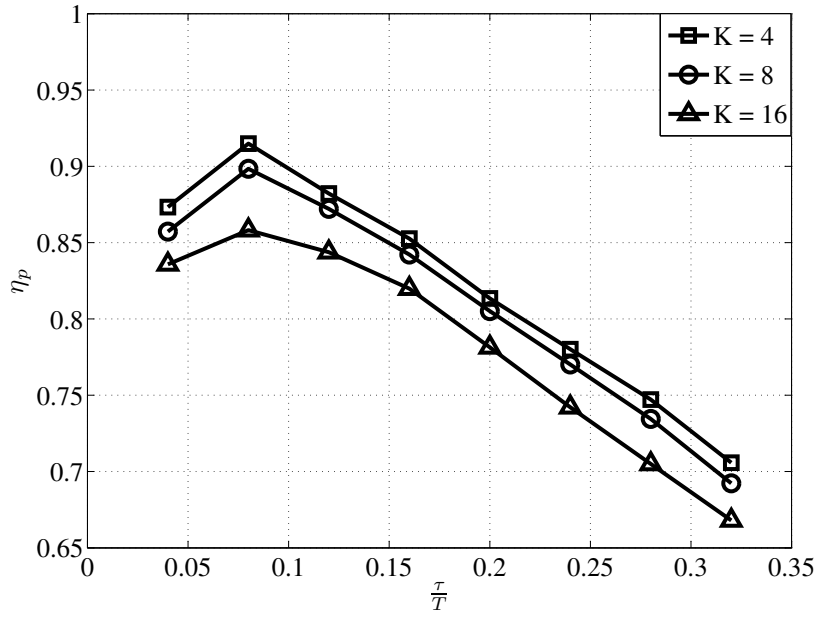

Figure 6.8: Ratio between the achievable spectral efficiency of the MBS for imperfect CSIT and perfect CSIT in the second tier, $SNR = 10$ dB, $K \in \{4, 8, 16\}$ SBSs, $N = 128, L = 32$ and bandwidth of 1.92 Mhz.

the target average spectral efficiency per macro-cell in LTE-A, ranging between 2.4 and 3.7 bit/s/Hz [138], a target average SNR ranging between 9 and 11 dB is required for practical modulation and coding schemes [139]. Accordingly, in this analysis we assume SNR = 10 dB, i.e., a likely occurring value in future LTE-A networks to be able to meet the target performance. Similarly to the previous study, we note that the pre-log factor is dominant for the spectral efficiency of the first tier only for $\frac{\tau}{T} > 0.08$, $\forall K \in \{4, 8, 16\}$. Remarkably, the optimal value for $\frac{\tau}{T}$ is then independent of the number of considered active SBSs. On the other hand, as could be intuitively expected, the spectral efficiency loss experienced by the first tier increases with K, due to the superior cross-tier interference generated by the SBSs. However, the difference between the loss induced in the three considered case is rather low. In particular, the difference in spectral

efficiency loss between $K = 4$ and $K = 16$ is less than 10%. These results confirm our previous findings, showing a promising robustness of the proposed distributed CIA approach against imperfect CSIT.

As a final step, we study the overall performance of the two-tiered network, to evaluate the advantages, if any, brought by the proposed technique. We consider as a reference performance the achievable spectral efficiency of a standalone OFDMA MBS serving $M = 4$ MUEs, by means of an optimal power allocation strategy, given by a classic water-filling algorithm [59]. We consider a second tier composed of $K \in \{4, 16\}$ SBS/SUE pairs. This allows to model two scenarios, characterized by different density of SBSs in the second tier , i.e., a rather sparse ($K = 4$) and a more dense ($K = 16$) deployment. Given the previous results, we assume $\frac{\tau}{T} = 0.08$. For clarity, we compute the percent increase in achievable spectral efficiency brought to the single standalone MBS (reference performance) by the co-channel deployment of a second tier of self-organizing SBSs adopting CIA. Note that, for completeness, the percent increase achievable in case of TDMA approach in the second tier is computed as well. As can be seen in Figure 6.9, a second tier adopting CIA provides significant additional spectral efficiency to the legacy single tier performance at any SNR regime. Remarkably, CIA outperforms the TDMA approach

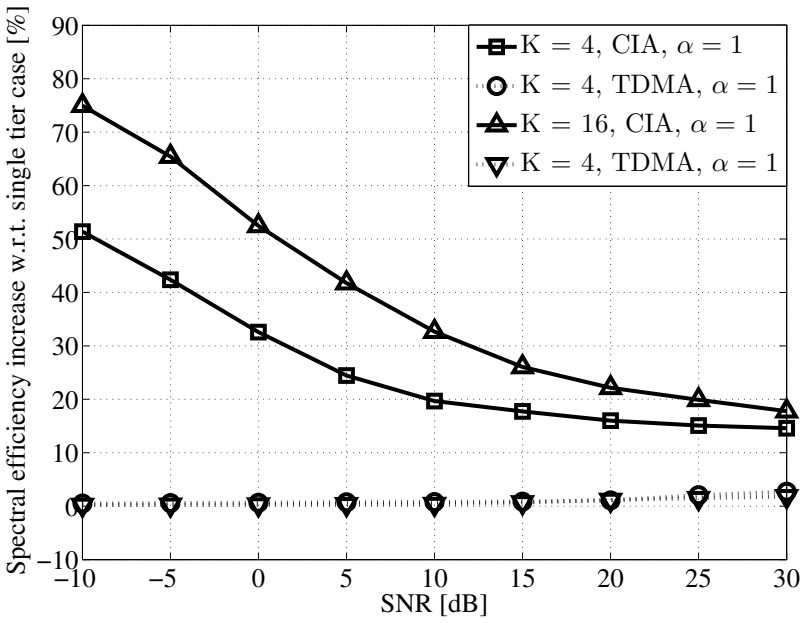

Figure 6.9: Percent increase in spectral efficiency w.r.t. the single OFDMA-based tier case. $K \in \{4, 16\}$, $N = 128, L = 32$ and bandwidth of 1.92 Mhz. Full cross-tier interference from the MBS to the SUEs.

for both values of K. Interestingly, the lower the target SNR the larger is the advantage of CIA w.r.t. TDMA, showing the effectiveness of CIA for practically relevant SNR values. We note that, the high cross-tier interference generated by the MBS towards the SUEs has a significant impact on the spectral efficiency increase experience by the two-tiered

network. This can be clearly seen for very high target SNR values, where an increase in the number of SBSs from $K = 4$ to $K = 16$ does not yield a significant advantage. Conversely, for lower target SNR values, the presence of larger number of SBSs brings non-negligible additional spectral efficiency. Specifically, for SNR= 0 dB, $K = 4$ SBSs deliver a percent increase in spectral increase of as much as 33% over the single tier case, whereas a percent increase of as much as 53% is brought by the deployment of $K = 16$ SBSs (more than 35% of relative increase). An even higher relative increase, i.e., more than 40%, is experienced when going from $K = 4$ to $K = 16$ SBSs for SNR = 10 dB, for which the percent increase in spectral efficiency w.r.t. the single tier case is 20% for $K = 4$ and 34% for $K = 16$.

Similar insights for low to medium target SNR values can be drawn from Figure 6.10, where the analysis is repeated for $\alpha = 0$, i.e., no cross-tier interference generated by the MBS towards the SUEs.

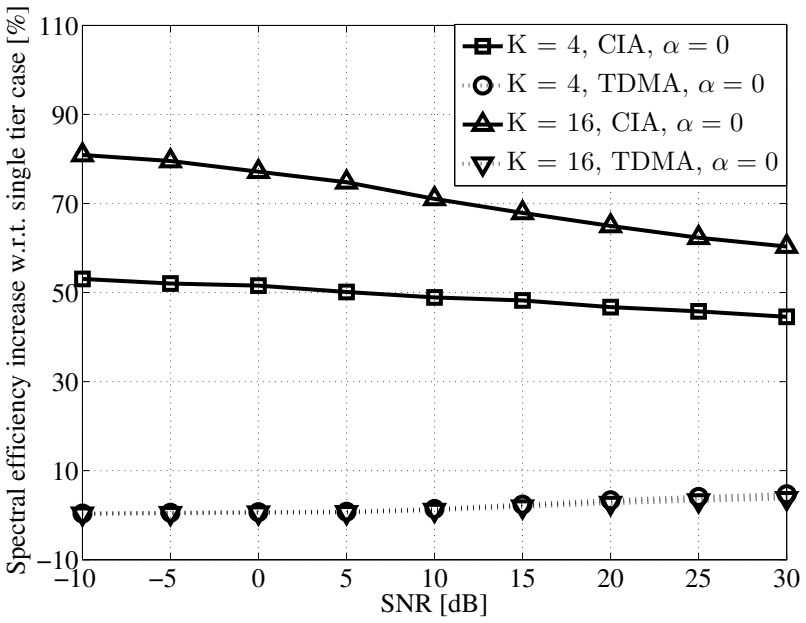

Figure 6.10: Percent increase in spectral efficiency w.r.t. the single OFDMA-based tier case. $K \in \{4, 16\}$, $N = 128, L = 32$ and bandwidth of 1.92 Mhz. No cross-tier interference from the MBS to the SUEs.

In particular, for target SNR= 0 dB, the percent increase in spectral efficiency is as much as 54% for $K = 4$ and 80% for $K = 16$, whereas for SNR= 10 dB, the percent increase goes from 49% to 70% (30% of relative increase). However, differently from the previous case, the deployment of $K = 16$ provides around 60% of percent increase for very high SNR, i.e. SNR= 30 dB, whereas the result for $K = 4$ is around 44% (more than 35% of relative increase). We note that, by comparing the performance for $K = 4$ and $K = 16$, a larger difference in percent increase, w.r.t. to the single tier network, is experienced in the latter case, when going from very low to very high target SNR values.

This confirms the result provided in Figure 6.8, where we showed the larger impact that a more dense second tier has on the performance of the first tier, in case of imperfect CSIT, due to the imperfectly derived cross-interference cancelation precoder.

The numerical findings in this section show that the robustness and consistency of the proposed distributed solution for co-tier interference mitigation is such that the achievable spectral efficiency in the second tier compensates the loss experienced in the first tier due to the imperfect computation of $\mathbf{Z}^{(k)}$. This is verified $\forall \alpha \in [0, 1]$, particularly from very low to medium SNR regime. Therefore, additional capacity can always be added to the network by deploying a second tier of self-organizing SBSs, even if no cooperation is established between the two tiers or within the second tier, regardless of the distance between the MBS and the SUEs.

Furthermore, significant spectral efficiency improvements with respect to legacy TDMA/FDMA approaches have been shown, regardless of the experienced SNR at the receiver, as the number of self-organizing SBSs increases. Accordingly, thanks to an appropriate input signal subspace reduction at each SBS, a more efficient transmission can be performed in the second tier, if compared to state-of-the-art user orthogonalization approaches, while always mitigating (or canceling[3]) the cross-tier interference mitigation generated towards the MUEs. Interestingly, the design of the proposed linear cascaded precoder only requires that each SBS is aware of the number of SUEs inside its coverage area, and disposes of a perfect local CSI w.r.t. the link towards the served SUEs and the MUEs reached by its transmission. On the other hand, CIA exhibits consistent robustness against channel estimation errors, yielding promising spectral efficiency results.

From a practical point of view, the distributed co-tier mitigation solution solves some very challenging issues discussed Chapter 5, affecting the centralized solution proposed in Chapter 4. Specifically, the distributed solution does not require signaling between the SBSs, hence no backhaul or network interface is necessary for its implementation. As a consequence, even if some problem occurred at one or more SBSs, the remaining transmitter in the second tier would still be able to operate, without incurring performance limitations. Furthermore, no dimensionality constraint has to be satisfied to mitigate the co-tier interference in an efficient way in terms of achievable spectral efficiency of the second tier. Thus, the SBSs do not need more than one antenna to be able to communicate with the SUEs in an effective way. Due to the CSI requirements at each SBS, the presence of different mobility patterns and profiles among the SUEs would not compromise the implementation of the proposed technique. In fact, one of its most interesting features is that only the CSI w.r.t. to its served SUE is required by the k^{th} SBS, to derive the precoder $\mathbf{\Theta}^{(k)}$. Finally, concerning the synchronization of the received signals at the receiver, largely discussed in Chapter 5, the distributed approach yields a simpler task for the SBSs. In particular, only the synchronization of the CIA signal with the OFDMA signal at each MUE is required (to realize the perfect cross-interference cancelation), whereas no synchronization among the SBSs is needed to implement the co-tier interference mitigation mechanism.

[3]If perfect CSIT is available.

This discussion concludes the analysis of the multiple small-cells deployment case in two-tiered networks. In the last three chapters, the inherent benefits of the complete spectrum sharing approach w.r.t. to the classical spectrum partitioning have been investigated, for a second tier populated by both cooperative and self-organizing SBSs. Accordingly, we showed that a paradigm shift in the spectrum access strategies in such networks may yield to significant spectral efficiency enhancements, if compared to state-of-the-art approaches. In the next chapters, we will take a step back and illustrate the flexibility of CIA, whose applicability is not necessarily limited to CR settings. In particular, we will focus on a simpler single transmitter downlink scenario, and show how CIA can be adopted to increase the energy efficiency of an OFDM transmission, both from a theoretical and practical perspective.

Part III

Applications and Implementations

Chapter 7

Hybrid Transceiver Design: Recycling Wasted Resources

The results provided so far have shown the enhancements that a paradigm shift in the spectrum access strategies may yield to the spectral efficiency of two-tiered networks. Accordingly, we have discussed the inherent benefits of the complete spectrum sharing approach w.r.t. to the classical spectrum partitioning. Nevertheless, the presented techniques, devised for a cognitive radio setting, are not only key enablers towards opportunistic spectrum access, but more generally a set of flexible mathematical tools that may be used to accomplish other goals. In this section, we give an example of this flexibility. Accordingly, we show how the transmission of a standalone OFDM FBS [4] can be complemented by a second physical layer strategy, i.e., CIA, to enhance the energy efficiency of the legacy transmission. In other words, we model the system given by an FBS communicating with two user equipments as a virtual two-tiered network and show the effectiveness of CIA from an energy efficiency perspective. Numerical findings demonstrate the feasibility of this approach, and that energy efficiency enhancements are achieved due to the spectral efficiency gains, maintaining the same power at the FBS.

7.1 Motivation

As seen in Chapter 1, one of the most promising strategies to increase the flexibility and the robustness of next generation networks is believed to be a hierarchical base station deployment [4]. This is leading to a progressive deployment of small form factor base stations, already available on the market under the name of FBSs. Nowadays, more than 16% of the total traffic from the macro-cellular tier is already being diverted to femto-cells, and this is expected to grow to 48% by 2015 [6]. In fact, the flexibility of femto-cells opens new perspectives for mobile operators to satisfy future traffic demands, both in an economical and ecological way.

The importance of this potentially twofold advantage has been recently emphasized by the SMART 2020 report [140]. Therein, it is foreseen that FBSs should not only lead to performance enhancement, but also operate in a more energy efficient and green way [3]. At a first glance, these two goals may seem contradictory, but research and development on femto-cells is at full speed in both industrial and academic research communities to achieve them. In this spirit, the LTE standard core has included several energy efficient techniques along with capacity increasing solutions, e.g., bandwidth reduction, carrier aggregation strategies and cell switch-off approaches [141]. We note that, the state-of-the-art research on this subject is not specifically targeting either the network level or the device level. In fact, both approaches could yield benefits in terms of energy efficiency. Examples of these solutions at the network level are the many self-organizing techniques being studied to enable traffic demand tracking, aiming at a reduction of the energy expenses in LTE [14]. Otherwise, at the device level, link adaptation strategies for OFDM transmissions, base physical layer technique for most of the modern standard proposals, have been studied and proposed (see [142] and references therein). Usually, such approaches involve a design shift in both RF circuitry and resource allocation strategies to improve energy efficiency.

Herein, we show how the energy efficiency of legacy OFDM-based femto-cells can be improved, by enhancing their spectral efficiency while preserving power consumption. This new device level approach is based on the previously introduced CIA and, unlike currently proposed strategies [141, 142], we show that spectral efficiency can be improved without changing the hardware design, link adaptation, bandwidth or transmit power. More specifically, our power efficient approach recycles the redundant resources of OFDM transmissions (i.e., guard bands or CPs) introduced to combat the frequency selectivity. Interestingly, our approach does not stand as a competitor for the aforementioned current proposal, but can be implemented alongside them, adding up the total energy efficiency.

We recall that, in its classical form seen in Chapter 3, CIA allows a cognitive SBS (or FBS) to serve a secondary user by sharing the spectrum with a licensee OFDM primary macro-cell, protecting the primary OFDM receiver from undesired interference. Herein, we exploit the flexibility of CIA to design a clever hybrid transceiver that simultaneously sends both primary and secondary signals. Remarkably, this hybrid approach does not suffer from some issues inherent to CIA, such as synchronization at the primary receiver and interference channel knowledge acquisition. On the other hand, the simultaneous transmission of primary and secondary messages introduces a new challenge since the femto-cell receiver is now subject to strong primary interference. This issue prompts the adoption of an appropriate linear receiver at the femto-cell receiver, as discussed in the final part of the chapter.

7.2 Hybrid OFDM-CIA transceiver

Consider the layout presented in Figure 7.1, where a single OFDM FBS, adopted to extend coverage and capacity of a generic OFDM macro-cell, serves both the primary and secondary users. As discussed in previous sections, a transmitter adopting OFDM

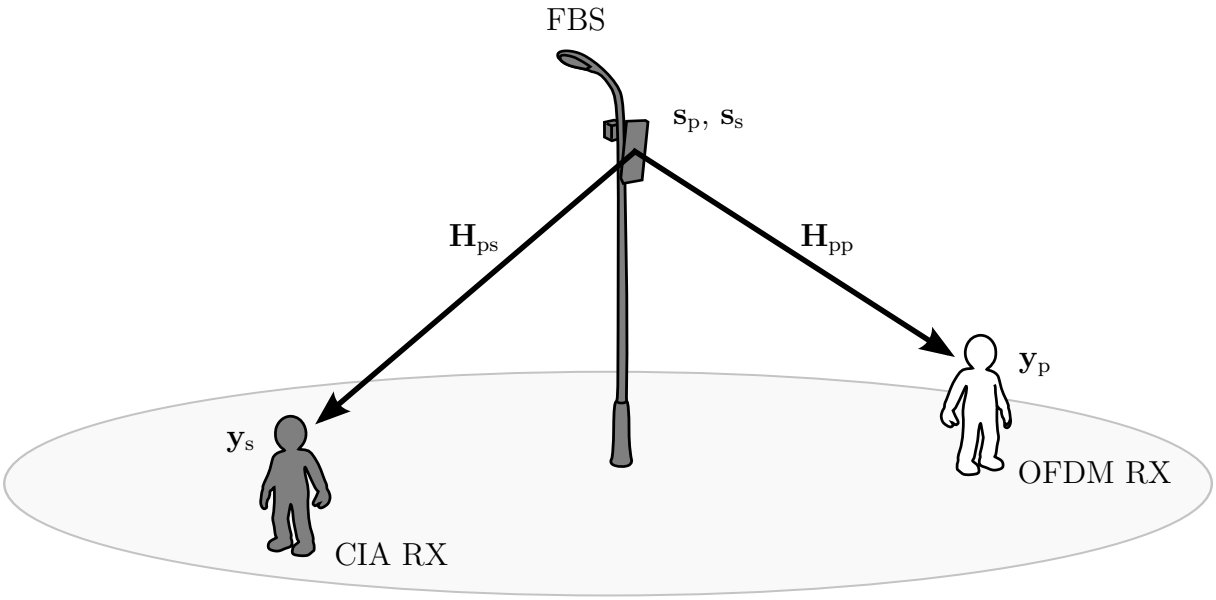

Figure 7.1: Layout for simultaneous primary and secondary transmissions.

introduces a redundancy, i.e., the CP, to combat the frequency-selectivity of the channel. Then, the CP is discarded at the receiver to avoid IBI, and thus, all power invested in the CP is lost. This results in both spectral and energy inefficiencies. We aim at showing how this wasted information resources can be compensated by the simultaneous transmission of a primary (OFDM) and a secondary (CIA) signal at the FBS. In order to emphasize the hybrid nature of the resulting transmission, hereafter we will refer to the FBS as hybrid transceiver (HT). We note that, the implementation of this hybrid scheme does not require the installation of an additional antenna. This contrasts with the conventional CIA approach, where the OFDM and CIA signals are transmitted by two different devices (thus antennas).

Adopting the same notation as in Section 3.2 when introducing CIA, we define $\mathbf{s}_\mathrm{p} \in \mathcal{CN}(0, \mathrm{d}(\mathbf{p}_\mathrm{p}))$ and $\mathbf{s}_\mathrm{s} \in \mathcal{CN}(0, \mathrm{d}(\mathbf{p}_\mathrm{s}))$ as the input symbol vector for the primary and secondary system, of size N and L respectively. Then, $\tilde{\mathbf{y}}_\mathrm{p} \in \mathbb{C}^N$ and $\mathbf{y}_\mathrm{s} \in \mathbb{C}^{N+L}$, received symbol vector at the OFDM and CIA receiver, respectively, are given by

$$\tilde{\mathbf{y}}_\mathrm{p} = \tilde{\mathbf{H}}_\mathrm{pp}\mathbf{A}\mathbf{F}^{-1}\mathbf{s}_\mathrm{p} + \tilde{\mathbf{H}}_\mathrm{pp}\mathbf{E}\mathbf{s}_\mathrm{s} + \mathbf{F}\tilde{\mathbf{n}}_\mathrm{p} \tag{7.1}$$

$$\mathbf{y}_\mathrm{s} = (\Delta^{(l)}(\mathbf{H}_\mathrm{ps}) + \Delta^{(u)}(\mathbf{H}_\mathrm{ps}))\mathbf{E}\mathbf{s}_\mathrm{s} + \mathbf{H}_\mathrm{ps}\mathbf{A}\mathbf{F}^{-1}\mathbf{s}_\mathrm{p} + \mathbf{n}_\mathrm{s}, \tag{7.2}$$

where, we recall, $\tilde{\mathbf{H}}_\mathrm{pp} = \mathbf{F}\mathbf{B}\mathbf{H}_\mathrm{pp} \in \mathbb{C}^{N\times(N+L)}$. We note that, the CIA receiver does not discard the CP according to our findings in Chapter 3. Additionally, we recall that, $\Delta^{(l)}(\cdot)$ and $\Delta^{(u)}(\cdot)$ are two operators yielding the lower and upper triangular part of a matrix argument, as shown in (3.5) and (3.5). In other words, in (7.2), the channel seen by the CIA signal is decomposed into $\Delta^{(l)}(\mathbf{H}_\mathrm{ps})$, $\Delta^{(u)}(\mathbf{H}_\mathrm{ps}) \in \mathbb{C}^{(\mathbb{N}+\mathbb{L})\times(\mathbb{N}+\mathbb{L})}$, channel contribution to ISI and IBI, respectively. In fact, since the secondary receiver does not discard the CP, IBI is not eliminated and has to be taken into account into the model. Moreover,

we recall that, if perfect CSIT w.r.t. $\mathbf{H}_{\text{pp}}$ is available at the HT, $\mathbf{E}$ can be designed such that $\tilde{\mathbf{H}}_{\text{pp}}\mathbf{E}\mathbf{s}_{\text{s}} = \mathbf{0}_{N\times 1}$ as in the conventional CIA case in Chapter 3. Remarkably, and differently from the classical CIA implementation, no adaptive procedure is required at the HT to design $\mathbf{E}$. This is due to the equivalence of the useful channel and interference channel in the hybrid scheme. In practice, only one CSIT, i.e., w.r.t $\mathbf{H}_{\text{pp}}$, is needed both to derive $\mathbf{E}$ and perform power allocation for the OFDM transmission, and this considerably increases the feasibility of the precoder design even in case of high mobility scenarios. We note that, a similar approach is adopted in [63] for physical layer security, where a Vandermonde precoder is used to transmit a common and a private message to two different receivers. In spite the fact that our HT structure is similar, we do not need to enforce secure communications since our focus is on energy efficiency. Therefore, we do not encode all messages with $\mathbf{E}$ nor discard the CP in our reception strategy. These characteristics are at the heart of CIA, a more robust technique w.r.t. diverse PDP configurations, than [63].

We remark that, even though from the primary receiver's point of view the interfering and useful channels coincide, i.e., $\mathbf{H}_{\text{pp}} = \mathbf{H}_{\text{sp}}$, interference and useful signals are subject to different precoding strategies, yielding two independent equivalent channel representations. Therefore, only the secondary message is canceled, with no effect whatsoever to the primary reception. Likewise, the secondary channel is the same for the intended message and interference, a fact that impacts the performance of the secondary system. The secondary receiver can cope with the issue, by means of an appropriate linear equalizer, as shown in the following how

Now, let $\mathbf{x}_{\text{p}} = \mathbf{A}\mathbf{F}^{-1}\mathbf{s}_{\text{p}}$ and $\mathbf{x}_{\text{s}} = \mathbf{E}\mathbf{s}_{\text{s}}$, both of size $N+L$, be the primary and secondary signal components at the HT's antenna. Let us assume that the power budget for the standalone OFDM transmission at the legacy FBS is P. Then, if we let $\mathbf{x} = \mathbf{x}_{\text{p}} + \mathbf{x}_{\text{s}}$ be the HT overall transmit vector, we have that in order to maintain the same power consumption as the OFDM case, it must hold that

$$\text{tr}(\mathbb{E}[\mathbf{x}\mathbf{x}^{\text{H}}]) \leq P. \tag{7.2}$$

In the proposed scheme, both primary and secondary messages are transmitted at the same time, hence they share the transmitter's power budget. We note that, while the CIA precoder is designed to protect the primary receiver from undesired interference, the converse is not true for the OFDM transmission w.r.t. the secondary receiver. Neither deterministic nor stochastic information about this interference is available at the HT. In fact, $\mathbf{H}_{\text{ps}}$ is a finite dimension Toeplitz matrix, whose eigenvalue and eigenvector distribution is not currently known. As a consequence, analytic optimization of the power splitting strategy between the two transmissions is not feasible, and only numerical iterative approaches could be adopted to solve it. Then, since the HT won't be able to find the optimal power splitting strategy due to computational and time constraints, we assume that it will statically split the maximum power between the two transmissions.

Accordingly, $\mathbf{x}_\mathrm{p}$ and $\mathbf{x}_\mathrm{s}$ are derived disjointly, such that

$$\begin{aligned} \mathrm{tr}(\mathbf{x}_\mathrm{p}\mathbf{x}_\mathrm{p}^\mathrm{H}) &\leq P_\mathrm{p} && (7.3)\\ \mathrm{tr}(\mathbf{x}_\mathrm{s}\mathbf{x}_\mathrm{s}^\mathrm{H}) &\leq P_\mathrm{s} && (7.4)\\ P_\mathrm{p} + P_\mathrm{s} &= P && (7.5) \end{aligned}$$

where the optimal power loading strategy for both cases is adopted separately. Specifically, a classical WF algorithm is adopted for the OFDM transmission [59], whereas for CIA the HT can operate as described in Chapter 3. In general, such an approach will induce an SNR loss w.r.t. the legacy standalone OFDM FBS' transmission. The impact of this loss on the performance of the system will be analyzed in Section 7.5, where a study on the spectral efficiency maximizing power splitting strategy is provided.

7.3 Practical Advantages

As seen in Chapter 3, the perfect interference cancelation provided by CIA is possible if perfect CSIT w.r.t. $\mathbf{H}_\mathrm{sp}$ is available at the secondary transmitter, and perfect synchronization of the OFDM and CIA signals is ensured at the primary receiver. If one or both assumptions are not verified, the effectiveness of CIA would be highly reduced. In the following we discuss how the HT structure can facilitate the design of the CIA precoder, increasing its feasibility and effectiveness.

7.3.1 Channel Estimation Issue

A crucial aspect of CIA is the availability of an estimation of $\mathbf{H}_\mathrm{sp}$ at the secondary transmitter. In general, the CSIT acquisition in CR settings requires operations which are not always feasible under the tight delay constraints imposed by the coherence time of the channel, especially in high mobility scenarios. Indeed, two main drawbacks can be identified. Firstly, the secondary transmitter must be aware of the channel estimation procedures adopted in the primary system to be able to adapt its own strategy and acquire the needed CSIT w.r.t. the interference channel. Secondly, the quality of the CSIT highly depends on the SINR at the transmitter and on the available time for estimation.

In TDD networks, the first issue may be addressed by exploiting the training/transmission scheme usually adopted in such scenarios to allow for the necessary channel estimations, as described in [103]. Specifically, for a block fading channel model characterized by a coherence time T, the channel estimations in the primary system are performed during a time interval $\tau \leq T$. This scheme could be opportunistically exploited by a CIA transmitter to acquire the CSIT with periodicity T, to derive $\mathbf{E}$ and be able to engage in the transmission during each time interval of length $T - \tau$, as discussed in Chapter 5 for the multiple secondary transmitters case.

The second issue highly hinges on the characteristics of the operating scenario. For instance, in the case of low SINR at the transmitter, a longer time would be necessary

to acquire a high quality channel estimation [103]. However, even for high SINR at the transmitter the quality of the channel estimations may not be satisfactory. As previously said, the available time for the channel estimation in wireless communications is directly dependent on the coherence time of the channel. Thus, if the receivers in both systems are mobile user equipments, the coherence time of their channel would vary depending on the mobility pattern, speed, and changes in the surrounding environment. This would complicate the resource allocation process in the primary system, possibly reducing the time available for the channel estimations. Consequently, a secondary CIA transmitter operating in such scenarios would face very stringent time constraints. As a result, the whole feasibility of the precoder design could be compromised by wrong or outdated CSIT yielding imperfectly designed precoders and poor overall system performance.

Remarkably, the HT design does not require adaptive procedure to obtained the necessary CSIT to design $\mathbf{E}$. In fact, the aforementioned equivalence $\mathbf{H}_{\text{pp}} = \mathbf{H}_{\text{ps}}$ implies that only the CSI related to the link between the HT and the primary user equipment needs to acquired (i.e., to perform optimal power loading strategy for the OFDM transmission). Consequently, the HT design increases the feasibility of the CIA precoder design, even in case of high mobility scenarios.

7.3.2 Synchronization

As shown in 3.2, CIA's interference cancelation is completely dependent on the CP removal at the primary receiver, where $\mathbf{K}$ is dropped, making the whole interference term $\mathbf{F}\bar{\mathbf{H}}_{\text{sp}}\mathbf{E}\mathbf{s}_{\text{s}} = \mathbf{0}_{N\times L}$. On the other hand, as discussed in Section 5.3, this effect is guaranteed only if perfect synchronization of OFDM and CIA signals at the primary receiver is ensured. In practical implementations of CIA, satisfying this condition could be an extremely challenging task, especially if the position of the primary receiver is not known at the secondary transmitter.

This problem is not present in the proposed hybrid scheme, resulting in a significant simplification of the implementation requirements of CIA. In fact, both the OFDM and CIA messages are transmitted simultaneously by the HT and experience the same channel. Thus, synchronization discrepancies at the receiver are always avoided. In other words, the OFDM and CIA messages are always synchronized at the primary receiver at sample level, regardless of the adopted time synchronization algorithm. Consequently, thanks to the HT design, the precision of the synchronization at the primary receiver has no impact on the residual interference potentially generated by a practical CIA implementation.

7.4 Receiver Structure

As described before, one of the most striking differences between the hybrid scheme proposed herein and the conventional CIA, is the fact that the secondary receiver's physical interference and main channel coincide, i.e., $\mathbf{H}_{\text{ps}}$. This issue imposes a tough interference

cost. In fact, the inevitable presence of the OFDM transmission will always cause high interference at the secondary receiver, irrespective of the channel fading state. As such, the secondary receiver becomes the weak link of the technique, and needs to be addressed carefully. In the following, we let $R_{\rm p}$, $R_{\rm s}$ be the spectral efficiency of the primary and secondary link, respectively. Then, the overall spectral efficiency of the HT's transmission is defined as $R_{\rm h} = R_{\rm p} + R_{\rm s}$.

7.4.1 CIA Receiver

Before starting, let us consider 7.2 and rewrite the received signal at the secondary receiver as

$$\mathbf{y}_{\rm s} = \widetilde{\mathbf{H}}_{\rm ps}^{(l)}\mathbf{s}_{\rm s} + \widetilde{\mathbf{H}}_{\rm ps}^{(u)}\mathbf{s}_{\rm s} + \widetilde{\mathbf{H}}_{\rm ps}^{(p)}\mathbf{s}_{\rm p} + \mathbf{n}_{\rm s}, \tag{7.5}$$

where $\widetilde{\mathbf{H}}_{\rm ps}^{(l)} = \Delta^{(l)}(\mathbf{H}_{\rm ps})\mathbf{E}$, $\widetilde{\mathbf{H}}_{\rm ps}^{(u)} = \Delta^{(u)}(\mathbf{H}_{\rm ps})\mathbf{E} \in \mathbb{C}^{(N+L)\times L}$ are equivalent representations of the ISI and IBI channel contribution, respectively. $\widetilde{\mathbf{H}}_{\rm ps}^{(p)} = \mathbf{H}_{\rm ps}\mathbf{A}\mathbf{F}^{-1} \in \mathbb{C}^{(N+L)\times N}$ is the equivalent channel matrix related to the primary transmission contribution at the CIA receiver.

We know from [59], that the linear equalizer that maximizes the output SINR for any variance of the Gaussian noise is the so-called MMSE receiver. Therefore, let us assume that the secondary receiver possesses perfect CSI w.r.t. to the equivalent channel matrices, by means of a channel estimation made possible by the TDD structure [103]. Accordingly, the experienced interference plus noise component is obtained as $\boldsymbol{\eta}_{\rm s} = \widetilde{\mathbf{H}}_{\rm ps}^{(p)}\mathbf{s}_{\rm p} + \widetilde{\mathbf{H}}_{\rm ps}^{(u)}\mathbf{s}_{\rm s} + \mathbf{n}_{\rm s}$, with covariance matrix $\mathbf{S}_\eta = \mathbb{E}[\boldsymbol{\eta}_{\rm s}\boldsymbol{\eta}_{\rm s}^{\rm H}]$. Then, the MMSE equalizer $\mathbf{C}_{\rm s}$ can be derived as [59]

$$\mathbf{C}_{\rm s} = \widetilde{\mathbf{H}}_{\rm ps}^{(l)\rm H}\left(\mathbf{S}_\eta + \widetilde{\mathbf{H}}_{\rm ps}^{(l)}\widetilde{\mathbf{H}}_{\rm ps}^{(l)\rm H}\right)^{-1}. \tag{7.5}$$

The estimated symbols at the secondary receiver can be obtained as

$$\hat{\mathbf{s}}_{\rm s} = \mathbf{C}_{\rm s}\mathbf{y}_{\rm s}, \tag{7.5}$$

resulting in an effective SINR of the k^{th} decoded symbol of

$$\gamma_{{\rm s},k} = p_{{\rm s},k}\widetilde{\mathbf{h}}_{{\rm ps},k}^{(l)\rm H}\left(\widetilde{\mathbf{H}}_{\rm ps}^{(u)}d(\mathbf{p}_{\rm s})\widetilde{\mathbf{H}}_{\rm ps}^{(u)\rm H} + \widetilde{\mathbf{H}}_{\rm ps}^{(p)}d(\mathbf{p}_{\rm p})\widetilde{\mathbf{H}}_{\rm ps}^{(p)\rm H} + \widetilde{\mathbf{H}}_{{\rm ps},[k]}^{(u)}d(\mathbf{p}_{{\rm s},[k]})\widetilde{\mathbf{H}}_{{\rm ps},[k]}^{(u)\rm H} + \sigma^2\mathbf{I}_{N+L}\right)^{\dagger}\widetilde{\mathbf{h}}_{{\rm ps},k}^{(l)}, \tag{7.5}$$

where, $\widetilde{\mathbf{H}}_{\rm ps}^{(l)} = [\ \widetilde{\mathbf{h}}_{{\rm ps},1}^{(l)} \mid \ldots \mid \widetilde{\mathbf{h}}_{{\rm ps},L}^{(l)}\ ]$, $\widetilde{\mathbf{H}}_{{\rm ps},[k]}^{(u)} = [\ \widetilde{\mathbf{h}}_{{\rm ps},1}^{(u)} \mid \ldots \mid \widetilde{\mathbf{h}}_{{\rm ps},k-1}^{(u)} | \widetilde{\mathbf{h}}_{{\rm ps},k+1}^{(u)} \mid \ldots \mid \widetilde{\mathbf{h}}_{{\rm ps},L}^{(u)}\ ]$ and $\mathbf{p}_{{\rm s},[i]} = [p_{{\rm s},1}, \ldots, p_{{\rm s},k-1}, p_{{\rm s},k+1}, \ldots, p_{{\rm s},L}]$, for the sake of compactness. Accordingly, the spectral efficiency of the CIA transmission can be computed as

$$R_{\rm s} = \frac{1}{N+L}\sum_{k=1}^{L}\log_2\left(1+\gamma_{{\rm s},k}\right). \tag{7.5}$$

7.4.2 OFDM Receiver

Looking back at the primary receiver, we remark that thanks to adoption of CIA's precoder $\mathbf{E}$, no interference is generated by the secondary transmission and the OFDM receiver can apply the decoding procedure adopted in classical OFDM systems. As a consequence, a ZF equalizer is adopted to obtain an estimate of the received symbol vector $\hat{\mathbf{s}}_{\mathrm{p}}$, and the corresponding spectral efficiency R_{p} can be computed as detailed in [59].

7.5 Performance Evaluation

In this section we evaluate the performance of the proposed HT by means of extensive Monte Carlo simulations. The spectral efficiency of a legacy OFDM-based FBS is taken as a reference to assess the performance of the proposed approach. For the simulations, we assume $N = 128$ subcarriers and a CP of $L = 32$. This corresponds to the extended mode of the least resource demanding LTE-A's configurations [58]. This mode is characterized by the lowest $\frac{N}{L}$ ratio, i.e., typically 4. Thus, the power carried by the CP in this mode is roughly 20% of the total, resulting in both a reduced spectral and energy efficiency. As a result, this configuration is a good candidate for energy efficiency improvements, to test the effectiveness of the proposed approach.

In the simulations, noise is generated w.r.t. the average SNR per symbol of our reference legacy OFDM system, equivalent to set $P_p = P$ and $P_s = 0$. The average SNR (in dB) of the i^{th} received symbol is given by

$$\mathrm{SNR}_i = \log_{10} \mathbb{E} \left[\frac{p_{\mathrm{p},i} \bar{\mathbf{h}}_{\mathrm{pp},i}^{\mathrm{H}} \bar{\mathbf{h}}_{\mathrm{pp},i}}{\sigma^2} \right],$$

$\forall i \in [1, N]$, $\sum_i^N p_{\mathrm{p},i} = P$ and with $\bar{\mathbf{h}}_{\mathrm{pp},i}$ i^{th} column of $\bar{\mathbf{H}}_{\mathrm{pp}} = \mathbf{F}\mathbf{B}\mathbf{H}_{\mathrm{pp}}\mathbf{A}\mathbf{F}^{-1}$. For the hybrid system, we keep the same noise power (σ^2), and split the total power P for the OFDM and CIA transmission as in (7.5), such that we provide a fair comparison with the proposed legacy scheme. In other words, by ensuring the same noise level for both reference and hybrid cases, we take into account the SNR reduction experienced by the primary and secondary receivers w.r.t. the reference legacy OFDM femtocell receiver, due to the power splitting strategy adopted in the hybrid scheme.

Let R_{OFDM} be the spectral efficiency of the OFDM transmission, and

$$\mathcal{E}_{\mathrm{OFDM}} \triangleq \frac{R_{\mathrm{OFDM}}}{P} \tag{7.5}$$

its energy efficiency, measured in bit/s/Hz/W. If we define the energy efficiency of the hybrid transmission as

$$\mathcal{E}_{\mathrm{h}} \triangleq \frac{R_{\mathrm{h}}}{P}, \tag{7.5}$$

then we can define $\xi \in \mathbb{R}$, percent change in the energy efficiency experienced by the FBS when switching from legacy OFDM to the proposed hybrid scheme, as

$$\xi = 100\left(\frac{\mathcal{E}_{\mathrm{h}}}{\mathcal{E}_{\mathrm{OFDM}}} - 1\right) = 100\left(\frac{R_{\mathrm{h}}}{R_{\mathrm{OFDM}}} - 1\right).$$

Thus, any change in spectral efficiency is translated into an equivalent change in energy efficiency, since the total transmit power remains the same. To numerically obtain the semi-unitary $\mathbf{E}$, we compute the LQ decomposition [61] of $\bar{\mathbf{H}}_{\mathrm{pp}} = \mathbf{L}_{\mathrm{pp}}\mathbf{Q}_{\mathrm{pp}}$, with $\mathbf{L} \in \mathbb{R}^{N\times(N+L)}$ lower triangular matrix and $\mathbf{Q} = [\ \mathbf{q}_1 \mid \mathbf{q}_2 \mid \cdots \mid \mathbf{q}_{(N+L)}\ ] \in \mathbb{R}^{(N+L)\times(N+L)}$ unitary matrix. Then, we make $\mathbf{E} = \left[\ \mathbf{q}_{N+1} \mid \cdots \mid \mathbf{q}_{(N+L)-1} \mid \mathbf{q}_{N+L}\ \right]$. Other methods to obtain an equally optimal semi-unitary $\mathbf{E}$ can be found in [61]

Firstly, we analyze the effect of the power splitting strategy on the energy efficiency of the HT. As previously said, this analysis can be pursued only by means of a numerical approach. Accordingly, we restrain to some significant configuration useful to grasp the fundamental features of the proposed approach. All channel vectors are obtained as described in Chapter 3, with $l = L$ number of channel taps and uniform PDP. To determine the best ξ we let P_{p}/P vary from 0.5 to 1 and adjust P_{s} accordingly. In Figure 7.2 the best value for ξ, obtained for $P_{\mathrm{p}}/P = 0.87$, is of about 15%, 11% and 4% for the SNRs of 35, 20 and 5 dB, respectively. This shows that the higher efficiency of an OFDM transmission

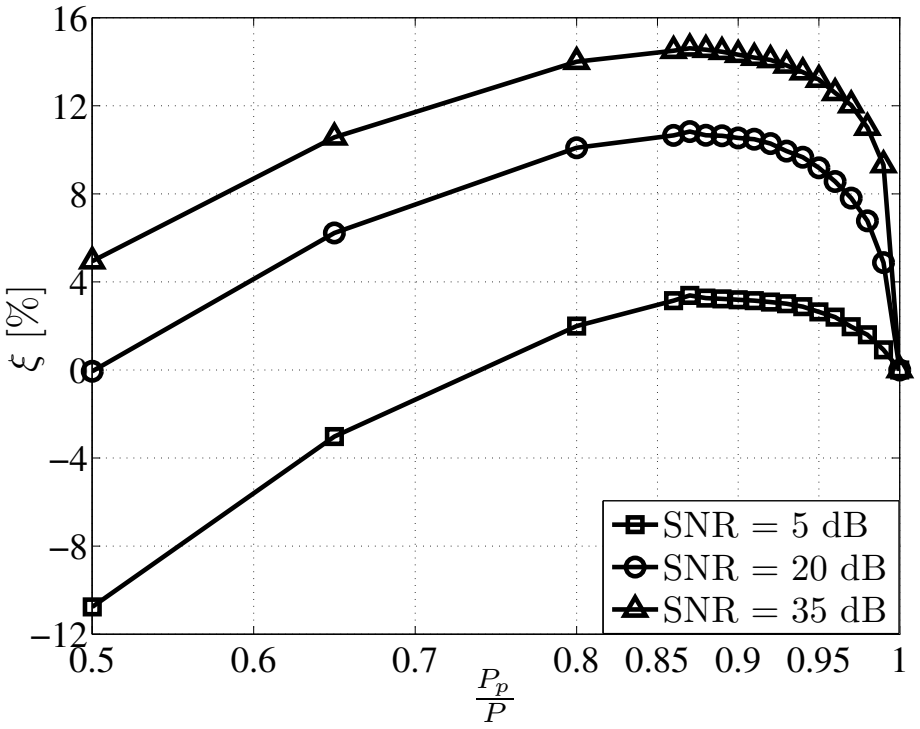

Figure 7.2: Percent energy efficiency change w.r.t. the legacy OFDM FBS for a uniform Rayleigh fading channel.

w.r.t. CIA calls for an unbalanced power splitting in favor of the former, which can carry

more information per block. On the other hand, evident energy efficiency enhancements are experienced at the optimal value $P_{\mathrm{p}}/P = 0.87$ for the three considered SNR regimes. Remarkably, for a medium-to-high SNR regime, the hybrid approach yields a gain of 15% to the legacy standalone OFDM transmission. We note that, for non-optimal values of P_p/P, ξ experiences different trends. This is due to the unbalanced spectral efficiency contribution from the OFDM and CIA parts to the overall HT performance.

We know that uniform PDP channels are not realistic in nature. To grasp the effect of realistic channels on the performance of the HT, we analyze the effect of an exponentially decreasing PDP for the considered Rayleigh fading channel. In the result that follows, we adopt a rather fast channel decay of $T_s/\tau_d = 1.25$, where T_s is the sample time and τ_d the R.M.S. delay spread of the channel. As before, we let the values of P_{p}/P vary from 0.5 to 1 and adjust P_{s} accordingly. In Figure 7.3, we see that the best power splitting strategy is identical to the uniform PDP case, showing that the PDP has no evident influence on this criterion. Nevertheless, the gains at medium-to-high SNR regime are accentuated

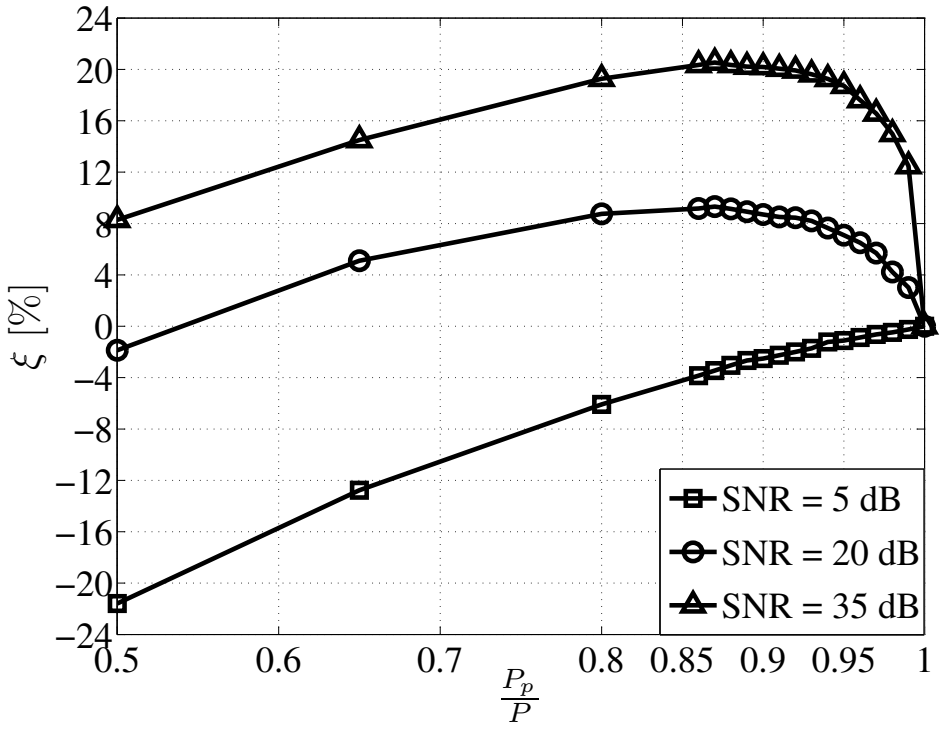

Figure 7.3: Percent energy efficiency change w.r.t. the legacy OFDM FBS for a Rayleigh fading channel, exponentially decreasing PDP.

(up to 20% for 35 dB), while in the low SNR regime they disappear. This is due to CIA's behavior for exponential PDPs. In fact, as discussed in Chapter 3 for exponential PDPs, the efficiency of CIA increases with the SNR, compensating the reduction on the amount of effective eigenmodes of the equivalent channel thanks to the lower experienced IBI, due to a smaller delay spread of the channel.

So far we have seen that the HT provides the best performance when the contribution from CIA adds up on the contribution of the OFDM transmission, occurring at a P_{p}/P of about 0.87. In this final part, we focus on the best P_{p}/P and extend the considered SNR range, to understand how the gains of the hybrid scheme behave w.r.t. the standalone OFDM transmission for both PDP cases. In Figure 7.4 we see the performance of the hybrid scheme for both uniform and exponential PDP channels. Corroborating

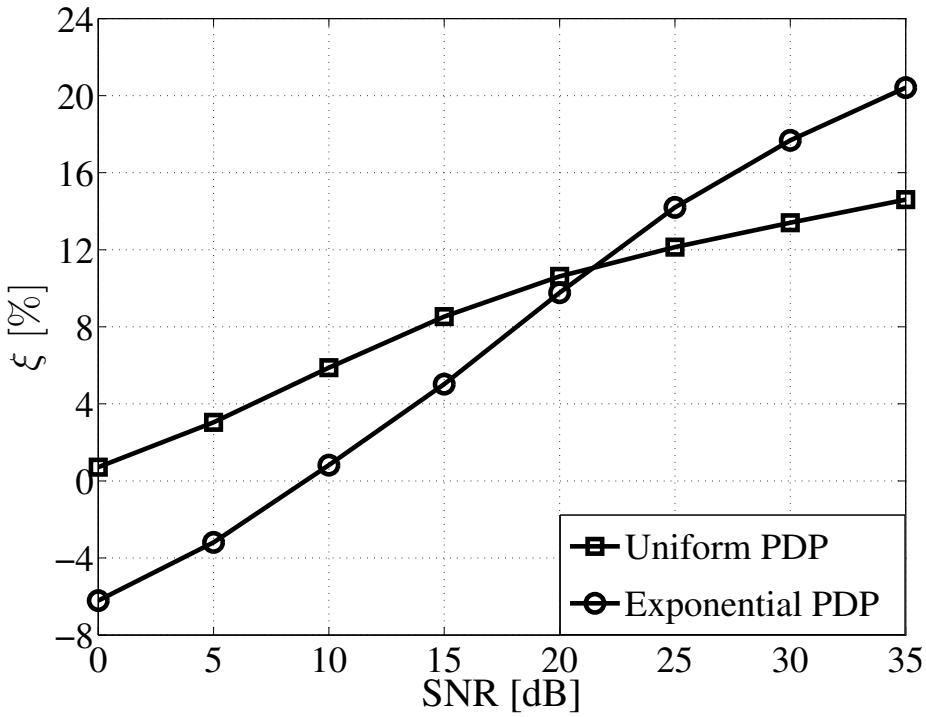

Figure 7.4: Percentage of the maximum achievable spectral efficiency of CIA that can be achieved by the secondary transmission in the hybrid scheme.

our previous findings, for the uniform PDP case the proposed scheme always provides gains, i.e., $\xi > 0$, even when the SNR is as low as 0 dB. Conversely, for the exponential PDP case, the hybrid approach experiences energy efficiency gains w.r.t. the standalone OFDM transmission only for SNRs larger than 8 dB. On the other hand, higher values for ξ are achievable if compared to the uniform PDP case for SNRs larger than 21 dB, exceeding the performance for the latter by about 6% at 35 dB.

The results presented in this chapter show that CIA can be used to open a new research front towards the energy efficiency improvement of legacy OFDM FBSs, without requiring specific hardware modifications or complicated link layer adaptation. Therefore, the techniques developed so far, are not only key enablers towards opportunistic spectrum access, but more generally a set of flexible mathematical tools that may be exploited to accomplish other goals. In the next section, we will further validate these achievements by proposing a proof-of-concept of the herein designed HT, thanks to a suitable SDR approach.

Chapter 8

Reconfigurable Transceiver Design for Flexible Cognitive Networks

In the previous chapter we have seen how CIA can be adopted not only as a DSA enabler technique for a secondary system coexisting with an OFDM primary system, but also to increase the spectral and energy efficiency of a standalone OFDM transmission. Herein, we aim at providing a proof-of-concept of this latter application, thus we focus on the point to point primary and secondary system considered in Chapter 7. This is achieved by designing a novel reconfigurable transceiver architecture, providing the base-band design of both primary and secondary transmitter chains on the same radio device, by means of an SDR approach. As a first step, we show that the proposed transceiver is fast enough to exploit the channel reciprocity within the channel coherence time, an issue of TDD communications. Subsequently, a performance study of the primary and secondary links under an interference cancelation constraint at the secondary system is provided. Field tests are performed to validate the proposed reconfigurable transceiver design, providing encouraging results. Specifically, a non-negligible throughput is achieved at CIA while maintaining the performance of the OFDM transmission. In other words, we show how additional spectral efficiency can be added to the standalone OFDM transmission, while maintaining constant the transmit power at the transceiver. The energy efficiency of the device is then increased, confirming the previously obtained theoretical and numerical results.

8.1 Base-band Design

In this chapter, we aim at designing a novel reconfigurable transceiver architecture, to be used to provide a proof of concept of the hybrid system described in Chapter 7. Similarly to the approach adopted in Chapter 2, the base-band design presented herein is based on the concept of SDR [143]. This flexible approach to radio device design has been introduced from the basis that processing power has become cheap enough to allow

	UL	**DL**
HT	OFDM receiver	OFDM & CIA transmitter
OT	OFDM transmitter	OFDM receiver
CT	CIA receiver	CIA receiver

Figure 8.1: Operating mode of the devices for UL and DL phases.

offloading base-band processing to general purpose processors. From that seminal paper in 1995, until nowadays, SDRs have evolved a long way, going from a military conceptual technology [144] to actual commercially available products [64, 145].

The SDR toolkit adopted in the following is known as GNU Radio library [146]. This flexible tool has been chosen due to its popularity and ease of use. Indeed, the GNU Radio toolkit offers a simple way to create base-band designs, by connecting ready-made signal processing basic blocks using python or by creating such blocks in C and C++ [146]. The adopted RF hardware is based on the same USRP version 1 cards adopted in Chapter 2.

Let us focus on the hybrid scheme proposed in Chapter 7. Therein, HT was acting as both OFDM and CIA transmitter. As a consequence, in this chapter, we aim at obtaining a network layout where primary and secondary transmitter chains are implemented on the same device, whereas two separate devices should host the primary and secondary receiver chains. Interestingly, the flexibility provided by the SDR approach allows for the design of a unique reconfigurable transceiver architecture, that can be tailored at each device to act according to its role in the communication. In particular, depending on the current phase of the communication (UL or DL), each device may operate according to the appropriate transceiver mode, acting as a transmitter or as a receiver thanks to a simple software reconfiguration. In order to improve the readability of the work, given that all devices can switch from transmitter to receiver state, we redefine the device names as follows: in order o ensure consistency with the nomenclature so far adopted, the hybrid device encompassing OFDM and CIA transmitters is named HT, as done in Chapter 7; the primary receiver becomes OFDM transceiver (OT); and the secondary receiver becomes CIA transceiver (CT). The dynamic of the reconfiguration at each device can be modeled as a state machine, implemented at software level during the UL/DL phase, with states as shown in Table 8.1. For the sake of clarity, the structure of the three devices is provided in Figure 8.2 provides, where the configuration of the chains is shown according to the states described in Table 8.1. We note that, any device in the considered network can potentially act as an OFDM/CIA transceiver through minimal software reconfiguration, without any change to the RF chain at the USRPs. Additionally, as further detailed in the following, many signal processing blocks could be common to both receiver chains, due to the similarity of the receiver structures (OT and CT).

We remind that all communications are in TDD, thus the transmitters and receivers access the channel in an alternating manner. Thus, we introduce a small notation change w.r.t. the signal model adopted in Chapter 7 to emphasize the TDD structure, and be able to refer to the DL and UL channels separately. Accordingly, we let $\mathbf{h}_{\mathrm{ab}}^{\mathrm{d}} = [h_{\mathrm{ab},0}^{\mathrm{d}}, \ldots, h_{\mathrm{ab},l}^{\mathrm{d}}]$

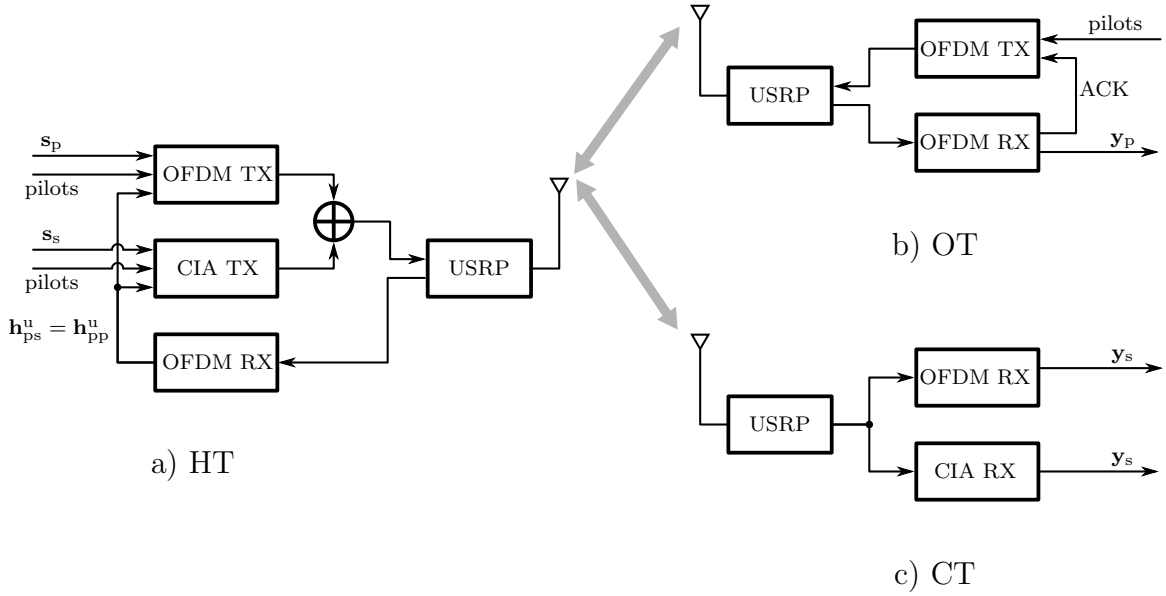

Figure 8.2: Transceivers structure.

be fading channel vectors of size $l+1$ taps, representing the DL between the transmitter in system "a" and the receiver in system "b". Analogously, we let $\mathbf{h}^\mathrm{u}_\mathrm{ab} = [h^\mathrm{u}_{\mathrm{ab},0}, \ldots, h^\mathrm{u}_{\mathrm{ab},l}]$ be fading channel vectors of size $l+1$ taps, representing the UL between the receiver in system "a" and the transmitter in system "b". Finally, we modify the scenario depicted in Fig 7.1 for clarity, such that The communications between the devices are performed according to the following.

8.1.1 Channel estimation and triggering

As a first step, OT sends a "handshake" frame to HT in the UL. Pilots are included in this frame to allow for channel estimation at the HT. This is necessary for equalization of the handshake and, in the future (next version of the software), to perform optimal power allocation. We remind the reader that the $\mathbf{h}^\mathrm{u}_\mathrm{ps}$ CSI is required to construct the null-space precoder $\mathbf{E}$. With the hybrid structure, such knowledge of $\mathbf{h}^\mathrm{u}_\mathrm{ps}$ is always available since its accessible by both the OFDM and CIA transceiver chains, as shown in Figure 8.2.

Thanks to TDD and channel reciprocity, we can consider that within the coherence time, $\mathbf{h}^\mathrm{d}_\mathrm{sp} = \mathbf{h}^\mathrm{u}_\mathrm{ps}$. For the moment, the $\mathbf{h}^\mathrm{u}_\mathrm{ps}$ channel estimation is stored in the CIA transmitter chain for a subsequent precoder generation during the DL phase. We note that no handshake message is sent by CT during the UL phase. As a consequence, differently from Chapter 3, no optimal power allocation is performed for the DL CIA transmission, thus reducing the computational burden for HT.

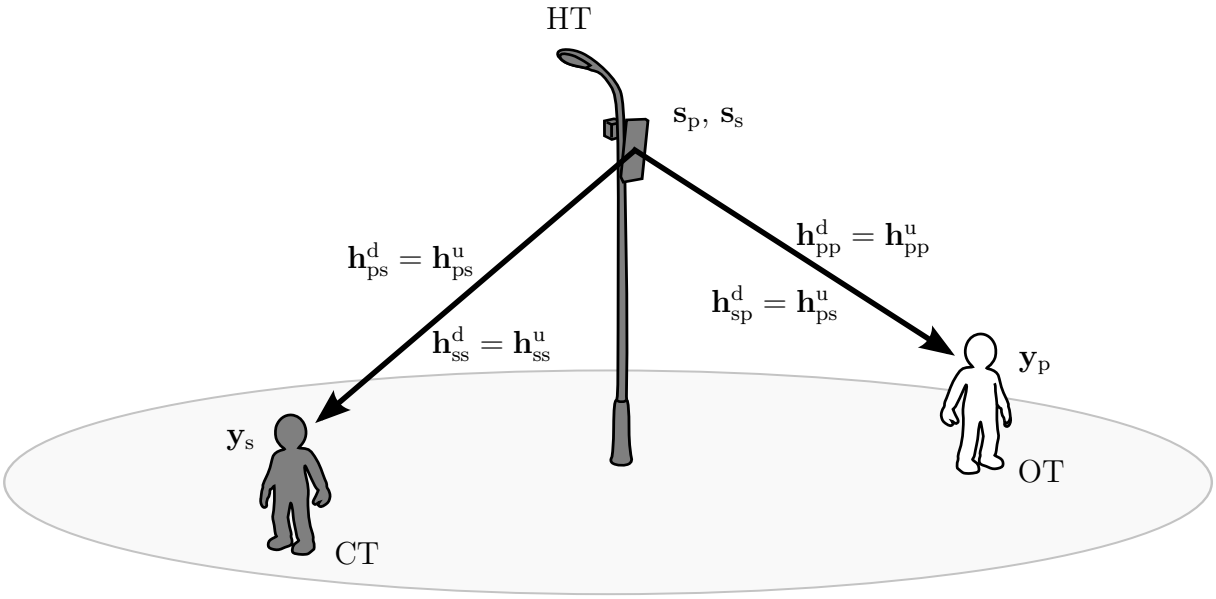

Figure 8.3: Layout of the hybrid scheme.

8.1.2 DL transmission

Triggered by the handshake, the DL phase starts. Two independent frames are generated in parallel, one for OFDM and one for CIA. Note that, no optimal power allocation is performed in the CIA frame generation, thus a CSI w.r.t. $\mathbf{h}^\mathrm{d}_\mathrm{ss} = \mathbf{h}^\mathrm{d}_\mathrm{pp}$ is not required. For simplicity, the input symbol size is set such that the two frames have the same size. Then, the two frames are summed and sent to the USRP for transmission. We recall that, in Chapter 3, the secondary transmitter was introduced as an opportunistic device that can obtain the necessary CSI to design $\mathbf{E}$. Herein, the cognitive nature is represented by HT's ability to act both as an OFDM receiver during the channel estimation phase, and as a CIA transmitter in the DL phase, under the adopted hybrid approach. As previously said, this scheme ensures synchronization of the OFDM and CIA signals at the OT, satisfying a fundamental condition to guarantee the effectiveness of CIA. Concerning the CSI acquisition to obtain an estimation of $\mathbf{h}^\mathrm{d}_\mathrm{sp}$, HT exploits the reciprocity of the channel as done by any standalone CIA cognitive transceiver (without OFDM transmitter capabilities) in a two-tiered network operating in TDD mode. Specifically, the estimation of only one channel is needed, being $\mathbf{h}^\mathrm{d}_\mathrm{sp} = \mathbf{h}^\mathrm{d}_\mathrm{pp}$.

8.1.3 DL reception

During the DL phase, both OT and CT receive and decode their respective signals. The received symbols (after equalization) are stored for further analysis. Then, an "ACK" frame is constructed (including pilots) and transmitted from OT back to HT, to confirm

the positive reception and trigger a new transmission. We note that no UL transmission by CT is required. For simplicity, no channel coding scheme is considered in this work. The analysis of channel coding on the performance of the reconfigurable transceiver is a matter of future research.

8.2 Transceiver Chains Description

As previously seen, the cognitive transceiver has four possible operating modes, namely OFDM transmitter/receiver and CIA transmitter/receiver. In the following, the block structure of each mode is described.

In the remainder of the chapter, the following specific mathematical notation is adopted. The result of the integer division of m, $n \in \mathbb{N}$ is denoted as $\lfloor \frac{m}{n} \rfloor$. Let $\mathbf{b}$ be a vector, then we denote as b_m its m^{th} element. The *vec* operator is denoted by $\mathrm{vec}\,(\cdot)$, and applied to the matrix $\mathbf{B} = [\mathbf{b}_1, \ldots, \mathbf{b}_N]$ it yields $\mathrm{vec}\,(\mathbf{B}) = [\mathbf{b}_1^{\mathrm{T}}, \ldots, \mathbf{b}_N^{\mathrm{T}}]^{\mathrm{T}}$. Finally, given $c \in \mathbb{C}$, we denote by c^* and $\angle c$ the complex conjugate and the phase angle of c, respectively.

8.2.1 OFDM transmitter

Consider the block representation given in Figure 8.4. A detailed description is provided

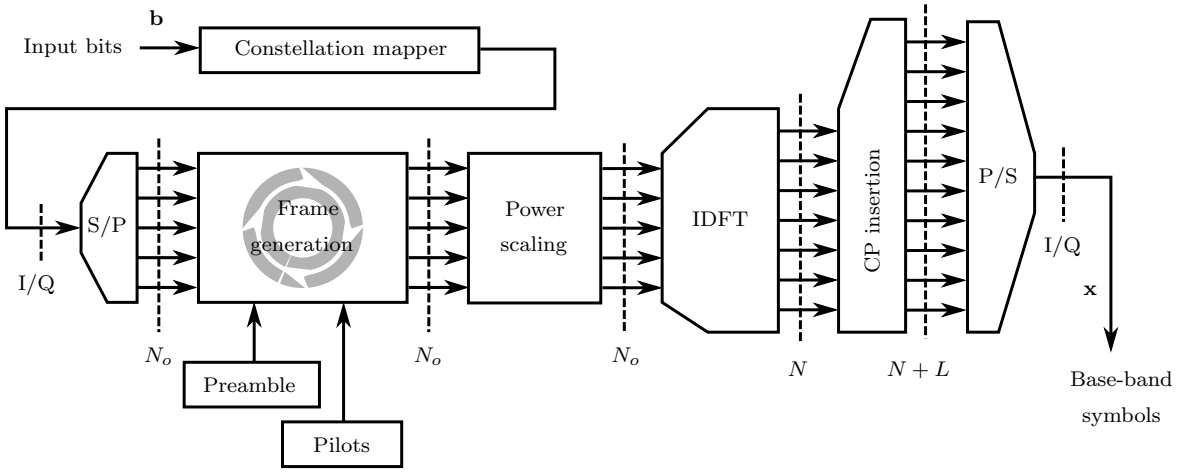

Figure 8.4: OFDM transmitter chain.

in the following.

Constellation Mapper

The constellation mapper accepts a bit sequence as input and yields its digitally modulated version as output. We define $\mathcal{A}$ as the modulated symbol alphabet of order M. Now, let $\mathbf{b} \in [0,1]^K$ be the K-sized row input bit vector fed to the constellation mapper such that $\overline{K} = \frac{K}{log_2 M} \in \mathbb{N}$. Consequently, we define $\overline{\mathbf{d}} \in \mathcal{A}^{\overline{K}}$ as the data row vector at the output of the constellation mapper, representing the digitally modulated version of $\mathbf{b}$. We note that $\mathbf{b}$ can be either a binary file or a pseudo-random binary sequence, with the addition of an appropriate padding to satisfy the above size condition. Any mapping function can be implemented in this block to provide support for the corresponding digital modulation scheme.

Serial to Parallel

A serial to parallel operation is performed on $\overline{\mathbf{d}}$, to prepare the modulated symbols for the frame generation in the frequency domain. Let us assume that only a central portion of the available spectrum may be used to obtain a smoother impulse response of the transmit/receive filters in the USRPs. In particular, we let N_o be the number of active subcarriers, i.e., *occupied tones*, out of the N available for the OFDM transmission. Accordingly, a check on the size of $\overline{\mathbf{d}}$ is performed before the serial to parallel operation. If $\frac{\overline{K}}{N_o} \notin \mathbb{N}$, then a padding vector of dummy symbols $\mathbf{d}_\mathrm{p} \in \mathbb{C}^{N_o(1+\lfloor \frac{\overline{K}}{N_o} \rfloor)-\overline{K}}$ is appended to $\overline{\mathbf{d}}$, such that $\mathbf{d} = [\overline{\mathbf{d}}\, \mathbf{d}_\mathrm{p}]$, new padded data row vector of size $\tilde{K} = N_o(1 + \lfloor \frac{\overline{K}}{N_o} \rfloor)$, is obtained. Naturally, if $\frac{\overline{K}}{N_o} \in \mathbb{N}$, then $\mathbf{d} = \overline{\mathbf{d}}$ and $\tilde{K} = \overline{K}$. The serial to parallel block transforms the data vector $\mathbf{d}$ in a data matrix $\mathbf{D}^{(\mathrm{O})} \in \mathcal{A}^{N_o \times \frac{\tilde{K}}{N_o}}$, mapping the m^{th} element of $\mathbf{d}$ to $[\mathbf{D}^{(\mathrm{O})}]_{(m-N_o\lfloor \frac{m}{N_o} \rfloor, \lfloor \frac{m}{N_o} \rfloor + 1)}$.

Frame Generation

The frame generated by the OFDM transmitter has three main components. Accordingly, the frame generation block accepts data matrix $\mathbf{D}^{(\mathrm{O})}$, as input and construct a frame $\mathbf{S}$ as

$$\mathbf{S} = [\mathbf{G}\ \ \mathbf{P}^{(\mathrm{O})}\ \ \mathbf{D}^{(\mathrm{O})}], \tag{8.0}$$

where $\mathbf{P}^{(\mathrm{O})} \in \mathbb{C}^{N_o \times R_p^{(\mathrm{O})}}$ is a deterministic matrix, known a priori by the frame generator, and $\mathbf{G} \in \mathbb{C}^{N_o \times R_g}$ is a matrix with pseudo-random entries. In particular, they are denoted as *preamble* and *pilot* matrix, respectively, with R_g and $R_p^{(\mathrm{O})}$ detailed in the following.

We start by describing the preamble matrix $\mathbf{G}$, adopted for time and frequency synchronization purposes at the receiver. We consider a preamble structure according to the classical Schmidl-Cox (S-C) procedure proposed in [147]. This approach makes use of the statistical properties of specially constructed sequences, characterized by interesting auto-correlation properties. In our implementation, we set $R_g = 1$ and $\mathbf{G}$ degenerates into a N_o-sized vector $\mathbf{g}$, obtained by alternating binary phase shift keying (BPSK) symbols

g_i, $\forall i \in [1, \frac{N_o}{2}]$, and zeros such that $\mathbf{g} = [g_1, 0, g_2, 0, \ldots, g_{\frac{N_o}{2}}]^T$. We remark that, the seed adopted to generate the pseudo-random sequence of BPSK symbol is defined by the user and shared with the OFDM receiver, to allow for a more precise time synchronization as detailed in the following. Note that, an inverse discrete Fourier transform (IDFT) over the N available subcarriers will be performed in the following block, to generate the OFDM symbols to be transmitted. Thanks to the properties of the IDFT, the time domain representation of $\mathbf{g}$ will consist of a repeated sequence over one full OFDM symbol, required structure for the correct application of the S-C algorithm.

The realization of the preamble is known at the receiver, as previously stated, hence the latter could estimate the channel (for equalization purposes) by evaluating the received instance of $\mathbf{g}$, as done in classical pilot-based estimations [62]. Nevertheless, the presence of a significant number of zeros in $\mathbf{g}$ may decrease the quality of said estimation, even if linear interpolation techniques were to be adopted [148]. Therefore, the pilot matrix $\mathbf{P}^{(\mathrm{O})}$ of size $N_o \times R_p^{(\mathrm{O})}$ is appended to the frame after $\mathbf{g}$, to provide the receiver with a more reliable tool for channel estimation. In particular, we let $\mathbf{P}^{(\mathrm{O})} = \mathbf{p}^{(\mathrm{C})}\mathbf{1}^{\mathrm{T}}_{R_p^{(\mathrm{O})}}$, with $\mathbf{p}^{(\mathrm{C})} \in \mathbb{C}^{N_o}$ deterministic vector known both at the transmitter and receiver. We remark that, a bigger $R_p^{(\mathrm{O})}$ could yield more accurate channel estimations at the receiver but reduces the spectral efficiency of the transmission. Thus, a careful adjustment of this parameter depending on the environment, e.g., perceived SNR at the receiver and coherence time of the channel, could become necessary during the field tests.

Power Scaling

At this point, power scaling may be applied to shape a desired power profile for $\mathbf{S}$ before the IDFT. Let $\alpha_g^{(\mathrm{O})}$, $\alpha_p^{(\mathrm{O})}$, $\alpha_d^{(\mathrm{O})} \in \mathbb{R}$ be parameters adopted to scale independently the power of $\mathbf{g}$, $\mathbf{P}^{(\mathrm{O})}$ and $\mathbf{D}^{(\mathrm{O})}$. Then, the frame obtained at the output of the power scaling block can be written as $\mathbf{S} = [\alpha_g^{(\mathrm{O})}\mathbf{g} \;\; \alpha_p^{(\mathrm{O})}\mathbf{P}^{(\mathrm{O})} \;\; \alpha_d^{(\mathrm{O})}\mathbf{D}^{(\mathrm{O})}]$.

IDFT

The matrix $\mathbf{S}$, input to the IDFT block, has size $N_o \times (1 + R_p^{(\mathrm{O})} + \frac{\tilde{K}}{N_o})$, thus a further padding to $\mathbf{S}$ has to be appended to prepare the frame for the N-point IDFT. In fact, the number of occupied tones in the proposed scheme is lower than the number of available subcarriers, i.e., $N_o < N$. Let $\mathbf{N} = \mathbf{0}_{\frac{(N-N_o)}{2} \times (1+R_p^{(\mathrm{O})} + \frac{\tilde{K}}{N_o})}$ be a suitable zero padding matrix. The frequency domain representation of the full OFDM frame is defined as

$$\mathbf{S}_{\mathcal{F}} = \begin{bmatrix}\mathbf{N}^{\mathrm{T}} & \mathbf{S}^{\mathrm{T}} & \mathbf{N}^{\mathrm{T}}\end{bmatrix}^{\mathrm{T}} \in \mathbb{C}^{N \times (1+R_p^{(\mathrm{O})} + \frac{\tilde{K}}{N_o})}. \tag{8.0}$$

Then, $\mathbf{S}_{\mathcal{T}}$, time domain representation of $\mathbf{S}_{\mathcal{F}}$, is obtained by stacking the N-point IDFT of $\mathbf{S}_{\mathcal{T}}$ and an additional padding matrix $\mathbf{Z} = \mathbf{0}_{N \times R_z}$, included for SNR estimation purposes at the OFDM receiver, as further detailed in Section 8.2.2. Then, $\mathbf{S}_{\mathcal{T}}$ reads

$$\mathbf{S}_{\mathcal{T}} = [\mathbf{F}^{-1}\mathbf{S}_{\mathcal{F}} \quad \mathbf{Z}] \in \mathbb{C}^{(N+L) \times (1+R_p^{(\mathrm{O})} + \frac{\tilde{K}}{N_o} + R_z)}, \tag{8.0}$$

with $\mathbf{F}$ unitary DFT matrix as defined in Section 3.1 and $R_z \in \mathbb{R}$. We remark that the matrix representation adopted so far has been provided only for the sake of compactness. In fact, in the operating framework provided by the adopted platform, (GNU Radio), algorithms based upon matrix-wise operations are not computationally efficient. Consequently, the N-point IDFTs (and DFTs) are implemented by means of the computationally efficient algorithms provided by the fastest Fourier transform in the West (FFTW) [149] C library, based on vector-wise operations. This choice has been made to decrease the required computational time of the IDFT block.

Cyclic Prefix Insertion

As detailed in Section 3.1, the CP insertion can be modeled as a matrix operation consisting in a left multiplication of $\mathbf{S}_{\mathcal{T}}$ by the CP insertion matrix $\mathbf{A}$, yielding $\mathbf{S}_{\mathcal{T}}^{\mathrm{CP}} = \mathbf{A}\mathbf{S}_{\mathcal{T}} \in \mathbb{C}^{(N+L)\times(1+R_p^{(\mathrm{O})}+\frac{\tilde{K}}{N_o}+R_z)}$. In practice, if we let $\overline{\mathbf{S}}_{\mathcal{T}} \in \mathbb{C}^{L\times(1+R_p^{(\mathrm{O})}+\frac{\tilde{K}}{N_o}+R_z)}$ be the matrix carrying the last L rows of $\mathbf{S}_{\mathcal{T}}$, then the CP insertion operation can be implemented without matrix operations by constructing $\mathbf{S}_{\mathcal{T}}^{\mathrm{CP}} = [\overline{\mathbf{S}}_{\mathcal{T}}^{\mathrm{T}} \ \mathbf{S}_{\mathcal{T}}^{\mathrm{T}}]^{\mathrm{T}}$.

Parallel to Serial

We denote the output of the parallel to serial block as $\mathbf{x}^{(\mathrm{O})} \in \mathbb{C}^{(N+L)(1+R_p^{(\mathrm{O})}+\frac{\tilde{K}}{N_o}+R_z)}$, i.e., the serialized version of the stream, ready to be fed to the USRP for RF modulation. This operation can be written as $\mathbf{x}^{(\mathrm{O})} = \mathrm{vec}\,(\mathbf{S}_{\mathcal{T}}^{\mathrm{CP}})^{\mathrm{T}}$, with $\mathbf{x}^{(\mathrm{O})}$ being a row vector.

8.2.2 OFDM receiver

Consider the block representation given in Figure 8.5. A detailed block-by-block description is provided in the following.

Synchronization

The first operation performed by the OFDM receiver on $\mathbf{y}$, frame received by the USRP and fed as input to the OFDM receiver base-band chain, is the time and frequency synchronization. By construction, OFDM is based upon a large number of closely spaced orthogonal subcarrier signals, used to bear data on several parallel data streams or channels. In case of missed synchronization of the received frame, such carrier orthogonality is lost. Specifically, if the CP L is not much larger than the delay spread of the channel, imperfect time synchronization of the frame may cause IBI and decrease the signal to interference plus noise ratio of the useful portion of the signal. Conversely, in case of imperfect frequency synchronization, issues such as inter-carrier interference or phase noise may arise [62], breaking the orthogonality between the subcarriers and reducing the quality of the decoding. Unfortunately, any communication system may experience a

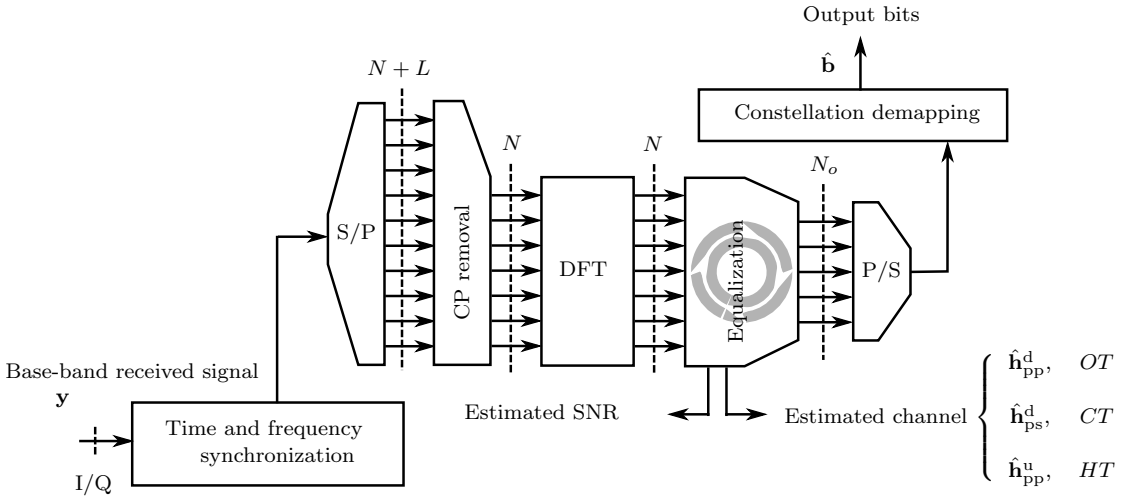

Figure 8.5: OFDM receiver chain.

carrier frequency offset due to issues such as Doppler shifts, or imperfections in the phase lock loop responsible for the generation of the carrier frequency at the receiver (used in the RF demodulation step to obtain the base-band representation of the received signal), just to name a few. Thus, an appropriate procedure to achieve time and frequency synchronization is required.

Herein, we exploit the special structure of the preamble, described in Section 8.2.1, and adopt the S-C method [147] to achieve both time and frequency synchronization. First the timing of the first sample of the preamble is identified. Then the carrier frequency offset is detected and corrected to achieve frequency synchronization.

By construction, the time domain representation of the considered preamble (CP excluded) is composed by two halves of size $\frac{N}{2}$, for a total preamble size of N samples. The receiver disposes of the same seed adopted at the transmitter to generate the preamble, as explained in Section 8.2.1. Thus, a copy of $\mathbf{g}_{\mathcal{T}} = \mathbf{F}^{-1}[\mathbf{0}_{1\times\frac{N-N_o}{2}}\ \mathbf{g}^{\mathrm{T}}\ \mathbf{0}_{1\times\frac{N-N_o}{2}}]^{\mathrm{T}}$, time domain version of the N-sized preamble (CP excluded) is locally available at the receiver. Now, let us consider a window of N received samples. We define t as the time index corresponding to the first sample of the window. If we let the window slide along in time, we have that the receiver can search for the preamble by computing A_t, auto-correlation function of the received signal evaluated at the instant t, $\forall t \in \mathbb{N}$, given by

$$A_t = \sum_{m=1}^{\frac{N}{2}} y^*_{t+m} y_{t+m+\frac{N}{2}}. \tag{8.0}$$

Let T^c_t be a timing metric, defined as

$$T^c_t = \frac{|A_t|^2}{E^2_t} \in [0,1], \tag{8.0}$$

where $E_t = \sum_{m=1}^{N/2} |y_{t+m+(N/2)}|^2$ is the received energy for the second half-window. In correspondence with the start of the actual frame, T_t^c reaches a plateau whose length is equal to $L - l$, thanks to the auto-correlation properties of the adopted preamble, with l number of channel taps (excluding the line-of-sight component) as defined in Section 8.1. The starting sample of the preamble may be taken to be anywhere within this plateau [147], leading to some uncertainty for the receiver. A two-step timing estimation is adopted to solve this issue. First, a *coarse* timing estimation, i.e., $\hat{t}_c$, is computed to identify the approximate position of the preamble within the received sequence by

$$\hat{t}_c = \arg\max_t \{T_t\}. \tag{8.0}$$

Then, we select a fixed window of received samples of size $\frac{N}{2} + 2L$, including the sample at $\hat{t}_c$ (as the $(L+1)^{th}$ sample), and compute its cross-correlation with the $\mathbf{g}_{\mathcal{T}}$ as

$$\tilde{A}_t = \sum_{m=1}^{N/2+2L} y^*_{\hat{d}_c - L + m} \mathbf{g}_{\mathcal{T},m}. \tag{8.0}$$

Note that, (8.2.2) is feasible if $L \leq \frac{N}{4}$, condition usually verified in practical systems for matters of spectral efficiency [50]. Now, the *fine* estimation of the timing of the first sample of the preamble, i.e., $\hat{t}_f$, is obtained by exploiting the property of the peak of the cross-correlation $\tilde{A}_t$ as

$$\hat{t}_f = \hat{t}_c + \arg\max_t \{\tilde{A}_t\} - L - 1. \tag{8.0}$$

From now on, we will let $\tilde{\mathbf{y}}$ be the received frame after the time synchronization, for clarity. It is obtained by discarding the first $\hat{t}_f - 1$ samples of $\mathbf{y}$.

Once the best timing point $\hat{t}_f$ has been identified, frequency synchronization can be achieved. In particular, the carrier frequency offset f_Δ can be directly estimated by evaluating $\hat{\phi}$, phase difference between the two halves of the received preamble, in radians, estimated at $\hat{t}_f$ as

$$\hat{\phi} = \angle(A_{t,\hat{t}_f}). \tag{8.0}$$

Accordingly, f_Δ can be computed as

$$\hat{f_\Delta} = \frac{\phi}{\pi N} + \frac{2z}{N}, \tag{8.0}$$

sum of a fractional and an integer part, with $z = 0$ for $|\hat{\phi}| < \pi$[1] and $z \in \mathbb{Z} \setminus \{0\}$ otherwise [147]. Thus, no estimator for the integer part of f_Δ has been implemented in the synchronization block, in order to not cause an unneeded increase in complexity. However, the interested reader may refer to [147] for a description of the algorithm that can be adopted to estimate z.

Finally, $\hat{\mathbf{x}}^{(\mathrm{O})}$, synchronized version of the received frame is obtained as

$$\hat{\mathbf{x}}^{(O)} = e^{-2\pi \hat{f}_\Delta} \tilde{\mathbf{y}}, \tag{8.0}$$

[1]We note that in the preliminary experimental trials performed to assess the effectiveness of the synchronization algorithms, the condition $|\hat{\phi}| < \pi$ was always satisfied.

with $\hat{\mathbf{x}}^{(O)} \in \mathbb{C}^{(N+L)(1+R_p^{(\mathrm{O})}+\frac{\tilde{K}}{N_o}+R_z)+N}$ carrying the first $(N+L)(1+R_p^{(\mathrm{O})}+\frac{\tilde{K}}{N_o}+R_z)+N$ received samples after the $\hat{t}_f^{th}$. At this stage, the OFDM receiver discards the leading N samples of $\hat{\mathbf{x}}^{(O)}$, i.e., the preamble, and feeds the resulting $\hat{\mathbf{x}}^{(O)} \in \mathbb{C}^{(N+L)(1+R_p^{(\mathrm{O})}+\frac{\tilde{K}}{N_o}+R_z)}$ to the serial to parallel block.

Serial to Parallel

The output of this block is the stream ready for the CP removal operation, i.e., the matrix $\hat{\mathbf{X}}_{\mathcal{T}} = \mathbf{H}_{\mathrm{pp}}\mathbf{S}_{\mathcal{T}}^{\mathrm{CP}} + \mathbf{W}^{(\mathrm{O})} \in \mathbb{C}^{(N+L)\times(1+R_p^{(\mathrm{O})}+\frac{\tilde{K}}{N_o}+R_z)}$, with $\mathbf{W}^{(\mathrm{O})} \in \mathbb{C}^{(N+L)\times(1+R_p^{(\mathrm{O})}+\frac{\tilde{K}}{N_o}+R_z)}$ matrix collecting the overall effect of both the thermal noise and the residual interference generated by the secondary transmission, if perfect CSI is not available at HT. In particular, the m^{th} element of $\hat{\mathbf{x}}^{(O)}$ is mapped to $[\hat{\mathbf{X}}_{\mathcal{T}}]_{(m-(N+L)\lfloor\frac{m}{N+L}\rfloor,\lfloor\frac{m}{N+L}\rfloor)}$.

CP Removal

The CP removal block performs the dual operation w.r.t. the CP insertion block at the transmitter. In practice, the first L rows of the matrix $\hat{\mathbf{X}}$ are removed to obtain a matrix $\hat{\mathbf{X}}_{\mathcal{T},N}$, ready to be processed by the DFT block. We can represent this operation in matrix form by

$$\hat{\mathbf{X}}_{\mathcal{T},N} = \mathbf{B}\mathbf{X}, \tag{8.0}$$

with $\mathbf{B}$ CP removal matrix as defined in Section 3.1.

DFT

A DFT operation is performed after the CP removal to yield $\hat{\mathbf{X}}_{\mathcal{T},F} \in \mathbb{C}^{N\times(1+R_p^{(\mathrm{O})}+\frac{\tilde{K}}{N_o}+R_z)}$, representation of the received frame in the frequency domain, given by $\hat{\mathbf{X}}_{\mathcal{F},N} = \mathbf{F}\hat{\mathbf{X}}_{\mathcal{T},N}$. We remark that the matrix representation is adopted for the sake of compactness, as done for the dual block at the transmitter. For practical implementation, the N-point DFT is computed by means of computationally efficient algorithms provided by the FFTW C library, based on vector-wise operations.

Equalizer

A channel equalization is performed after the DFT, to be able to remove the effect of the channel on the received signal and proceed to the decoding. We recall that, thanks to the orthogonality between the subcarriers, OFDM transforms the wide-band frequency-selective channel into a set of parallel narrow-band flat-fading channels. Thus, a classical low-complexity ZF strategy can be implemented to equalize the received frame, as typically done in OFDM receivers [59]. First, the portion of the spectrum with no active subcarrier is discarded from $\hat{\mathbf{X}}_{\mathcal{F},N}$, to recover the received noisy version of $\mathbf{S}$. Accordingly, we remove both the first and the last $\frac{N-N_o}{2}$ rows from the matrix $\hat{\mathbf{X}}_{\mathcal{F},N}$, obtaining

$\hat{\mathbf{S}} = \mathbf{Q}\hat{\mathbf{X}}_{\mathcal{F},N} = [\hat{\mathbf{g}}\ \hat{\mathbf{P}}^{(\mathrm{O})}\ \hat{\mathbf{D}}^{(\mathrm{O})}\ \hat{\mathbf{Z}}^{(\mathrm{O})}]$, with $\mathbf{Q} = \left[\mathbf{0}_{N_o \times \frac{N-N_o}{2}}\ \mathbf{I}_{N_o}\ \mathbf{0}_{N_o \times \frac{N-N_o}{2}}\right]$. Note that, $\hat{\mathbf{Z}}^{(\mathrm{O})} = \mathbf{QFBZ} \in \mathbb{C}^{N_o \times R_z}$ is the frequency domain representation of the received noisy version of the padding matrix $\mathbf{Z}$.

Now, before the actual equalization, the receiver can exploit the structure of the received frame to obtain $\widehat{SNR}$, approximate estimation of the average SNR experienced during the reception. Specifically, $\widehat{SNR}$ is computed as the ratio between the energy of the preamble $\mathbf{g}$ and the energy of the AWGN as

$$\widehat{SNR} = 10\log_{10}\left(\frac{\hat{\mathbf{g}}^{\mathrm{H}}\hat{\mathbf{g}}}{\mathrm{tr}\left(\hat{\mathbf{Z}}^{(\mathrm{O})}\hat{\mathbf{Z}}^{(\mathrm{O})\mathrm{H}}\right)}\right). \tag{8.0}$$

This approximation is more suitable for medium and high SNR regime, due to the presence of a noise component in $\mathbf{g}$ that affects the precision of $\widehat{SNR}$. Additionally, the precision of $\widehat{SNR}$ depends on the size of $\mathbf{g}$ and $\mathbf{Z}$, being more accurate for $1 << R_z$, condition that guarantees a more reliable estimation of the energy of the AWGN.

At this stage, the receiver evaluates $\hat{\mathbf{P}}^{(\mathrm{O})}$ to compute the diagonal equalizer matrix $\hat{\mathbf{H}}_{\mathrm{eq}} = diag([\frac{1}{\hat{h}_1}, \ldots, \frac{1}{\hat{h}_{N_o}}]) \in \mathbb{C}^{N_o \times N_o}$. Accordingly, the knowledge of the deterministic transmitted pilot matrix $\mathbf{P}^{(\mathrm{O})}$ is exploited to obtain $\hat{h}_k$ as

$$\hat{h}_k = \frac{1}{R_p^{(\mathrm{O})}} \sum_{m=1}^{R_p^{(\mathrm{O})}} \frac{[\hat{\mathbf{P}}^{(\mathrm{O})}]_{k,m}}{[\mathbf{P}^{(\mathrm{O})}]_{k,m}}, \quad \forall k \in [1, N_o]. \tag{8.0}$$

Then, the equalized version of the data matrix $\hat{\mathbf{D}}_{\mathrm{eq}}^{(\mathrm{O})}$ reads

$$\hat{\mathbf{D}}_{eq}^{(\mathrm{O})} = \hat{\mathbf{H}}_{eq}\hat{\mathbf{D}}^{(\mathrm{O})}, \tag{8.0}$$

and this ends the equalization process.

Parallel to Serial

A parallel to serial operation is performed on $\hat{\mathbf{D}}_{eq}^{(\mathrm{O})}$ to yield $\hat{d} \in \mathbb{C}^{\frac{\tilde{K}}{N_o}} = \mathrm{vec}(\hat{\mathbf{D}}_{eq}^{(\mathrm{O})})^{\mathrm{T}}$, row vector carrying the received version of the digitally modulated symbol vector $\mathbf{d}$, of size $\frac{\tilde{K}}{N_o}$, ready to be fed to the constellation demapper.

Constellation Demapper

The constellation demapper implements the appropriate function to recover the received bit vector $\hat{\mathbf{b}}$, ending the receiver processing. The block does not impose any restriction on the modulation order that can be adopted. Any demapping function can be implemented to provide support for the corresponding digital modulation scheme.

8.2.3 CIA transmitter

Consider the block representation in Figure 8.6. The main difference between this scheme

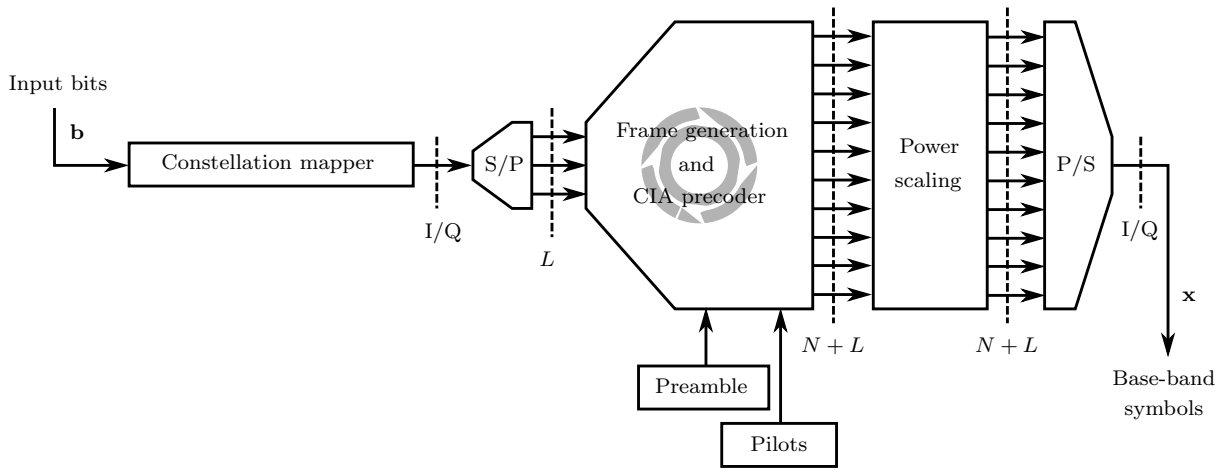

Figure 8.6: CIA transmitter chain.

and the one presented for the OFDM transmitter implementation in Section 8.2.1 is the precoding block. In particular, in the OFDM transmitter an IDFT is applied to the frequency domain representation of the signal, to obtain its time domain version. Conversely, in the CIA transmitter a linear precoder is applied on the signal to project it onto the null-space of the interference channel $\mathbf{h}_{\text{sp}}^{\text{d}}$. We note that the CIA precoder is built upon an appropriate channel estimation performed by HT, by evaluating the pilots appended by OT to the OFDM UL frame. A detailed block-by-block description is provided in the following.

Constellation Mapper

The constellation mapper provides the same functions as its previously described OFDM counterpart. In this case, we let $\mathbf{b} \in [0,1]^J$ be the J-sized row input bit vector fed to the constellation mapper, such that $\overline{J} = \frac{J}{log_2 M} \in \mathbb{N}$. As before, $\mathbf{b}$ can be either a binary file or a pseudo-random binary sequence, with the addition of an appropriate padding to satisfy the above size condition. Then, we let $\overline{\mathbf{d}} \in \mathcal{A}^{\overline{J}}$ be the data row vector at the output of the constellation mapper, representing the digitally modulated version of $\mathbf{b}$.

Serial to Parallel

The serial to parallel block provides the same functions as its previously described OFDM counterpart. As before, a check on the size of $\overline{\mathbf{d}}$ is performed before the serial to parallel operation. In particular, we note that the precoder $\mathbf{E}$ adopted in the following block

operates on sequences of size L (i.e., $\dim\ker(\tilde{\mathbf{H}}^{\mathrm{d}}_{\mathrm{sp}}) = L$), as detailed in Section 8.1. Then (if $\frac{\overline{J}}{L} \notin \mathbb{N}$), a padding vector of dummy symbols $\mathbf{d}_{\mathrm{p}} \in \mathbb{C}^{L(1+\lfloor\frac{\overline{J}}{L}\rfloor)-\overline{L}}$ is appended to $\overline{\mathbf{d}}$, such that $\mathbf{d} = [\overline{\mathbf{d}}\,\mathbf{d}_{\mathrm{p}}]$. A new padded data row vector of size $\tilde{J} = L(1+\lfloor\frac{\overline{J}}{L}\rfloor)$, is obtained. Naturally, if $\frac{\overline{J}}{L} \in \mathbb{N}$, then $\mathbf{d} = \overline{\mathbf{d}}$ and $\tilde{J} = \overline{J}$. The serial to parallel block transforms the data vector $\mathbf{d}$ into a data matrix $\mathbf{D}^{(\mathrm{C})} \in \mathcal{A}^{L\times\frac{\tilde{J}}{L}}$, by mapping the m^{th} element of $\mathbf{d}$ to $[\mathbf{D}^{(\mathrm{C})}]_{(m-L\lfloor\frac{m}{L}\rfloor,\lfloor\frac{m}{L}\rfloor+1)}$.

Frame Generation and CIA Precoder

This composite block is responsible for the CIA frame generation and linear precoding. Similarly to the OFDM frame generation, the CIA frame includes four parts, namely a preamble $\mathbf{g} \in \mathbb{C}^{N+L}$, a pilot matrix $\mathbf{P}$ detailed in the following, the data matrix $\mathbf{D}^{(\mathrm{C})}$ obtained as input after the serial to parallel conversion and a padding matrix $\mathbf{Z} = \mathbf{0}_{(N+L)\times R_z}$, with $\mathbf{g}$ and $\mathbf{Z}$ obtained as described in Section 8.2.1.

On the other hand, the size of the input symbol vector is smaller for CIA than OFDM, L and N respectively. Thus, the design of the pilot matrix $\mathbf{P}^{(\mathrm{C})}$ for CIA is different if compared to the analogous operation for OFDM described in Section 8.2.1. Specifically, we let $\mathbf{P}^{(\mathrm{C})} \in \mathbb{C}^{L\times R_p^{(\mathrm{C})}}$, (with $R_p^{(\mathrm{C})} \geq L$) be a matrix such that $\mathbf{P}^{(\mathrm{C})}\mathbf{P}^{(\mathrm{C})\mathrm{H}} = \mathbf{I}_L$, i.e., a semi-unitary matrix. In Section 8.2.4 we will see how this choice allows for a simpler channel estimation at CT. In this implementation, we assume that $[\mathbf{P}^{(\mathrm{C})}]_{(l+1,k+1)} = \frac{1}{\sqrt{L}}e^{-i2\pi\frac{lk}{L}}$, with $l = \{0,\ldots,L-1\}$ and $k = \{0,\ldots,R_p^{(\mathrm{C})}-1\}$, semi-unitary by construction. We remark that any other semi-unitary matrix would be equivalently viable.

After generating the aforementioned matrices, the block derives the CIA precoder $\mathbf{E}$. As previously explained, HT operates as an OFDM receiver during the UL phase. In particular, a channel estimation in frequency domain, i.e., $\hat{\mathbf{h}}^{\mathrm{u}}_{\mathrm{ps}} = \hat{\mathbf{h}}^{\mathrm{d}}_{\mathrm{sp}}$, is acquired and stored to be successively fed to the precoder block during the DL phase, as shown in Figure 8.6. The time domain version of $\hat{\mathbf{h}}^{\mathrm{d}}_{\mathrm{sp}} \in \mathbb{C}^{L+1}$, necessary to build the circulant channel matrix $\tilde{\mathbf{H}}^{\mathrm{d}}_{\mathrm{sp}} \in \mathbb{C}^{N\times(N+L)}$ as in (3.1), is then obtained by taking the IDFT of $\hat{\mathbf{h}}^{\mathrm{d}}_{\mathrm{sp}}$, by means of the efficient methods provided by the FFTW library. At this stage, the CIA precoder $\mathbf{E}$ satisfying (3.2) can be derived by computing the SVD of $\tilde{\mathbf{H}}^{\mathrm{d}}_{\mathrm{sp}}$, and selecting its right singular vectors generating $\ker(\tilde{\mathbf{H}}^{\mathrm{d}}_{\mathrm{sp}})$, as detailed in Chapter 3. In practice, this is implemented by the efficient algorithms provided by the portable linear algebra library linear algebra PACKage (LAPACK) [150]. We remark that, differently from Chapter 3, the block providing the frame generation and CIA precoder functions does not adopt any optimal power allocation strategy. Accordingly, a uniform power allocation strategy is adopted as in the OFDM transmitter chain, to simplify the computational burden for the general purpose processor performing the base-band processing.

Finally, the CIA frame is constructed as

$$\mathbf{C} = [\mathbf{g}\ \ \mathbf{E}\mathbf{P}^{(\mathrm{C})}\ \ \mathbf{E}\mathbf{D}^{(\mathrm{C})}\ \ \mathbf{Z}] \in \mathbb{C}^{(N+L)\times(1+R_p^{(\mathrm{C})}+\frac{\tilde{J}}{L}+R_z)}, \tag{8.0}$$

where only the pilot and data matrices are precoded with $\mathbf{E}$. We note that the preamble

g is not precoded in order to preserve its useful properties in the time domain for synchronization purposes. The padding matrix does not need to be precoded, being entirely composed of null entries.

Power Scaling

At this stage, a power scaling may be applied to shape a desired power profile for **C** before the parallel to serial operation. Let $\alpha_g^{(\mathrm{C})}$, $\alpha_p^{(\mathrm{C})}$, $\alpha_d^{(\mathrm{C})} \in \mathbb{R}$ be parameters adopted to scale independently the power of **g**, $\mathbf{EP}^{(\mathrm{C})}$ and $\mathbf{ED}^{(\mathrm{C})}$. Then, the frame obtained at the output of the power scaling block can be written as $\mathbf{C} = [\alpha_g^{(\mathrm{C})}\mathbf{g} \;\; \alpha_p^{(\mathrm{C})}\mathbf{EP}^{(\mathrm{C})} \;\; \alpha_d^{(\mathrm{C})}\mathbf{ED}^{(\mathrm{C})} \;\; \mathbf{Z}]$.

Parallel to Serial

We denote the output of the parallel to serial block as $\mathbf{x} \in \mathbb{C}^{(N+L)(1+R_p^{(\mathrm{C})}+\frac{\tilde{J}}{L}+R_z)}$, serialized version of the stream, ready to be fed to the USRP for the RF modulation. This operation can be written as $\mathbf{x}^{(\mathrm{C})} = \mathrm{vec}\,(\mathbf{C})^{\mathrm{T}}$, with $\mathbf{x}^{(\mathrm{C})}$ being a row vector.

8.2.4 CIA receiver

Consider the block representation in Figure 8.7. The main difference between this scheme

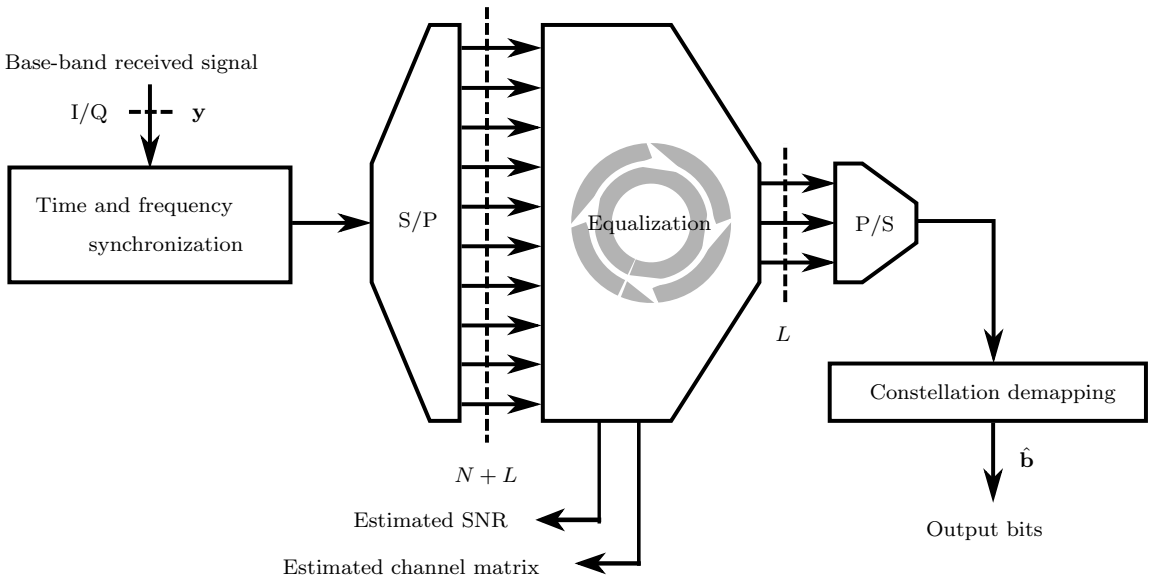

Figure 8.7: CIA receiver chain.

and the one presented for the OFDM receiver implementation in Section 8.2.2 is the absence of the DFT and CP removal blocks. In fact, in the CIA receiver, no CP removal

operation and DFT are required and the received signal can be directly equalized after an appropriate channel estimation. A detailed block-by-block description is provided in the following.

Synchronization

The synchronization block provides the same functions as its previously described OFDM counterpart. Accordingly, time and frequency synchronization operations are performed as described therein. The output of this block is $\hat{\mathbf{x}}^{(\mathrm{C})} \in \mathbb{C}^{(N+L)(1+R_p^{(\mathrm{C})}+\frac{\tilde{J}}{L}+R_z)}$ a synchronized and corrected vector carrying the first $(N+L)(1+R_p^{(\mathrm{C})}+\frac{\tilde{J}}{L}+R_z)$ samples after the $(\hat{t}_f+N)^{th}$ sample of the received vector $\mathbf{y}$.

Serial to Parallel

A serial to parallel conversion is performed on $\hat{\mathbf{x}}^{(\mathrm{C})}$ to prepare the received stream for the channel estimation and equalization. The output of this block is the matrix $\hat{\mathbf{C}} = [\hat{\mathbf{g}}\ \hat{\mathbf{E}}\hat{\mathbf{P}}^{(\mathrm{C})}\ \hat{\mathbf{E}}\hat{\mathbf{D}}^{(\mathrm{C})}\ \hat{\mathbf{Z}}^{(\mathrm{C})}] \in \mathbb{C}^{(N+L)\times(1+R_p^{(\mathrm{C})}+\frac{\tilde{J}}{L}+R_z)}$, such that the m^{th} element of $\hat{\mathbf{x}}^{(\mathrm{C})}$ is mapped to $[\hat{\mathbf{C}}]_{(m-(N+L)\lfloor\frac{m}{N+L}\rfloor,\lfloor\frac{m}{N+L}\rfloor)}$.

Equalizer

In this block a channel estimation and a subsequent equalization are performed, to remove the combined effect of channel and precoder on the received signal. Before the actual equalization, the receiver can exploit the structure of the received noisy frame $\hat{\mathbf{C}}$ to obtain $\widehat{SNR}$, approximate estimation of the average SNR experienced during the reception. Specifically, $\widehat{SNR}$ can be computed by means of (8.2.2) as explained in Section 8.2.2, as the ratio between the energy of the preamble $\mathbf{g}$ and the energy of the AWGN, obtained by evaluating the Frobenius norm of the padding matrix $\hat{\mathbf{Z}}^{(\mathrm{C})}$.

Now, let us rewrite the received frame as

$$\begin{aligned} \hat{\mathbf{C}} &= [\hat{\mathbf{g}}\ \hat{\mathbf{E}}\hat{\mathbf{P}}^{(\mathrm{C})}\ \hat{\mathbf{E}}\hat{\mathbf{D}}^{(\mathrm{C})}\ \hat{\mathbf{Z}}^{(\mathrm{C})}] && (8.1)\\ &= \mathbf{H}_{\mathrm{ss}}^{\mathrm{d}}[\mathbf{g}\ \mathbf{E}\mathbf{P}^{(\mathrm{C})}\ \mathbf{E}\mathbf{D}^{(\mathrm{C})}\ \mathbf{Z}] + \mathbf{W}^{(\mathrm{C})}, && (8.2)\end{aligned}$$

where the channel matrix $\mathbf{H}_{\mathrm{ss}}^{\mathrm{d}}$ has been isolated, for clarity. Note that, in (8.1), the matrix $\mathbf{W}^{(\mathrm{C})} = [\mathbf{g}_W\ \mathbf{E}_W\mathbf{P}_W^{(\mathrm{C})}\ \mathbf{E}_W\mathbf{D}_W^{(\mathrm{C})}\ \mathbf{Z}_W] \in \mathbb{C}^{(N+L)\times(1+R_p^{(\mathrm{C})}+\frac{\tilde{J}}{L}+R_z)}$ collects the overall effect of both the thermal noise and the interference generated by the OFDM transmission, with $\mathbf{g}_W \in \mathbb{C}^{N+L}$, $\mathbf{E}_W \in \mathbb{C}^{(N+L)\times L}$, $\mathbf{P}_W^{(\mathrm{C})} \in \mathbb{C}^{(N+L)\times R_p^{(\mathrm{C})}}$, $\mathbf{D}_W^{(\mathrm{C})} \in \mathbb{C}^{(N+L)\times\frac{\tilde{J}}{L}}$ and $\mathbf{Z}_W \in \mathbb{C}^{(N+L)\times R_z}$.

Now, let us consider an equivalent representation of the channel faced by the pilot and data matrices, given by the contribution of the CIA precoder and the actual channel. Let

$\mathbf{H}^{(\mathrm{C})} = \mathbf{H}_{\mathrm{ss}}^{\mathrm{d}}\mathbf{E} \in \mathbb{C}^{(N+L)\times L}$ be the equivalent channel matrix. Then, an estimation of $\mathbf{H}^{(\mathrm{C})}$ is computed in this block by evaluating the received pilot matrix $\hat{\mathbf{P}}^{(\mathrm{C})}$ to obtain

$$\hat{\mathbf{H}}^{(\mathrm{C})} = (\mathbf{H}^{(\mathrm{C})}\mathbf{P}^{(\mathrm{C})} + \mathbf{P}_W^{(\mathrm{C})})\mathbf{P}^{(\mathrm{C})\mathrm{H}} \tag{8.3}$$

$$= \mathbf{H}^{(\mathrm{C})} + \underbrace{\mathbf{P}_W^{(\mathrm{C})}\mathbf{P}^{(\mathrm{C})\mathrm{H}}}_{\text{interference plus noise}}, \tag{8.4}$$

where the properties of the semi-unitary pilot matrix $\mathbf{P}^{(\mathrm{C})}$ have been exploited. Now, let $\hat{\mathbf{H}}^{(\mathrm{C})} = \mathbf{U}^{(\mathrm{C})}\mathbf{\Sigma}^{(\mathrm{C})}\mathbf{V}^{(\mathrm{C})\mathrm{H}}$ be the SVD of $\hat{\mathbf{H}}^{(\mathrm{C})}$, with $\mathbf{U}^{(\mathrm{C})} \in \mathbb{C}^{(N+L)\times(N+L)}$ and $\mathbf{V} \in \mathbb{C}^{L\times L}$ unitary matrices and $\mathbf{\Sigma} = [\mathbf{\Sigma}^{\sigma}\ \mathbf{\Sigma}^{0}]^{\mathrm{T}}$, with $\mathbf{\Sigma}^{\sigma} = diag(\sigma_1, \ldots, \sigma_L)$ diagonal matrix carrying the L ordered singular vectors of $\hat{\mathbf{H}}^{(\mathrm{C})}$ and $\mathbf{\Sigma}^{0} = \mathbf{0}_{L\times(N-L)}$. We note that as before, this operation is implemented by means of the efficient algorithms provided by the library LAPACK. Then, we can obtain $\hat{\mathbf{H}}_{eq}^{(\mathrm{C})}$, ZF equalizer for the equivalent channel, as

$$\hat{\mathbf{H}}_{eq}^{(\mathrm{C})} = \mathbf{V}^{(\mathrm{C})}\tilde{\Sigma}^{(\mathrm{C})}\mathbf{U}^{(\mathrm{C})\mathrm{H}} \in \mathbb{R}^{L\times(N+L)}, \tag{8.4}$$

with $\tilde{\Sigma}^{(\mathrm{C})} = [diag(\frac{1}{\sigma_1}, \ldots, \frac{1}{\sigma_L})\ \mathbf{\Sigma}^{0}]^{\mathrm{T}}$. The estimated version of data matrix $\mathbf{D}^{(\mathrm{C})}$ after the equalization is computed as

$$\hat{\mathbf{D}}_{eq}^{(\mathrm{C})} = \hat{\mathbf{H}}_{eq}^{(\mathrm{C})}(\hat{\mathbf{H}}^{(\mathrm{C})}\mathbf{D}^{(\mathrm{C})} + \mathbf{W}^{(\mathrm{C})}) \tag{8.5}$$

$$= \mathbf{U}^{(\mathrm{C})}\mathbf{\Sigma}^{(\mathrm{C})}\mathbf{V}^{(\mathrm{C})\mathrm{H}}(\mathbf{V}^{(\mathrm{C})}\tilde{\Sigma}^{(\mathrm{C})}\mathbf{U}^{(\mathrm{C})\mathrm{H}}\mathbf{D}^{(\mathrm{C})} + \mathbf{W}^{(\mathrm{C})}) \tag{8.6}$$

$$= \mathbf{D}^{(\mathrm{C})} + \underbrace{\mathbf{U}^{(\mathrm{C})}\mathbf{\Sigma}^{(\mathrm{C})}\mathbf{V}^{(\mathrm{C})\mathrm{H}}\mathbf{W}^{(\mathrm{C})}}_{\text{interference plus noise}}. \tag{8.7}$$

and this ends the equalization process.

Parallel to Serial

A parallel to serial operation is performed on $\hat{\mathbf{D}}_{eq}^{(\mathrm{C})}$ to yield $\hat{d} = \mathrm{vec}(\hat{\mathbf{D}}_{eq}^{(\mathrm{C})})^{\mathrm{T}} \in \mathbb{C}^{\frac{\tilde{J}}{L}}$, row vector carrying the received version of the digitally modulated symbol vector $\mathbf{d}$, of size $\frac{\tilde{J}}{L}$, ready to be fed to the constellation demapper.

Constellation Demapper

The constellation demapper provides the same functions as its previously described OFDM counterpart. Accordingly, it implements the appropriate function to recover the received bit vector $\hat{\mathbf{b}}$, ending the receiver processing.

8.3 Experimental Results

In this section we describe and discuss the results of the field tests performed to assess the performance of the proposed reconfigurable transceiver. In Figure 8.8, the environment

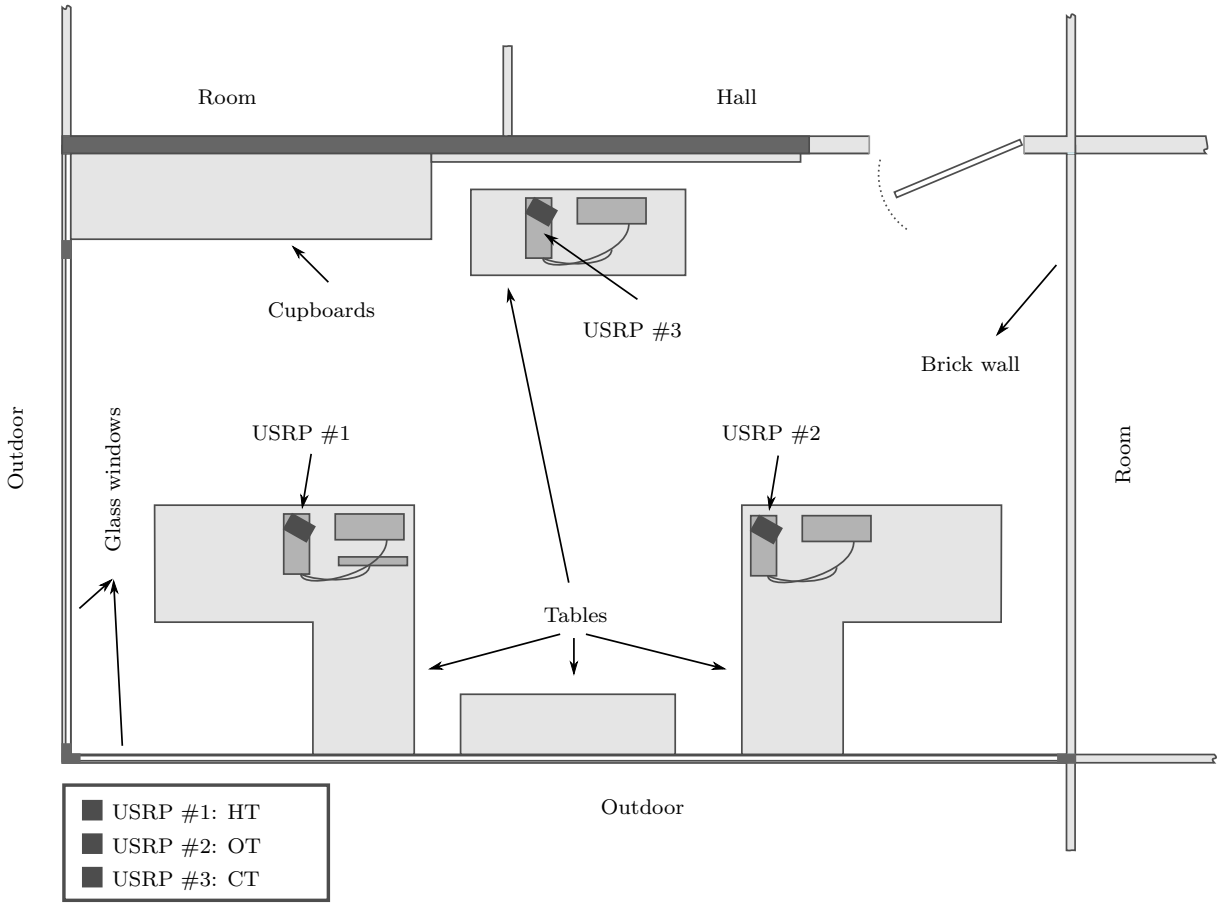

Figure 8.8: Environment hosting the field tests.

hosting the field tests is depicted, whereas the description of the parameters configuration adopted throughout the test is described in Table 8.1.

We note that as seen in Section 8.2.1 and 8.2.3, the preamble size is identical in both OFDM and CIA chains. Then, the first $N + L$ samples of $\mathbf{x}$, serialized version of the sum of the OFDM and CIA streams, i.e., $\mathbf{S}$ and $\mathbf{C}$, are obtained as the weighted sum of the OFDM and CIA preambles, identical by construction, with weights given by the power scaling factors $\alpha_g^{(\mathrm{O})}$ and $\alpha_g^{(\mathrm{C})}$, respectively. Furthermore, we remark that, the effectiveness of the CIA precoder is strictly dependent on the reliability of the channel state information, acquired by HT during the UL phase. In practice, HT must be able to exploit the reciprocity of the UL and DL channels, i.e., $\mathbf{h}_{\mathrm{sp}}^{\mathrm{d}} = \mathbf{h}_{\mathrm{ps}}^{\mathrm{u}}$, inherent to TDD communications. Accordingly, its responsiveness has be to such that UL and DL transmissions are performed within the coherence time of the channel.

	OFDM	**CIA**
Carrier Frequency	ISM 2.422 GHz	ISM 2.422 GHz
Bandwidth	1 MHz	1 MHz
Transmit Power	1-20 mW	1-20 mW
Input Type	binary sequence	binary sequence
M	2 (BPSK)	2 (BPSK)
N	128	-
N_o	48	-
L	16	-
K	48	-
J	-	48
$R_p^{(O)}$	35	-
$R_p^{(C)}$	-	33
R_z	4	4

Table 8.1: User defined parameters for the experimental setup.

8.3.1 Channel Reciprocity

With the following experiment, we test the responsiveness of the transceiver and verify the reciprocity of the UL and DL channels in the considered scenario. Consider the three devices depicted in Figure 8.8. We focus on the primary pair composed by HT and OT. Both devices engage in an OFDM transmission according to the procedure described in Section 8.1, and perform a channel estimation (UL channel for HT and DL channel for OT), obtaining $\hat{\mathbf{h}}_{\mathrm{pp}}^{\mathrm{u}}$ and $\hat{\mathbf{h}}_{\mathrm{pp}}^{\mathrm{d}}$, respectively. Additionally, we let CT operate as an OFDM receiver that decodes the received signal and performs a channel estimation, obtaining $\hat{\mathbf{h}}_{\mathrm{ps}}^{\mathrm{d}}$. We note that in our 1×2 scenario $\mathbf{h}_{\mathrm{pp}}^{\mathrm{d}}$ coincides with $\mathbf{h}_{\mathrm{sp}}^{\mathrm{d}}$, whereas $\mathbf{h}_{\mathrm{ps}}^{\mathrm{d}}$ coincides with $\mathbf{h}_{\mathrm{ss}}^{\mathrm{d}}$, by construction.

Now, some perturbations are generated in the channel between HT and OT, by placing an object between them and changing its position periodically. No action is performed w.r.t. to CT. Furthermore, the position of the three devices and the duration of the experiment, i.e., more than 30 s, have been selected in order to ensure similar values of average SNR at the receiver, thus equivalent conditions at the different devices. To simplify the representation of the results, due to space constraints, we select one subcarrier inside the spectrum, i.e., the 20^{th} occupied subcarrier, and plot the time evolution of its normalized channel gain in Figure 8.9. Remarkably, the time evolution of the channel gain associated to 20^{th} subcarrier for the UL and DL channel between HT and OT is almost identical. We remark that, the negligible differences between the UL and DL channel are due to estimation errors, small differences in the experienced SNR and non-perfectly symmetric characteristics of the RF circuitry in the two USRPs [100]. Conversely, no clear relationship is present between $\hat{\mathbf{h}}_{\mathrm{pp}}^{\mathrm{d}}$ and $\hat{\mathbf{h}}_{\mathrm{ps}}^{\mathrm{d}}$, channel between HT and CT.

The importance of this result is twofold. On the one hand, we verified that the

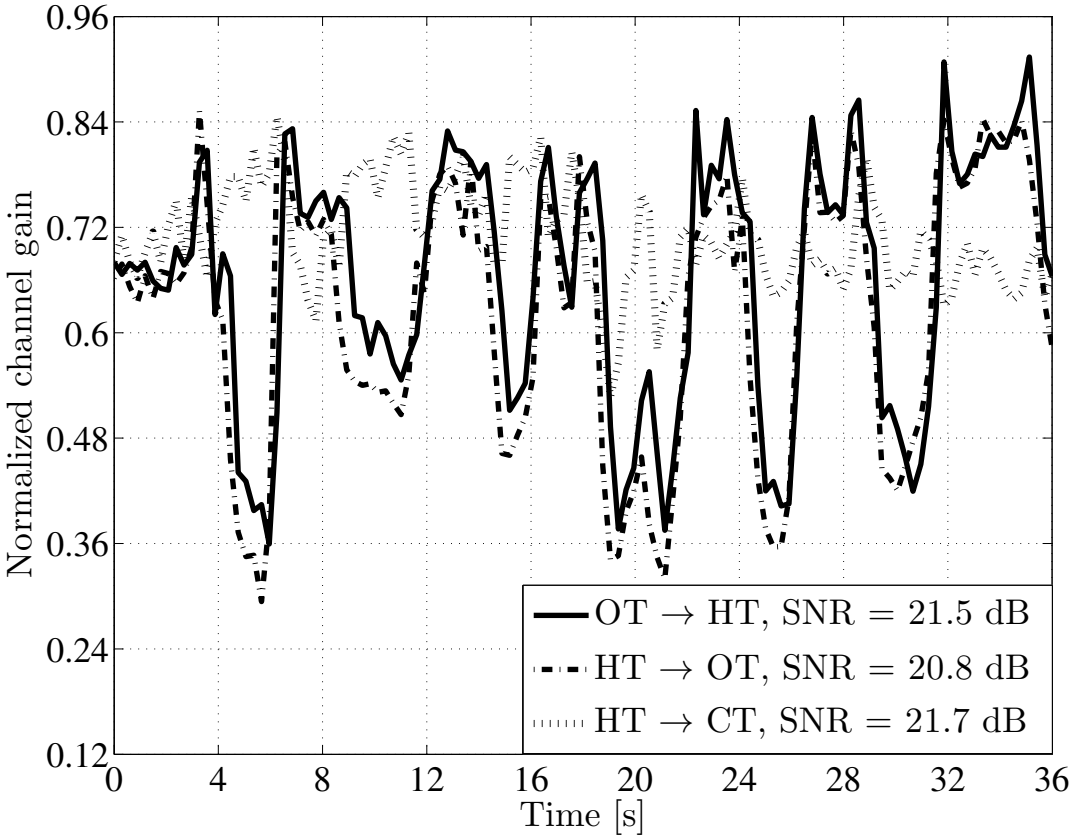

Figure 8.9: Time evolution of the channel gains (20th subcarrier out of the 48 occupied subcarriers).

responsiveness of the proposed transmitter is such that the UL and DL channel reciprocity holds in the considered scenario. On the other hand, the difference between $\hat{\mathbf{h}}^{\mathrm{d}}_{\mathrm{pp}}$ and $\hat{\mathbf{h}}^{\mathrm{d}}_{\mathrm{ps}}$ proves that the CIA precoder $\mathbf{E}$ designed at HT to project to signal onto the null-space precoder of $\mathbf{h}^{\mathrm{d}}_{\mathrm{pp}}$, would not incur interference cancelation effect when facing $\mathbf{h}^{\mathrm{d}}_{\mathrm{ps}}$. We note that this last insight, actively shows the feasibility of the CIA transmission, whose performance will be evaluated in the next section.

8.3.2 Performance Evaluation

So far we described the structure of our tests, and presented a preliminary result to show the responsiveness of the proposed architecture, necessary step before performing the set of complete experiments. Herein, we aim at showing that in a cognitive radio setting, different primary and secondary devices may be effectively implemented adopting the same hardware, i.e., the USRPs, thanks to specific base-band operations and configurations performed at software level. We note that the OFDM and CIA architectures described in

Section 8.2 are not optimized, but are the first step towards more refined architectures, object of future research. As a consequence, due to practical limitations, no meaningful comparison with theoretical results [62, 59] can be established. Accordingly, specific benchmarks for both the OFDM and CIA transmissions are required, to assess the performance of primary and secondary system. We first focus on the OFDM transmission, i.e., the link between HT and OT.

OFDM performance

Let us consider a standalone OFDM transmission performed by HT and OT, according to the parameters in Table 8.1, as if no secondary link were present. We note that a BPSK modulation is adopted for simplicity. We appropriately control the power scaling parameters such that the two devices may vary the transmit power between 1 and 20 mW, for a resulting SNR at the receiving antenna ranging between 10 and 30 dB. Now, let $\mathcal{B}$ be the transmit bandwidth at HT, then we can define T_o, maximum achievable throughput of the OFDM transmission as the maximum number of information bits that HT can transmit per second to OT, given by

$$T_o = \frac{N_o \mathcal{B}}{(N+L)(R_p^{\mathrm{O}} + R_z^{\mathrm{O}} + \frac{\overline{K}}{N_o} + 1)}, \tag{8.7}$$

that, according to the parameters in Table 8.1, corresponds to 8.13 kbps. We first compute the experimental throughput of the aforementioned standalone OFDM transmission, in order to obtain a specific benchmark to evaluate the performance of the primary transmission, when coexisting with the secondary CIA transmission. Subsequently, the CIA frame will be generated and added to the transmit signal at HT to evaluate its impact on the experimental throughput of the primary transmission. Concerning the CIA frame, we want to characterize the effectiveness of $\mathbf{E}$ as mean to reduce (if not null) the interference generated by the secondary transmission towards OT. Thus, we test two different channel realizations to obtain the null-space precoder $\mathbf{E}$, namely the estimation of $\hat{\mathbf{h}}_{\mathrm{sp}}^{\mathrm{d}}$ performed by HT and a Rayleigh fading random channel, generated according to the model described in Section 3.1. The rationale for this is that if the precoder built upon $\hat{\mathbf{h}}_{\mathrm{sp}}^{\mathrm{d}}$ were not more effective than a randomly generated null-space precoder, then CIA would lose its attractiveness, and there would be no use in further pursuing the development. The three so-obtained throughput curves are depicted in Figure 8.10. As previously said, our system is not optimized, thus an analysis on the quantitative results is not extremely significant. Despite this fact, we notice that for SNR$>$ 20 dB the throughput of the OFDM transmission is already very close to T_o. Conversely, a direct comparison between the three curves provides the qualitative insights we need to assess the effectiveness of CIA. We note that the throughput loss experienced by the OFDM transmission when coexisting with the CIA transmission diminishes as the SNR increases if $\mathbf{E}$ is built upon $\hat{\mathbf{h}}_{\mathrm{sp}}^{\mathrm{d}}$, whereas it increases with the SNR if $\mathbf{E}$ is computed using the random channel realization. In particular, in the latter case, the throughput is clearly interference limited. Despite the imperfections due to the non-optimized practical implementation, these findings show

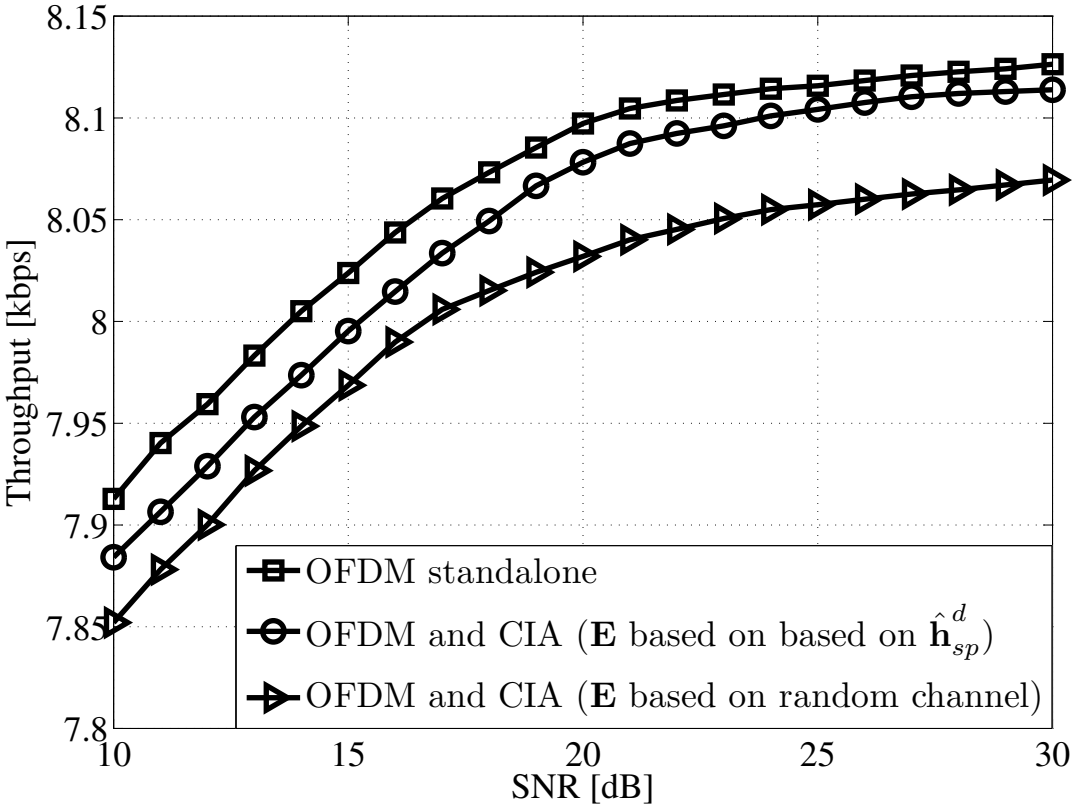

Figure 8.10: Throughput of the primary transmission at OT for both standalone CIA and hybrid (OFDM and CIA) transmissions.

the effectiveness of the CIA precoder built upon the actual channel estimation, as a mean to protect the primary receiver from undesired interference.

We now perform a last test w.r.t. the primary transmission and activate only the CIA transmitter chain at HT and switch our focus on the received power at OT after the CP removal operation and DFT. With this experiment, we aim at measuring the actual residual interference experienced by OT, to better characterize the previous results. Now, let $\mathbf{M} = \mathbf{QFB}(\mathbf{H}_{\text{pp}}^{\text{d}}\mathbf{ED}^{(\text{C})} + \mathbf{W}) \in \mathbb{C}^{N_o \times \frac{J}{L}}$ be the residual interference plus noise component at OT after the CP removal operation and DFT, with $\mathbf{W} \in \mathbb{C}^{N_o \times \frac{J}{L}}$ matrix collecting the effect of the thermal noise. Now, let us introduce a metric called interference plus noise to noise ratio (INNR), as the ratio between the energy of the interference plus thermal noise component and the energy of the thermal noise, given by

$$\text{INNR} = 10\log_{10}\left(\frac{\text{tr}\left(\mathbf{M}\mathbf{M}^{\text{H}}\right)}{\text{tr}\left(\hat{\mathbf{Z}}^{(\text{O})}\hat{\mathbf{Z}}^{(\text{O})\text{H}}\right)}\right), \tag{8.7}$$

with $\hat{\mathbf{Z}}^{(\text{O})}$ as defined in Section 8.2.2. Note that, herein $\mathbf{E}$ is derived according to the two aforementioned strategies, i.e., first the precoder is built upon the actual channel

estimation then upon a random channel realization. As shown in Figure 8.11, the INNR

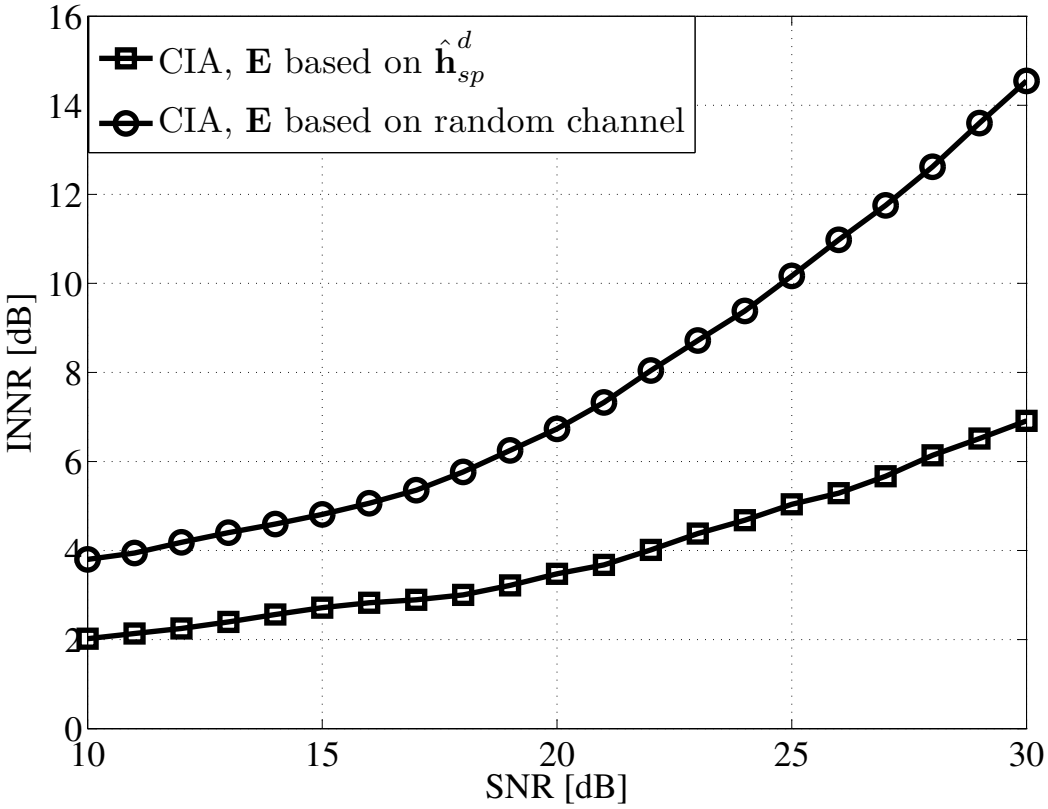

Figure 8.11: Residual interference at OT.

for the randomly derived **E** is significantly higher than the result for the actual CIA precoder, with the former inducing a residual interference to OT almost 50% larger than the latter for SNR= 10 dB and 500% for SNR= 30 dB. These findings confirm the previous results. On the other hand, we note that the INNR for the actual CIA precoder can reach up to 7 dB at high SNR. This shows the non-negligible impact of the hardware imperfections on the quality of the $\hat{\mathbf{h}}_{\mathrm{sp}}^{\mathrm{d}}$ channel estimation, even for very favorable SNR values, i.e., SNR> 20 dB.

CIA decoding

As a final test, we focus on the link between HT and CT to evaluate the performance of the secondary transmission. We first perform a standalone CIA transmission using a previously built **E**, upon one of the many $\hat{\mathbf{h}}_{\mathrm{sp}}^{\mathrm{d}}$ estimations, according to the parameters in Table 8.1. As before, we can define T_c, maximum throughput of the CIA transmission as the maximum number of information bits that HT can transmit per second to CT, given

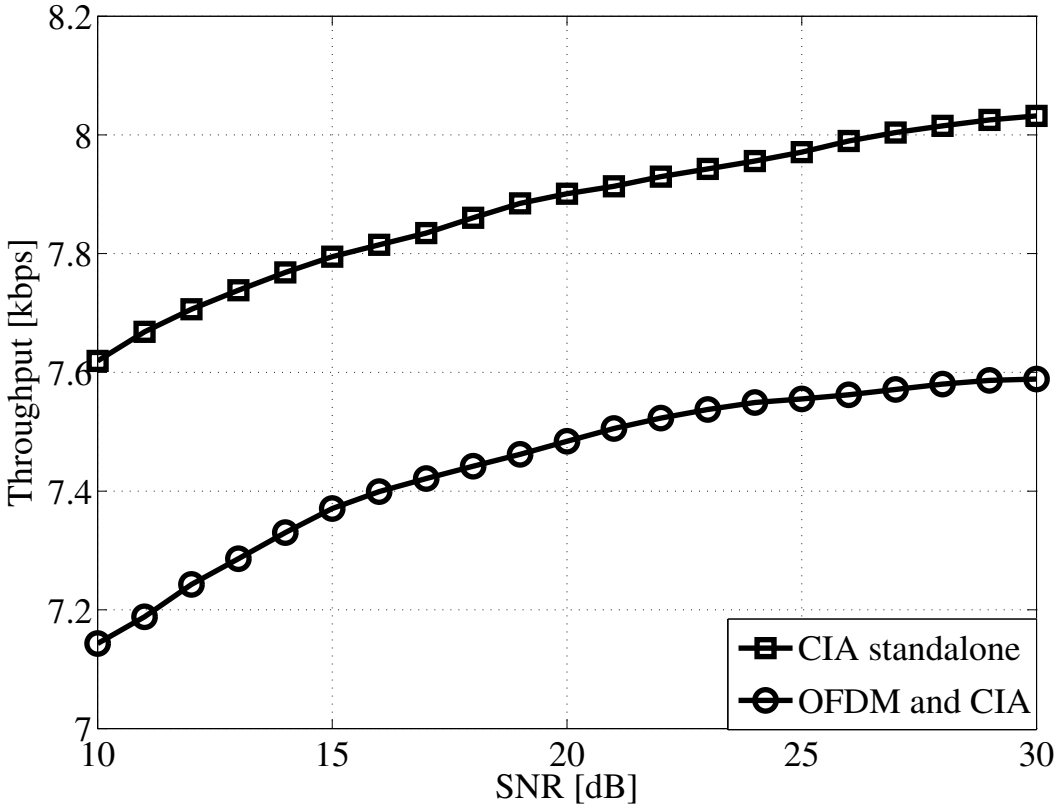

Figure 8.12: Throughput of the secondary transmission at CT for both standalone CIA and hybrid (OFDM and CIA) transmissions.

by

$$T_c = \frac{J\mathcal{B}}{(N+L)(R_p^{\mathrm{C}} + R_z^{\mathrm{C}} + \frac{\overline{J}}{J} + 1)}, \tag{8.7}$$

whose value is identical to the previous case, i.e., 8.13 kbps, due to the identical size of the OFDM and CIA frame by construction. The impact of the primary transmission on the experimental throughput at CT is evaluated by activating the OFDM transmitter chain at HT, whose transmitted signal is, as before, the serialized version of the sum of the CIA and OFDM frame. The results of this test are provided in Figure 8.12. The throughput of the secondary transmission is lower than the performance of the primary system, even though the difference is not large due to the adopted low modulation order, i.e., BPSK. This is due to the presence of the OFDM transmission causing the interference limited performance of the secondary system. Once again the performance loss of around 5% is mitigated by the adopted low modulation order, but its trend is evident throughout the whole range of experienced SNR.

These results show the effectiveness and feasibility of the hybrid approach proposed in Chapter 7. From a quantitative point of view, additional throughput is achievable for a

HT adopting a hybrid transmission based on OFDM and CIA w.r.t. a standalone OFDM transmission, as can be seen by comparing the results in 8.10 and 8.12 with T_o. This is possible thanks to the shielding effect provided by CIA, that effectively mitigates the interference generated by the secondary transmission to the primary OFDM transmission. These findings confirm the promising outcomes of the previously performed theoretical and numerical analysis, further motivating the study of new flexible architectures for reconfigurable transceivers for next generation two-tiered networks.

Part IV

Conclusions, Perspectives and Appendices

Chapter 9

Conclusions and Future Directions

Future cellular networks are expected to provide ubiquitous broadband access to a large number of mobile users, and satisfy the ever-growing user data demand [1]. Accordingly, the capacity of the already stressed existing 3G networks will not be able to accommodate the explosion in mobile data demands created by new-generation wireless devices. Recent academic and industry trends are pointing towards the adoption of a new network planning approach that could break away from the traditional cellular structure, to enable future wireless networks to sustain users' data demand. In this novel paradigm, a second tier of densely deployed SBSs is required to coexist with a pre-existing first tier populated by legacy MBSs, in the same band, yielding two-tiered networks capable of delivering the expected capacity increase for the future of wireless communications.

This thesis aimed at studying the coexistence problem arising in such networks due to the co-channel deployment of the two tiers. In fact, solutions to allow the two tiers to operate side-by-side in a spectrum sharing fashion must be identified, in order to experience the expected capacity gains. Specifically, we focused on the downlink of a two-tiered network where a first tier composed of an OFDM MBS is underlaid by a second tier populated by densely deployed SBSs, in compliance with what is proposed by many recent standards, e.g., LTE/LTE-A. On the one hand, the co-channel deployment guarantees the most efficient spectrum usage, potentially increasing the spectral efficiency. On the other hand, very large levels of co- and cross-tier interference may arise in such scenarios. A significant spectral efficiency reduction could be experienced, if appropriate mechanism is adopted to mitigate this interference.

The nature of the OFDM transmission and the absence of cooperation between the two tiers disqualify traditional cooperative approaches to interference cancelation/mitigation in multi-cellular networks, e.g., coordinated beamforming, joint signal processing, interference alignment, just to name a few. Furthermore, if the SBSs do not dispose of genie-provided informations about the transmission performed by the MBS, e.g., power allocation at the transmitter, spectrum holes, presence of multiple antennas at the MUEs

and so on, no degrees of freedom are available for the SBSs in the time, frequency or spatial domain. Accordingly, the implementation of state-of-the-art opportunistic versions of the aforementioned interference avoidance techniques is not possible in the second tier as well.

This thesis started from these observations to provide effective solutions for co- and cross-tier interference cancelation/mitigation in two-tiered networks that do not rely on cooperation between the two tiers, or genie-provided informations. The flexibility of the proposed techniques has been assessed by showing how they can be applied to different cases, depending on the underlying network layout. Practical insights concerning real-life implementations of said approaches have been discussed, identifying the main limitations and open problems. This allowed the design of a proof-of-concept demonstrator that concluded the thesis and proved the effectiveness of the proposed approach in a simplified scenario, providing the basis for future extensions of this work.

9.1 Conclusions

Herein, we summarize the contributions and conclusions of this work, according to the overall structure of the thesis. As a consequence, the remainder of the section is divided into three parts, for the sake of clarity.

9.2 Single Small-cell

In this part, we focused on a simplified two-tiered network, in which an OFDM MBS coexists with one SBS/SUE pair. We started from the design and implementation of a test-bed to study the feasibility of the state-of-the-art technique for such scenario, i.e., VFDM [56], and discuss the issues and problems affecting this approach. We considered the secondary link and performed the transmission of a known file by means of the VFDM-based precoding, confirming its feasibility for several values of the average SNR per symbol at the receiver. This metric could be computed by the receiver by evaluating a known preamble, added to the VFDM frame for synchronization and SNR estimation purposes. On the other hand, the estimation of the average SNR per received symbol showed inconsistency with the resulting BER at the receiver, due to the severe PAPR affecting the VFDM signal. In particular, a significant detriment of the achieved practical BER w.r.t. the theoretical results provided in [56] was evident. Accordingly, the performed tests showed that the estimation of the average SNR of the preamble cannot be used to have a reliable estimation of the average SNR of the VFDM payload, and correctly assess the performance of the transmission.

A more general approach to solve the interference cancelation problem in the second tier has been adopted, to better characterize the structure of the precoded signal. Accordingly, a thorough analysis of the structure of a general null-space precoder to null the

cross-tier interference generated by a secondary transmitter towards a primary receiver has been carried out. In particular, we assumed to precode a given input symbol vector with a null-space precoder built upon interference channels characterized by different R.M.S delay spread and PDP profiles. A comparison of the resulting transmitted and received signals in such scenarios has been performed, and a strong connection between the R.M.S delay spread (and PDP profile) of the interference channel and the power profile of the corresponding transmitted and received signals has been identified. The obtained results confirmed the impact of a less time dispersive channel on the power profile of the null-space precoded signal, i.e., the shorter the channel the more the power of the precoded signal is concentrated inside a portion of the signal whose length is equal to the CP size, yielding a larger PAPR.

In order to minimize the spectral efficiency loss caused by this issue, a structural change in the signal model of the considered scenario has been proposed. Accordingly, a technique called CIA has been designed and the optimal precoder structure to maximize the spectral efficiency of the secondary link has been derived and tested for several channel models. Similarly to VFDM, this technique preserves the degrees of freedom of the legacy transmission[1], while providing additional transmit dimensions to the opportunistic SBS (upper bounded by the dimension of the kernel of the cross-tier interference channel matrix). We have shown that, for uniform PDP channels, the performance of the CIA and VFDM root-based precoder coincide, providing the optimal performance. For exponentially decaying PDP channels, CIA precoder shows a higher consistency w.r.t. the other considered approaches, outperforming both VFDM root-based and non optimally designed precoders. Nevertheless, the spectral efficiency of the secondary link highly hinges on the R.M.S. delay spread and PDP of the channel, and a greater frequency selectivity is preferable in terms of performance for CIA. Finally, a comparison between the achievable spectral efficiency in case of legacy receiver architecture and an alternative scheme not including the CP removal step has provided, confirming the previous findings. In particular, in the latter case the spectral efficiency loss for the secondary transmission when facing shorter channels is significantly reduced (if compared to the theoretical result obtained for channels characterized by uniform PDP), and the shorter the channel the lower is the IBI affecting the first part of the CIA symbol[2].

9.3 Multiple Small-cells

In this part, we started from the insights drawn for the single small-cell case, and considered a more complex network layout, where an OFDMA MBS serving a group of MUEs is underlaid by densely deployed SBSs cognitive SBSs serving one SUE each. The nature of the ICI in such a scenario is twofold. In fact, each standalone base station operating in these networks generates co-tier interference towards receivers belonging to the same tier, and cross-tier interference towards receivers belonging to a different tier. We have

[1] In case of perfect CSIT.

[2] We recall that the CP removal step eliminates the IBI by construction.

shown that the interference avoidance technique presented for the single small-cell case can be seamlessly extended in case of multiple MUEs hosted in the first tier, thanks to a distributed design of an appropriate cross-tier interference nulling precoder at the SBSs. On the other hand, the co-tier interference management task in the second tier can be addressed by means of either a centralized or a distributed approach. We first studied the former case.

In the centralized case, we assumed the presence of an infinite-capacity backhaul connecting all the SBSs in the second tier, realizing a network MIMO system, making a potentially interference limited system become a MIMO-BC. Several linear precoding techniques involving cooperation between transmitters have been taken into account. The inherent dimensionality constraint faced by the SBSs to mitigate the co-tier interference, due to the structure of the problem, has been identified. The search for a suitable scheme brought us to the proposed flexible cascaded precoder approach, i.e., a combination of an inner precoder to cancel the cross-tier interference and an outer precoder to mitigate the co-tier interference.

Furthermore, we have shown that increasing the number of transmit dimensions, while keeping the receiver layout, is a viable way to design a second tier that overcomes the aforementioned dimensionality constraints and achieves relevant performance in terms of sum-rate. Such a configuration can be obtained either by extra antenna installation, denser SBS deployment or a flexible combination of both. A comparison with state-of-the-art techniques has shown a consistent advantage of the proposed technique for a large range of SNR values and perfect CSIT in the second tier. This reinforced our previous findings and confirmed the effectiveness of the proposed approach to deploy SBSs and MBS coexisting inside the same coverage area, sharing the same band.

From a practical perspective, many of the assumptions made in the centralized case may lead to results that are hardly reproducible in real-life scenarios. Accordingly, we discussed some critical issues affecting this approach, providing insights to better characterize its implementability. First we studied the importance of the perfect CSIT assumption for the correct design of the cascaded precoder, we have studied the performance of the two-tiered network in case of imperfect CSIT in the second tier. Accordingly, a rate loss experienced by both systems has been shown for this case, due to the imperfectly devised precoder. The best compromise between training and transmission time has been investigated, for various SNR values, as well as the best performing strategy to deploy a dense network for the imperfect CSIT case. The comparison with state-of-the-art techniques has been provided for the imperfect CSIT case as well, yielding results qualitatively similar to the previously analyzed perfect CSIT case. Afterwards, we considered other critical problems that may affect or prevent the implementation of the centralized solution in real-life scenario. Accordingly, we discussed about issues such as the perfect synchronization of the SBSs in the second tier, the possible absence or limited performance of a backhaul among the SBSs, the impact of the dimensionality constraint on the structure of the second tier, the difficulty faced by the cell-edge SBSs to cancel the interference generated towards MUEs belonging to different macro-cells and the problems that the SBSs may face to design the cascaded precoder in case of SUEs and MUEs characterized by different

mobility patterns and profiles.

To conclude this part, a distributed solution to the co-tier interference management problem has been provided, to address some of the most critical issues affecting the centralized solution. Specifically, a completely self-organizing approach has been proposed to mitigate the co-tier interference in the second tier by means of an appropriate input signal subspace reduction at the autonomous SBSs. The optimal precoder that maximizes the spectral efficiency of the link connecting each SBS to its served SUE has been found through a distributed one-shot strategy. Our numerical findings showed significant spectral efficiency improvements with respect to legacy TDMA/FDMA approaches as the number of self-organizing SBSs in the second tier increases. Remarkably, the design of the resulting linear cascaded precoder only requires that each SBS is aware of the number of SUEs inside its coverage area, and disposes of a perfect local CSI w.r.t. the link towards the served SUEs and the MUEs reached by its transmission. The distributed solution exhibited consistent robustness against channel estimation errors, yielding promising spectral efficiency results. Finally, the percent increase in spectral efficiency that a two-tiered network deployed by means of the proposed approach experiences w.r.t an OFDMA-based single tier network has been evaluated, accounting for the presence of channel estimation errors in the second tier. Performance enhancements brought by the two-tiered structure over the single tier layout are evident at any SNR regime, despite the non-negligible cross-tier interference generated by the MBS towards the devices in the second tier.

9.4 Applications and Implementations

In this part, we took a step back and we considered a simpler single transmitter downlink scenario, given by an OFDM FBS communicating with two user equipments. We specifically aimed at demonstrating the flexibility of CIA, whose applicability is not necessarily limited to CR settings. Accordingly, a green approach to recycle unused resources of the legacy OFDM transmission has been proposed, with the goal to increase the spectral efficiency of the FBS while maintaining the same total transmit power, thus increasing the energy efficiency as well. In order to achieve this result, we modeled the considered scenario as a virtual two-tiered network, and proposed a hybrid approach to the FBS design by means of CIA. Thanks to this approach, the OFDM transmission does not suffer from undesired interference if perfect CSIT is available, and two critical issues of CIA are solved. In fact, by means of the hybrid scheme, perfect synchronization of the OFDM and CIA signals at the MUE is always guaranteed (regardless of the channel between the FBS and the MUE), and the necessary CSIT to design the CIA precoder is always available at the FBS without the need of a special adaptive channel estimation procedures. On the other hand, the sharing of a channel for both intended and interfering messages generates a strong unavoidable interference on the SUE, due to the simultaneous transmission of the OFDM primary and CIA secondary signals. However, we showed that the SUE is able to cope with this problem by adopting a suitable MMSE linear equalizer that provides an effective decoding of the CIA signal. Simulation results demonstrated that, if a suitable

power allocation strategy is adopted at the FBS (i.e., the total budget is split among the OFDM and CIA signals appropriately), non-negligible energy efficiency gains are possible for uniform and exponential PDP channels, due to the CIA contribution. In particular, we showed how the optimal performance for the hybrid scheme when the power budget is split in favor of the OFDM transmission, since it carries more information than CIA.

Subsequently, we proposed an SDR approach for the design of a reconfigurable transceiver for interference management in CR networks, to be adopted to implement the aforementioned hybrid scheme, and demonstrate the practical feasibility of a CIA-based transmission. The proposed architecture permits the implementation of transceivers adopting several physical layer technologies, i.e., OFDM, CIA or a flexible combination of both. The SDR framework adopted to implement the primary and secondary radios is composed by the GNU Radio toolkit and a set of single antenna USRPs. Accordingly, the base-band operations are performed at software level, whereas the actual transmissions are done by means of the USRPs' hardware RF. Field tests were performed to validate the proposed transceiver design, an demonstrate the feasibility of the hybrid OFDM/CIA scheme. We first verified that all necessary conditions for CIA were fulfilled (reciprocity, channel estimation and others). Then, the performance of the primary and secondary links has been studied under an interference cancelation constraint for the secondary CIA transmission (as done throughout the whole thesis). Accordingly, we have analyzed the residual interference generated by the secondary CIA transmission over the primary. We have shown that CIA does indeed provide interference shielding with respect to a deliberately wrong precoder, and that not only an actual CIA implementation makes sense, but it achieves a non-negligible performance as a secondary system.

9.5 Future Directions

The studies presented within this thesis offer several possible scopes for future directions of the work. Some of theses directions are:

- **PAPR.** We have seen that the signal obtained at each SBS by means of the CIA precoding is plagued by high PAPR, regardless of the PDP and R.M.S. delay spread of the interference channel used to build the precoder. On the other hand, when dealing with very short channels, the CIA signal carries the largest portion of its power in the first symbols of each block, reducing the effectiveness of the transmission in terms of spectral efficiency. Accordingly, the study of suitable ad-hoc techniques to mitigate this effect may increase the spectral efficiency of the CIA transmission, thus the performance of the two-tiered network.

- **Centralized co-tier interference management.** The analysis of the performance of the centralized approach proposed in Chapter 4, under limited backhaul capacity assumption, could be matter of future research, along with the impact of a partial cooperation between the SBSs. In fact, if a backhaul were present in

the second tier, different and more practically implementable ways to manage the co-tier interference, while guaranteeing the cross-tier interference cancelation, could be found by moving from a fully coordinated to a clustered network MIMO scenario.

- **Distributed co-tier interference management.** The study in Chapter 6 is the first step towards the characterization of the performance of a two-tiered network, with second tier composed of self-organizing SBSs, where the self-organization is realized at physical layer (i.e., without requiring signaling or cooperation between the SBSs). Accordingly, the extension of this solution to cellular layouts including structured SBSs' positioning and practical channel models (i.e., distance dependent path-loss, shadow fading and so on) could be matter of future research, to better assess the impact of real-life signal propagation effects on the performance of the proposed technique.

- **System level aspects.** In order to propose a working system level deployment strategy for OFDM-based two-tiered networks, adopting the techniques proposed in this work, a further analysis of the critical issues discussed in Chapter 5 is needed. Some examples of these are: What could be the performance of the proposed approaches when multiple OFDM MBS populate the first tier?What could be the limitations that the cell-edge SBSs would suffer, to be able to operate along with the MBSs in the first tier, while guaranteeing an effective cross-tier interference cancelation?What are the constraints in terms of mobility patterns and profiles of MUEs and SUEs to ensure the feasibility of both the centralized and distributed solutions?We note that, some of the answers to these questions may not be valid in general terms, but rather depend on the peculiar configuration of the given two-tiered network layout.

- **Synchronization.** Despite the discussion provided in Chapter 5, the impact of the transmission of imperfectly synchronized SBSs, adopting the centralized strategy proposed in Chapter 4, on the performance of the two-tiered network, remains an open problem. An analysis of the practical algorithms proposed in the literature for this task would allow a better characterization of the practical constraints and limitations of the centralized approach. If unsatisfactory results were achieved, the study of new solutions to ensure the feasibility of the proposed approach could be necessary. Note that, even though simpler and less demanding in terms of synchronization requirements, the distributed solution proposed in Chapter 6 for self-organizing SBSs' deployments still relies on perfect synchronization of primary and secondary signals at each MUE, to guarantee the absence of cross-tier interference. The impact of a wrong synchronization of the two signals on the performance of the MUEs, when the SBSs in the second tier operate according to the distributed solution, should be assessed in a continuation of this work as well.

- **Hybrid transmitter scheme.** A deeper analysis of the nature of the contributions from OFDM and CIA transmissions to the performance of the hybrid transmitter is needed to assess its flexibility. This could lead to more flexible power splitting

strategies, depending both on the surrounding environment and the scope of the hybrid transmission, to achieve specific target performance for the transmission. Additionally, a study of the performance of the hybrid scheme in more realistic scenarios would be a logical step to characterize the feasibility of its practical implementations. Accordingly, the impact of channel estimation errors at the transmitter and the limitations of the proposed approach in case of multi-FBS network layouts (if any) should be considered.

- **Reconfigurable transceiver.** In a continuation of this work, the study of suitable software improvements and the optimization of the proposed reconfigurable transceiver architecture may lead to significant performance improvements for the hybrid transmitter scheme. Furthermore, an analysis of the performance when perfect synchronization of primary and secondary signals at the MUE is not ensured, i.e., a complete 2×2 scenario implemented by means of the reconfigurable transceiver, could be carried out. If the outcome of the aforementioned analysis were not satisfying, the consequent study of alternative solutions, to guarantee the synchronization of the received signals at the MUE, would be necessary.

- **Uplink.** The focus of this work has been on the downlink of OFDM-based two-tiered networks. Nevertheless, if we consider the complete full duplex scenario, the study of the problems related to the uplink is necessary to fully characterize the communications in such networks. Accordingly, solutions for the SUEs to guarantee interference-free uplink communications in the first tier, and mitigate the multi-user uplink interference in the second tier, have to be found to ensure the feasibility of uplink communications in such two-tiered networks.

Appendix A

Null-space precoder structure

A.1 Two-path channels

Consider a channel with two paths, including the LOS, i.e., $l = 1$, i.e., $\mathbf{h}_{\mathrm{p}} = [h_{\mathrm{p},0}, h_{\mathrm{p},1}]$ and $\mathbf{h}_{\mathrm{s}} = [h_{\mathrm{s},0}, h_{\mathrm{s},1}]$. We focus on the channel matrix representing the link between TX2 and the receiver in the tier "a", and obtain

$$\mathbf{H}_{\mathrm{a}} = \begin{bmatrix} h_{\mathrm{a},1} & h_{\mathrm{a},0} & 0 & 0 & 0 & 0 & \dots & 0 \\ 0 & h_{\mathrm{a},1} & h_{\mathrm{a},0} & 0 & 0 & 0 & \dots & 0 \\ 0 & 0 & h_{\mathrm{a},1} & h_{\mathrm{a},0} & 0 & 0 & \dots & 0 \\ 0 & 0 & 0 & h_{\mathrm{a},1} & h_{\mathrm{a},0} & 0 & \dots & 0 \\ 0 & 0 & 0 & 0 & h_{\mathrm{a},1} & h_{\mathrm{a},0} & \dots & 0 \\ \vdots & \ddots & & & & & \ddots & \vdots \\ 0 & 0 & 0 & 0 & \dots & 0 & h_{\mathrm{a},1} & h_{\mathrm{a},0} \end{bmatrix}.$$

In the following we proceed to the explicit computation of the null-space precoder columns, for several values of $L > l$ providing $L - l$ precoding columns each. Note that, $N = 4$ for simplicity if not otherwise stated.

A.1.1 $L = l + 1$

In this case the precoder is given by

$$\mathbf{v}_1 = \left[w_1, -c_{41} \left(\frac{h_{\mathrm{p},0}}{h_{\mathrm{p},1}}\right)^3, c_{41} \left(\frac{h_{\mathrm{p},0}}{h_{\mathrm{p},1}}\right)^2, -c_{41} \left(\frac{h_{\mathrm{p},0}}{h_{\mathrm{p},1}}\right), c_{41}, -c_{41} \left(\frac{h_{\mathrm{p},1}}{h_{\mathrm{p},0}}\right) \right]^{\mathrm{T}}$$

$$\mathbf{v}_2 = \left[t_1, c_{42} \left(\frac{h_{\mathrm{p},0}}{h_{\mathrm{p},1}}\right)^3, c_{42} \left(\frac{h_{\mathrm{p},0}}{h_{\mathrm{p},1}}\right)^2, -c_{42} \left(\frac{h_{\mathrm{p},0}}{h_{\mathrm{p},1}}\right), c_{42}, -c_{42} \left(\frac{h_{\mathrm{p},1}}{h_{\mathrm{p},0}}\right) \right]^{\mathrm{T}},$$

where w_i,$t_i \in \mathbb{C}$, for all $i \in \mathbb{N}$. Its orthonormalized version is given by

$$\mathbf{e}_1 = \frac{1}{\sqrt{D_1}}\left[w_1, -c_{41}\left(\frac{h_{\mathrm{p},0}}{h_{\mathrm{p},1}}\right)^3, c_{41}\left(\frac{h_{\mathrm{p},0}}{h_{\mathrm{p},1}}\right)^2, -c_{41}\left(\frac{h_{\mathrm{p},0}}{h_{\mathrm{p},1}}\right), c_{41}, -c_{41}\left(\frac{h_{\mathrm{p},1}}{h_{\mathrm{p},0}}\right)\right]^{\mathrm{T}}$$

$$\mathbf{e}_2 = \frac{1}{\sqrt{D_3}}\left[t_1 - \frac{D_2 w_1}{D_1}, \left(\frac{h_{\mathrm{p},0}}{h_{\mathrm{p},1}}\right)^3\left(\frac{c_{41}D_2}{D_1} - c_{42}\right), \left(\frac{h_{\mathrm{p},0}}{h_{\mathrm{p},1}}\right)^2\left(c_{42} - \frac{c_{41}D_2}{D_1}\right), \right.$$
$$\left.\left(\frac{h_{\mathrm{p},0}}{h_{\mathrm{p},1}}\right)\left(\frac{c_{41}D_2}{D_1} - c_{42}\right), c_{42} - \frac{c_{41}D_2}{D_1}, \left(\frac{h_{\mathrm{p},1}}{h_{\mathrm{p},0}}\right)\left(\frac{c_{41}D_2}{D_1} - c_{42}\right)\right]^{\mathrm{T}}$$

with

$$D_1 = |w_1|^2 + |c_{41}|^2\left[\left|\frac{h_{\mathrm{p},0}}{h_{\mathrm{p},1}}\right|^6 + \left|\frac{h_{\mathrm{p},0}}{h_{\mathrm{p},1}}\right|^4 + \left|\frac{h_{\mathrm{p},0}}{h_{\mathrm{p},1}}\right|^2 + \left|\frac{h_{\mathrm{p},0}}{h_{\mathrm{p},1}}\right|^{-2} + 1\right]$$

$$D_2 = t_1 w_1^* + c_{42}c_{41}^*\left[\left|\frac{h_{\mathrm{p},0}}{h_{\mathrm{p},1}}\right|^6 + \left|\frac{h_{\mathrm{p},0}}{h_{\mathrm{p},1}}\right|^4 + \left|\frac{h_{\mathrm{p},0}}{h_{\mathrm{p},1}}\right|^2 + \left|\frac{h_{\mathrm{p},0}}{h_{\mathrm{p},1}}\right|^{-2} + 1\right]$$

$$D_3 = \left|t_1 - \frac{D_2 w_1}{D_1}\right|^2 + \left|\left(\frac{c_{41}D_2}{D_1} - c_{42}\right)\right|^2\left[\left|\frac{h_{\mathrm{p},0}}{h_{\mathrm{p},1}}\right|^6 + \left|\frac{h_{\mathrm{p},0}}{h_{\mathrm{p},1}}\right|^4 + \left|\frac{h_{\mathrm{p},0}}{h_{\mathrm{p},1}}\right|^2 + \left|\frac{h_{\mathrm{p},1}}{h_{\mathrm{p},0}}\right|^{-2} + 1\right]$$

A.1.2 $L = l + 2$

In this case, the precoder $\mathbf{V}$ is given by

$$\mathbf{v}_1 = \left[w_1, w_2, -c_{41}\left(\frac{h_{\mathrm{p},0}}{h_{\mathrm{p},1}}\right)^3, c_{41}\left(\frac{h_{\mathrm{p},0}}{h_{\mathrm{p},1}}\right)^2, -c_{41}\left(\frac{h_{\mathrm{p},0}}{h_{\mathrm{p},1}}\right), c_{41}, -c_{41}\left(\frac{h_{\mathrm{p},1}}{h_{\mathrm{p},0}}\right)\right]^{\mathrm{T}}$$

$$\mathbf{v}_2 = \left[t_1, t_2, -c_{42}\left(\frac{h_{\mathrm{p},0}}{h_{\mathrm{p},1}}\right)^3, c_{42}\left(\frac{h_{\mathrm{p},0}}{h_{\mathrm{p},1}}\right)^2, -c_{42}\left(\frac{h_{\mathrm{p},0}}{h_{\mathrm{p},1}}\right), c_{42}, -c_{42}\left(\frac{h_{\mathrm{p},1}}{h_{\mathrm{p},0}}\right)\right]^{\mathrm{T}}$$

$$\mathbf{v}_3 = \left[s_1, s_2, c_{43}\left(\frac{h_{\mathrm{p},0}}{h_{\mathrm{p},1}}\right)^3, c_{43}\left(\frac{h_{\mathrm{p},0}}{h_{\mathrm{p},1}}\right)^2, -c_{43}\left(\frac{h_{\mathrm{p},0}}{h_{\mathrm{p},1}}\right), c_{43}, -c_{43}\left(\frac{h_{\mathrm{p},1}}{h_{\mathrm{p},0}}\right)\right]^{\mathrm{T}}$$

where $s_i \in \mathbb{C}$, $\forall i \in \mathbb{N}$. Its orthonormalized version is given by

$$\mathbf{e}_1 = \frac{1}{\sqrt{D_1}}\left[w_1, w_2, -c_{41}\left(\frac{h_{\mathrm{p},0}}{h_{\mathrm{p},1}}\right)^3, c_{41}\left(\frac{h_{\mathrm{p},0}}{h_{\mathrm{p},1}}\right)^2, -c_{41}\left(\frac{h_{\mathrm{p},0}}{h_{\mathrm{p},1}}\right), c_{41}, -c_{41}\left(\frac{h_{\mathrm{p},1}}{h_{\mathrm{p},0}}\right)^3\right]^{\mathrm{T}}$$

$$\begin{aligned}\mathbf{e}_2 = \frac{1}{\sqrt{D_3}}\Bigg[&t_1 - \frac{D_2 w_1}{D_1}, t_2 - \frac{D_2 w_2}{D_1}, \left(\frac{h_{\mathrm{p},0}}{h_{\mathrm{p},1}}\right)^3\left(\frac{c_{41}D_2}{D_1} - c_{42}\right), \left(\frac{h_{\mathrm{p},0}}{h_{\mathrm{p},1}}\right)^2\left(c_{42} - \frac{c_{41}D_2}{D_1}\right),\\ &\left(\frac{h_{\mathrm{p},0}}{h_{\mathrm{p},1}}\right)\left(\frac{c_{41}D_2}{D_1} - c_{42}\right), c_{42} - \frac{c_{41}D_2}{D_1}, \left(\frac{h_{\mathrm{p},1}}{h_{\mathrm{p},0}}\right)\left(\frac{c_{41}D_2}{D_1} - c_{42}\right)\Bigg]^{\mathrm{T}}\end{aligned}$$

$$\begin{aligned}\mathbf{e}_3 = \frac{1}{\sqrt{D_6}}\Bigg[&s_1 - \frac{D_4 w_1}{D_1} - \frac{D_5\left(t_1 - \frac{D_2 w_1}{D1}\right)}{D_3}, s_2 - \frac{D_4 w_2}{D_1} - \frac{D_5\left(t_2 - \frac{D_2 w_2}{D1}\right)}{D_3},\\ &\left(\frac{h_{\mathrm{p},0}}{h_{\mathrm{p},1}}\right)^3\left[\frac{D_5}{D_3}\left(c_{42} - \frac{c_{41}D_2}{D_1}\right) + \frac{c_{41}D_4}{D_1} - c_{43}\right], \left(\frac{h_{\mathrm{p},0}}{h_{\mathrm{p},1}}\right)^2\left[\frac{D_5}{D_3}\left(\frac{c_{41}D_2}{D_1} - c_{42}\right) + c_{43} - \frac{c_{41}D_4}{D_1}\right],\\ &\left(\frac{h_{\mathrm{p},0}}{h_{\mathrm{p},1}}\right)\left[\frac{D_5}{D_3}\left(c_{42} - \frac{c_{41}D_2}{D_1}\right) + \frac{c_{41}D_4}{D_1} - c_{43}\right], \frac{D_5}{D_3}\left(\frac{c_{41}D_2}{D_1} - c_{42}\right) + c_{43} - \frac{c_{41}D_4}{D_1},\\ &\left(\frac{h_{\mathrm{p},1}}{h_{\mathrm{p},0}}\right)\left[\frac{D_5}{D_3}\left(c_{42} - \frac{c_{41}D_2}{D_1}\right) + \frac{c_{41}D_4}{D_1} - c_{43}\right]\Bigg]^{\mathrm{T}}\end{aligned}$$

with

$$D_1 = |w_1|^2 + |w_2|^2 + |c_{41}|^2\left(\left|\frac{h_{\mathrm{p},0}}{h_{\mathrm{p},1}}\right|^6 + \left|\frac{h_{\mathrm{p},0}}{h_{\mathrm{p},1}}\right|^4 + \left|\frac{h_{\mathrm{p},0}}{h_{\mathrm{p},1}}\right|^2 + \left|\frac{h_{\mathrm{p},0}}{h_{\mathrm{p},1}}\right|^{-2} + 1\right)$$

$$D_2 = t_1 w_1^* + t_2 w_2^* + c_{42}c_{41}^*\left(\left|\frac{h_{\mathrm{p},0}}{h_{\mathrm{p},1}}\right|^6 + \left|\frac{h_{\mathrm{p},0}}{h_{\mathrm{p},1}}\right|^4 + \left|\frac{h_{\mathrm{p},0}}{h_{\mathrm{p},1}}\right|^2 + \left|\frac{h_{\mathrm{p},0}}{h_{\mathrm{p},1}}\right|^{-2} + 1\right)$$

$$D_3 = \left|t_1 - \frac{D_2 w_1}{D_1}\right|^2 + \left|t_2 - \frac{D_2 w_2}{D_1}\right|^2 + \left|\left(\frac{c_{41}D_2}{D_1} - c_{42}\right)\right|^2\left[\left|\frac{h_{\mathrm{p},0}}{h_{\mathrm{p},1}}\right|^6 + \left|\frac{h_{\mathrm{p},0}}{h_{\mathrm{p},1}}\right|^4 + \left|\frac{h_{\mathrm{p},0}}{h_{\mathrm{p},1}}\right|^2 + \left|\frac{h_{\mathrm{p},1}}{h_{\mathrm{p},0}}\right|^{-2} + 1\right]$$

$$D_4 = s_1 w_1^* + s_2 w_2^* + c_{43}c_{41}^*\left(\left|\frac{h_{\mathrm{p},0}}{h_{\mathrm{p},1}}\right|^6 + \left|\frac{h_{\mathrm{p},0}}{h_{\mathrm{p},1}}\right|^4 + \left|\frac{h_{\mathrm{p},0}}{h_{\mathrm{p},1}}\right|^2 + \left|\frac{h_{\mathrm{p},0}}{h_{\mathrm{p},1}}\right|^{-2} + 1\right)$$

$$\begin{aligned}D_5 = &s_1\left(t_1^* - \frac{D_2^* w_1^*}{D_1}\right) + s_2\left(t_2^* - \frac{D_2^* w_2 *}{D_1}\right) +\\ &+ c_{43}\left(c_{42}^* - \frac{D_2^* c_{41}^*}{D_1}\right)\left(\left|\frac{h_{\mathrm{p},0}}{h_{\mathrm{p},1}}\right|^6 + \left|\frac{h_{\mathrm{p},0}}{h_{\mathrm{p},1}}\right|^4 + \left|\frac{h_{\mathrm{p},0}}{h_{\mathrm{p},1}}\right|^2 + \left|\frac{h_{\mathrm{p},0}}{h_{\mathrm{p},1}}\right|^{-2} + 1\right)\end{aligned}$$

$$D_6 = \left| s_1 - \frac{D_4 w_1}{D_1} - \frac{D_5\left(t_1 - \frac{D_2 w_1}{D_1}\right)}{D_3} \right|^2 + \left| s_2 - \frac{D_4 w_2}{D_1} - \frac{D_5\left(t_2 - \frac{D_2 w_2}{D_1}\right)}{D_3} \right|^2 + \\ + \left| \frac{D_5}{D_3}\left(c_{42} - \frac{c_{41} D_2}{D_1}\right) + \frac{c_{41} D_4}{D_1} - c_{43} \right|^2 \left[\left| \frac{h_{\mathrm{p},0}}{h_{\mathrm{p},1}} \right|^6 + \left| \frac{h_{\mathrm{p},0}}{h_{\mathrm{p},1}} \right|^4 + \left| \frac{h_{\mathrm{p},0}}{h_{\mathrm{p},1}} \right|^2 + \left| \frac{h_{\mathrm{p},0}}{h_{\mathrm{p},1}} \right|^{-2} + 1 \right]$$

A.2 Three-path channels

Now we consider a channel with three paths, including the LOS, i.e., $l = 2$. Let $\mathbf{h}_{\mathrm{p}} = [h_{\mathrm{p},0}, h_{\mathrm{p},1}, h_{\mathrm{p},2}]$ and $\mathbf{h}_{\mathrm{s}} = [h_{\mathrm{s},0}, h_{\mathrm{s},1}, h_{\mathrm{s},2}]$ be the primary and secondary system channel, respectively. The matrices $\mathbf{H}_{\mathrm{p}}$, $\mathbf{H}_{\mathrm{s}}$ are built according to the scheme presented previously. As before we consider different values for L.

A.2.1 $L = l$

In this case, the precoder $\mathbf{V}$ is given by

$$\mathbf{v}_1 = \left[\frac{1}{h_{\mathrm{p},2}^3}\left[c_{51}\left(h_{\mathrm{p},0}h_{\mathrm{p},1}^2 - h_{\mathrm{p},0}^2 h_{\mathrm{p},2}\right) - c_{41}\left(h_{\mathrm{p},1}^3 - 2h_{\mathrm{p},0}h_{\mathrm{p},1}h_{\mathrm{p},2}\right)\right], \frac{1}{h_{\mathrm{p},2}^2}[c_{51}h_{\mathrm{p},0}h_{\mathrm{p},1} + \right. \\ \left. + c_{41}\left(h_{\mathrm{p},1}^2 - h_{\mathrm{p},0}h_{\mathrm{p},2}\right)], -\frac{1}{h_{\mathrm{p},2}}\left(c_{51}h_{\mathrm{p},0} + c_{41}h_{\mathrm{p},1}\right), c_{41}, c_{51}, -\frac{1}{h_{\mathrm{p},0}}\left(c_{51}h_{\mathrm{p},1} + c_{41}h_{\mathrm{p},2}\right) \right]^{\mathrm{T}}$$

$$\mathbf{v}_2 = \left[\frac{1}{h_{\mathrm{p},2}^3}\left[c_{52}\left(h_{\mathrm{p},0}h_{\mathrm{p},1}^2 - h_{\mathrm{p},0}^2 h_{\mathrm{p},2}\right) - c_{42}\left(h_{\mathrm{p},1}^3 - 2h_{\mathrm{p},0}h_{\mathrm{p},1}h_{\mathrm{p},2}\right)\right], \frac{1}{h_{\mathrm{p},2}^2}[c_{52}h_{\mathrm{p},0}h_{\mathrm{p},1} + \right. \\ \left. + c_{42}\left(h_{\mathrm{p},1}^2 - h_{\mathrm{p},0}h_{\mathrm{p},2}\right)], -\frac{1}{h_{\mathrm{p},2}}\left(c_{52}h_{\mathrm{p},0} + c_{41}h_{\mathrm{p},1}\right), c_{42}, c_{52}, -\frac{1}{h_{\mathrm{p},0}}\left(c_{52}h_{\mathrm{p},1} + c_{42}h_{\mathrm{p},2}\right) \right]^{\mathrm{T}}$$

Its orthonormalized version is given by

$$\mathbf{e}_1 = \frac{1}{\sqrt{D_1}}\left[\frac{1}{h_{\mathrm{p},2}^3}\left[c_{51}\left(h_{\mathrm{p},0}h_{\mathrm{p},1}^2 - h_{\mathrm{p},0}^2 h_{\mathrm{p},2}\right) - c_{41}\left(h_{\mathrm{p},1}^3 - 2h_{\mathrm{p},0}h_{\mathrm{p},1}h_{\mathrm{p},2}\right)\right], \frac{1}{h_{\mathrm{p},2}^2}[c_{51}h_{\mathrm{p},0}h_{\mathrm{p},1} + \right. \\ \left. + c_{41}\left(h_{\mathrm{p},1}^2 - h_{\mathrm{p},0}h_{\mathrm{p},2}\right)], -\frac{1}{h_{\mathrm{p},2}}\left(c_{51}h_{\mathrm{p},0} + c_{41}h_{\mathrm{p},1}\right), c_{41}, c_{51}, -\frac{1}{h_{\mathrm{p},0}}\left(c_{51}h_{\mathrm{p},1} + c_{41}h_{\mathrm{p},2}\right) \right]^{\mathrm{T}}$$

$$\mathbf{e}_2 = \frac{1}{\sqrt{D_3}}\left[-\frac{1}{h_{\mathrm{p},2}^3}\left(\left(\frac{D_2 c_{51}}{D_1} - c_{52}\right)\left(h_{\mathrm{p},0}h_{\mathrm{p},1}^2 - h_{\mathrm{p},0}^2 h_{\mathrm{p},2}\right) - \left(\frac{D_2 c_{41}}{D_1} - c_{42}\right)\left(h_{\mathrm{p},1}^3 - 2h_{\mathrm{p},0}h_{\mathrm{p},1}h_{\mathrm{p},2}\right)\right), \right. \\ -\frac{1}{h_{\mathrm{p},2}^2}\left(\left(\frac{D_2 c_{51}}{D_1} - c_{52}\right)h_{\mathrm{p},0}h_{\mathrm{p},1} + \left(\frac{D_2 c_{41}}{D_1} - c_{42}\right)\left(h_{\mathrm{p},1}^2 - h_{\mathrm{p},0}h_{\mathrm{p},2}\right)\right), \\ \frac{1}{h_{\mathrm{p},2}}\left(\left(\frac{D_2 c_{51}}{D_1} - c_{52}\right)h_{\mathrm{p},0} + \left(\frac{D_2 c_{41}}{D_1} - c_{42}\right)h_{\mathrm{p},1}\right), c_{42} - \frac{c_{41}D_2}{D_1}, c_{52} - \frac{c_{51}D_2}{D_1}, \\ \left. \frac{1}{h_{\mathrm{p},0}}\left(\left(\frac{D_2 c_{51}}{D_1} - c_{52}\right)h_{\mathrm{p},1} + \left(\frac{D_2 c_{41}}{D_1} - c_{42}\right)h_{\mathrm{p},2}\right) \right]^{\mathrm{T}}$$

with

$$D_1 = |c_{41}|^2 + |c_{51}|^2 + \left|\frac{c_{41}h_{\mathrm{p},2} + c_{51}h_{\mathrm{p},1}}{h_{\mathrm{p},0}}\right|^2 + \left|\frac{c_{51}h_{\mathrm{p},0} + c_{41}h_{\mathrm{p},1}}{h_{\mathrm{p},2}}\right|^2 + \\ + \left|\frac{c_{51}h_{\mathrm{p},0}h_{\mathrm{p},1} + c_{41}\left(h_{\mathrm{p},1}^2 - h_{\mathrm{p},0}h_{\mathrm{p},2}\right)}{h_{\mathrm{p},2}^2}\right|^2 + \\ + \left|\frac{c_{51}\left(h_{\mathrm{p},0}h_{\mathrm{p},1}^2 - h_{\mathrm{p},0}^2h_{\mathrm{p},2}\right) - c_{41}\left(h_{\mathrm{p},1}^3 - 2h_{\mathrm{p},0}h_{\mathrm{p},1}h_{\mathrm{p},2}\right)}{h_{\mathrm{p},2}^3}\right|^2$$

$$D_2 = c_{42}c_{41}^* + c_{52}c_{51}^* + \left|\frac{1}{h_{\mathrm{p},0}}\right|^2 [(c_{42}h_{\mathrm{p},2} + c_{52}h_{\mathrm{p},1})(c_{41}h_{\mathrm{p},2} + c_{51}h_{\mathrm{p},1})^*] \\ + \left|\frac{1}{h_{\mathrm{p},2}}\right|^2 [(c_{52}h_{\mathrm{p},0} + c_{42}h_{\mathrm{p},1})(c_{51}h_{\mathrm{p},0} + c_{41}h_{\mathrm{p},1})^*] + \\ + \left|\frac{1}{h_{\mathrm{p},2}}\right|^4 [c_{52}h_{\mathrm{p},0}h_{\mathrm{p},1} + c_{42}(h_{\mathrm{p},1}^2 - h_{\mathrm{p},0}h_{\mathrm{p},2})][c_{51}h_{\mathrm{p},0}h_{\mathrm{p},1} + c_{41}(h_{\mathrm{p},1}^2 - h_{\mathrm{p},0}h_{\mathrm{p},2})]^* + \\ + \left|\frac{1}{h_{\mathrm{p},2}}\right|^6 [c_{52}(h_{\mathrm{p},0}h_{\mathrm{p},1}^2 - h_{\mathrm{p},0}^2h_{\mathrm{p},2}) - c_{42}(h_{\mathrm{p},1}^3 - 2h_{\mathrm{p},0}h_{\mathrm{p},1}h_{\mathrm{p},2})][c_{51}(h_{\mathrm{p},0}h_{\mathrm{p},1}^2 - h_{\mathrm{p},0}^2h_{\mathrm{p},2}) - \\ - c_{41}(h_{\mathrm{p},1}^3 - 2h_{\mathrm{p},0}h_{\mathrm{p},1}h_{\mathrm{p},2})]^*$$

$$D_3 = \left|c_{42} - \frac{c_{41}D_2}{D_1}\right|^2 + \left|c_{52} - \frac{c_{51}D_2}{D_1}\right|^2 + \left|\frac{1}{h_{\mathrm{p},0}}\right|^2 \left|\left(\frac{D_2c_{51}}{D_1} - c_{52}\right)h_{\mathrm{p},1} + \left(\frac{D_2c_{41}}{D_1} - c_{42}\right)h_{\mathrm{p},2}\right|^2 + \\ + \left|\frac{1}{h_{\mathrm{p},2}}\right|^2 \left|\left(\frac{D_2c_{51}}{D_1} - c_{52}\right)h_{\mathrm{p},0} + \left(\frac{D_2c_{41}}{D_1} - c_{42}\right)h_{\mathrm{p},1}\right|^2 + \\ + \left|\frac{1}{h_{\mathrm{p},2}}\right|^4 \left|\left(\frac{D_2c_{51}}{D_1} - c_{52}\right)h_{\mathrm{p},0}h_{\mathrm{p},1} + \left(\frac{D_2c_{41}}{D_1} - c_{42}\right)(h_{\mathrm{p},1}^2 - h_{\mathrm{p},0}h_{\mathrm{p},2})\right|^2 + \\ + \left|\frac{1}{h_{\mathrm{p},2}}\right|^6 \left|\left(\frac{D_2c_{51}}{D_1} - c_{52}\right)(h_{\mathrm{p},0}h_{\mathrm{p},1}^2 - h_{\mathrm{p},0}^2h_{\mathrm{p},2}) - \left(\frac{D_2c_{41}}{D_1} - c_{42}\right)(h_{\mathrm{p},1}^3 - 2h_{\mathrm{p},0}h_{\mathrm{p},1}h_{\mathrm{p},2})\right|^2$$

A.2.2 $L = l + 1$

In this case, the precoder $\mathbf{V}$ is given by

$$\mathbf{v}_1 = \Bigg[w_1, \frac{1}{h_{\mathrm{p},2}^3}\left(c_{51}\left(h_{\mathrm{p},0}h_{\mathrm{p},1}^2 - h_{\mathrm{p},0}^2h_{\mathrm{p},2}\right) - c_{41}\left(h_{\mathrm{p},1}^3 - 2h_{\mathrm{p},0}h_{\mathrm{p},1}h_{\mathrm{p},2}\right)\right), \\ \frac{1}{h_{\mathrm{p},2}^2}\left(c_{51}h_{\mathrm{p},0}h_{\mathrm{p},1} + c_{41}\left(h_{\mathrm{p},1}^2 - h_{\mathrm{p},0}h_{\mathrm{p},2}\right)\right), -\frac{1}{h_{\mathrm{p},2}}(c_{51}h_{\mathrm{p},0} + c_{41}h_{\mathrm{p},1}), c_{41}, c_{51}, \\ -\frac{1}{h_{\mathrm{p},0}}(c_{51}h_{\mathrm{p},1} + c_{41}h_{\mathrm{p},2})\Bigg]^{\mathrm{T}}$$

$$\mathbf{v}_2 = \Bigg[t_1, \frac{1}{h_{\mathrm{p},2}^3}\left(c_{52}\left(h_{\mathrm{p},0}h_{\mathrm{p},1}^2 - h_{\mathrm{p},0}^2 h_{\mathrm{p},2}\right) - c_{42}\left(h_{\mathrm{p},1}^3 - 2h_{\mathrm{p},0}h_{\mathrm{p},1}h_{\mathrm{p},2}\right)\right), \\ \frac{1}{h_{\mathrm{p},2}^2}\left(c_{52}h_{\mathrm{p},0}h_{\mathrm{p},1} + c_{42}\left(h_{\mathrm{p},1}^2 - h_{\mathrm{p},0}h_{\mathrm{p},2}\right)\right), -\frac{1}{h_{\mathrm{p},2}}(c_{52}h_{\mathrm{p},0} + c_{42}h_{\mathrm{p},1}), c_{42}, c_{52}, \\ -\frac{1}{h_{\mathrm{p},0}}(c_{52}h_{\mathrm{p},1} + c_{42}h_{\mathrm{p},2})\Bigg]^{\mathrm{T}}$$

$$\mathbf{v}_3 = \Bigg[s_1, \frac{1}{h_{\mathrm{p},2}^3}\left(c_{53}\left(h_{\mathrm{p},0}h_{\mathrm{p},1}^2 - h_{\mathrm{p},0}^2 h_{\mathrm{p},2}\right) - c_{43}\left(h_{\mathrm{p},1}^3 - 2h_{\mathrm{p},0}h_{\mathrm{p},1}h_{\mathrm{p},2}\right)\right), \\ \frac{1}{h_{\mathrm{p},2}^2}\left(c_{53}h_{\mathrm{p},0}h_{\mathrm{p},1} + c_{43}\left(h_{\mathrm{p},1}^2 - h_{\mathrm{p},0}h_{\mathrm{p},2}\right)\right), -\frac{1}{h_{\mathrm{p},2}}(c_{53}h_{\mathrm{p},0} + c_{43}h_{\mathrm{p},1}), c_{43}, c_{53}, \\ -\frac{1}{h_{\mathrm{p},0}}(c_{53}h_{\mathrm{p},1} + c_{43}h_{\mathrm{p},2})\Bigg]^{\mathrm{T}}.$$

Its orthonormalized version is given by

$$\mathbf{e}_1 = \frac{1}{\sqrt{D_1}}\Bigg[w_1, \frac{1}{h_{\mathrm{p},2}^3}\left(c_{51}(h_{\mathrm{p},0}h_{\mathrm{p},1}^2 - h_{\mathrm{p},0}^2 h_{\mathrm{p},2}) - c_{41}(h_{\mathrm{p},1}^3 - 2h_{\mathrm{p},0}h_{\mathrm{p},1}h_{\mathrm{p},2})\right), \\ \frac{1}{h_{\mathrm{p},2}^2}\left(c_{51}h_{\mathrm{p},0}h_{\mathrm{p},1} + c_{41}(h_{\mathrm{p},1}^2 - h_{\mathrm{p},0}h_{\mathrm{p},2})\right), -\frac{1}{h_{\mathrm{p},2}}(c_{51}h_{\mathrm{p},0} + c_{41}h_{\mathrm{p},1}), c_{41}, c_{51}, \\ -\frac{1}{h_{\mathrm{p},0}}(c_{51}h_{\mathrm{p},1} + c_{41}h_{\mathrm{p},2})\Bigg]^{\mathrm{T}}$$

$$\mathbf{e}_2 = \frac{1}{\sqrt{D_3}}\Bigg[t_1 - \frac{D_2 w_1}{D_1}, \\ \frac{1}{h_{\mathrm{p},2}^3}\left(\left(\frac{D_2 c_{41}}{D_1} - c_{42}\right)(h_{\mathrm{p},1}^3 - 2h_{\mathrm{p},0}h_{\mathrm{p},1}h_{\mathrm{p},2}) - \left(\frac{D_2 c_{51}}{D_1} - c_{52}\right)(h_{\mathrm{p},0}h_{\mathrm{p},1}^2 - h_{\mathrm{p},0}^2 h_{\mathrm{p},2})\right), \\ -\frac{1}{h_{\mathrm{p},2}^2}\left(\left(\frac{D_2 c_{41}}{D_1} - c_{42}\right)(h_{\mathrm{p},1}^2 - h_{\mathrm{p},0}h_{\mathrm{p},2}) + \left(\frac{D_2 c_{51}}{D_1} - c_{52}\right)h_{\mathrm{p},0}h_{\mathrm{p},1}\right), \\ \frac{1}{h_{\mathrm{p},2}}\left(\left(\frac{D_2 c_{41}}{D_1} - c_{42}\right)h_{\mathrm{p},1} + \left(\frac{D_2 c_{51}}{D_1} - c_{52}\right)h_{\mathrm{p},0}\right), c_{42} - \frac{c_{41}D_2}{D_1}, c_{52} - \frac{c_{51}D_2}{D_1}, \\ \frac{1}{h_{\mathrm{p},0}}\left(\left(\frac{D_2 c_{41}}{D_1} - c_{42}\right)h_{\mathrm{p},2} + \left(\frac{D_2 c_{51}}{D_1} - c_{52}\right)h_{\mathrm{p},1}\right)\Bigg]^{\mathrm{T}}$$

$$
\begin{aligned}
\mathbf{e}_3 = \Bigg[& s_1 - \frac{D_4 w_1}{D_1} - \frac{D_5 \left(t_1 - \frac{D_2 w_1}{D_1} \right)}{D_3}, \\
& \frac{1}{h_{\mathrm{p},2}^3} \Bigg(\frac{c_{51}(h_{\mathrm{p},0} h_{\mathrm{p},1}^2 - h_{\mathrm{p},0}^2 h_{\mathrm{p},2}) - c_{41}(h_{\mathrm{p},1}^3 - 2 h_{\mathrm{p},0} h_{\mathrm{p},1} h_{\mathrm{p},2})}{D_1} \left(\frac{D_5 D_2}{D_3} - D_4 \right) + \\
& + \left(c_{53} - \frac{D_5}{D_3} c_{52} \right) (h_{\mathrm{p},0} h_{\mathrm{p},1}^2 - h_{\mathrm{p},0}^2 h_{\mathrm{p},2}) - \left(c_{43} - \frac{D_5}{D_3} c_{42} \right) (h_{\mathrm{p},1}^3 - 2 h_{\mathrm{p},0} h_{\mathrm{p},1} h_{\mathrm{p},2}) \Bigg), \\
& \frac{1}{h_{\mathrm{p},2}^2} \Bigg(\frac{c_{51} h_{\mathrm{p},0} h_{\mathrm{p},1} + c_{41}(h_{\mathrm{p},1}^2 - h_{\mathrm{p},0} h_{\mathrm{p},2})}{D_1} \left(\frac{D_5 D_2}{D_3} - D_4 \right) + \left(c_{53} - \frac{D_5}{D_3} c_{52} \right) h_{\mathrm{p},0} h_{\mathrm{p},1} + \\
& + \left(c_{43} - \frac{D_5}{D_3} c_{42} \right) (h_{\mathrm{p},1}^2 - h_{\mathrm{p},0} h_{\mathrm{p},2}) \Bigg), \frac{1}{h_{\mathrm{p},2}} \Bigg(\frac{c_{51} h_{\mathrm{p},0} + c_{41} h_{\mathrm{p},1}}{D_1} \left(D_4 - \frac{D_5 D_2}{D_3} \right) - \\
& - \left(c_{53} - \frac{D_5}{D_3} c_{52} \right) h_{\mathrm{p},0} - \left(c_{43} - \frac{D_5}{D_3} c_{42} \right) h_{\mathrm{p},1} \Bigg), c_{43} - \frac{\left(c_{42} - \frac{c_{41} D_2}{D_1} \right) D_5}{\mathrm{D3}} - \frac{c_{41} D_4}{D_1}, \\
& c_{53} - \frac{\left(c_{52} - \frac{c_{51} D_2}{D_1} \right) D_5}{\mathrm{D3}} - \frac{c_{51} D_4}{D_1}, \frac{1}{h_{\mathrm{p},0}} \Bigg(\frac{c_{51} h_{\mathrm{p},1} + c_{41} h_{\mathrm{p},2}}{D_1} \left(D_4 - \frac{D_5 D_2}{D_3} \right) - \\
& - \left(c_{53} - \frac{D_5}{D_3} c_{52} \right) h_{\mathrm{p},1} - \left(c_{43} - \frac{D_5}{D_3} c_{42} \right) h_{\mathrm{p},2} \Bigg) \Bigg]^{\mathrm{T}}
\end{aligned}
$$

with

$$
\begin{aligned}
D_1 = & |c_{41}|^2 + |c_{51}|^2 + |w|^2 + \left| \frac{c_{51} h_{\mathrm{p},0} + c_{41} h_{\mathrm{p},1}}{h_{\mathrm{p},2}} \right|^2 + \left| \frac{c_{51} h_{\mathrm{p},1} + c_{41} h_{\mathrm{p},2}}{h_{\mathrm{p},0}} \right|^2 + \\
& + \left| \frac{c_{51} h_{\mathrm{p},0} h_{\mathrm{p},1} + c_{41} \left(h_{\mathrm{p},1}^2 - h_{\mathrm{p},0} h_{\mathrm{p},2} \right)}{h_{\mathrm{p},2}^2} \right|^2 + \left| \frac{c_{51} \left(h_{\mathrm{p},0} h_{\mathrm{p},1}^2 - h_{\mathrm{p},0}^2 h_{\mathrm{p},2} \right) - c_{41} \left(h_{\mathrm{p},1}^3 - 2 h_{\mathrm{p},0} h_{\mathrm{p},1} h_{\mathrm{p},2} \right)}{h_{\mathrm{p},2}^3} \right|^2
\end{aligned}
$$

$$
\begin{aligned}
D_2 = & c_{42} c_{41}^* + c_{52} c_{51}^* + t_1 w_1^2 + \left| \frac{1}{h_{\mathrm{p},2}} \right|^2 [(c_{52} h_{\mathrm{p},0} + c_{42} h_{\mathrm{p},1})(c_{51} h_{\mathrm{p},0} + c_{41} h_{\mathrm{p},1})^*] + \\
& + \left| \frac{1}{h_{\mathrm{p},0}} \right|^2 [(c_{52} h_{\mathrm{p},1} + c_{42} h_{\mathrm{p},2})(c_{51} h_{\mathrm{p},1} + c_{41} h_{\mathrm{p},2})^*] + \\
& + \left| \frac{1}{h_{\mathrm{p},2}} \right|^4 [c_{52} h_{\mathrm{p},0} h_{\mathrm{p},1} + c_{42}(h_{\mathrm{p},1}^2 - h_{\mathrm{p},0} h_{\mathrm{p},2})][c_{51} h_{\mathrm{p},0} h_{\mathrm{p},1} + c_{41}(h_{\mathrm{p},1}^2 - h_{\mathrm{p},0} h_{\mathrm{p},2})]^* + \\
& + \left| \frac{1}{h_{\mathrm{p},2}} \right|^6 [c_{52}(h_{\mathrm{p},0} h_{\mathrm{p},1}^2 - h_{\mathrm{p},0}^2 h_{\mathrm{p},2}) - c_{42}(h_{\mathrm{p},1}^3 - 2 h_{\mathrm{p},0} h_{\mathrm{p},1} h_{\mathrm{p},2})][c_{51}(h_{\mathrm{p},0} h_{\mathrm{p},1}^2 - h_{\mathrm{p},0}^2 h_{\mathrm{p},2}) - \\
& - c_{41}(h_{\mathrm{p},1}^3 - 2 h_{\mathrm{p},0} h_{\mathrm{p},1} h_{\mathrm{p},2})]^*
\end{aligned}
$$

$$
\begin{aligned}
D_3 = &\left| c_{42} - \frac{c_{41}D_2}{D_1} \right|^2 + \left| c_{52} - \frac{c_{51}D_2}{D_1} \right|^2 + \left| t_1 - \frac{D_2 w_1}{D_1} \right|^2 + \\
&+ \left| \frac{1}{h_{\mathrm{p},2}} \right|^2 \left| \left(\frac{D_2 c_{41}}{D_1} - c_{42} \right) h_{\mathrm{p},1} + \left(\frac{D_2 c_{51}}{D_1} c_{52} \right) h_{\mathrm{p},0} \right|^2 + \\
&+ \left| \frac{1}{h_{\mathrm{p},0}} \right|^2 \left| \left(\frac{D_2 c_{41}}{D_1} - c_{42} \right) h_{\mathrm{p},2} + \left(\frac{D_2 c_{51}}{D_1} - c_{52} \right) h_{\mathrm{p},1} \right|^2 + \\
&+ \left| \frac{1}{h_{\mathrm{p},2}} \right|^4 \left| \left(\frac{D_2 c_{41}}{D_1} - c_{42} \right) (h_{\mathrm{p},1}^2 - h_{\mathrm{p},0} h_{\mathrm{p},2}) + \left(\frac{D_2 c_{51}}{D_1} - c_{52} \right) h_{\mathrm{p},0} h_{\mathrm{p},1} \right|^2 + \\
&+ \left| \frac{1}{h_{\mathrm{p},2}} \right|^6 \left| \left(\frac{D_2 c_{41}}{D_1} - c_{42} \right) (h_{\mathrm{p},1}^3 - 2 h_{\mathrm{p},0} h_{\mathrm{p},1} h_{\mathrm{p},2}) - \left(\frac{D_2 c_{51}}{D_1} - c_{52} \right) (h_{\mathrm{p},0} h_{\mathrm{p},1}^2 - h_{\mathrm{p},0}^2 h_{\mathrm{p},2}) \right|^2
\end{aligned}
$$

$$
\begin{aligned}
D_4 = &\, c_{43}[c_{41}^* + c_{53} c_{51}^* + s_1 w_1^* + \left| \frac{1}{h_{\mathrm{p},2}} \right|^2 [(c_{53} h_{\mathrm{p},0} + c_{43} h_{\mathrm{p},1})(c_{51} h_{\mathrm{p},0} + c_{41} h_{\mathrm{p},1})^*] + \\
&+ \left| \frac{1}{h_{\mathrm{p},0}} \right|^2 [(c_{53} h_{\mathrm{p},1} + c_{43} h_{\mathrm{p},2})(c_{51} h_{\mathrm{p},1} + c_{41} h_{\mathrm{p},2})^*] + \\
&+ \left| \frac{1}{h_{\mathrm{p},2}} \right|^4 [c_{53} h_{\mathrm{p},0} h_{\mathrm{p},1} + c_{43}(h_{\mathrm{p},1}^2 - h_{\mathrm{p},0} h_{\mathrm{p},2})][c_{51} h_{\mathrm{p},0} h_{\mathrm{p},1} + c_{41}(h_{\mathrm{p},1}^2 - h_{\mathrm{p},0} h_{\mathrm{p},2})]^* + \\
&+ \left| \frac{1}{h_{\mathrm{p},2}} \right|^6 [c_{53}(h_{\mathrm{p},0} h_{\mathrm{p},1}^2 - h_{\mathrm{p},0}^2 h_{\mathrm{p},2}) - c_{43}(h_{\mathrm{p},1}^3 - 2 h_{\mathrm{p},0} h_{\mathrm{p},1} h_{\mathrm{p},2})][c_{51}(h_{\mathrm{p},0} h_{\mathrm{p},1}^2 - h_{\mathrm{p},0}^2 h_{\mathrm{p},2}) - \\
&- c_{41}(h_{\mathrm{p},1}^3 - 2 h_{\mathrm{p},0} h_{\mathrm{p},1} h_{\mathrm{p},2})]^*
\end{aligned}
$$

$$
\begin{aligned}
D_5 = &\, c_{43} \left(c_{42}^* - \frac{D_2^* c_{41}^*}{D_1} \right) + c_{53} \left(c_{52}^* - \frac{D_2^* c_{51}^*}{D_1} \right) + s_1 \left(t_1^* - \frac{D_2^* w_1^*}{D_1} \right) - \\
&- \left| \frac{1}{h_{\mathrm{p},2}} \right|^2 (c_{53} h_{\mathrm{p},0} + c_{43} h_{\mathrm{p},1}) \left[\left(\frac{D_2 c_{51}}{D_1} - c_{52} \right) h_{\mathrm{p},0} + \left(\frac{D_2 c_{41}}{D_1} - c_{42} \right) h_{\mathrm{p},1} \right]^* - \\
&- \left| \frac{1}{h_{\mathrm{p},0}} \right|^2 (c_{53} h_{\mathrm{p},1} + c_{43} h_{\mathrm{p},2}) \left[\left(\frac{D_2 c_{51}}{D_1} - c_{52} \right) h_{\mathrm{p},1} + \left(\frac{D_2 c_{41}}{D_1} - c_{42} \right) h_{\mathrm{p},2} \right]^* - \\
&- \left| \frac{1}{h_{\mathrm{p},2}} \right|^4 \left[c_{53} h_{\mathrm{p},0} h_{\mathrm{p},1} + c_{43}(h_{\mathrm{p},1}^2 - h_{\mathrm{p},0} h_{\mathrm{p},2}) \right] \left[\left(\frac{D_2 c_{51}}{D_1} - c_{52} \right) h_{\mathrm{p},0} h_{\mathrm{p},1} + \right. \\
&\left. + \left(\frac{D_2 c_{41}}{D_1} - c_{42} \right) (h_{\mathrm{p},1}^2 - h_{\mathrm{p},0} h_{\mathrm{p},2}) \right]^* - \left| \frac{1}{h_{\mathrm{p},2}} \right|^6 \left[c_{53}(h_{\mathrm{p},0} h_{\mathrm{p},1}^2 - h_{\mathrm{p},0}^2 h_{\mathrm{p},2}) - \right. \\
&\left. - c_{43}(h_{\mathrm{p},1}^3 - 2 h_{\mathrm{p},0} h_{\mathrm{p},1} h_{\mathrm{p},2}) \right] \left[\left(\frac{D_2 c_{51}}{D_1} - c_{52} \right) (h_{\mathrm{p},0} h_{\mathrm{p},1}^2 - h_{\mathrm{p},0}^2 h_{\mathrm{p},2}) - \right. \\
&\left. - \left(\frac{D_2 c_{41}}{D_1} - c_{42} \right) (h_{\mathrm{p},1}^3 - 2 h_{\mathrm{p},0} h_{\mathrm{p},1} h_{\mathrm{p},2}) \right]^*
\end{aligned}
$$

$$
\begin{aligned}
D_6 = &\left| c_{43} - \frac{c_{41}D_4}{D_1} - \frac{\left(c_{42} - \frac{c_{41}D_2}{D_1}\right)D_5}{D_3} \right|^2 + \left| c_{53} - \frac{c_{51}D_4}{D_1} - \frac{\left(c_{52} - \frac{c_{51}D_2}{D_1}\right)D_5}{D_3} \right|^2 + \\
&+ \left| s_1 - \frac{D_4 w_1}{D_1} - \frac{D_5\left(t_1 - \frac{D_2 w_1}{D_1}\right)}{D_3} \right|^2 + \left|\frac{1}{h_{\mathrm{p},2}}\right|^2 \left| \left(D_4 - \frac{D_5 D_2}{D_3}\right)\frac{c_{51}h_{\mathrm{p},0} + c_{41}h_{\mathrm{p},1}}{D_1} + \right. \\
&\left. + \left(\frac{D_5 c_{52}}{D_3} - c_{53}\right)h_{\mathrm{p},0} + \left(\frac{D_5 c_{42}}{D_3} - c_{43}\right)h_{\mathrm{p},1} \right|^2 + \left|\frac{1}{h_{\mathrm{p},0}}\right|^2 \left| \left(D_4 - \frac{D_5 D_2}{D_3}\right)\frac{c_{51}h_{\mathrm{p},1} + c_{41}h_{\mathrm{p},2}}{D_1} + \right. \\
&\left. + \left(\frac{D_5 c_{52}}{D_3} - c_{53}\right)h_{\mathrm{p},1} + \left(\frac{D_5 c_{42}}{D_3} - c_{43}\right)h_{\mathrm{p},2} \right|^2 + \\
&+ \left|\frac{1}{h_{\mathrm{p},2}}\right|^4 \left| \left(\frac{D_5 D_2}{D_3} - D_4\right)\frac{c_{51}h_{\mathrm{p},0}h_{\mathrm{p},1} + c_{41}(h_{\mathrm{p},1}^2 - h_{\mathrm{p},0}h_{\mathrm{p},2})}{D_1} - \left(\frac{D_5 c_{52}}{D_3} - c_{53}\right)h_{\mathrm{p},0}h_{\mathrm{p},1} - \right. \\
&\left. - \left(\frac{D_5 c_{42}}{D_3} - c_{43}\right)(h_{\mathrm{p},1}^2 - h_{\mathrm{p},0}h_{\mathrm{p},2}) \right|^2 + \\
&+ \left|\frac{1}{h_{\mathrm{p},2}}\right|^6 \left| \left(\frac{D_5 D_2}{D_3} - D_4\right)\frac{c_{51}(h_{\mathrm{p},0}h_{\mathrm{p},1}^2 - h_{\mathrm{p},0}^2 h_{\mathrm{p},2}) - c_{41}(h_{\mathrm{p},1}^3 - 2h_{\mathrm{p},0}h_{\mathrm{p},1}h_{\mathrm{p},2})}{D_1} - \right. \\
&\left. - \left(\frac{D_5 c_{52}}{D_3} - c_{53}\right)(h_{\mathrm{p},0}h_{\mathrm{p},1}^2 - h_{\mathrm{p},0}^2 h_{\mathrm{p},2}) + \left(\frac{D_5 c_{42}}{D_3} - c_{43}\right)(h_{\mathrm{p},1}^3 - 2h_{\mathrm{p},0}h_{\mathrm{p},1}h_{\mathrm{p},2}) \right|^2
\end{aligned}
$$

Bibliography

[1] Cisco, "Visual networking index: Global mobile data traffic forecast update, 2010–2015," White Paper, URL: http://www.cisco.com/en/US/solutions/collateral/ns341/ns525/ns537/ns705/ns827/white_paper_c11-520862.pdf, 2011, Accessed: 31/12/2012.

[2] G. Staple and K. Werbach, "The end of spectrum scarcity [spectrum allocation and utilization]," *IEEE Spectrum*, vol. 41, no. 3, pp. 48–52, March 2004.

[3] J. Hoydis, M. Kobayashi, and M. Debbah, "Green Small-Cell Networks," *IEEE Vehicular Technology Magazine*, vol. 6, no. 1, pp. 37–43, March 2011.

[4] V. Chandrasekhar, J. Andrews, and A. Gatherer, "Femtocell networks: a survey," *IEEE Communications Magazine*, vol. 46, no. 9, pp. 59–67, September 2008.

[5] V. Chandrasekhar, J. G. Andrews, T. Muharemovic, S. Zukang, and A. Gatherer, "Power control in two-tier femtocell networks," *IEEE Transactions on Wireless Communications*, vol. 8, no. 8, pp. 4316–4328, August 2009.

[6] D. Srinivasan, J. Dey, S. Kumar M, and R. N. Mukherjee, URL: http://www.wipro.com/Documents/resource-center/Data_Offload_Approaches_for_Mobile_Operators.pdf, Wipro, 2012, Accessed: 31/12/2012.

[7] NGMN, "NGMN recommendation on SON and O&M requirements," URL: http://www.ngmn.org/uploads/media/NGMN_Recommendation_on_SON_and_O_M_Requirements.pdf, 2008, Accessed: 31/12/2012.

[8] D. Lopez-Perez, A. Valcarce, G. de la Roche, and J. Zhang, "Ofdma femtocells: A roadmap on interference avoidance," *IEEE Communications Magazine*, vol. 47(9), no. 9, pp. 41–48, September 2009.

[9] 3GPP, "TR 36.300, Evolved Universal Terrestrial Radio Access (E-UTRA) and Evolved Universal Terrestrial Radio Access Network (E-UTRAN), Overall description, Stage 2, v.10.8.0," 3GPP, Tech. Rep., July 2012.

[10] M. Andrews, V. Capdevielle, A. Feki, and P. Gupta, "Autonomous Spectrum Sharing for Mixed LTE Femto and Macro Cells Deployments," in *IEEE Conference on Computer Communications (INFOCOM) Workshops*, March 2010, pp. 1–5.

[11] J. D. Hobby and H. Claussen, "Deployment options for femtocells and their impact on existing macrocellular networks," *Bell Labs Technical Journal*, vol. 13, no. 4, pp. 145–160, 2009.

[12] M. Bernaschi, F. Cacace, and G. Iannello, "Vertical handoff performance in heterogeneous networks," in *Proceedings of 2004 International Conference on Parallel Processing (ICCP) Workshops*, August 2004, pp. 100–107.

[13] D. Gesbert, S. Hanly, H. Huang, S. Shamai Shitz, O. Simeone, and W. Yu, "Multi-Cell MIMO Cooperative Networks: A New Look at Interference," *IEEE Journal on Selected Areas in Communications*, vol. 28, no. 9, pp. 1380–1408, December 2010.

[14] 3GPP, "TR 36.902, Evolved Universal Terrestrial Radio Access Network (E-UTRAN); Self-configuring and self-optimizing network (SON) use cases and solutions, v.9.3.1," 3GPP, Tech. Rep., May 2011.

[15] ARTIST4G, "Innovative advanced signal processing algorithms for interference avoidance," URL: https://ict-artist4g.eu/projet/work-packages/wp1/documents/d1.2/d1.2.pdf/at_download/file, Accessed: 28/11/2012.

[16] C. H. M. de Lima, M. Bennis, and M. Latva-aho, "Coordination Mechanisms for Self-Organizing Femtocells in Two-Tier Coexistence Scenarios," *IEEE Transactions on Wireless Communications*, vol. 11, no. 6, pp. 2212–2223, June 2012.

[17] M. Costa, "Writing on dirty paper," *IEEE Transactions on Information Theory*, vol. 29, no. 3, pp. 439– 441, May 1983.

[18] V. R. Cadambe and S. A. Jafar, "Interference Alignment and Degrees of Freedom of the K-User Interference Channel," *IEEE Transactions onInformation Theory*, vol. 54, no. 8, pp. 3425–3441, August 2008.

[19] A. Ghasemi, A. Motahari, and A. Khandani, "Interference alignment for the K user MIMO interference channel," in *IEEE International Symposium on Information Theory Proceedings (ISIT)*, June 2010, pp. 360–364.

[20] B. Da and R. Zhang, "Exploiting Interference Alignment in Multi-Cell Cooperative OFDMA Resource Allocation," in *IEEE Global Telecommunications Conference (GLOBECOM)*, December 2011, pp. 1–5.

[21] H. Zhou and T. Ratnarajah, "A Novel Interference Draining Scheme for Cognitive Radio Based on Interference Alignment," in *IEEE Symposium on New Frontiers in Dynamic Spectrum Access Networks (DySPAN)*, April 2010, pp. 1–6.

[22] H. Dahrouj and W. Yu, "Coordinated beamforming for the multicell multi-antenna wireless system," *IEEE Transactions on Wireless Communications*, vol. 9, no. 5, pp. 1748–1759, May 2010.

[23] I. Mitola, J. and J. Maguire, G. Q., "Cognitive radio: making software radios more personal," *IEEE Personal Communications*, vol. 6, no. 4, pp. 13–18, August 1999.

[24] S. E. W. Group, "Report of the Spectrum Efficiency Working Group," FCC, Tech. Rep., November 2002.

[25] FCC, "Fcc et docket no. 03-108: Facilitating opportunities for flexible, efficient, and reliable spectrum use employing cognitive radio technologies," FCC, Tech. Rep., 2003.

[26] ——, "In the matter of unlicensed operation in the tv broadcast bands docket 04-186 incremental reform towards a boradcast underlay, and the radio traffic signal," FCC, Tech. Rep., 2008.

[27] S. Haykin, "Cognitive radio: brain-empowered wireless communications," *IEEE Journal on Selected Areas in Communications*, vol. 23, no. 2, pp. 201–220, February 2005.

[28] Q. Zhao and B. Sadler, "A Survey of Dynamic Spectrum Access," *IEEE Signal Processing Magazine*, vol. 24, no. 3, pp. 79–89, May 2007.

[29] A. Goldsmith, S. Jafar, I. Maric, and S. Srinivasa, "Breaking Spectrum Gridlock With Cognitive Radios: An Information Theoretic Perspective," *Proceedings of the IEEE*, vol. 97, no. 5, pp. 894 –914, May 2009.

[30] I. Akyildiz, W.-Y. Lee, M. Vuran, and S. Mohanty, "A survey on spectrum management in cognitive radio networks," *IEEE Communications Magazine*, vol. 46, no. 4, pp. 40–48, April 2008.

[31] S. Srinivasa and S. A. Jafar, "Cognitive radios for dynamic spectrum access - the throughput potential of cognitive radio: A theoretical perspective," *IEEE Communications Magazine*, vol. 45, no. 5, pp. 73–79, May 2007.

[32] I. Akyildiz, W. Lee, M. Vuran, and S. Mohanty, "NeXt generation/dynamic spectrum access/cognitive radio wireless networks: a survey," *Computer Networks*, vol. 50, no. 13, pp. 2127–2159, 2006.

[33] A. Ghasemi and E. Sousa, "Fundamental limits of spectrum-sharing in fading environments," *IEEE Transactions on Wireless Communications*, vol. 6, no. 2, pp. 649–658, 2007.

[34] S. Akoum, M. Zwingelstein-Colin, R. W. Heath Jr., and M. Debbah, "Cognitive cooperation for the downlink of frequency reuse small cells," *EURASIP Journal on Advances in Signal Processing, URL: http://asp.eurasipjournals.com/content/2011/1/525271*, vol. 2011, no. 1, p. 525271, 2011.

[35] W. Zhang and U. Mitra, "Spectrum shaping: a new perspective on cognitive radio-part I: coexistence with coded legacy transmission," *IEEE Transactions on Communications*, vol. 58, no. 6, pp. 1857–1867, June 2010.

[36] S. Perlaza, N. Fawaz, S. Lasaulce, and M. Debbah, "From Spectrum Pooling to Space Pooling: Opportunistic Interference Alignment in MIMO Cognitive Networks," *IEEE Transactions on Signal Processing*, vol. 58, no. 7, pp. 3728–3741, July 2010.

[37] M. Gastpar, "On Capacity Under Receive and Spatial Spectrum-Sharing Constraints," *IEEE Transactions on Information Theory*, vol. 53, no. 2, pp. 471–487, February 2007.

[38] C. Shen and M. P. Fitz, "Opportunistic Spatial Orthogonalization and Its Application in Fading Cognitive Radio Networks," *IEEE Journal of Selected Topics in Signal Processing*, vol. 5, no. 1, pp. 182–189, February 2011.

[39] M. Amir, A. El-Keyi, and M. Nafie, "Constrained Interference Alignment and the Spatial Degrees of Freedom of MIMO Cognitive Networks," *IEEE Transactions on Information Theory*, vol. 57, no. 5, pp. 2994–3004, May 2011.

[40] S. Ganesan, M. Sellathurai, and T. Ratnarajah, "Opportunistic interference alignment in cognitive MIMO with finite rate feedback," in *First UK-India International Workshop on Cognitive Wireless Systems (UKIWCWS)*, December 2009, pp. 1–5.

[41] R. Zhang and Y.-C. Liang, "Exploiting Multi-Antennas for Opportunistic Spectrum Sharing in Cognitive Radio Networks," *IEEE Journal of Selected Topics in Signal Processing*, vol. 2, no. 1, pp. 88–102, February 2008.

[42] K. Cumanan, L. Musavian, S. Lambotharan, and A. Gershman, "SINR Balancing Technique for Downlink Beamforming in Cognitive Radio Networks," *IEEE Signal Processing Letters*, vol. 17, no. 2, pp. 133–136, February 2010.

[43] J. Hoydis, M. Kobayashi, and M. Debbah, "Optimal Channel Training in Uplink Network MIMO Systems," *IEEE Transactions on Signal Processing*, vol. 59, no. 6, pp. 2824–2833, June 2011.

[44] T. L. Marzetta, "Noncooperative cellular wireless with unlimited numbers of base station antennas," *IEEE Transactions on Wireless Communications*, vol. 9, no. 11, pp. 3590–3600, November 2010.

[45] H. Huh, G. Caire, H. Papadopoulos, and S. Ramprashad, "Achieving "Massive MIMO" Spectral Efficiency with a Not-so-Large Number of Antennas," *IEEE Transactions on Wireless Communications*, vol. 11, no. 9, pp. 3226–3239, September 2012.

[46] R. Esmailzadeh, M. Nakagawa, and A. Jones, "TDD-CDMA for the 4th generation of wireless communications," *IEEE Wireless Communications*, vol. 10, no. 4, pp. 8–15, August 2003.

[47] G. Povey and M. Nakagawa, "A review of time division duplex-CDMA techniques," in *IEEE 5th International Symposium on Spread Spectrum Techniques and Applications*, vol. 2, September 1998, pp. 630–633.

[48] P. W. C. Chan, E. S. Lo, R. R. Wang, E. K. S. Au, V. K. N. Lau, R. S. Cheng, W. H. Mow, R. D. Murch, and K. B. Letaief, "The evolution path of 4G networks: FDD or TDD?" *IEEE Communications Magazine*, vol. 44, no. 12, pp. 42–50, December 2006.

[49] E. Ayanoglu, M. Burgess, M. Pollack, and A. Zamanian, "Frequency division duplexing and time division duplexing for broadband wireless applications, broadband wireless internet forum white paper, v1.2, february 2011," URL:http://www.inforede.net/Technical/Layer_1/Wireless_LAN/FDD_vs_TDD.pdf, Accessed: 31/12/2012.

[50] 3GPP, "TR 25.814, physical layer aspects for Evolved UTRA, v.2.0.0," 3GPP, Tech. Rep., October 2006.

[51] S. Shen and K. Takada, "China's ZTE to launch TD-LTE phone this year," URL: http://www.reuters.com/article/2012/06/20/net-us-zte-smartphone-idUSBRE85J0KN20120620, Reuters, Accessed: 31/12/2012.

[52] S. Chen, Y. Wang, W. Ma, and J. Chen, "Technical innovations promoting standard evolution: from TD-SCDMA to TD-LTE and beyond," *IEEE Wireless Communications*, vol. 19, no. 1, pp. 60–66, February 2012.

[53] X. Hou, Z. Zhang, and H. Kayama, "QRD-based MU-MIMO transmission scheme towards evolved LTE TDD system," in *IEEE GLOBECOM Workshops (GC Wkshps)*, December 2010, pp. 866–870.

[54] F. Sun, L. Lu, and T. B. Sø andrensen, "Designs of precoding for LTE TDD using cell specific reference signals," in *IEEE GLOBECOM Workshops (GC Wkshps)*, December 2010, pp. 871–875.

[55] L. S. Cardoso, M. Kobayashi, O. Ryan, and M. Debbah, "Vandermonde frequency division multiplexing for cognitive radio," in *IEEE 9th Workshop on Signal Processing Advances in Wireless Communications (SPAWC)*, July 2008, pp. 421–425.

[56] L. S. Cardoso, F. R. P. Cavalcanti, M. Kobayashi, and M. Debbah, "Vandermonde-subspace frequency division multiplexing receiver analysis," in *2010 IEEE 21st International Symposium on Personal Indoor and Mobile Radio Communications (PIMRC)*, September 2010, pp. 293–298.

[57] SDR4All, URL: http://www.flexible-radio.com/sdr4all, Accessed: 31/12/2012.

[58] 3GPP, "TR 36.814, Further advancements for E-UTRA physical layer aspects, v.9.0.0," 3GPP, Tech. Rep., March 2010.

[59] D. Tse and P. Viswanath, *Fundamentals of Wireless Communication*. Cambridge University Press, June 2005.

[60] S. Srinivasa and S. A. Jafar, "The throughput potential of Cognitive Radio: A theoretical perspective," in *Fortieth Asilomar Conference on Signals, Systems and Computers (ACSSC)*, November 2006, pp. 221–225.

[61] G. H. Golub and C. F. Van Loan, *Matrix Computations*, 3rd ed. The Johns Hopkins University Press, October 1996.

[62] N. Benvenuto and G. Cherubini, *Algorithms for Communications Systems and their Applications*. John Wiley & Sons, 2002.

[63] M. Kobayashi, M. Debbah, and S. Shamai, "Secured Communication over Frequency-Selective Fading Channels: a practical Vandermonde precoding," *CoRR*, vol. abs/0906.3192, 2009.

[64] ETTUS Research LLC, URL: http://www.ettus.com/, Accessed: 12/11/2012.

[65] IEEE, "Wireless LAN Medium Access Control (MAC) and Physical Layer (PHY) Specifications," URL: http://standards.ieee.org/getieee802/download/802.11-2012.pdf, Accessed: 31/12/2012.

[66] Bluetooth SIG, "Bluetooth Core Version 4.0", URL: https://www.bluetooth.org/Technical/Specifications/adopted.htm, Accessed: 31/12/2012.

[67] K. Etemad and M. Lai, *WiMAX Technology and Network Evolution*, ser. The ComSoc Guides to Communications Technologies. Wiley, 2011.

[68] SDR4All toolbox (Tools4SDR), URL: http://www.flexible-radio.com/tools4sdr, Accessed: 31/12/2012.

[69] F. A. Hamza, "The USRP under 1.5 x magnifying lens!" URL: https://microembedded.googlecode.com/files/USRP_Documentation.pdf, Accessed: 31/12/2012.

[70] M. Golay, "Complementary series," *IRE Transactions on Information Theory*, vol. IT-7, pp. 82–87, 1961.

[71] IEEE, "Wireless LAN Medium Access Control (MAC) and Physical Layer (PHY) Specifications – High speed physical layer in 5GHz band," URL: http://standards.ieee.org/getieee802/download/802.11a-1999.pdf, Accessed: 31/12/2012.

[72] ETSI, "Ts 101475 v1.2.2, broadband radio access networks (BRAN); HIPERLAN type 2; physical (PHY) layer," ETSI, Tech. Rep., 2002.

[73] C. Meyer, *Matrix Analysis and Applied Linear Algebra Book and Solutions Manual*, ser. Miscellaneous Titles in Applied Mathematics Series. Society for Industrial and Applied Mathematics, 2000.

[74] M. Debbah, "Short introduction to OFDM," URL: flexible-radio.org/sites/default/files/media/1/tutorial_ofdmtutorial.pdf, Accessed: 31/12/2012.

[75] S. Jing, D. Tse, J. Soriaga, J. Hou, J. Smee, and R. Padovani, "Multicell Downlink Capacity with Coordinated Processing," *EURASIP Journal on Wireless Communications and Networking, URL: http://jwcn.eurasipjournals.com/content/2008/1/586878*, vol. 2008, no. 1, p. 586878, 2008.

[76] O. Simeone, O. Somekh, G. Kramer, H. V. Poor, and S. Shamai, "Throughput of cellular systems with conferencing mobiles and cooperative base stations," *EURASIP Journal on Wireless Communications and Networking, URL: http://jwcn.eurasipjournals.com/content/2008/1/652325*, vol. 2008, no. 1, p. 652325, 2008.

[77] O. Somekh, O. Simeone, Y. Bar-Ness, A. Haimovich, U. Spagnolini, and S. Shamai, *An information theoretic view of distributed antenna processing in cellular systems*. Auerbach Publications, CRC Press, New York, NY, USA, 2007.

[78] M. K. Karakayali, G. J. Foschini, and R. A. Valenzuela, "Network coordination for spectrally efficient communications in cellular systems," *IEEE Wireless Communications*, vol. 13, no. 4, pp. 56–61, August 2006.

[79] H. Zhang, H. Dai, and Q. Zhou, "Base station cooperation for multiuser MIMO: Joint transmission and BS selection," in *Proceedings of the 2004 Conference on Information Sciences and Systems (CISS), Princeton, NJ, March*, 2004.

[80] S. Shamai, O. Somekh, and B. M. Zaidel, "Multi-cell communications: an information theoretic perspective," in *Proceedings of the 3rd Joint Workshop on Communications and Coding (JWCC), Donnini, Italy*, October 2004.

[81] H. Zhou, T. Ratnarajah, and Y.-C. Liang, "On secondary network interference alignment in cognitive radio," in *IEEE Symposium on New Frontiers in Dynamic Spectrum Access Networks (DySPAN)*, May 2011, pp. 637–641.

[82] H. Du and T. Ratnarajah, "Robust joint signal and interference alignment for MIMO cognitive radio network," in *IEEE Wireless Communications and Networking Conference (WCNC)*, April 2012, pp. 448–452.

[83] M. Andrews, K. Kumaran, K. Ramanan, A. Stolyar, P. Whiting, and R. Vijayakumar, "Providing quality of service over a shared wireless link," *IEEE Communications Magazine*, vol. 39, no. 2, pp. 150–154, February 2001.

[84] H. Holma and A. Toskala, *LTE for UMTS - OFDMA and SC-FDMA Based Radio Access*. Wiley, 2009.

[85] J. Ayres, *Theory and Problems of Matrices: Including 340 Solved Problems Completely Solved in Detail*, ser. Schaum's Outline Series. McGraw-Hill Books Company, 1962.

[86] A. Goldsmith, *Wireless Communications*. Cambridge University Press, August 2005.

[87] G. Caire and S. Shamai, "On the achievable throughput of a multiantenna Gaussian broadcast channel," *IEEE Transactions on Information Theory*, vol. 49, no. 7, pp. 1691–1706, July 2003.

[88] J. Lee and N. Jindal, "Dirty Paper Coding vs. Linear Precoding for MIMO Broadcast Channels," in *Fortieth Asilomar Conference on Signals, Systems and Computers (ACSSC)*, November 2006, pp. 779 –783.

[89] Q. H. Spencer, A. L. Swindlehurst, and M. Haardt, "Zero-forcing methods for downlink spatial multiplexing in multiuser MIMO channels," *IEEE Transactions on Signal Processing*, vol. 52, no. 2, pp. 461–471, February 2004.

[90] C. Peel, B. Hochwald, and A. Swindlehurst, "A vector-perturbation technique for near-capacity multiantenna multiuser communication (part I): channel inversion and regularization," *IEEE Transactions on Communications*, vol. 53, no. 1, pp. 195–202, January 2005.

[91] R. de Miguel and R. R. Muller, "Vector precoding for a single-user MIMO channel: Matched filter vs. distributed antenna detection," in *First International Symposium on Applied Sciences on Biomedical and Communication Technologies (ISABEL)*, October 2008, pp. 1–4.

[92] P. Viswanath, D. Tse, and R. Laroia, "Opportunistic beamforming using dumb antennas," *IEEE Transactions on Information Theory*, vol. 48, no. 6, pp. 1277–1294, June 2002.

[93] M. Sharif and B. Hassibi, "On the capacity of MIMO broadcast channels with partial side information," *IEEE Transactions on Information Theory*, vol. 51, no. 2, pp. 506–522, February 2005.

[94] V. Stankovic and M. Haardt, "Multi-user MIMO downlink precoding for users with multiple antennas," in *Proc. 12-th Meeting of the Wireless World Research Forum*, 2004.

[95] ——, "Generalized Design of Multi-User MIMO Precoding Matrices," *IEEE Transactions on Wireless Communications*, vol. 7, no. 3, pp. 953–961, March 2008.

[96] T. Yoo and A. Goldsmith, "On the optimality of multiantenna broadcast scheduling using zero-forcing beamforming," *IEEE Journal on Selected Areas in Communications*, vol. 24, no. 3, pp. 528–541, March 2006.

[97] G. Dimic and N. Sidiropoulos, "On downlink beamforming with greedy user selection: performance analysis and a simple new algorithm," *IEEE Transactions on Signal Processing*, vol. 53, no. 10, pp. 3857–3868, October 2005.

[98] ETSI, "EN 302 755 V1.3.1, Digital Video Broadcasting (DVB); Frame structure channel coding and modulation for a second generation digital terrestrial television broadcasting system (DVB-T2)," ETSI, Tech. Rep., April 2012.

[99] IEEE, "IEEE 802.16: Broadband Metropolitan Area Networks (MANs)," IEEE, 2009.

[100] M. Guillaud, D. Slock, and R. Knopp, "A practical method for wireless channel reciprocity exploitation through relative calibration," in *Proceedings of the Eighth International Symposium on Signal Processing and Its Applications*, vol. 1, August 2005, pp. 403–406.

[101] S. Sesia, I. Toufik, and M. Baker, *LTE, The UMTS Long Term Evolution: From Theory to Practice*. John Wiley & Sons, 2009.

[102] D. Grieco, J.-L. Pan, R. Olesen, and N. Shah, "Uplink Single-User MIMO for 3GPP LTE," in *IEEE 18th International Symposium on Personal, Indoor and Mobile Radio Communications (PIMRC)*, September 2007, pp. 1–5.

[103] B. Hassibi and B. Hochwald, "How much training is needed in multiple-antenna wireless links?" *IEEE Transactions on Information Theory*, vol. 49, no. 4, pp. 951–963, April 2003.

[104] 3GPP, "TR 36.211, Evolved UTRA; physical channels and modulation, v.10.5.0," 3GPP, Tech. Rep., 2012.

[105] E. Alsusa and C. Masouros, "Adaptive code allocation for interference management on the downlink of DS-CDMA systems," *IEEE Transactions on Wireless Communications*, vol. 7, no. 7, pp. 2420–2424, July 2008.

[106] Y. Zhou, J. Wang, and T.-S. Ng, "Downlink Transmission of Broadband OFCDM Systems-Part V: Code Assignment," *IEEE Transactions on Wireless Communications*, vol. 7, no. 11, pp. 454 –4557, November 2008.

[107] M. Kobayashi and X. Mestre, "Impact of CSI on distributed space-time coding in wireless relay networks," *IEEE Transactions on Wireless Communications*, vol. 8, no. 5, pp. 2580–2591, May 2009.

[108] F. Gao, R. Zhang, and Y.-C. Liang, "Channel Estimation for OFDM Modulated Two-Way Relay Networks," *IEEE Transactions on Signal Processing*, vol. 57, no. 11, pp. 4443–4455, November 2009.

[109] H. Gacanin, T. Sjodin, and F. Adachi, "On Channel Estimation for Analog Network Coding in a Frequency-Selective Fading Channel," *EURASIP Journal on Wireless Communications and Networking, URL: http://jwcn.eurasipjournals.com/content/2011/1/980430*, vol. 2011, no. 1, p. 980430, 2011.

[110] Y. Wang, S. Frattasi, T. Sorensen, and P. Mogensen, "Network Time-Synchronization in TDD Based LTE-Advanced Systems," in *IEEE 69th Vehicular Technology Conference, VTC Spring*, April 2009, pp. 1–5.

[111] K. Tan, J. Fang, Y. Zhang, S. Chen, L. Shi, J. Zhang, and Y. Zhang, "Fine-grained channel access in wireless LAN," in *Proceedings of the ACM SIGCOMM 2010 Conference on Applications, Technologies, Architectures, and Protocols for Computer Communications*. ACM, 2010, pp. 147–158.

[112] H. S. Rahul, H. Hassanieh, and D. Katabi, "SourceSync: a distributed wireless architecture for exploiting sender diversity," in *Proceedings of the ACM SIGCOMM 2010 Conference on Applications, Technologies, Architectures, and Protocols for Computer Communications*. ACM, 2010, pp. 171–182.

[113] D. C. Jenn, J. H. Ryu, T. Yen-Chang, and R. Broadston, "Adaptive phase synchronization in distributed digital arrays," in *NASA/ESA Conference on Adaptive Hardware and Systems (AHS)*, June 2010, pp. 199–204.

[114] S. H. Lim, Y.-H. Kim, A. El Gamal, and S.-Y. Chung, "Noisy Network Coding," *IEEE Transactions on Information Theory*, vol. 57, no. 5, pp. 3132–3152, May 2011.

[115] H. S. Rahul, S. Kumar, and D. Katabi, "JMB: scaling wireless capacity with user demands," in *Proceedings of the ACM SIGCOMM 2012 Conference on Applications, Technologies, Architectures, and Protocols for Computer Communications*. ACM, 2012, pp. 235–246.

[116] L. S. Cardoso, "Orthogonal precoder for dynamic spectrum access in wireless networks," Ph.D. dissertation, Supélec, November 2011.

[117] ARTIST4G, "Feedback from RAN constraints," URL: https://ict-artist4g.eu/projet/work-packages/wp4/offiial-deliverables/d4.2_v1.0-feedback-from-ran-constraints.pdf, Accessed: 28/11/2012.

[118] Alcatel Lucent, "lightRadio: Evolve your wireless broadband network", URL: http://www.alcatel-lucent.com/lightradio/, Accessed: 12/11/2012.

[119] G. Li and H. Liu, "Downlink Radio Resource Allocation for Multi-Cell OFDMA System," *IEEE Transactions on Wireless Communications*, vol. 5, no. 12, pp. 3451–3459, December 2006.

[120] I. Koutsopoulos and L. Tassiulas, "Cross-Layer Adaptive Techniques for Throughput Enhancement in Wireless OFDM-Based Networks," *IEEE/ACM Transactions on Networking*, vol. 14, no. 5, pp. 1056–1066, October 2006.

[121] A. Abrardo, A. Alessio, P. Detti, and M. Moretti, "Centralized Radio Resource Allocation for OFDMA Cellular Systems," in *IEEE International Conference on Communications (ICC)*, June 2007, pp. 5738–5743.

[122] M. Pischella and J.-C. Belfiore, "Distributed resource allocation for rate-constrained users in multi-cell OFDMA networks," *IEEE Communications Letters*, vol. 12, no. 4, pp. 250–252, April 2008.

[123] B. D. Van Veen and K. M. Buckley, "Beamforming: a versatile approach to spatial filtering," *IEEE ASSP Magazine*, vol. 5, no. 2, pp. 4–24, April 1988.

[124] B. Sklar, "Rayleigh fading channels in mobile digital communication systems .I. Characterization," *IEEE Communications Magazine*, vol. 35, no. 7, pp. 90 –100, July 1997.

[125] M. Grossglauser and D. Tse, "Mobility increases the capacity of ad-hoc wireless networks," in *Proceedings of the 20th Annual Joint Conference of the IEEE Computer and Communications Societies (INFOCOM)*, vol. 3, 2001, pp. 1360–1369.

[126] S. Borst, A. Proutiere, and N. Hegde, "Capacity of wireless data networks with intra- and inter-cell mobility," in *Proceedings of 25th IEEE International Conference on Computer Communications (INFOCOM)*, April 2006, pp. 1–12.

[127] S. A. Jafar, "Too much mobility limits the capacity of wireless ad hoc networks," *IEEE Transactions on Information Theory*, vol. 51, no. 11, pp. 3954–3965, November 2005.

[128] H. W. Je, H. Lee, K. Kwak, S. Choi, Y.-J. Hong, and B. Clerckx, "Long-Term Channel Information-Based CoMP Beamforming in LTE-Advanced Systems," in *IEEE Global Telecommunications Conference (GLOBECOM)*, December 2011, pp. 1–6.

[129] A. Adhikary, H. Papadopoulos, S. Ramprashad, and G. Caire, "Multi-user MIMO with outdated CSI: Training, feedback and scheduling," in *49th Annual Allerton Conference on Communication, Control, and Computing (Allerton)*, September 2011, pp. 886–893.

[130] E. Aryafar, M. Khojastepour, K. Sundaresan, S. Rangarajan, and E. Knightly, "ADAM: An adaptive beamforming system for multicasting in wireless LANs," in *Proceedings of the 31st IEEE International Conference on Computer Communications (INFOCOM)*, March 2012, pp. 1467–1475.

[131] I. Wajid, M. Pesavento, Y. Eldar, and A. Gershman, "Robust downlink beamforming for cognitive radio networks," in *IEEE Global Telecommunications Conference (GLOBECOM)*, December 2010, pp. 1–5.

[132] H. Kim, H. Wang, S. Lim, and D. Hong, "On the impact of outdated channel information on the capacity of secondary user in spectrum sharing environments," *IEEE Transactions on Wireless Communications*, vol. 11, no. 1, pp. 284–295, January 2012.

[133] N. Devroye, P. Mitran, and V. Tarokh, "Achievable rates in cognitive radio channels," *IEEE Transactions on Information Theory*, vol. 52, no. 5, pp. 1813–1827, May 2006.

[134] Y. Ma, D. I. Kim, and Z. Wu, "Optimization of OFDMA-based cellular cognitive radio networks," *IEEE Transactions on Communications*, vol. 58, no. 8, pp. 2265–2276, August 2010.

[135] P. Bertrand, "Channel Gain Estimation from Sounding Reference Signal in LTE," in *IEEE 73rd Vehicular Technology Conference (VTC Spring)*, May 2011, pp. 1–5.

[136] W. Ho, T. Quek, S. Sun, and R. Heath, "Decentralized Precoding for Multicell MIMO Downlink," *IEEE Transactions on Wireless Communications*, vol. 10, no. 6, pp. 1798–1809, June 2011.

[137] I. Rhee, A. Warrier, J. Min, and L. Xu, "DRAND: Distributed Randomized TDMA Scheduling for Wireless Ad Hoc Networks," *IEEE Transactions on Mobile Computing*, vol. 8, no. 10, pp. 1384–1396, October 2009.

[138] 3GPP, "TR 36.913, Requirements for further advancements for Evolved Universal Terrestrial Radio Access (E-UTRA) (LTE-Advanced), v.10.0.0," 3GPP, Tech. Rep., April 2011.

[139] ——, "TR 36.942, Evolved Universal Terrestrial Radio Access (E-UTRA); Radio Frequency (RF) system scenarios, v.8.2.0," 3GPP, Tech. Rep., July 2009.

[140] The Climate Group and Global e-Sustainability Initiative (GeSI), "SMART 2020: Enabling the low carbon economy in the information age", URL: http://www.smart2020.org, 2008, Accessed: 31/12/2012.

[141] T. Chen, Y. Yang, H. Zhang, H. Kim, and K. Horneman, "Network energy saving technologies for green wireless access networks," *IEEE Wireless Communications*, vol. 18, no. 5, pp. 30–38, October 2011.

[142] G. Miao, N. Himayat, and G. Y. Li, "Energy-efficient link adaptation in frequency-selective channels," *IEEE Transactions on Communications*, vol. 58, no. 2, pp. 545–554, February 2010.

[143] J. Mitola, "The software radio architecture," *IEEE Communications Magazine*, vol. 33, no. 5, pp. 26–38, May 1995.

[144] R. Lackey and D. Upmal, "Speakeasy: the military software radio," *IEEE Communications Magazine*, vol. 33, no. 5, pp. 56–61, May 1995.

[145] G. Hillerström and A. Olofsson, "SDR and Cognitive Radio on Parallella," URL: http://www.adapteva.com/white-papers/sdr-and-cognitive-radio-on-parallella/, Accessed: 12/11/2012.

[146] GNURadio, URL: http://www.gnuradio.org, Accessed: 12/11/2012.

[147] T. Schmidl and D. Cox, "Robust frequency and timing synchronization for OFDM," *IEEE Transactions on Communications*, vol. 45, no. 12, pp. 1613–1621, December 1997.

[148] G. Cariolaro, *Unified Signal Theory*, ser. SpringerLink : Bücher. Springer, 2011.

[149] M. Frigo and S. Johnson, "The design and implementation of FFTW3," *Proceedings of the IEEE*, vol. 93, no. 2, pp. 216–231, February 2005.

[150] LAPACK, URL: http://www.netlib.org, Accessed: 12/11/2012.